Aus der Medizinischen Klinik III für Hämatologie, Onkologie und Palliativmedizin,
Universitätsmedizin Rostock

Direktor: Prof. Dr. med. Christian Junghanß

Combined immunotherapy approaches in preclinical models of mismatch-repair-deficiency-associated tumorigenesis

Inauguraldissertation
(Kumulative Promotionsschrift)
zur
Erlangung des akademischen Grades:
Doktor der Naturwissenschaften
Doktor rerum naturalium (Dr. rer. nat.)
der Universitätsmedizin Rostock

Vorgelegt von
Inken Salewski | geb. am 06.12.1994 in Heidenheim
aus Rostock

Rostock | (30.01.2023)

DOKTORARBEIT
UNIVERSITÄTSMEDIZIN ROSTOCK
https://doi.org/10.18453/rosdok_id00004407

Gutachter:

Prof. Dr. Ulrike Gimsa, Universität Rostock, Forschungsinstitut für Nutztierbiologie, Institut für Verhaltensbiologie

PD Dr. Claudia Maletzki, Universitätsmedizin Rostock, Medizinische Klinik III für Hämatologie, Onkologie und Palliativmedizin

Prof. Dr. Sebastian Stintzing, Charité – Universitätsmedizin Berlin, Medizinische Klinik mit Schwerpunkt Hämatologie, Onkologie und Tumorimmunologie

Jahr der Einreichung: 2023

Jahr der Verteidigung: 2023

Table of contents

List of illustrations

List of tables

List of abbreviations

CalR	Calreticulin
CDK	Cyclin dependent kinase
CDKi	Cyclin- dependent kinase inhibitor
cMS	Coding Microsatellite
CRC	Colorectal cancer
CTLA-4	Cytotoxic T-lymphocyte-associated protein 4
DC	Dendritic cell
dMMR	Mismatch-repair deficiency
FDA	*US Food and Drug Administration*
HMGB1	High-mobility group protein 1
IC	Immune checkpoint
ICD	Immunogenic cell death
ICI	Immune checkpoint inhibitor
i.p.	Intraperitoneal
LAG-3	Lymphocyte-activation gene 3
MDSC	Myeloid- derived suppressor cells
MMR	Mismatch-repair
MS	Microsatellite
MSI	Microsatellite instability
PD-1	Programmed cell death protein 1
PD-L1	Programmed cell death-ligand 1
s.c.	Subcutaneous
5-FU	5-Fluorouracil

1. Introduction

1.1 Microsatellite instability

Microsatellite instability (MSI) is a form of genetic instability. It acts as a diagnostic marker for solid and hematological malignancies and has become an excellent biomarker for immunotherapy. Microsatellites are short DNA regions of repetitive mono-, di-, tri-, or tetranucleotides, such as AGAGAG [1]. MSI results from deletions or insertions in microsatellites which are particularly present in non-coding regions of the DNA. During replication, the polymerase can detach from the DNA strand, a process called DNA replication slippage [2,3]. As a consequence, the double strand separates. When these two strands reattach incorrectly a loop can be created. The resulting replicated DNA strand is reduced or elongated. The mismatch repair (MMR) system recognizes the loop and corrects the error. MLH1, MSH2, MSH6, and PMS2 are the four main proteins involved in this repair system [4]. When a cell has a dysfunctional MMR system, the loop can lead to frameshift mutations and dysfunctional, usually, C-terminally truncated proteins [5,6]. These novel proteins, with deletions of 4 to 12 base pairs, depending on the type of cancer, act as neo-antigens, which are foreign to the immune system. Hence, MMR-deficient (dMMR) tumors are highly immunogenic and ideal candidates for immunotherapy.

In clinical diagnostics, the Bethesda panel is used to test for MSI. Five microsatellites are examined *via* fragment length analysis. Two mononucleotide loci (Bid Adenosine Tract [BAT]-25 and BAT-26) and three dinucleotide loci (D2S123, D5S346, D17S250) are part of the Bethesda panel. Instability in two or more of these regions is defined as MSI-high, instability in one of the MS is defined as MSI-low and no instability is called MS stable [7–10].

Germline mutations in one of the MMR genes, i.e. *hMLH1, hMSH2, hMSH6*, or *hPMS2* result in a dysfunctional MMR system and finally drive MSI. This can either occur sporadic or hereditary. In fact, dMMR is present in 15-18 % of all colorectal cancers (CRC). Hereditary dMMR--related cancers arise in the context of Lynch syndrome – the most common hereditary tumor syndrome in men.

1.2 dMMR-associated tumors

Humans can inherit mono- or bi-allelic mutations in one of the MMR genes. These are the driver mutations [11–13]. When a somatic inactivation of the second allele appears additionally to the mono-allelic germline mutation, tumors develop in the affected organs. In most cases, gastrointestinal adenomas or carcinomas arise. Besides, extra-gastrointestinal malignancies, including the endometrium, ovary, and bile duct are likewise detectable in Lynch syndrome patients [14]. This disease is named after the researcher Henry Lynch who described this syndrome in 1971 [15]. The median age of onset is 44 years [16,17]. It is the most frequent hereditary cancer syndrome in men with a prevalence of 1:400 and [18,19] and accounts for 3 %

of all CRCs [20,21]. The lifetime risk of germline mutation carriers to develop tumors is over 80 %. Two subgroups exist: subtype G1 is highly immunogenic and subtype G2 is low immunogenic [8,22,23]. Men are twice more affected as women. This disease is characterized by MSI [24–27].

In the case of the bi-allelic inherited mutation, children develop tumors all over their bodies; this is called constitutional mismatch-repair-deficiency (cMMR-D). In both syndromes, developing tumors show a high mutational burden [28–30].

Another reason for developing dMMR-related tumors is the epigenetic modification of the *MLH1* promoter, which results in the inactivation of *MLH1* [31,32].

Table 1: Clinical characteristics of Lynch syndrome [16,17,33–39]

Age	~40 - 50 years old
Sex	Higher risk in men
Tumor localization	Colon, endometrium, ovarium, stomach, urothel, bile duct, small intestine, central nerve system
Mutation in *hMLH1*	~35 % of patients
Mutation in *hMSH2*	~40 % of patients
Life time risk of tumorigenesis of patients with dMMR	Men: 27 – 74 % Women: 22 – 53 %
MSI status	Usually MSI-high

1.3 Clinical and preclinical approaches for dMMR related diseases

Conventional chemotherapy is still used as first-line therapy for many tumor entities. Cytostatic drugs stop the uncontrolled cell division of tumor cells. 5-Flourouracil (5-FU) for example, is inserted into the newly synthesized DNA as a base. Depending on the stage of the tumor, different schemes of chemotherapy are applied, for example, FOLFOX4 [40,41]. This starts 5 to 8 weeks after surgery and includes a sequence of oxaliplatin, folinic acid, and 5-FU. Nowadays, XELOX II is increasingly used [42]. Herein the oral drug capecitabine is given instead of 5-FU, which is transformed into 5-FU in the body, especially in the tumor tissue [43]. Besides the cytotoxic effects against tumor cells, certain cytostatic drugs can trigger endogenous antitumor immune responses. One of the most important effects is the induction of immunogenic

cell death, which in turn, leads to an activation of cytotoxic T-lymphocytes, and finally to tumor infiltration [44]. In addition, chemotherapy can increase the tumor mutational burden [22,23]. Another commonly used drug in the clinic is Gemcitabine. This drug inhibits DNA synthesis by acting as a deoxycytidine nucleoside analog and consequently activates the immune system. In this cascade, the tumor microenvironment shifts to an inflammatory milieu [45,46]. Gemcitabine is, among others, approved for the treatment of pancreatic carcinoma and metastatic breast cancer [47,48]. Currently, gemcitabine is not part of the treatment regimen for Lynch syndrome or CRC, but due to its immunomodulatory properties, it is a potential candidate for combinational immunotherapies [49]. Indeed, in a previous *in vitro* study, our group could show that gemcitabine reduces the amount of intracellular IDO-1 and triggers immunogenic cell death, characterized by translocation of CalR and HMGB1 secretion [50]. *In vivo*, combined chemo-immunotherapy prolonged the overall survival of dMMR mice [50].

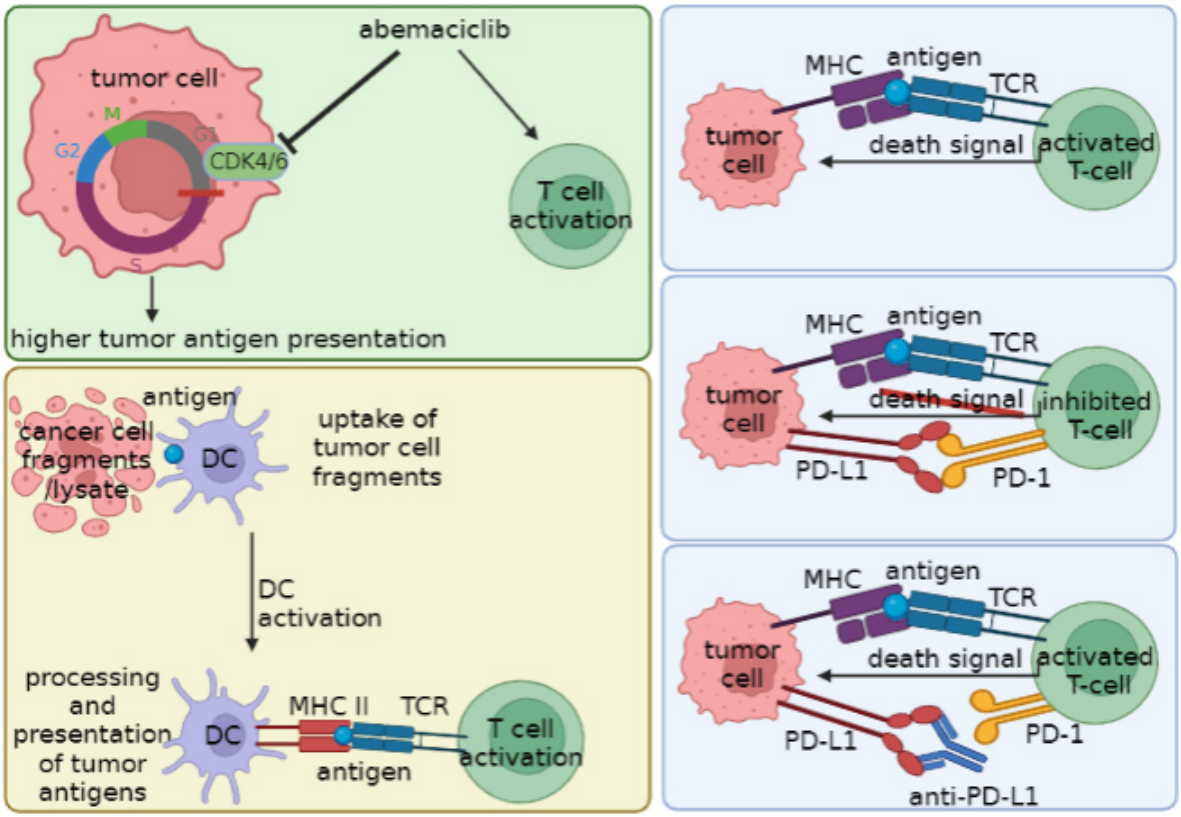

Figure 1
Schematic overview of the mechanism of action of the different immunotherapies: green box: abemaciclib, yellow box: Dendritic cells, blue boxes: α-PD-L1. DC = dendritic cell, TCR = T-cell receptor.

Nowadays, immunotherapy is increasingly clinically approved. The most widely applied immunotherapy is based on immune checkpoint inhibitors (ICIs). Immune checkpoints are natural regulators of the immune system. Physiologically, these checkpoints prevent autoimmunity by mediating immune tolerance. They are primarily found in immune cells, including T-lymphocytes. However, tumor cells utilize immune checkpoints to obtain self-tolerance by preventing

the immune system to attack the body's own cells. ICIs activate the immune defense by stopping the immune inhibiting impact, a mechanism termed "*breaking the breaks*". Their main function is to reactivate exhausted T-lymphocytes. The main targets for ICIs are cytotoxic T-lymphocyte-associated Protein 4 (CTLA-4 or CD152), programmed cell death protein 1 (PD-1 or CD279), and programmed cell death- ligand protein 1 (PD-L1 or CD274).

Cytotoxic T-lymphocyte-associated Protein 4 (CTLA-4) also known as CD152, is expressed on T-lymphocytes to prevent overreaction of the immune system when T-lymphocytes are activated [51–54]. Already in the 1990s, the blockade of CTLA-4 was tested to improve antitumor immunity [55]. Ipilimumab was the first FDA-approved ICI for metastatic melanoma in 2011 [56,57].

PD-1-targeting antibodies, such as Nivolumab, Pembrolizumab, and Cemiplimab are approved for 1st line therapy of unresectable or metastatic dMMR CRC [58–60]. Response rates for patients with metastatic CRC to α-PD-1 monotherapy are described to be between 31-54 % [61–63]. PD-1 is an inhibitory receptor on the surface of activated monocytes, dendritic cells, NK cells, T, and B cells. When bound to its ligand PD-L1, it takes part in programmed death signaling which regulates T cell-mediated responses [64]. PD-1 reduces cytokine secretion, like TNFα, IFNγ, and IL-2 which in turn blocks cell proliferation [65,66]. This blockade induces a cell cycle arrest in the G0/G1 phase more than by apoptosis [67].

PD-L1 is a transmembrane protein that helps to maintain peripheral tolerance, but it is also involved in tumor immune escape (Figure 1) [68]. Antibodies against PD-L1, such as Atezolizumab are FDA-approved for entities like progressive advanced urothelial carcinoma [69,70].

Another ICI that just started to gain attention, is the antibody against the lymphocyte-activation gene 3 (LAG-3). It is expressed on activated immune cells, maintains the homeostasis of $CD8^+$ T-lymphocytes, participates in the activation of dendritic cells, and blocks cellular proliferation [71–73]. LAG-3 and CD4 are structural homologs, but LAG-3 expressed on tumor cells outcompetes CD4 when binding to MHC class II, which leads to calming of NK and T-lymphocytes [74–77]. As a consequence, LAG-3 promotes tumor immune escape in the local tumor microenvironment [73]. Indeed, a recent study showed that inhibition of LAG-3 leads to the downregulation of anti-apoptotic signals in tumor cells and to the reactivation of NK and T-lymphocytes [78]. The safety of LAG-3 antibodies is currently tested in several clinical trials for unresectable or metastatic solid tumors (*Clinicaltrials.gov* identifier: *NCT03489369*). Additionally, a combination with Nivolumab is tested (*Clinicaltrials.gov* identifier: *NCT03607890, NCT01968109, NCT04811027*). On 18 March 2022, the FDA approved the combination of Nivolumab (α-PD-1) with Relatlimab (α-LAG-3) for unresectable or metastatic melanoma which doubled the time of progression-free survival compared to Nivolumab monotherapy. This combinational therapy is called Opdualag [79].

Since not all patients respond to ICI therapy, predictive markers are investigated to identify patients with a high likelihood to benefit from this treatment [80–83]. Additionally, combination treatments with conventional chemotherapy are under clinical investigation.

Since nearly all Lynch syndrome tumors are MSI and thus hypermutated, cancer vaccines constitute a promising therapy option. Commonly used are antigen-loaded dendritic cells, these are already safety proven and induce long-lasting immunity in some cases [78,84,85]. Vaccines can delay or prevent relapse. Furthermore, whole tumor lysate vaccines provide a far more variety of neo-antigens that can be combated by the immune system than peptide-based vaccines do (Figure 1) [86]. In clinical trials, the vaccines did not show the desired effects [87,88]. In prophylactic settings, tumor lysate vaccination may prevent tumorigenesis in high-risk patients [89]. Indeed, a recent study showed that a combination of four synthetic frameshift peptide neoantigens decreased the tumor burden and prolong the overall survival of mice with an *Msh2* knock-out in the intestine. Furthermore, the adaptive immunity towards those four neoantigens was significantly increased [90]. In previous studies of our group, comparable preventive effects were found in *Mlh1* knock-out mice (*Mlh*1$^{-/-}$ mice) repetitively treated with murine whole tumor lysates. Survival could be prolonged, especially in combination with chemotherapy [50,91].

1.4 Preclinical tumor models

Given the high clinical relevance of *hMLH1* and *hMSH2* mutations in human dMMR-related cancers, mouse lines with a constitutional or conditional knock-out in these genes have been developed [33,34,92,93]. The group of Prof. Edelmann pioneered the experimental development of dMMR mouse lines. In our lab, we bred two knock-out mouse models which develop tumors spontaneously to nearly 100% [94–97]. The Mlh1$^{-/-}$ mice (strain: B6.129-Mlh1^{tmRak}) have a dominant negative null mutation of exon 2 of the *Mlh1* gene [97]. Infertility of Mlh1$^{-/-}$ mice is a side effect, therefore heterozygous mice are used for breeding. Within the first months, Mlh1$^{-/-}$ mice can develop lymphomas, which represent cMMR-D. These can arise either in the thymus or as generalized lymphomas in the liver or spleen. Additionally, skin lesions can appear [98]. At an age of around 8 months, these mice develop gastrointestinal tumors, which show characteristics of Lynch syndrome [99]. Both tumor syndromes evolve at around the same distribution in Mlh1$^{-/-}$ mice, still female mice are more prone to develop lymphomas, whereas males rather develop gastrointestinal tumors [98]. Msh2$^{loxP/loxP\ ;TgTg(Vil1\text{-}cre)}$ mice have a conditional knock-out that manifests in the gut. Accordingly, the Msh2$^{loxP/loxP\ ;TgTg(Vil1\text{-}cre)}$ mice only develop tumors in the intestine due to their targeted knock-out only in the gastrointestinal tract.

1.5 Targeted therapies: Cyclin-dependent kinase inhibitors

It is known that dysregulation and overexpression of cyclin-dependent kinases (CDK) are involved in the development of tumors, hence, CDK inhibitors (CDKi) have been developed and are increasingly used in the clinic [100–104]. There are 13 human CDKs that all belong to the serine/threonine kinases. CDKs regulate the cell cycle and are dependent on the oscillation of cytokines which are up- and down-regulated throughout the cell cycle [100]. Furthermore, they are involved in the metabolism, transcription, epigenetic regulation, neuronal function, and self-renewal of stem cells [105]. CDKis can be categorized into global and selective agents. Global CDKis have a broad mode of action, usually targeting multiple CDKs. Examples of global CDKis include dinaciclib and THZ1. The first one inhibits CDK1, 2, 5, and 9 [106] and is known to turn immunological cold microenvironments in pancreatic cancers into hot [107]. THZ1 blocks CDK7, 12, and 13 [108] and affects the phosphorylation and transcription of RNA polymerase 2 [109,110]. In a recent study on glioblastoma multiforme cell lines, dinaciclib significantly affected the viability in 2D as well as in 3D cell culture. Visible changes were found in morphology such as small vacuoles and cell shrinkage. Additionally, dinaciclib induced senescence, necrosis, and mitochondrial dysfunction. RNA analysis revealed downregulation of genes related to cell cycle, mitosis, transcription regulation, cell migration, and E3 ubiquitination, and in contrast, upregulation of genes involved in chemotaxis, DNA damage, and stress. Long-term treatment exhibited resistance in only 1 of 5 cell lines [111]. For CRC, riviciclib, a CDK1, 4, and 9 inhibitor was found to inhibit colony formation *in vitro* and induce apoptosis. Furthermore, riviciclib showed synergistic effects with various chemotherapeutics in different tumor entities [112]. In another study, the CDK9 inhibitor CDKI-73 induced apoptosis in two human CRC cell lines and inhibited tumor growth significantly in xenograft mouse models [113]. The same effects were found for samuraciclib, also called ICEC0942, in CRC cell lines [114]. The advantage of CDKI-73 over dinaciclib is, that CDKI-73 can be applied orally [113]. Selective CDKis have a narrower spectrum of activity and target specific CDKs. These include, among others, the CDK4 and 6 inhibitors abemaciclib, ribociclib, and palbociclib [115]. All agents stop the cell cycle at the G1 phase [116,117]. CDK4/6 inhibitors indirectly improve tumor antigen presentation and suppress the proliferation of regulatory T-lymphocytes, but reactivate T-lymphocytes and produce an inflamed microenvironment [118–120]. They can improve long-term immunity by transforming $CD8^+$ T-lymphocytes into memory cells [121]. All three CDK4/6 inhibitors are FDA-approved for the treatment of hormone receptor-positive, human epidermal growth factor receptor 2 negative breast cancer [122,123], and clinical trials are ongoing for other solid tumors. Although these three CDK4/6 inhibitors have the same targets, they differ in efficacy and side effects [124]. Additionally, palbociclib and ribociclib show higher affinity to CDK6, while abemaciclib rather binds to CDK4 (Figure 1) [125–127]. The latter leads to swollen and dysfunctional lysosomes and induces apoptosis, necrosis [116], and

senescence. Besides, abemaciclib blocks DNA synthesis, which reduces cell proliferation [117,119,128,129]. The CDK4/6 blockade leads to the upregulation of the transcriptional repressor MXD4, which negatively regulates MYC [121]. CDKis are good candidates to treat dMMR malignancies because these patients already have preformed antitumor immune responses that can be boosted using CDKis [130–132].

1.6 Combination therapies

Combination treatments are used to increase the effects of a certain monotherapy and to neutralize or prevent the development of escape mechanisms. The addition of chemotherapy to ICIs is promising to prevent resistance mechanisms and to combat the tumor by activating the patient's own immune system [44]. Clinical trials are ongoing for combination therapy of α-PD-L1 together with chemotherapy for solid tumors (*Clinicaltrials.gov* identifier: *NCT03572400, NCT03324282, NCT03093922*).

Additionally, combination treatments of ICI with CDKi are tested. *In vitro* tests revealed that dinaciclib enhances T cell proliferation and induces DC activation which leads to immunogenic cell death. These outcomes increase the effectiveness of PD-1 blockade [133]. In an *in vitro* study, abemaciclib triggered proinflammatory immune responses in ovarian cancer cells, enhanced immune cell infiltration, and PD-L1 expression [134]. The combination with α-PD-1 additionally induced $CD8^+$ T cell activation and can therefore be a great option for low-immunogenic cancer types [135].

In another study, it was found that the deletion of *CDKN2A* contributed to α-PD-1 (Nivolumab) resistance in malignant pleural mesothelioma patients, but sensitized cells to CDK blockade [136]. In mice, a combination with a CDK4/6 inhibitor was applied to overcome resistance mechanisms induced by the α-PD-1 monotherapy. This finally reduced the tumor size [136]. The sensitivity towards abemaciclib was also found in HNSCC cell lines with deletions in the *CDKN2a* gene [137].

In preclinical as well as in a phase 1 study, Pembrolizumab and dinaciclib were combined and showed strong antitumor activity and good tolerance in patients with relapsed or refractory chronic lymphocytic leukemia (rrCLL) and diffuse large B-cell lymphoma (rrDLBCL) [138].

2. Aim of the study

The study aimed to test the efficacy of different immunotherapies in two preclinical mouse models of dMMR. *In vivo* experiments were done on mice, either harboring a constitutional (*Mlh1)* or conditional (*Msh2)* knock-out.

Given the growing relevance of immune checkpoint inhibitors in first- and second-line treatment of dMMR-related tumors, in this thesis, we focused on PD-L1 as a novel target receptor and applied different combination strategies. Whole tumor vaccination, chemotherapy, and the CDK inhibitor abemaciclib were used as combination partners to improve the outcome. Treatments included therapeutic and prophylactic interventions intended to reduce or prevent dMMR tumor growth.

To evaluate the efficacy of either treatment, the general condition of mice was monitored daily, accompanied by longitudinal PET/CT screens using $^{[18]}$FDG-PET/CT and routine blood sampling to track immunological changes by flow cytometry. After the experimental endpoint, Kaplan-Meier survival curves were displayed. Additionally, the tumor microenvironment was examined *via* immunofluorescence, the MSI status was determined with fragment length analysis, and changes in gene expression were recorded using Nanostring-based arrays.

With this project, we intended to provide new insights into the underlying mechanisms of response and resistance toward state-of-the-art treatments for patients with MMR-D-related tumors.

3. Methods

As part of this project medical PhD students (Steffen Kuntoff, Julia Henne, Leonie Engster, Paula Krone, Julia Teichmann) were incorporated and guided. Part of their work is included in this thesis. Therefore, methods were performed by different people.

3.1 *In vitro* experiments

Cell culture & treatments

Cell lines A7450 T1 M1 and 328 cells (both adherent) were established from gastrointestinal tumors and 1351 (suspension) was generated from a splenic lymphoma of $Mlh1^{-/-}$ mice in our lab. Cells were cultured in complete medium DMEM/HamsF12, supplemented with 10 % fetal calf serum, 2 mmol/L glutamine, and antibiotics. Treatments were applied as IC_{30}. Abemaciclib: 1 µM, Palbociclib: 1 µM, Dinaciclib: 100 nM, THZ1: 0.83 µM.

Dendritic cells were extracted from the bone marrow of euthanized $Mlh1^{+/-}$ mice. The femur was extracted and rinsed with PBS to gain the dendritic cells. Cells were sieved and washed and cultured in RPMI medium, + 10 % fetal calf serum, 2 mmol/L glutamine + antibiotics and seeded in 6 well plates with 300,000 cells/ml and 3 ml/well. After 3 days 1 ml medium/well was exchanged with 2 ml of fresh medium. After additional 3 days and 2 days 2 ml medium/well were exchanged with 2 ml fresh medium, respectively. After 9 days in total, dendritic cells were harvested by collecting the supernatant medium, washing the wells with PBS and centrifugation (300 x g, 8 min).

Apoptosis/necrosis assay

Cells were treated for 48 h, 72 h and 2x 72 h with CDKis. Cells were harvested and incubated with 0.2 µM Yo-Pro iodide (Thermo Scientific, Ex/Em 491/509 nm; blue laser 488 nm) for 20 min at RT. Afterwards cells were washed and mixed with 7-AAD viability staining solution (250 ng, Biolegend, San Diego, United States) before measurements started. Measurements were performed at a FACSVerse Cytometer (BD Pharmingen, San Diego, USA) and were analyzed using BD FACSuite software (BD Pharmingen).

Cell cycle analysis

Cells were treated for 48 h, 72 h and 2x 72 h with CDKis. Cells were harvested and incubated with ice-cold ethanol overnight at -20°C. RNase (1mg/ml Carl Roth, Karlsruhe, Germany) was preheated for 90 min at 37°C. Cells were washed twice with 2 ml PBS and centrifuged at 300 x g for 10 min. 500 µl RNase was added to each sample, mixed and incubated for 45 min at 37°C in the water bath. Cells were washed twice with 2 ml PBS and centrifuged at 300 x g for 10 min. Cells were mixed with 400 µl propidium iodide (50 µg/ml) and incubated for 30 min in the fridge covered from light. Measurements were performed at a FACSVerse Cytometer (BD

Pharmingen, San Diego, USA) and were analyzed using BD FACSuite software (BD Pharmingen) and FlowJo™ Version 10.6.1.

Immunogenic cell death analysis

Cells were treated for 48 h, 72 h and 2x 72 h either with abemaciclib, palbociclib, dinaciclib or THZ1. Cells were harvested and incubated with poyclonal rabbit CalR primary antibody (10 µg/ml, Abgent, San Diego, CA, USA) for 30 min at 4°C. Then, the secondary donkey anti rabbit FITC-labeled antibody (10 µg/ml; Biolegend, San Diego, USA) was added and incubated for 30 min at 4°C. Control cells were only incubated with the secondary antibody. Measurements were performed at a FACSVerse Cytometer (BD Pharmingen, San Diego, USA) and were analyzed using BD FACSuite software (BD Pharmingen).

ELISA to quantify HMGB1 level in supernatant

Supernatants were collected from tumor cells upon incubation. The level of high-mobility group protein 1 (HMGB1) were measured *via* ELISA following the manufacturers' protocol (Abbexa, Cambridge, UK).

Colony formation assay

500 cells were seeded per well in 6 well plates and allowed to rest overnight. Treatment was added. After 6 days cells were stained with 500 µl 0.2% crystal violet for 10 min on a rocking plate. Afterwards cells were washed with PBS. The number of colonies was counted *via* ImageJ-win64. The well in the image was cropped and cleared out. The image type was set to 8-bit. Outliers were removed using: radius = 5 pixel, threshold = 1, which outliers = dark. The threshold was adjust to 0 to 119 and black and white. The watershed function was applied and particles were analyzed with parameters: size = 20-infinity, circularity = 0-1, snow = outliers.

Co-culture assay

Tumor cells were stained with 5 µM CMFDA for 15 min at 37°C and 5% CO_2. 20 000 cells were seeded per well in a 24 well plate. After 24 h 200 000 blood cells were added per well. Blood was lysed before with erythrocyte lysis buffer (155 mM NH_4Cl (MERCK Millipore, Darmstadt, Germany), 10 mM $KHCO_3$ (MERCK Millipore), and 0.1 mM EDTA (Applichem, Darmstadt, Germany)). Treatment was added (abemaciclib 1 µM). 24 h later, the anti-PD-L1 antibody (10 µg/ml) was added. After 48 h, tumor cells were quantified. Cells were mixed with fluorescent microsphere beads (1.4 x 10^5 beads/ml, size: 10 µm, Polyscience, Hirschberg an der Bergstrasse, Germany). Measurements were performed at a FACSVerse Cytometer (BD Pharmingen, San Diego, USA) and were analyzed using BD FACSuite software (BD Pharmingen).

Immunofluorescence of cytoskeleton and ROS

Cells were treated twice for 72 h with 1 µM abemaciclib. Then cells were stained with 7.5 µM ROS Brite 670 (AAT Bioquest, CA, USA) for 30 min at 37°C. Then, 125 nM Mitolite Green (AAT Bioquest) were added for 45 min at 37°C. Cells were fixed with 4% PFA for 30 min at RT. After three times washing with PBS cells were permeabilized with 0.2% TritonX for 15 min at RT. Afterwards Phalloidin-iFluor (1 test unit/ml in 1% BSA; AAT Bioquest) was added for 30 min at RT. Cells were washed thrice and incubated with 1.5 µg/ml DAPI for 2 min. Images were taken on a confocal laser scanning microscope (ZEISS Elyra 7 Confocal Laser Microscope, Zeiss, Jena, Germany).

Whole exome sequencing data analysis (Dr. rer. nat. Yvonne Gladbach)

The cell lines 328 and A7450 T1 M1 were sequenced using the Agilent SureSelectXT panel on a Genome Sequencer Illumina HiSeq in paired-end mode (GATC, Konstanz, Germany). Their genomic correlations were presented in oncoprint. Then single nucleotide variants (SNV) were searched both missense and nonsense mutations. With the help of a “lollipop” mutation diagram generator mutations on proteins of interest were mapped. Candidate genes, with a high probability to mutate, were selected based on human MMR-D counterparts and their involvement in tumorigenesis.

3.2 *In vivo* experiments

Ethical statement

All animal experiments were authorized by the Landesamt für Landwirtschaft, Lebensmittelsicherheit und Fischerei Mecklenburg-Vorpommern (7221.3-1-062/19; -025/20; -026/17) in accordance to the german animal welfare act and the EU policy 2010/63/EU. Mice were bred in the animal facility of the University Medical Center Rostock under specific pathogen-free conditions. Genotyping of $MLlh1^{-/-}$ [130] and $Msh2^{loxP/loxP\ ;TgTg(Vil1\text{-}cre)}$ [139,140] was performed. All mice got enrichment like mouse-igloos, nest material, paper rolls, and nailwood. Mice were kept in type III cages during experiment in a 12-hour dark-light rhythm, a temperature of 21 + /- 2 °C and a relative humidity of 60 + /- 20 %. Food pellets and tap water was given *ad libitum*. For manufacturing of tumor lysate, tumor fragments were transplanted subcutaneously into mice under ketamine/xylazin anesthesia (90/6 mg/kg bw i.p.). After reach of a critical tumor size, mice were euthanized and tissue was resected for further processing.

Methods

Experimental protocol

Treatment schedules were as followed:

1) Combined chemo-vaccine in Mlh1$^{-/-}$ mice

Prophylactic approach: four weekly injections of tumor lysate subcutaneously and afterwards every four weeks, to a total of 12 injections (s.c., 10 mg/kg bw, 328 vaccine n = 10, A7459 T1 M1 vaccine: n = 9, q1wx4 + q4wx8). Control mice were left untreated (n = 15 mice).

Therapeutic approach: four weekly injections of tumor lysate subcutaneously and afterwards biweekly, to a total of 12 injections (s.c., 10 mg/kg bw, 328 vaccine n = 8, A7459 T1 M1 vaccine: n = 8, q1wx4 + q2wx8). Additionally, mice received thrice gemcitabine every four weeks (i.p., 100 mg/kg bw). Control mice were left untreated (Mlh1$^{-/-}$ n = 7 mice).

2) Vaccine-ICI combination in Mlh1$^{-/-}$ mice

Vaccine was given biweekly (s.c., 10 mg/kg bw, n = 10 mice, 12 times in total, q2wx12). The α-PD-L1 antibody in the first experiments was given intravenously (i.v., 2.5 mg/kg bw) once n = 4 mice) or thrice biweekly (q2wx3, n = 10 mice). Mice receiving the combination were first vaccinated, followed by α-PD-L1 injection (n = 10 mice/group; q2wx1 and q2wx3). Control mice were left untreated (n = 10 mice).

3) Chemo-ICI combination in Mlh1$^{-/-}$ mice

The α-PD-L1 antibody was given intravenously biweekly (i.v., 2.5 mg/kg bw, q2wx3, n = 10 mice) and gemcitabine was given intraperitoneal every 4 weeks (i.p., 100 mg/kg bw, q4wx3, n = 10 mice). For combination, mice received first gemcitabine and after four weeks, α-PD-L1 therapy started (n = 9 mice). Control mice were left untreated (n = 9 mice).

4) CDKi-ICI combination in Mlh1$^{-/-}$ and Msh2$^{loxP/loxP\ ;TgTg(Vil1\text{-}cre)}$ mice

Abemaciclib was given weekly (oral gavage, 75 mg/kg body weight (bw), 8 times in total (q1wx8), Mlh1$^{-/-}$ n = 7 mice, Msh2$^{loxP/loxP}$ villin-cre n = 9 mice). The α-PD-L1 antibody was given biweekly, three times in total (i.p., 2.5 mg/kg bw, q2wx3, Mlh1$^{-/-}$ n = 7 mice, Msh2$^{loxP/loxP\ ;TgTg(Vil1\text{-}cre)}$ n = 10 mice). The combination was conducted with lead-in abemaciclib, followed by α-PD-L1 injection (Mlh1$^{-/-}$ n = 7 mice, Msh2$^{loxP/loxP\ ;TgTg(Vil1\text{-}cre)}$ n = 10 mice). Control mice were left untreated (Mlh1$^{-/-}$ n = 7 mice, Msh2$^{loxP/loxP\ ;TgTg(Vil1\text{-}cre)}$ n = 9 mice) or were treated with the isotype control antibody (i.p. 2.5 mg/kg bw, Mlh1$^{-/-}$ n = 7 mice, Msh2$^{loxP/loxP\ ;TgTg(Vil1\text{-}cre)}$ n = 7 mice).

The murine α-PD-L1 antibody, clone 6E11 was kindly provided by Genentech, a subsidiary of Roche, South San Francisco, USA.

Prophylactic application started at an age of around 8 to 10 weeks. Therapeutic treatment started after approved development of at least one gastrointestinal tumor *via* PET/CT imaging. Control mice were left untreated. Suffering was prevented by offering soaked pellets. In addition, health status was monitored twice a day. Mice were sacrificed when reaching human endpoints (weight loss > 15%, pain, changes in social behavior) to avoid pain and distress.

PET/CT imaging (measurements were done by Core Facility of Multimodal Small Animal Imaging under the head of Univ.-Prof. Dr. med. Brigitte Vollmar)

Small animal PET/CT (Inveon PET/CT scanner, Siemens Preclinical Solutions, Knoxville, TN, USA) measurements were performed following a standard protocol. Mice were anesthetized by isoflurane (1.5% to 2.5% supplemented with oxygen Baxter) and ^{18}F-FDG was injected intravenously (16,91 + /- 1.73 MBq Radiopharmacon ^{18}F-FDG) into the tail vein. Mice were left for 1 h for ^{18}F-FDG uptake. Mice were measured for 15 min in PET/CT scanner. During measurements of mice were kept warm constantly at 38°C on a heating pad. Additionally, respiration was supervised. Images were evaluated. Feldkamp algorithm was applied on CT images. PET data was converted into 2D data and a ordered subset expectation maximization algorithm with 16 subsets and four iterations was utilized. Mitigation was performed to correct CT data. The Inveon Research Workplace 4.2 software showed metabolic volumes and standardized uptake values. Tumor growth was divided into progressive disease, when tumor size increased more than 25% compared to day 0, stable disease when tumor size only changed less than 25% compared to day 0 and partial response when tumor size was reduced by over 50% compared to day 0. Short term follow-up measurements were performed 30 days after start of therapy and long-term follow-ups were done after 50 days of treatment.

Tumor expansion and lysate preparation

For expansion of tumor material, heterozygous Mlh1$^{+/-}$ mice of an age of around 8 to 10 weeks were implanted subcutaneously into the flank with a 3x3x3mm piece of A7450 tumor. During operation mice were anesthetized with ketamine/xylazin 90/6 mg/kg body weight (i.p.). When the tumor reached an appropriate volume (<1,500 mm³), mice were euthanized and the tumor was removed. Tumor was homogenized and washed. Then tumor solution was incubated for 5 min at 42 °C for heat stress followed by 4 cycles of freeze thaw of 5 min in liquid nitrogen and 5 min at 56°C in the water bath, respectively. Afterwards, the tumor lysate was irradiated with 60 Gray and centrifuged for 10 min at 10 000 rpm to get rid of cell scrap. The concentration of the remaining supernatant was measured and stored at -80°C.

Quantitative real-time PCR

RNA isolation was performed using the RNeasy Mini Kit (Qiagen). For cDNA synthesis 1 µg mRNA and 50 ng random Hexamer Primer were incubated for 10 min at 70°C. Then 5x RT buffer complete, dNTPs and 200 units reverase were added. PCR conditions were as followed: 120 min at 45°C and 10 min at 70°C. 25 ng cDNA was used for quantitative real-time PCR with the SensiFAST Probe Lo-ROX Kit (Bioline, Memphis, Tennessee, USA). Predesigned Taqman gene expression assays were used: 6-FAM-3'BHQ-1 *Mxd4* (Mm00487523_m1), 6-FAM-3'BHQ-1 *cMyc* (Mm00487804_m1), 5-VIC-3'BHQ-1 *Agr2* (Mm01 291804_m1), 6-FAM-3'BHQ-

1 *Tgfb1* (Mm01178820_m1), 6-FAM-3'BHQ-1 *Vimentin* (Mm01333430_m1), 5-VIC-3'BHQ- 1 *N-Cadherin* (Mm01162497_m1), 6-FAM-3'BHQ-1 *Fpr2* (Mm00484464_s1), 5-VIC-3'BHQ-1 *Csf1* (Mm00432686_m1), 6-FAM-3'BHQ-1 *Csf2* (Mm01290062_m1), 5-VIC-3'BHQ-1 *Tcf1/Pcbd2* (Mm01342270_m1), and 6-FAM-3'BHQ-1 *Alox5* (Mm01182747_m1). As a housekeeping gene the self-designed 5-VIC-3'BHQ-1 *GAPDH* was used. Measurements were taken in the light cycler Viia7 (Applied Biosystems, Foster City, USA). Following PCR conditions were applied: 10 min at 95°C, 40 cycles of 15 sec at 95°C and 1 min at 60°C. Reactions were performed in triplicates. GAPDH level were used to normalize the level of target genes. The corresponding level were examined by calculating $2^{-\Delta CT}$ ($\Delta Ct = Ct_{target} - Ct_{Housekeeping\ gene}$), followed by $2^{-\Delta\Delta CT}$ quantification.

Cytometry measurements were supervised by the core facility for cell sorting and cell analysis of Rostock university medical center under the head of Prof. Dr. Brigitte Müller-Hilke**.**

Immune phenotyping on FACSVerse™

Routinely blood was taken from the retrobulbar venous plexus of anesthetized mice. Spleen and tumor tissues were sieved through a 100 µm mesh to obtain single cell solutions. A penal of conjugated monoclonal antibodies (mAb, 1 µg each) was applied to stain single cells. Afterwards erythrocytes were lysed (155 mM NH_4Cl (MERCK Millipore, Darmstadt, Germany), 10 mM $KHCO_3$ (MERCK Millipore) and 0.1 mM EDTA (Applichem, Darmstadt, Germany). Isotype (Biolegend, San Diego, USA) stains were used as negative controls. After washing steps, cells were resuspended in PBS and measured on a Flow Cytometer (BD FACSVerse™, BD Pharmingen). BD FACSuite software (BD Pharmingen) was used for data analysis.

Immune phenotyping on Cytek™ Aurora

Routinely blood was taken from the retrobulbar venous plexus of anesthetized mice. Spleen and tumor tissues were sieved through a 100 µm mesh to gain single cell solutions. A panel of conjugated monoclonal antibodies (mAb, 0.125 mg to 1.5 µg each) was applied to stain single cells. Zombie NIR™ Fixable Viability Kit (1 test unit/5 ml; Biolegend, San Diego, US) was applied following the instructions of Zombie NIR™ Fixable Viability Kit. Afterwards, extracellular staining was executed applying the instructions of the protocol BD Horizon Brilliant Stain Buffer (BD Biosciences). Gr1 Alexa Fluor700, CD8 FITC, CD4 APC Fire, CD11b BV570, PD-L1 BV421, NK1.1 BV605, CD19 Spark Blue (Biolegend), CD25 PerCP-eFluor710 (Thermofisher), CD83 BV750, PD-1 BV650 (BD Bioscience) antibodies were used. Lysis was done followed by intracellular staining following the instructions of True-Nuclear™ Transcription Factor Buffer Set (Biolegend). CTLA-4 PE/Cy7, CD3 PerCP, and Foxp3 Alexa Fluor 647 (Biolegend) antibodies were applied. Cells were measured on a spectral flow cytometer (Cytek™ Aurora). Data

analysis was performed with the help of SpectroFlow™ Version 2.2.0.3 and FlowJo™ Version 10.6.1.

Procartaplex cytokine assay (performed by PD Dr. Claudia Maletzki)
Blood plasma of mice was taken routinely. Cytokine level were measured *via* the Procartaplex™ multiplex immunoassay (Thermo Fisher Scientific, Schwerte, Germany) following the manufacturers' protocol. Measurement was performed on a Bioplex 2000 (Bio-Rad Laboratories GmbH, Munich, Germany). The Bio-Plex Manager Software was used for quantification.

Multiplex cytokine assay
Blood plasma of mice was taken routinely. With the help of a multi-analyte flow assay kit cytokine levels in the plasma were analyzed following the manufacturers' protocol (LEGENDplex™, Biolegend). Measurements were performed on a spectral flow cytometer (Cytek™ Aurora). For evaluation the manufacturers' online software was used. Cytokine level are represented in [ng/ml].

Fragment length analysis (FLA itself was kindly performed by Dr. Bjoern Schneider and Dr. Maja Huehns of the Institute of Pathology)
gDNA was isolated from tumor tissue using Wizard Genomic DNA Purification Kit (Promega). Coding and non-coding MSI marker were selected and fluorescently labeled primer were used for PCR. PCR conditions were 1min at 95°C, then 35 cycles of 15 sec at 95°C, 30 sec at 58°C and 10 sec at 72°C followed by cooling at 10°C. Amplified DNA fragments were analyzed *via* fragment length analysis on a 3500 genetic analyzer. Evaluation was done using GeneMapper™ software v4.1. Novel peaks in comparison to control tissue were evaluated as instability.

Nanostring targeted gene expression profiling (Nanostring analysis itself was kindly performed by Dr. Caterina Redwanz of the Department of Internal Medicine B, Cardiology, University Medicine Greifswald and evaluated by PD Dr. Claudia Maletzki)
Cryostat sections of tumors were used to isolate RNA via RNeasy Mini Kit (Qiagen). A Nanostring Counter gene expression platform (NanoString Technologies, Seattle, WA) was used to analysis the gene expression. The PanCancer IO 360™ Panel was applied to analyze 770 genes that are involved in tumor-immune interface and immune response and escape. Data analysis was performed with the nSover™ Analysis Software 4.0 in combination with the nCounter Advanced Analysis (version2.0.115). Data are displayed as heat maps as well as in box plots.

Methods

Immunofluorescence on LSM780 (Images and evaluation was performed by PD Dr. Claudia Maletzki)

4 µm thick cryostat sections of tumors were fixed in methanol for 8 min and air-dried. 2% BSA was used to block unspecific binding sites for 2 h. 1 µg of FITC and PE labeled antibodies were applied for 4 h. Following antibodies were used: CD4, CD8α, CD11b, Gr.1 (Immunotools, Friesoythe, Germany), CD11c, CD104, LAG-3, PD-1, F4/80 and PD-L1 (Biolegend).

After washing, sections were embedded in Roti Mount Fluor Care DAPI (Roth, Karlsruhe). Images were taken on a confocal laser scanning microscope (LSM780, Zeiss, Jena, Germany).

Immunofluorescence on Elyra 7 (Images and evaluation was performed by PD Dr. Claudia Maletzki)

4 µm thick cryostat sections of tumors were fixed in methanol for 8 min and air-dried. 2% BSA (Serva, Heidelberg, Germany) was used to block unspecific binding sites for 2 h. 1 µg of Alexa Fluor 488, Alexa Fluor 594 and Alexa Fluor 647 labeled antibodies were applied for 4 h. Following antibodies were used: CD3, CD4, CD8, CD206, F4/80, CD11b, Gr.1, PD-L1, PD-1 and Irf5 (Biolegend). Before intracellular staining cells were fixed for 30 min with 4% paraformaldehyde w/o methanol (Thermo Scientific, Darmstadt, Germany). Then cells were permeabilized for 15 min with 0.5% Triton X-100 (Sigma-Aldrich, Darmstadt, Germany). Cells were blocked with 2% BSA and incubated overnight at 4°C with the monoclonal rabbit anti-IRF5 antibody (1:50; ThermoFisher Scientific, Darmstadt, Germany). On the next day slides were incubated with the secondary monoclonal goat anti-rabbit Alexa Fluor 647 antibody (1:500; Cell Signaling, Frankfurt am Main, Germany). After washing, sections were embedded in Roti Mount Fluor Care DAPI (Roth, Karlsruhe). Images were taken on a confocal laser scanning microscope (ZEISS Elyra 7 Confocal Laser Microscope, Zeiss, Jena, Germany) using 20 x objectives. Quantification of the infiltration pattern was done by selecting 2 to 3 high power fields (HPF) per slide. $CD3^+/CD4^+$ T helper cells and $CD3^+/CD8^+$ cytotoxic T-lymphocytes were counted on each HPF. Regulatory granulocytes and tumor-associated macrophages were semi-quantitatively scored, following a score system. 0 = no; 1 = mild (1-20 cells/HPF); 2 = moderate (21-40 cells/HPF); 3 = strong (>40 cells/HPF).

Immunofluorescence on LSM780 (Images and evaluation was performed by PD Dr. Claudia Maletzki)

4 µm thick cryostat sections of tumors were fixed in methanol for 8 min and air-dried. 2% BSA was used to block unspecific binding sites for 2 h. 1 µg of FITC and PE labeled antibodies were applied for 4 h. The following antibodies were used: CD4, CD8α, CD11b, Gr.1 (Immunotools, Friesoythe, Germany), CD11c, CD104, LAG-3, PD-1, F4/80 and PD-L1 (Biolegend). For

other stainings1 µg of Alexa Fluor 488, Alexa Fluor 594 and Alexa Fluor 647 labeled antibodies were applied for 4 h. Following antibodies were used: CD3, CD4, CD8, CD206, F4/80, CD11b, Gr.1, PD-L1, PD-1 and Irf5 (Biolegend). Before intracellular staining cells were fixed for 30 min with 4% paraformaldehyde w/o methanol (Thermo Scientific, Darmstadt, Germany). Then cells were permeabilized for 15 min with 0.5% Triton X-100 (Sigma-Aldrich, Darmstadt, Germany). Cells were blocked with 2% BSA and incubated overnight at 4°C with the monoclonal rabbit anti-IRF5 antibody (10 µg/ml; ThermoFisher Scientific, Darmstadt, Germany). On the next day slides were incubated with the secondary monoclonal goat anti-rabbit Alexa Fluor 647 antibody (4 µg/ml; Cell Signaling, Frankfurt am Main, Germany). After washing, sections were embedded in Roti Mount Fluor Care DAPI (Roth, Karlsruhe). Images were taken on a confocal laser scanning microscope (ZEISS Elyra 7 Confocal Laser Microscope, Zeiss, Jena, Germany) using 20 x objectives. Quantification of the infiltration pattern was done by selecting 2 to 3 high power fields (HPF) per slide. $CD3^+$ /$CD4^+$ T helper cells and $CD3^+$ /$CD8^+$ cytotoxic T-lymphocytes were counted on each HPF. Regulatory granulocytes and tumor-associated macrophages were semi-quantitatively scored, following a score system. 0 = no; 1 = mild (1-20 cells/HPF); 2 = moderate (21-40 cells/HPF); 3 = strong (>40 cells/HPF).

IFN-γ ELISpot (PD Dr. Claudia Maletzki)

A7450 T1 M1 cells, 328 cells, 1351 cells and YAC-1 cells were seeded as targeT-lymphocytes in IFN-γ-specific monoclonal antibody (Mabtech, 3321-3)-coated 96 microtiter plates (2.5 x 10^3 cells/well). Splenocytes (1 x 10^4 cells/well) or blood cells (5 x 10^4 cells/well) from untreated or treated mice were co-cultured overnight. Every sample was seeded in triplicates. On the next day visualization of the bound antibodies was performed using the BCIP/NBT (KPL, Gaithersburg, Maryland, USA). With the help of a ELISpot reader spots were counted. The number of IFN-γ secreting cells per 10 000 effector cells are presented. Background signal was measured in the absence of targeT-lymphocytes.

Statistics

Statistical analysis was performed using GraphPad PRISM, version 5.02 or 8.0.2 (GraphPad Software, San Diego, CA, USA). All data are represented as mean + /- SD. The only exception is publication 4. Here, mean + /- SEM are given. The value of significance was set to $p<0.05$. Date was tested first for normality using Shapiro-Wilk test. In case of normality one-way ANOVA (Bonferroni's multiple comparison or Dunnett's multiple comparison), two-way ANOVA (Tukey's multiple comparison test) or unpaired t-test were performed. In case of non-parametric data Kruskal-Wallis or U-Test was performed. Kaplan Meyer survival curves were analyzed using log rank (Mantel cox) test.

Dimensionality Reduction Analysis (t-SNE)

FlowJo software (version 10.6.1.) was loaded with individual fcs files. Then FlowJo randomly picks 10.000 cells per file and combines (command: “concatenate”) 6 to 8 of these files depending on the organ origin into one single file. T-SNE algorithm provided by FlowJo software then creates a dot-plot. For this algorithm only the gated live cells were used.

4. Results

The results of this dissertation can be found in the following publications.

Publication 1: **Salewski I***, Gladbach YS*, Kuntoff S, Irmscher N, Hahn O, Junghanss C, Maletzki C. In vivo vaccination with cell line-derived whole tumor lysates: neo-antigen quality, not quantity matters. J Transl Med. 2020 Oct 21;18(1):402. doi: 10.1186/s12967-020-02570-y. PMID: 33087163; PMCID: PMC7579816. (IF 5.531)

Publication 2: **Salewski I***, Kuntoff S*, Kuemmel A, Feldtmann R, Felix SB, Henze L, Junghanss C, Maletzki C. Combined vaccine-immune checkpoint inhibition constitutes a promising strategy for treatment of dMMR tumors. Cancer Immunol Immunother. 2021 Dec;70(12):3405-3419. doi: 10.1007/s00262-021-02933-4. Epub 2021 Apr 18. PMID: 33870463; PMCID: PMC8571220. (IF 6.968)

Publication 3: **Salewski I***, Henne J*, Engster L, Schneider B, Lemcke H, Skorska A, Berlin P, Henze L, Junghanss C, Maletzki C. Combined Gemcitabine and Immune checkpoint Inhibition Conquers Anti-PD-L1 Resistance in Low-Immunogenic Mismatch Repair-Deficient Tumors. Int J Mol Sci. 2021 Jun 1;22(11):5990. doi: 10.3390/ijms22115990. PMID: 34206051; PMCID: PMC8199186. (IF 5.542)

Publication 4: **Salewski I**, Henne J, Engster L, Krone P, Schneider B, Redwanz C, Lemcke H, Henze L, Junghanss C, Maletzki C. CDK4/6 blockade provides an alternative approach for treatment of mismatch-repair deficient tumors. Oncoimmunology. 2022 Jul 11;11(1):2094583. doi: 10.1080/2162402X.2022.2094583. PMID: 35845723; PMCID: PMC9278458. (IF 8.11)

*Both authors contributed equally

In the next chapter, summaries of the original publications are given. The full texts of the respective publications are attached in chapter 8.

4.1 Publication 1

Cancer vaccines contain a variety of tumor neoantigens. In this paper, we showed that the quality of these antigens matters, not their quantity.

We compared two cell-line-derived tumor lysates of $Mlh1^{-/-}$ mice. Cell line 328 was molecularly defined as tumor mutational burden ultra-high and cell line A7450 T1M1 was defined as moderate to high. *In vitro* analysis revealed that A7450 T1 M1 cells secreted higher levels of cytokines like IL-1b, GM-CSF, and IL-18. These cytokines strengthen the NK cell function and facilitate the progress of T helper cells. In contrast, 328 cells secreted chemokines that are in charge of the activation of monocytes and eosinophils such as MCP1, MCP3, and Eotaxin. In a co-culture of lymphocytes and DCs either loaded with A7450 T1 M1 tumor lysate or 328 tumor lysate, the former fostered the amount of $CD8^+$ T-lymphocytes and activated them. On the contrary, 328-loaded DCs did not influence the leukocyte profile. Then, the lysates were given prophylactic or therapeutic. Tumor formation was delayed after either prophylaxis and the median overall survival was prolonged from 25 weeks in the 328 lysate group to 37 weeks in the A7450 T1M1 group (Figure 2:A). The same effects were seen when tumor lysates were administered as therapy (Figure 2:B). Therapy was started after PET/CT confirmation of tumor growth. The analysis discovered antigen-driven immune stimulation. In IFNγ ELISpot assay, *Mlh1* knock-out tumor cells were co-cultured with T-lymphocytes from mice of the A7450 T1M1 lysate treatment. These immune cells perceived the tumor cells. Furthermore, *ex vivo* evaluation revealed that vaccine therapy influenced the tumor microenvironment. A7450 T1M1 prophylactic treated mice developed tumors with reduced tumor-infiltrating MDSCs but in contrast, increased amounts of $CD8^+$ T-lymphocytes (Figure 2:C). In comparison, MDSC levels were elevated in tumors of 328 lysate-treated mice. Again, therapeutic effects reflect prophylactic results. The therapy with the A7450 T1M1 vaccine led to stable disease. Besides that, high numbers of $LAG\text{-}3^+$ and $PD\text{-}L1^+$ immune cells were a good biomarker for a bad outcome, whereas long-term survival was associated with the absence of immune checkpoint-expressing T-lymphocytes (Figure 2:D).

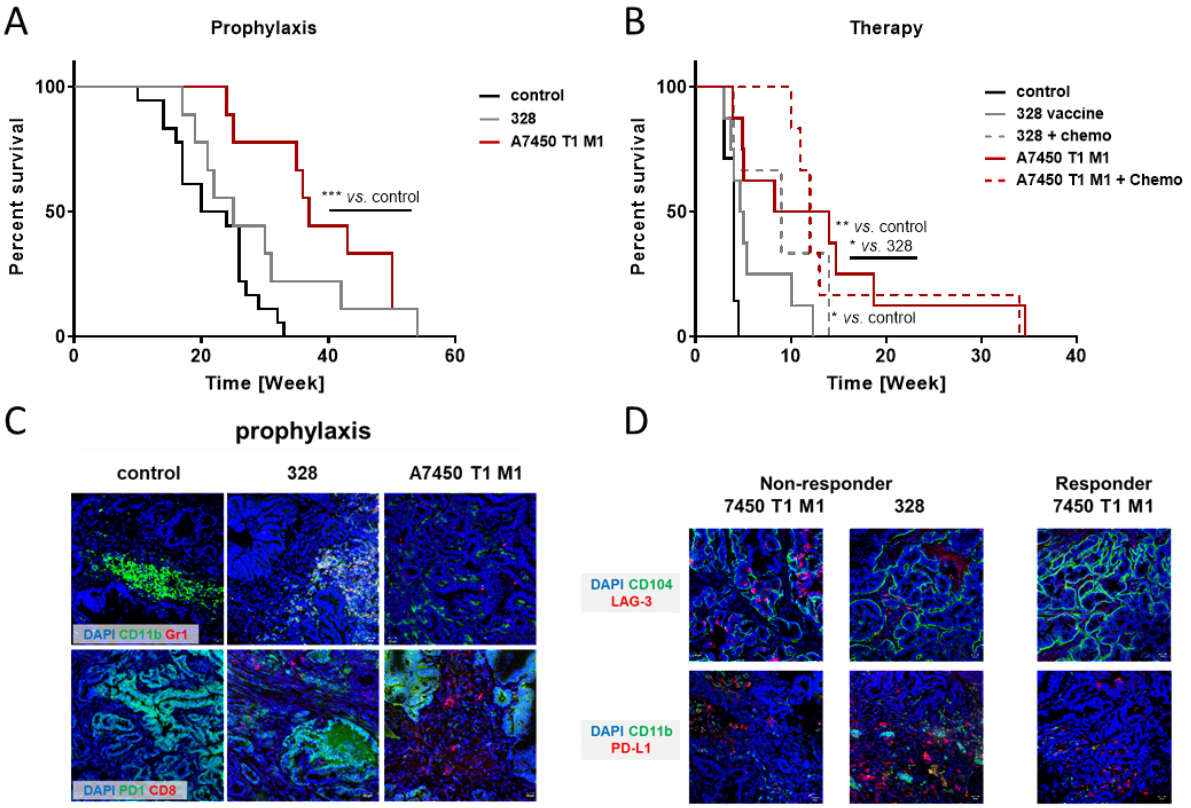

Figure 2:
(A, B) Kaplan-Meier survival curve after prophylactic and therapeutic vaccination of Mlh1$^{-/-}$ mice using whole tumor lysates 328 or A7450 T1 M1, respectively. Control mice did not receive any treatment. The best outcome was achieved upon vaccination with the A7450 T1 M1 lysate. Log-rank (Mantel–Cox) Test. A) Vaccine 10 mg/kg bw, s.c., n = 9 mice/group; control n = 15 mice. *p < 0.001 A7450 T1 M1 *vs.* control. B) n = 8 mice /group. Chemo = gemcitabine (100 mg/kg bw; A7450 T1 M1 n = 6 and 328 = 3 mice). *p < 0.05 328 + chemo *vs.* control;**p < 0.01 A7450 T1 M1 *vs.* control; *p < 0.05 A7450 T1 M1 *vs.* 328. (C, D) Immunofluorescence of 4 µm tumor tissue slides stained with mAbs. DAPI was used to stain cell nuclei. Images were taken on a laser scanning microscope (Zeiss) using 20x objectives. C) Prophylactic approach. Tumors of control mice showed higher infiltration with CD11b^{+} granulocytes. D) Therapeutic approach. Residual tumors of responders showed less infiltration of exhausted (LAG-3^{+}, PD-L1^{+}) T-lymphocytes. Non-responder = treatment failed, responder = treatment succeeded. Representative images are shown.

4.2 Publication 2

The above study revealed the efficacy of whole tumor lysates as vaccines for dMMR-driven tumors. Tumor vaccines delayed tumor growth significantly but immune escape mechanisms arose such as the upregulation of immune checkpoints like LAG-3 and PD-L1.

To counteract immune escape, a combination of vaccination with a PD-L1 blocking antibody was applied. In a pilot experiment, the α-PD-L1 antibody was tested in monotherapy being given once or thrice. Therapy was started after PET/CT confirmation of tumor growth. The first one prolonged the overall survival of mice from 4.0 weeks in the control to 6.0 weeks (Figure 3:A) and the second treatment even to 9.2 weeks (Figure 3:B), which was similar to vaccine monotherapy-treated mice which survived 10.2 weeks. The combination with α-PD-L1 once applied did not change the survival rate. But when the vaccine was combined with thrice α-PD-L1 treatment, this therapy even nearly doubled the time to 19.4 weeks. PET/CT imaging revealed reduced tumor growth for all therapies by far the best in the combination group. Three of 10 mice even reached complete remission and experienced long-term survival (Figure 3:C). Flow cytometry analysis identified increased T helper cell levels at day 84, as well as NK cell and myeloid-derived suppressor cell (MDSC) levels under all treatments. In contrast, splenic and intratumoral MDSC levels decreased, especially in the combination, accompanied by reduced numbers of immune checkpoint positive splenic T-lymphocytes, such as CTLA-4 and LAG-3 (Figure 3:D). Only under α-PD-L1 monotherapy, MDSC levels were increased. The number of B-lymphocytes was only elevated in the combination. Vaccine-based therapies stimulated the immune system, as determined by increased numbers of $CD83^+$ dendritic cells. On the contrary, in spleens, the level of DCs was downregulated in all treatments. The amount of $PD\text{-}1^+$ cells was unaffected in both spleens and tumors. T cell levels were not altered in spleens but increased under combination in the tumor.

Ex vivo immunological assays like multiplex cytokine expression assay showed fluctuation of IL-10 in all groups. Furthermore, gene expression analysis resulted in suppression of PI3K/Akt/Wnt and TGF pathways (Figure 3:F). This led to T cell infiltration, and reduced amounts of macrophages, neutrophils, and MDSCs (Figure 3:E). To sum up, the safety and efficacy of our combined immunotherapy approach were proven by the successful uncoupling of the PD-1/PD-L1 axis.

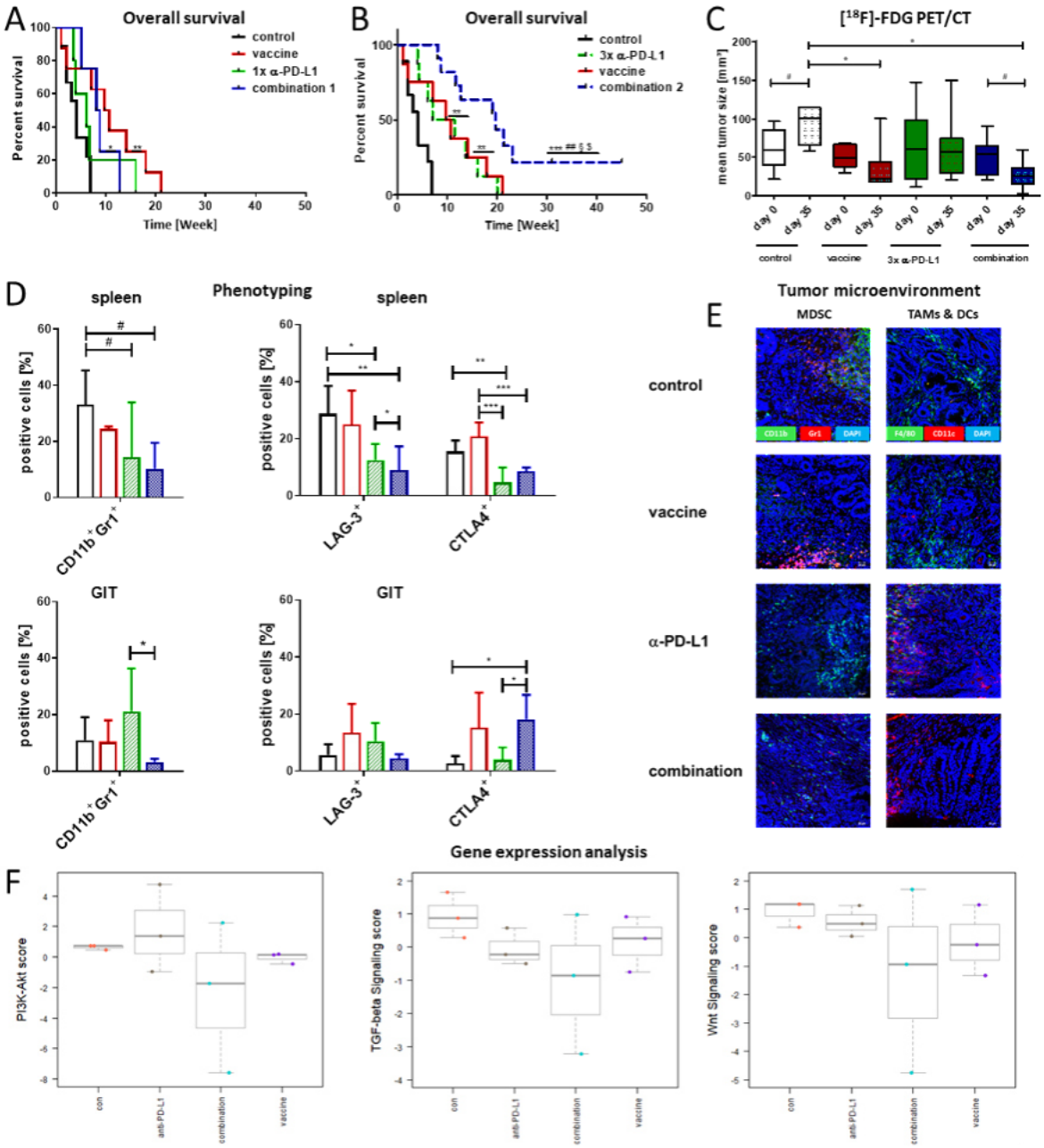

Figure 3:

(A, B) Kaplan-Meier survival curves of therapeutically treated mice (vaccine 10 mg/kg bw, n = 10 mice, α-PD-L1 clone 6E11, 2.5 mg/kg bw once n= 4 mice or thrice n = 10 mice). Control mice were left untreated (n = 10 mice). *p < 0.05 *vs.* control; **p < 0.01 *vs.* control; ***p < 0.001 *vs.* control; ##p < 0.01 *vs.* 1x α-PD-L1; §p < 0.05 *vs.* 3x α-PD-L1; $p < 0.05 *vs.* vaccine. C) PET/CT measurements of mean tumor size ± SD (n = 4-10 mice/group and time point). Combination therapy reduced the tumor size significantly. *p < 0.05 *vs.* control, one-way ANOVA (Bonferroni's multiple comparison test); #p < 0.05 *vs.* day 0; t-test. D) Phenotyping of spleen and GIT *via* flow cytometry. Shown are the percentage of positive cells ± SD from 20,000 measured events. The amount of immune checkpoints like LAG-3 and CTLA-4 was decreased under α-PD-L1 mono-and combination therapy. *p < 0.05; **p < 0.01; ***p < 0.001 one-way ANOVA (Bonferroni's multiple comparison test); #p < 0.05 one-way ANOVA (Dunnett's multiple comparison test). E) Immunofluorescence of 4 µm slides of residual tumors. Staining was done with mAbs and DAPI for nuclear staining. Reduced amount of $CD11b^+$ $Gr.1^+$ myeloid- derived suppres-sor cells (MDSCs) were detected under combination therapy. Images were taken on a laser scanning microscope (Zeiss) using 20x objectives. F) Nanostring gene expression analysis of tumors with Pan-Cancer IO 360 Gene Expression Panel. Increasing expression is shown as increasing scores (n = 3 samples/group).

4.3 Publication 3

Side effects are common when tumors are treated with conventional therapy like surgery, radiation, or chemotherapy. Nowadays, immunotherapies like ICIs are widely used because of their safety and efficacy. The aim is to reactivate exhausted T-lymphocytes which compel the killing of tumor cells. Hypermutated tumors in the context of Lynch syndrome and cMMR-D are likely to show good responses toward ICI treatment. Still, ICI-treated tumors often develop resistance mechanisms or relapse, therefore combination therapies are needed. In addition to classical inhibition of DNA synthesis, chemotherapy, such as the DNA pyrimidine analog gemcitabine has the potential to activate endogenous antitumor immune responses *via* the induction of immunogenic cell death. This finally activates cytotoxic T-lymphocytes and induces an inflamed TME. Furthermore, chemotherapy may increase the level of mutational burden in low immunogenic tumors like in the subgroup G2 of Lynch syndrome. Consequently, combinations of ICIs and chemotherapy are under clinical investigation and are likewise increasingly approved for the treatment of advanced solid cancers.

In our preclinical study, combined gemcitabine and α-PD-L1 treatment prolonged survival of $Mlh1^{-/-}$ mice to 12 weeks (vs. 7.5 weeks in gemcitabine monotherapy and 9.2 weeks in α-PD-L1 monotherapy) (Figure 4:A) accompanied by strong inhibition of tumor growth as determined by PET/CT imaging (Figure 4:B). Additionally, the combination therapy increased the level of IL-13, TNFα, and MIP1β in the plasma (Figure 4:F). In contrast, the amount of circulating and intratumoral MDSCs and M2 macrophages decreased whereas the number of infiltrating cytotoxic T-lymphocytes increased (Figure 4:C, D, G). Fragment length analysis detected novel mutations in tumor cells, while mutations in *APC*, *Tmem60*, and *Casc3* completely disappeared. This can be interpreted by the elimination of single mutated cell clones (Figure 4:E).

In summary, this study proved the safety of the gemcitabine/α-PD-L1 combination to overcome resistance mechanisms and control tumor growth.

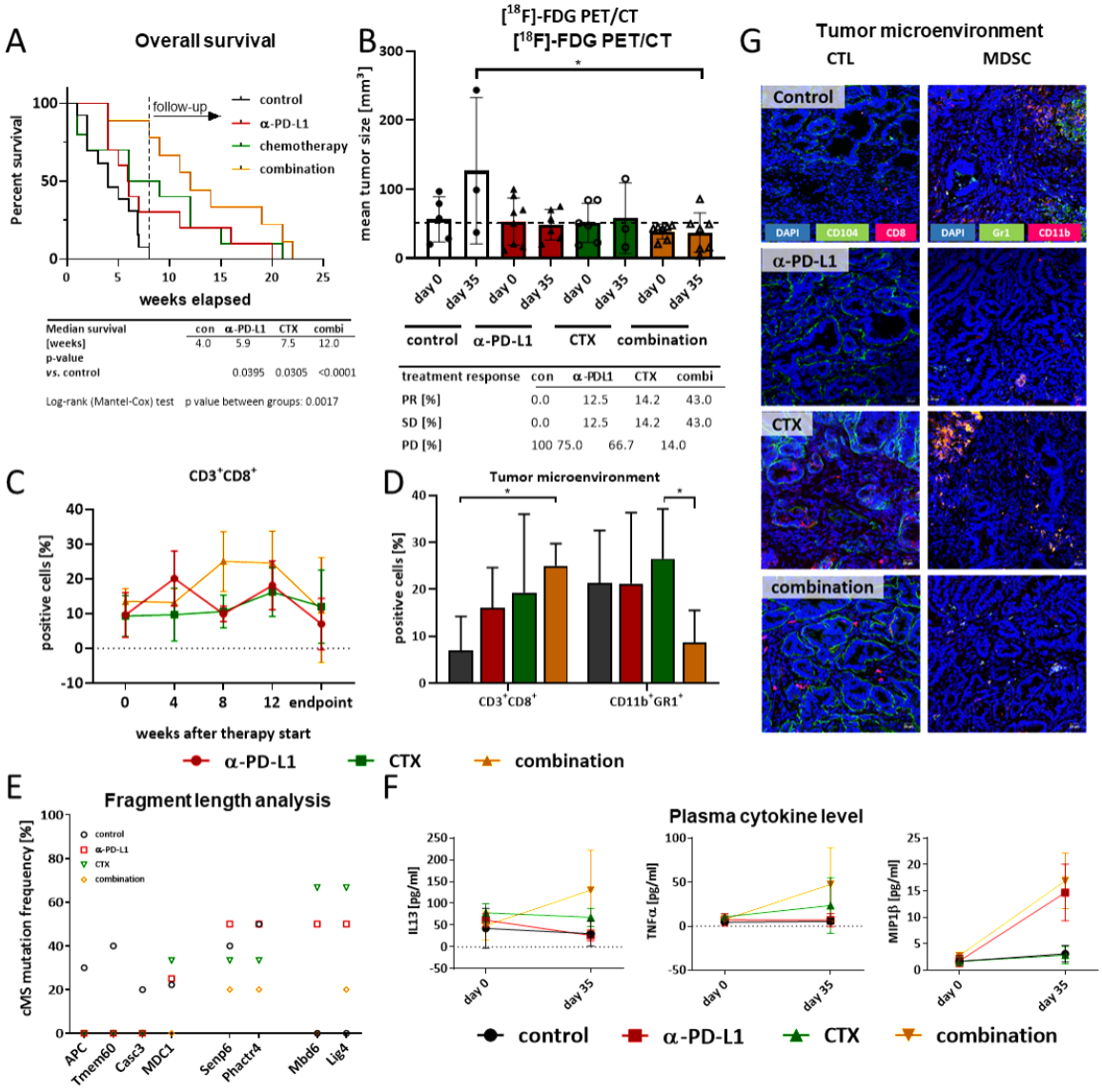

Figure 4:

A) Kaplan-Meier survival curve of therapeutically treated Mlh1$^{-/-}$ mice. (α-PD-L1 clone 6E11, 2.5 mg/kg bw thrice n = 10 mice; CTX = gemcitabine 100 mg/kg bw; n = 10 mice; combination n = 9 mice). Control mice were left untreated (n = 9 mice). B) The mean tumor volume ± SD in mm³ measured *via* [^{18}F]-FDG-PET/CT to track the tumor growth from start of therapy to day 35 (n = 3-8 mice/group and time-point). * $p < 0.05$; one-way ANOVA (Dunnett's multiple comparison test). (C, D) Flow cytometry phenotyping. Shown are the percentage of positive of cells ± SD from 20,000 events. (n = 3–5 mice/group) C) Rou-tinely blood sampling was used to track the blood phenotype status. Under combination therapy, cyto-toxic T cell level were elevated. ** $p < 0.01$ *vs.* CTX; one-way ANOVA (Bonferroni's multiple comparison test); ## $p < 0.01$ *vs.* α-PD-L1 mono-therapy one-way ANOVA (Dunnett's multiple comparison test). D) Tumor cells were screened for immunological markers. CD11b^{+}Gr1^{+} myeloid-derived suppressor cells (MDSCs) level were decreased under combination therapy. * $p < 0.05$ one-way ANOVA (Bonferroni's multiple comparison test). E) The coding microsatellite (cMS) mutation frequency of selected genes in Mlh1$^{-/-}$ mice. In *APC*, *Tmem60* and *Casc3* the results indicated a loss of single mutated cell clones. F) Immunofluorescence of 4 µm slides of residual tumors. Staining was done with mAbs and DAPI for nuclear staining. Infiltration of CD8^{+} cytotoxic T-lymphocytes was increased under combination therapy. Images were taken on a laser scanning microscope (Zeiss) using 20x objectives. G) Plasma cytokine levels were quantified at start of therapy and after 35 days. Shown are the mean cytokine levels [pg/ml] ± SD. All level were elevated under combination therapy.

4.4 Publication 4

In this study, we compared the therapeutic activity of the α-PD-L1 antibody with the CDKi abemaciclib either alone or in combination therapy. *In vitro* experiments on murine dMMR tumor cell lines revealed reduced colony formation abilities and increased amounts of cells with G1-arrest after abemaciclib treatment. Additional effects included significantly elevated levels of HMGB1, indicative of immunogenic cell death induction, which was confirmed in subsequent tumor-immune cell co-culture. In the *in vivo* combination approach, abemaciclib was administered first, and later in the therapy protocol α-PD-L1 was added. Both therapies were tested in two preclinical mouse models. Additionally, to the well-established $Mlh1^{-/-}$ mouse model, we here included another dMMR mouse line $Msh2^{loxP/loxP\ ;TgTg(Vil1\text{-}cre)}$ to compare treatment efficacy. Prolonged survival of $Mlh1^{-/-}$ and $Msh2^{loxP/loxP\ ;TgTg(Vil1\text{-}cre)}$ mice was achieved under both α-PD-L1 and abemaciclib monotherapy ($Mlh1^{-/-}$: 14.5 wks vs. 9.0 wks (α-PD-L1), and 3.5 wks (control); $Msh2^{loxP/loxP\ ;TgTg(Vil1\text{-}cre)}$: 11.7 wks vs. 9.6 wks (α-PD-L1), and 2.0 wks (control)) (Figure 5:A, D). The combination treatment did not boost efficacy. PET/CT imaging revealed decreased tumor sizes in $Mlh1^{-/-}$ mice under therapy and stable disease in $Msh2^{loxP/loxP\ ;TgTg(Vil1\text{-}cre)}$ mice (Figure 5:B, E). Immunological effects included increased amounts of tumor-infiltrating $CD4^+$ T helper and $CD8^+$ cytotoxic T-lymphocytes and decreased levels of M2-macrophages (Figure 5:G, H) as well as reduced numbers of regulatory T cell and T cell exhaustion markers after blood phenotyping. In contrast, expression of neutrophils and DCs was elevated as well as the expression of DNA damage repair genes (Figure 5:C, F). Abemaciclib treatment led to inhibition of the PI3K/Akt signaling pathway in $Mlh1^{-/-}$ mice but contrary it induced *Mxd4* and *Myc* expression and activation of the Wnt signaling pathway. In conclusion, we identified abemaciclib as a potential candidate to treat dMMR tumors not suitable for ICI treatment.

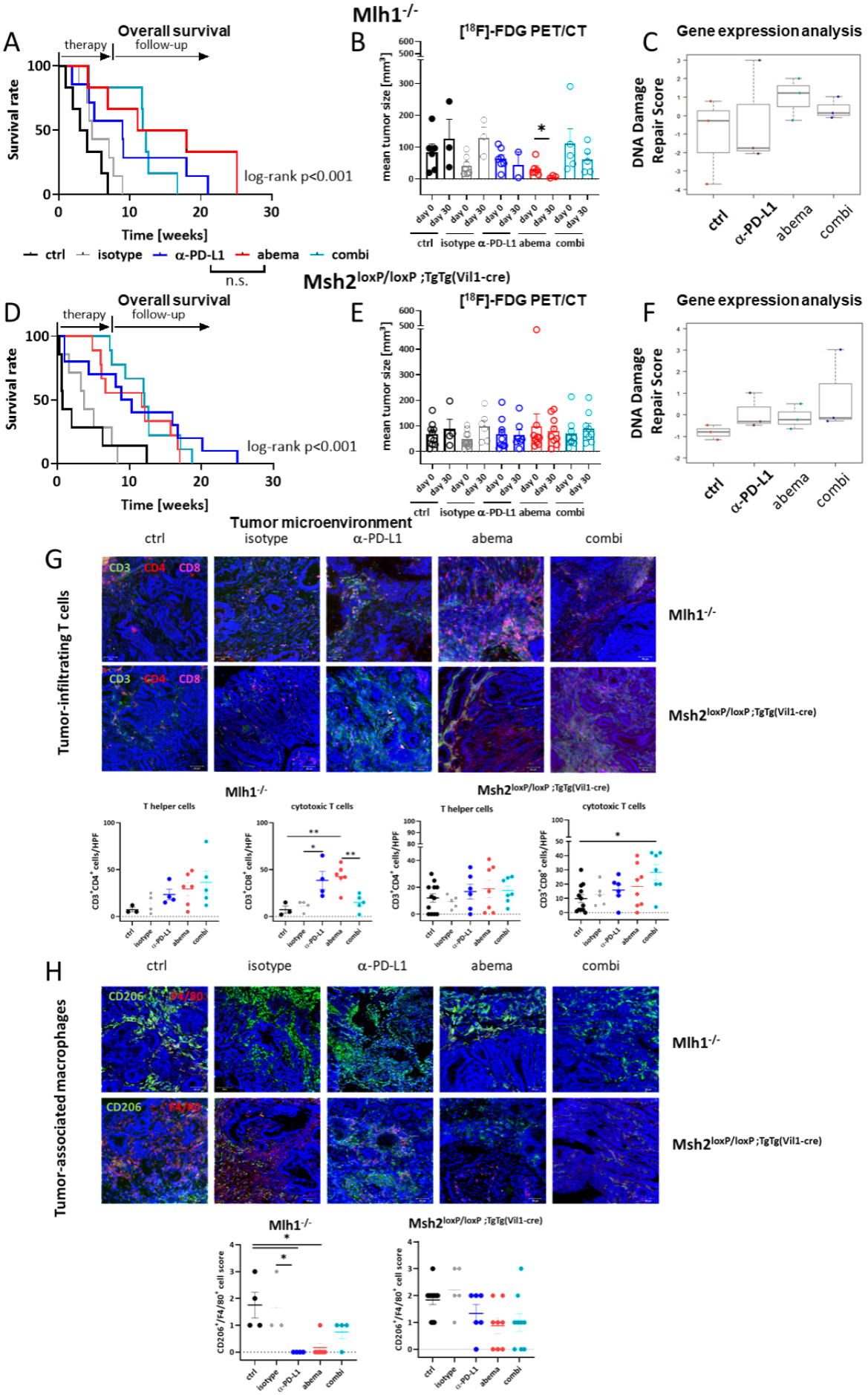
Mlh1-/-
A
Overall survival
therapy
follow-up
Survival rate
Time [weeks]
log-rank p<0.001
ctrl
isotype
α-PD-L1
abema
combi
n.s.
B
[18F]-FDG PET/CT
mean tumor size [mm3]
C
Gene expression analysis
DNA Damage Repair Score
Msh2loxP/loxP ;TgTg(Vil1-cre)
D
Overall survival
E
[18F]-FDG PET/CT
F
Gene expression analysis
Tumor microenvironment
G
Tumor-infiltrating T cells
CD3 CD4 CD8
T helper cells
cytotoxic T cells
H
Tumor-associated macrophages
CD206 F4/80

Figure 5:
(A, D) Kaplan-Meier survival curves of therapeutically treated mice. Log-rank analysis (Mantel Cox). (B, E) [^{18}F]-FDG-PET/CT measurements to track tumor growth at start of therapy and after 30 days of ther-apy. Each dot represents one mouse. (C, F) Nanostring gene expression analysis of tumors with Pan-Cancer IO 360 Gene Expression Panel. Expression of DNA damage repair pathways was elevated under abemaciclib therapy. Relative values are represented (n = 3 samples/group). A) Mlh1$^{-/-}$: isotype *vs*. α-PD-L1: $p < 0.05$; control *vs*. abemaciclib: $p < .01$; control *vs*. combination: $p < .01$; ctrl: n = 6, iso-type: n = 7, α-PD-L1 n = 7, abemaciclib: n = 6, combination n = 6. B) Mlh1$^{-/-}$ mice: * $p < 0.05$; one-way ANOVA (Dunnett's multiple comparison test). D) Msh2$^{loxP/loxP\ VillinCre}$: isotype *vs*. α-PD-L1: $p < 0.05$; con-trol *vs.* abemaciclib: $p < 0.01$; control *vs*. combination: $p < 0.001$. ctrl: n = 10, isotype: n = 7, α-PD-L1 n = 10, abemaciclib: n = 9, combination n = 9. E) Msh2$^{loxP/loxP\ VillinCre}$ (G, H) Immunofluorescence of 4 µm slides of residual tumors from Mlh1$^{-/-}$ and Msh2$^{loxP/loxP;TgTg(Vil1-cre)}$ mice. Staining was done with mAbs and DAPI for nuclear staining. Images were taken on a laser scanning microscope (Zeiss Elyra 7) using 20x objectives. Upper panel: representative images of tumor microenvironment. Lower panel: quantita-tive analysis of tumor-infiltrating immune cells. Number of tumor infiltrating T helper cells, cytotoxic T-lymphocytes (G) and macrophages (H) counted in 2–3 HPFs/slide with n = 3–10 mice/group. The infil-tration pattern was semi-quantitatively analyzed using a scoring system. T cell level were elevated under therapy and in contrast the amount of macrophages was decreased. 0 = no; 1 = mild; 2 = moderate; 3 = strong. Each symbol represents one case. *$p < 0.05$; **$p < 0.01$, Two-way ANOVA (Tukey's multiple comparisons test).

5. Discussion

Immune escape is very common in solid tumors and re-balancing or re-activating natural anti-tumor immunity is the ultimate goal of immunotherapy. In this study, we applied combined immunotherapy approaches to bypass dMMR-driven immune escape mechanisms. Two mouse models of spontaneous dMMR-driven tumorigenesis were employed to reflect the clinical situation experimentally. Initial experiments (Publication 1, 2, 3) were done on $Mlh1^{-/-}$ mice and to a later date also in $Msh2^{loxP/loxP\ ;TgTg(Vil1\text{-}cre)}$ mice (Publication 4). Given the fact that MLH1 and MSH2 are the main drivers of dMMR-associated tumors in men, results obtained from this study may have a direct translational value [139].

In a previous study, the significantly prolonged survival of $Mlh1^{-/-}$ mice after vaccination with a whole tumor lysate was shown [141]. As resistance mechanisms eventually developed, the inclusion of additional combination partners is necessary to prevent tumor progression. Here, we focused on immune checkpoint blockade (α-PD-L1), whole tumor vaccination, and targeted therapy with the CDK inhibitor abemaciclib.

The ultimate goal was to prolong the overall survival of $Mlh1^{-/-}$ mice and $Msh2^{loxP/loxP\ ;TgTg(Vil1\text{-}cre)}$ mice in therapeutic and prophylactic settings. By applying different combination strategies, a significant survival benefit was reached in all investigated treatments (please see Table 2 for details). Still, differences in terms of tumor growth control, immune activation, and modulation of the tumor microenvironment were seen. The results of each therapeutic approach are discussed below.

A direct comparison of all treatment regimens included in this dissertation identifies the combination therapy of immune checkpoint blockade using α-PD-L1 and whole tumor vaccine as the most promising approach to combat dMMR-driven cancer (Publication 2). By applying this combination therapeutically, the overall survival of $Mlh1^{-/-}$ mice was significantly prolonged from 4 weeks in the control to 19.4 weeks after treatment with 30 % of mice showing complete tumor remission. Notably, the overall survival of mice was twice as long as under either monotherapy. This shows that not only one target point in the whole "*immune system versus tumor*" cascade should be addressed, but instead different directions are mutually dependent and ideally act synergistic. Mechanistically, whole tumor vaccines present a bunch of immunogenic tumor neo-antigens. These, in turn, are taken up by dendritic cells, intracellularly processed and presented to T-lymphocytes to stimulate antigen-specific T cell responses. To prevent or abrogate tumor-driven T cell exhaustion, immune checkpoint blockade is indicated. Together, this combined treatment approach effectively controlled tumor growth in our preclinical mouse model. By contrast, particularly PD-L1 blockade alone had minor impact on tumor growth. This may be due to increased uptake of [^{18}F]-FDG, as previously shown on non-small cell lung cancer patients upon treatment with α-PD-1 antibodies and can be interpreted as pseudo-progress

[142]. Hence, the tumor size of α-PD-L1 treated mice inversely correlates with the survival, raising the need for more sophisticated *in vivo* monitoring systems and additional (bio-) markers to reliably predict treatment response.

To induce activation of the immune system two murine tumor vaccines of Mlh1$^{-/-}$ mice were established and tested. Both cell lines exhibited the same germline mutation and comparable behavior in cell culture, like growth kinetics, phenotype, and response toward drugs. 328 was established from an ultra-hypermutated tumor, that showed mutations known to result in a bad outcome for the patient, whereas A7450 T1 M1 was established from a moderately mutated tumor. Different characteristics were found for their cytokine secretion profile. 328 induced secretion of immunosuppressive cytokines, whereas A7450 T1 M1 secreted cytokines that are associated with a good outcome in patients, for example GM-CSF, and cytokines that induce NK cell activation and promote the development of T helper cells. Therefore, we concluded that the quality of the tumor vaccine is highly important (Publication 1). In fact, the whole tumor lysate A7450 T1 M1 was able to prolong the overall survival of tumor-bearing mice from 4 weeks to 11 weeks, much longer than the tumor lysate 328 (Publication 1).

Another study found that glioma vaccination blocks tumor cell proliferation and induces apoptosis *in vitro* [143]. *In vivo*, inhibition of tumor growth and prolonged survival of glioma-bearing rats was seen. The same result was achieved in our studies, with more than doubled survival times and a significantly reduced tumor volume under vaccine therapy.

The way of application of α-PD-L1 had no influence on the survival time (9 weeks for both applications). In combination with either gemcitabine (Publication 3) or abemaciclib (Publication 4) the survival time was prolonged to 12 weeks, which was a synergistic improvement in comparison to gemcitabine monotherapy (7.5 weeks), but a deterioration in contrast to abemaciclib monotherapy (14.5 weeks).

The co-culture experiment could also be a good predictor for the subsequent PET/CT results aiming to quantify tumor sizes. Co-culture of murine blood cells with A7450 T1 M1 tumor cells showed reduced tumor cell levels under α-PD-L1 treatment and even more under combination treatment of α-PD-L1 with chemotherapy (Publication 3). These effects reflected the results of the PET/CT measurements when imaging the tracking the tumor growth. α-PD-L1 treated mice showed slightly decreased tumor sizes, while mice who received chemotherapy developed slightly increased tumor sizes. The combination therapy could reduce the tumor size significantly. This was equal to the co-culture where the combination treatment reduced the tumor cell amount the strongest, too. This could be transferred to the co-culture experiment when tumor cells were treated with abemaciclib either alone or in combination with α-PD-L1 (Publication 4). Both therapies reduced the amount of tumor cells significantly, which could also be

seen when measuring the tumor growth *via* PET/CT of Mlh1$^{-/-}$ mice. Here again, strongest effects could be seen under abemaciclib therapy, followed by combination group and α-PD-L1 monotherapy. This evidence was supported by the *in vitro* colony formation assay. Reduced colony counts were found under 6 days of abemaciclib therapy. After an additional 6 days of rest, the colony amount increased slightly, which can be seen in the long-term follow-up PET/CT measurements, where only 2 of 4 mice had reduced tumor volumes, whereas the other 2 mice had increased tumor volumes.

Prolonged overall survival upon combined immunotherapy is the result of the successful breaking of tolerance *via* the complex interaction between the tumor and host immunity. Although all agents applied in this thesis were previously reported to activate T-lymphocytes and to trigger T-cell infiltration into the tumor microenvironment, we found striking differences between the individual approaches. Generally, immune-modulating effects were more evident in spleens and residual tumors compared to the periphery. With regard to the latter, we have to keep in mind, that immunological changes were only measured before the start of therapy and at the experimental endpoint. The human endpoint was defined by bad general conditions, like body weight, social behavior, and body posture. Therefore, the mouse already was at a critical point of its disease, independently of its therapy group. It would be more meaningful to evaluate the status of the immune system at the point of tumor reduction. At this moment the mouse is in good health status, but this time point would differ strongly between therapy groups. Especially for control mice without any therapy and consequently without any improvement in their health status, it would be problematic to set a time point to evaluate the current immune status.

Analysis of spleens from mice after chemo-vaccination showed faint increases of CD4$^+$ T helper cells. This marginal effect was also seen in combination with α-PD-L1.

When having a look at the tumor microenvironment, the success or failure of either treatment was detectable in residual tumors. Most therapies, i.e. A7450 T1 M1 vaccination, PD-L1 blockade, gemcitabine, and abemaciclib either alone or in combination decreased the amount of tumor-infiltrating MDSCs and M2 macrophages. In contrast, therapeutic vaccination with 328 resulted in an elevated level of MDSCs (Publication 1).

The combined vaccine-checkpoint blockade also led to a significant increase in tumor-infiltrating CD4$^+$ and CD8$^+$ T-lymphocytes (Publication 2). This effect was shown before in murine colon cancer and lymphoma cells where the application of a peptide vaccine led to a tumor infiltration with CD8$^+$ cytotoxic T-lymphocytes and an increase of regulatory T-lymphocytes [149]. Also, the combination of tumor vaccine with Pembrolizumab increased the number of intratumoral lymphocytes in melanoma patients [150]. In addition, another group found elevated CD4$^+$ and CD8$^+$ T cell infiltration in murine colon and breast cancer models using a vaccine and PD-L1 antibody [151]. The same effect of activating CD8$^+$ T-lymphocytes was

shown for ICIs in renal cell carcinoma [152]. Notably, the level of tumor-infiltrating $CD8^+$ T-lymphocytes correlates with clinical outcomes in most cancer patients. This is in line with our findings, in which the combination of vaccine with α-PD-L1 had the highest T cell level, resulting in synergistically improved overall survival. Hence, with all of these tested treatments, the amount of tumor-infiltrating $CD4^+$ and $CD8^+$ T-lymphocytes increased, confirming the active combat of the immune system against the tumor. Additionally, the infiltration with dendritic cells was observed after the combined vaccine-immune checkpoint blockade. This implies that our specific neoantigens present in the tumor vaccine were recognized by the immune system and activated dendritic cells, which then activated T-lymphocytes to infiltrate the tumor. Another interesting finding was the higher abundance of immune checkpoints PD-L1 and LAG-3 in non-responders compared to responders receiving whole tumor vaccines A7450 T1 M1 or 328. Residual tumors of long-term vaccine responders showed no immune checkpoint expression at all.

Interesting effects were observed for IFNγ, a cytokine secreted by T-lymphocytes after contact with neoantigens [156]. Co-culture of peripheral blood mononuclear cells with loaded DCs led to an increase in $CD3^+$ $CD8^+$ $IFN\gamma^+$ cells. This effect could also be seen *ex vivo*, when leukocytes of A7450 T1 M1 treated mice were co-cultured with A7450 T1 M1 tumor cells overnight, and IFNγ was quantified.

Furthermore, α-PD-L1 treatment likewise downregulated the expression of immune checkpoints on immune cells, confirming its biological relevance in mediating immune tolerance and the importance to target this molecule. Also, immunosuppressive cells like $CD11b^+$ $PD\text{-}L1^+$ cells and $CD206^+$ $PD1^+$ cells decreased upon immune checkpoint blockade, implying more global effects on immune cells as previously anticipated.

Systemically, we found elevated NK cell level under A7450 T1 M1 vaccine therapy in our $Mlh1^{-/-}$ mice, which was also found in the study of He *et al*., who tested a glioma cell lysate vaccine in a rat glioma model [143].

This might be due to the reduction of MDSC level accompanied by higher amounts of $CD8^+$ T-lymphocytes in A7450 T1 M1, but not 328-treated mice. In fact, low MDSC and high tumor-infiltrating T-cell level are related with a good clinical outcome because of the activated immune system. Already in 2014, low level of MDSCs were found as a prognostic marker for good clinical outcome in prostate cancer patients treated with a cancer vaccine in combination with Ipilimumab (α-CTLA-4) [160]. In contrast, high level of tumor-infiltrating T cells were found to predict good outcome in patients with neuroblastoma [161].

To refine our treatment approach and get a step closer to the clinical application, we then included two clinically-approved drugs: the chemotherapeutic gemcitabine and the CDK4/6 inhibitor abemaciclib (Publication 3 and 4). Both agents may reinforce immunotherapy responses *via* direct antitumoral and indirect immunomodulatory effects. Promising effects were

already found in 2012, when the CDK4/6 inhibitor PD0332991 was tested with paclitaxel preclinically as well as clinically in phase 1 and 2 studies [144]. Gemcitabine, on the one hand, already proved beneficial in a previous trial using combined chemo-vaccination [50]. Here, comparable positive effects on tumor growth and immune modulation were obtained after combining gemcitabine with PD-L1 blockade. Palmer *et al.* analyzed 13 reported phase 3 trials of different solid tumors treated with combinations containing ICIs [145]. In Summary, he found a great clinical benefits of ICI combinations because patients had the possibility to a response from different sides. In 2020, the FDA approved the combination of Nivolumab (α-PD-1), Ipilimumab (α-CTLA-4), and chemotherapy as first-line therapy for metastatic non-small cell lung cancer [146]. A case report of a patient with brain metastasis of nasopharyngeal carcinoma treated with conventional chemotherapy combined with novel immunotherapy showed a complete response [147].

Accompanying gene expression analysis was performed to investigate affected signaling pathways. Here, we focused on α-PD-L1-based combinations either showing synergistic (+ vaccination) or antagonistic (+ abemaciclib) effects *in vivo*. As anticipated, significant changes were seen with the α-PD-L1 monotherapy stimulating the PI3K signaling and suppressing the myeloid compartment score. Additionally, the neutrophils *vs*. TILs score was decreased. In contrast, *Wnt* signaling was once downregulated, when the application was performed intravenously and slightly upregulated when the application was performed intraperitoneal. In addition, the ratio of cytotoxic T-lymphocytes was higher upon intravenous *vs*. intraperitoneal application. This difference might be due to the small sample size of three mice. Nevertheless, the overall survival was the same for both application types.

When analyzing the influences of the different treatments, an important criterion was the MSI status of the tumor, because this is a hallmark of Lynch syndrome. Both application routes of α-PD-L1 increased the overall mutation frequency. Besides that, the loss of single-cell clones was found in all analyzed treatments though the affected genes were different. In conclusion, the application route had no relevant influence on the immunological and overall outcome of the mice.

Abemaciclib, on the other hand, was lately found to mediate long-term protective anticancer immunity, eventually being combined with immune checkpoint blockade [148]. In our study, abemaciclib monotherapy improved the outcome of $Mlh1^{-/-}$ mice and $Msh2^{loxP/loxP\ ;TgTg(Vil1\text{-}cre)}$ mice (Publication 4). However, and contrary to all other combinations, no synergistic effects were obtained after combined application of abemaciclib and the a-PD-L1 antibody, with outcomes being comparable to either monotherapy. Hence, if and how abemaciclib can be incorporated in such combination approaches has to be tested prospectively.

Table 2: Survival time of $Mlh1^{-/-}$ mice and $Msh2^{loxP/loxP\ ;TgTg(Vil1\text{-}cre)}$ mice under therapy

Therapy	**Survival [weeks]**	
	Mlh1$^{-/-}$	**Msh2$^{loxP/loxP\ ;TgTg(Vil1\text{-}cre)}$**
Control	4.0	0.7
Vaccine 328	4.9	
Vaccine A7450 T1 M1	11.2	
gemcitabine	7.5	
isotype	4.7	3.7
α-PD-L1 i.v. 1x	6.0	
α-PD-L1 i.v. 3x	9.2	
α-PD-L1 i.p. 3x	9.0	9.6
abemaciclib	14.5	11.7
Vaccine 328 + gemcitabine	9.0	
Vaccine A7450 T1 M1 + gemcitabine	12.0	
α-PD-L1 i.v. 1x + vaccine A7450 T1 M1	8.4	
α-PD-L1 i.v. 3x + vaccine A7450 T1 M1	19.4	
α-PD-L1 i.v. 3x + gemcitabine	12.0	
α-PD-L1 i.p. 3x + abemaciclib	12.0	12.1

i.v. = intravenous, i.p. = intraperitoneal

The therapeutic effects differed between the two mouse lines (please see publication 4 for details [153]). The prolonged survival time after PD-L1 checkpoint blockade and abemaciclib therapy was comparable, but the tumor growth was decreased in Mlh1$^{-/-}$ mice whereas Msh2$^{loxP/loxP\ ;TgTg(Vil1\text{-}cre)}$ mice only showed stable disease. In the tumor microenvironment, T helper cell level were similar in both mouse lines, but cytotoxic T cell level were increased after either monotherapy in Mlh1$^{-/-}$ mice. This difference was also seen for tumor-infiltrating CD206^{+}/F4/80^{+} cells. These cells were nearly eliminated under therapy in Mlh1$^{-/-}$ mice whereas

in Msh2$^{loxP/loxP\ ;TgTg(Vil1\text{-}cre)}$, a low level was still detectable. The fragment length analysis showed similar percentages of mutations in microsatellites in both mouse lines, as shown before [154]. Gene expression analysis revealed an increased score of neutrophils in Msh2$^{loxP/loxP\ ;TgTg(Vil1\text{-}cre)}$ mice, whereas in Mlh1$^{-/-}$ mice this score was slightly decreased. This correlates with the fact that α-PD-L1-treated Msh2$^{loxP/loxP\ ;TgTg(Vil1\text{-}cre)}$ mice showed stable disease, whereas Mlh1$^{-/-}$ mice had a decreased tumor size. This is due to the fact that PD-L1 expressing neutrophils block cytotoxic T-lymphocytes and are therefore favor the tumor growth [155]. Possibly, Msh2$^{loxP/loxP\ ;TgTg(Vil1\text{-}cre)}$ neutrophils express PD-L1 but Mlh1$^{-/-}$ neutrophils do not.

To sum up our findings in therapeutic settings, we found promosing results with passive therapy like α-PD-L1, but the effects were even better when active therapy using whole tumor vaccines was applied. Therefore, our idea that the immune system should combat the tumor on its own can be brought to reality.

In support of this, prophylactic settings were additionally applied in this thesis, with the aim to prevent tumor growth (Publication 1). Cancer prevention is a smart approach for tumors arising in the context of Lynch syndrome. Although pharmacological prevention approaches were started many years ago, to date, aspirin remains the most studied drug intervention [157,158]. Recent advances in preclinical drug screening may thus help identifying novel and more effective agents with a better side-effect profile. Several clinical studies are recently performed to prevent tumorigenesis in patients with Lynch syndrome. They test immune checkpoint inhibitors, vaccines or even omega 3 fatty acids (*Clinicaltrials.gov* identifier: *NCT03831698*, *NCT04711434, NCT05419011*). The aim is to activate the patient's own immune system or in case of omega 3 fatty acids to change the microbiota in the patient's intestines.

In our study, we applied whole tumor vaccines to test whether the promising results seen in the therapeutic situation can be transferred to the prophylactic approach. In both settings, therapeutically and prophylactically, the vaccine A7450 T1 M1 worked better and delayed tumor growth longer than the vaccine 328 (25 weeks *vs*. 37 weeks). Prophylactic vaccines draw the attention of the immune system towards tumor antigens, before the tumor developed itself. An adaptive immune response is created. Therefore, tumorigenesis can be prevented or reduced [159].

In a recent study of Gerber *et al*. four synthetic frameshift-proteins were designed and used as vaccines in Msh2$^{loxP/loxP\ ;TgTg(Vil1\text{-}cre)}$ mice [90]. By applying these four peptides, the overall survival of mice was prolonged accompanied by reduced tumor burden. Hence, the development of universal usable synthetic vaccines might be a good sustainable therapy.

Outlook and perspectives

In a running trial, the vaccination approach is based on tumor-loaded dendritic cells. With this therapy, the step of tumor antigen recognition and processing by dendritic cells can be skipped, and tumor-antigens can be directly presented to T-lymphocytes [162,163]. Additionally, synthetic peptide-mixes of candidate genes specific for dMMR should be tested [164] to broaden the usability of one drug to treat many patients. Additionally, neoantigen peptides can be designed and mixed individually, depending on each patients biomarker and mutational profile [165]. This has already shown good response in patients with different solid tumor entities [165].

Furthermore, prophylactic interventions should be investigated more. Nowadays, the predisposition of people to develop dMMR-associated tumors can be detected easily, and the lifetime risk is high. A prophylactic strategy that prevents or at least delays the tumor development could help. Preclinically, the application of four synthetic frameshift peptides already showed good responses on mice with *Msh2* knockout [90]. Besides, several clinical trials actually explore the role of different immune modifiers in preventing polyps and second primary tumors in patients with Lynch Syndrome. This raises hope for improving the outcome of Lynch Syndrome patients prospectively.

6. Summary

In this thesis, different immunotherapy strategies were employed to combat mismatch-repair-deficient (dMMR) cancer. In men, *hMLH1* and *hMSH2* are the most affected genes and drivers for the development of highly immunogenic dMMR-associated tumors. Hence, we used two preclinical mouse models, either having constitutional (Mlh1) or conditional (Msh2) knock out. These mice develop tumors spontaneously to nearly 100%, hence, they can be included in therapeutic and prophylactic preclinical trials. Immunotherapy constitutes a state-of-the approach, aiming at stimulation and activation of the immune system to combat cancer. To prevent resistance development and improve outcome, we focused on combination strategies including whole tumor vaccines, immune checkpoint-inhibitors (α-PD-L1), classical chemotherapy or the Cyclin-dependent kinase inhibitor abemaciclib. Overall survival, tumor growth, immune status, and the tumor microenvironment were studied in detail.

By applying different combination strategies, a significant survival benefit was reached in all investigated treatments. The first study identified that the tumor neoantigen quality outranks quantity, i.e. not only the number of mutations provided by a vaccine, but rather their ability to evoke T cell responses are crucial for treatment responses. Here, prophylactic as well as therapeutic vaccination with the whole tumor vaccine A7450 T1 M1 significantly delayed tumor development and growth and may thus provide an optimal combination partner for subsequent trials. Hence, in the next study, this vaccine was combined with the α-PD-L1 antibody. With this approach, the overall survival was significantly prolonged, yielding 30% complete remission. Decreased levels of circulating splenic and intratumoral myeloid derived suppressor cells (MDSC) and reduced numbers of immune-checkpoint-positive splenic T-lymphocytes accompanied therapeutic effects. Gene expression and protein analysis of residual tumors revealed downregulation of PI3K/Akt/Wnt-and TGF-signaling, leading to T cell infiltration, reduced numbers of macrophages, neutrophils, and MDSCs. Comparable, though less pronounced effects were seen after combined application of α-PD-L1 with gemcitabine or abemaciclib, therapeutically applied in the third and fourth study of this thesis. However, the latter combination was the only that failed to show beneficial effects compared to either monotherapy. In all therapeu-tic approaches, increased levels of tumor infiltrating T-lymphocytes and decreased level of MDSCs were seen.

In conclusion, we found promising therapies to combat MMR-D related tumor entities. The deeper understanding of these results to finally enter clinical trials is the consequent next step.

7. Bibliography

1. Evrard C, Tachon G, Randrian V, Karayan-Tapon L, Tougeron D. Microsatellite Instability: Diagnosis, Heterogeneity, Discordance, and Clinical Impact in Colorectal Cancer. Cancers (Basel); 2019;11. DOI-Nr.10.3390/cancers11101567

2. Yang W. Structure and function of mismatch repair proteins. Mutat Res Repair. Elsevier; 2000;460:245–56.

3. Ellegren H. Microsatellites: simple sequences with complex evolution. Nature Publishing Group; 2004;5:435–45. DOI-Nr. 10.1038/nrg1348

4. Zhang C, Zhan Y, Ni K, Liu Z, Xin R, Han Q, et al. Effects of deficient mismatch repair on the prognosis of patients with stage II and stage III colon cancer during different postoperative periods. BMC Cancer. England; 2022;22:1156. DOI-Nr. 10.1186/s12885-022-10266-3

5. Lynch HT, De la Chapelle A. Genetic susceptibility to non-polyposis colorectal cancer. J Med Genet; 1999;36:801.

6. Chung H, Young DJ, Lopez CG, Le TAT, Lee JK, Ream-Robinson D, et al. Mutation rates of TGFBR2 and ACVR2 coding microsatellites in human cells with defective DNA mismatch repair. PLoS One; 2008;3:e3463. DOI-Nr. 10.1371/journal.pone.0003463

7. Boland CR, Thibodeau SN, Hamilton SR, Sidransky D, Eshleman JR, Burt RW, et al. A National Cancer Institute Workshop on Microsatellite Instability for cancer detection and familial predisposition: development of international criteria for the determination of microsatellite instability in colorectal cancer. Cancer Res. United States; 1998;58:5248–57.

8. Pawlik TM, Raut CP, Rodriguez-Bigas MA. Colorectal carcinogenesis: MSI-H versus MSI-L. Dis Markers; 2004;20:199. DOI-Nr. 10.1155/2004/368680

9. Raut CP, Pawlik TM, Rodriguez-Bigas MA. Clinicopathologic features in colorectal cancer patients with microsatellite instability. Mutat Res Mol Mech Mutagen. Elsevier; 2004;568:275–82. DOI-Nr. 10.1016/j.mrfmmm.2004.05.025

10. Zippl M, Jochum W Mikrosatelliten-Instabilität – Schweizer Zeitschrift für Onkologie. SZO 2019;4:19-25.

11. Ionov Y, Peinado MA, Malkhosyan S, Shibata D, Perucho M. Ubiquitous somatic mutations in simple repeated sequences reveal a new mechanism for colonic carcinogenesis. Nature. England; 1993;363:558–61. DOI-Nr. 10.1038/363558a0

12. Beckman RA, Loeb LA. Efficiency of carcinogenesis with and without a mutator mutation. Proc Natl Acad Sci U S A; 2006;103:14140. DOI-Nr. 10.1073/pnas.0606271103

13. Curtin NJ. DNA repair dysregulation from cancer driver to therapeutic target. Nature Publishing Group; 2012;12:801–17. DOI-Nr. 10.1038/nrc3399

14. Mäki-Nevala S, Valo S, Ristimäki A, Sarhadi V, Knuutila S, Nyström M, et al. DNA methylation changes and somatic mutations as tumorigenic events in Lynch syndrome-

associated adenomas retaining mismatch repair protein expression. EBioMedicine; 2019;39:280–91. DOI-Nr. 10.1016/j.ebiom.2018.12.018

15. Lynch HT, Snyder CL, Shaw TG, Heinen CD, Hitchins MP. Milestones of Lynch syndrome: 1895–2015. Nature Publishing Group; 2015;15:181–94. DOI-Nr. 10.1038/nrc3878

16. Patel SG, Ahnen DJ. Colorectal Cancer in the Young. Curr Gastroenterol Rep. Current Medicine Group LLC 1; 2018;20:1–12. DOI-Nr. 10.1007/s11894-018-0618-9

17. Strum WB, Boland CR. Clinical and Genetic Characteristics of Colorectal Cancer in Persons under 50 Years of Age: A Review. Dig Dis Sci; 2019;64:3059–65. DOI-Nr. 10.1007/s10620-019-05644-0

18. Gelsomino F, Barbolini M, Spallanzani A, Pugliese G, Cascinu S. The evolving role of microsatellite instability in colorectal cancer: A review. Cancer Treat Rev. W.B. Saunders; 2016;51:19–26. DOI-Nr. 10.1016/j.ctrv.2016.10.005

19. Koopman M, Kortman GAM, Mekenkamp L, Ligtenberg MJL, Hoogerbrugge N, Antonini NF, et al. Deficient mismatch repair system in patients with sporadic advanced colorectal cancer. Br J Cancer; 2009;100:266–73. DOI-Nr. 10.1038/sj.bjc.6604867

20. Kortüm B, Campregher C, Lang M, Khare V, Pinter M, Evstatiev R, et al. Mesalazine and thymoquinone attenuate intestinal tumour development in Msh2(loxP/loxP) Villin-Cre mice. Gut; 2015;64:1905–12. DOI-Nr. 10.1136/gutjnl-2014-307663

21. Boland CR, Goel A. Microsatellite instability in colorectal cancer. Gastroenterology; 2010;138. DOI-Nr. 10.1053/j.gastro.2009.12.064

22. Seth S, Ager A, Arends MJ, Frayling IM. Lynch syndrome - cancer pathways, heterogeneity and immune escape. J Pathol; 2018;246:129–33. DOI-Nr. 10.1002/path.5139

23. Binder H, Hopp L, Schweiger MR, Hoffmann S, Jühling F, Kerick M, et al. Genomic and transcriptomic heterogeneity of colorectal tumours arising in Lynch syndrome. J Pathol; 2017;243:242–54. DOI-Nr. 10.1002/path.4948

24. Goldstein J, Tran B, Ensor J, Gibbs P, Wong HL, Wong SF, et al. Multicenter retrospective analysis of metastatic colorectal cancer (CRC) with high-level microsatellite instability (MSI-H). Ann Oncol Off J Eur Soc Med Oncol; 2014;25:1032–8. DOI-Nr. 10.1093/annonc/mdu100

25. H Meijer TW, Hoogerbrugge N, Nagengast FM, L Ligtenberg MJ, Han M van Krieken JJ, W H MT, et al. In Lynch syndrome adenomas, loss of mismatch repair proteins is related to an enhanced lymphocytic response. Histopathology; 2009;55:414–22. DOI-Nr. 10.1111/j.1365-2559.2009.03403.x

26. Yurgelun MB, Kulke MH, Fuchs CS, Allen BA, Uno H, Hornick JL, et al. Cancer Susceptibility Gene Mutations in Individuals With Colorectal Cancer. J Clin Oncol. 2017;35:1086–95. DOI-Nr. 10.1200/JCO.2016.71.0012

27. Lorenzi M, Amonkar M, Zhang J, Mehta S, Liaw KL. Epidemiology of Microsatellite Instability High (MSI-H) and Deficient Mismatch Repair (dMMR) in Solid Tumors: A Structured

Literature Review. J Oncol. Hindawi Limited; 2020;2020. DOI-Nr. 10.1155/2020/1807929
28. Galon J, Bruni D. Approaches to treat immune hot, altered and cold tumours with combination immunotherapies. Nature Publishing Group; 2019;18:197–218. DOI-Nr. 10.1038/s41573-018-0007-y
29. Freeman GJ, Xiao Y. The microsatellite instable subset of colorectal cancer is a particularly good candidate for checkpoint blockade immunotherapy. Cancer Discov. 2015 Jan;5(1):16-8. DOI-Nr. 10.1158/2159-8290.CD-14-1397
30. Campbell BB, Light N, Fabrizio D, Zatzman M, Fuligni F, de Borja R, et al. Comprehensive Analysis of Hypermutation in Human Cancer. Cell; 2017;171:1042-1056.e10. DOI-Nr. 10.1016/j.cell.2017.09.048
31. Geurts-Giele WRR, Leenen CHM, Dubbink HJ, Meijssen IC, Post E, Sleddens HFBM, et al. Somatic aberrations of mismatch repair genes as a cause of microsatellite-unstable cancers. J Pathol; 2014;234:548–59. DOI-Nr. 10.1002/path.4419
32. Salewski I, Gladbach YS, Kuntoff S, Irmscher N, Hahn O, Junghanss C, et al. In vivo vaccination with cell line-derived whole tumor lysates: neoantigen quality, not quantity matters. J Transl Med; 2020;18:1–15. DOI-Nr. 10.1186/s12967-020-02570-y
33. Seppälä T, Pylvänäinen K, Evans DG, Järvinen H, Renkonen-Sinisalo L, Bernstein I, et al. Colorectal cancer incidence in path_MLH1 carriers subjected to different follow-up protocols: a Prospective Lynch Syndrome Database report. Hered Cancer Clin Pract; 2017;15:35. DOI-Nr. 10.1186/s13053-017-0078-5
34. Møller P, Seppälä T, Bernstein I, Holinski-Feder E, Sala P, Evans DG, et al. Original article: Cancer incidence and survival in Lynch syndrome patients receiving colonoscopic and gynaecological surveillance: first report from the prospective Lynch syndrome database. Gut; 2017;66:464. DOI-Nr. 10.1136/gutjnl-2015-309675
35. Niskakoski A, Pasanen A, Porkka N, Eldfors S, Lassus H, Renkonen-Sinisalo L, et al. Converging endometrial and ovarian tumorigenesis in Lynch syndrome: Shared origin of synchronous carcinomas. Gynecol Oncol; 2018;150:92–8. DOI-Nr. 10.1016/j.ygyno.2018.04.566
36. Muzny DM, Bainbridge MN, Chang K, Dinh HH, Drummond JA, Fowler G, et al. Comprehensive molecular characterization of human colon and rectal cancer. Nat 2012 4877407; 2012;487:330–7. DOI-Nr. 10.1038/nature11252
37. Jass JR. Classification of colorectal cancer based on correlation of clinical, morphological and molecular features. Histopathology. England; 2007;50:113–30. DOI-Nr. 10.1111/j.1365-2559.2006.02549.x
38. Idos G, Valle L. Lynch Syndrome. 2004 Feb 5 [Updated 2021 Feb 4]. In: Adam MP, Everman DB, Mirzaa GM, et al., editors. GeneReviews®. Seattle (WA): University of Washington, Seattle; 1993-2023.

39. Rodríguez-Soler M, Pérez-Carbonell L, Guarinos C, Zapater P, Castillejo A, Barberá VM, et al. Risk of cancer in cases of suspected lynch syndrome without germline mutation. Gastroenterology. W.B. Saunders; 2013;144. DOI-Nr. 10.1053/j.gastro.2013.01.044
40. Heyn G, Darmkrebs: Therapie nach Tumorstadium | PZ – Pharmazeutische Zeitung. [cited 2022 Sep 26]. Available from: https://www.pharmazeutische-zeitung.de/ausgabe-122017/therapie-nach-tumorstadium/
41. Leitlinienprogramm Onkologie: Home. [cited 2022 Sep 26]. Available from: https://www.leitlinienprogramm-onkologie.de/home/
42. Onkopedia. [cited 2022 Sep 26]. Available from: https://www.onkopedia.com/de
43. Wolf E, Capecitabin: Ein Zytostatikumin Tablettenform. Dtsch Arztebl 2001; 98(14): A-932 / B-793 / C-727
44. Li JY, Chen YP, Li YQ, Liu N, Ma J. Chemotherapeutic and targeted agents can modulate the tumor microenvironment and increase the efficacy of immune checkpoint blockades. Mol Cancer; 2021;20. DOI-Nr. 10.1186/s12943-021-01317-7
45. Parente P, Parcesepe P, Covelli C, Olivieri N, Remo A, Pancione M, et al. Crosstalk between the Tumor Microenvironment and Immune System in Pancreatic Ductal Adenocarcinoma: Potential Targets for New Therapeutic Approaches. Gastroenterol Res Pract; 2018;2018. DOI-Nr. 10.1155/2018/7530619
46. Sen T, Della Corte CM, Milutinovic S, Cardnell RJ, Diao L, Ramkumar K, et al. Combination Treatment of the Oral CHK1 Inhibitor, SRA737, and Low-Dose Gemcitabine Enhances the Effect of Programmed Death Ligand 1 Blockade by Modulating the Immune Microenvironment in SCLC. J Thorac Oncol; 2019;14:2152–63. DOI-Nr. 10.1016/j.jtho.2019.08.009
47. Réjiba S, Bigand C, Parmentier C, Hajri A. Gemcitabine-based chemogene therapy for pancreatic cancer using Ad-dCK::UMK GDEPT and TS/RR siRNA strategies. Neoplasia. Elsevier; 2009;11:637–50. DOI-Nr. 10.1593/neo.81686
48. fda, cder. Highlights of prescribing information [cited 2022 Nov 28]; Available from: www.fda.gov/medwatch.
49. Suzuki E, Sun J, Kapoor V, Jassar AS, Albelda SM. Gemcitabine has significant immunomodulatory activity in murine tumor models independent of its cytotoxic effects. Cancer Biol Ther. United States; 2007;6:880–5. DOI-Nr. 10.4161/cbt.6.6.4090
50. Maletzki C, Wiegele L, Nassar I, Stenzel J, Junghanss C. Chemo-immunotherapy improves long-term survival in a preclinical model of MMR-D-related cancer. J Immunother cancer [Internet]. J Immunother Cancer; 2019;7. DOI-Nr. 10.1186/s40425-018-0476-x
51. Brunet JF, Denizot F, Luciani MF, Roux-Dosseto M, Suzan M, Mattei MG, et al. A new member of the immunoglobulin superfamily--CTLA-4. Nature; 1987;328:267–70. DOI-Nr. 10.1038/328267a0
52. Shiravand Y, Khodadadi F, Mohammad S, Kashani A, Hosseini-Fard R, Hosseini S, et al.

Immune Checkpoint Inhibitors in Cancer Therapy. 2022; DOI-Nr. 10.3390/curroncol29050247
53. Egen JG, Allison JP. Cytotoxic T Lymphocyte Antigen-4 Accumulation in the Immunological Synapse Is Regulated by TCR Signal Strength. Immunity. Cell Press; 2002;16:23–35. DOI-Nr. 10.1016/s1074-7613(01)00259-x
54. Linsley PS, Wallace PM, Johnson J, Gibson MG, Greene JAL, Ledbetter JA, et al. Immunosuppression in Vivo by a Soluble Form of the CTLA-4 T Cell Activation Molecule. Science (80-); 1992;257:792–5. DOI-Nr. 10.1126/science.1496399
55. Leach DR, Krummel MF, Allison JP. Enhancement of Antitumor Immunity by CTLA-4 Blockade. Science (80-) ; 1996;271:1734–6. DOI-Nr. 10.1126/science.271.5256.1734
56. Callahan MK, Wolchok JD. At the Bedside: CTLA-4- and PD-1-blocking antibodies in cancer immunotherapy. J Leukoc Biol; 2013;94:41. DOI-Nr. 10.1189/jlb.1212631
57. Lipson EJ, Drake CG. Ipilimumab: an anti-CTLA-4 antibody for metastatic melanoma. Clin cancer Res an Off J Am Assoc Cancer Res. United States; 2011;17:6958–62. DOI-Nr. 10.1158/1078-0432.CCR-11-1595
58. Tan E, Sahin IH. Defining the current role of immune checkpoint inhibitors in the treatment of mismatch repair-deficient/microsatellite stability-high colorectal cancer and shedding light on future approaches. Taylor & Francis; 2021;15:735–42. DOI-Nr. 10.1080/17474124.2021.1886077
59. Trullas A, Delgado J, Genazzani A, Mueller-Berghaus J, Migali C, Müller-Egert S, et al. The EMA assessment of pembrolizumab as monotherapy for the first-line treatment of adult patients with metastatic microsatellite instability-high or mismatch repair deficient colorectal cancer. ESMO open; 2021;6. DOI-Nr. 10.1016/j.esmoop.2021.100145
60. Huang Q, Zheng Y, Gao Z, Yuan L, Sun Y, Chen H. Comparative Efficacy and Safety of PD-1/PD-L1 Inhibitors for Patients with Solid Tumors: A Systematic Review and Bayesian Network Meta-analysis. J Cancer; 2021;12:1133. DOI-Nr. 10.7150/jca.49325
61. Overman MJ, McDermott R, Leach JL, Lonardi S, Lenz HJ, Morse MA, et al. Nivolumab in patients with metastatic DNA mismatch repair-deficient or microsatellite instability-high colorectal cancer (CheckMate 142): an open-label, multicentre, phase 2 study. Lancet Oncol; 2017;18:1182–91. DOI-Nr. 10.1016/S1470-2045(17)30422-9
62. Mecklenburg-Vorpommern Ä, Maletzki C. Seite 454 Immuntherapeutische Kombinationsstrategien beim Lynch Syndrom und sporadischen Mismatch-Reparatur-defizienten Tumoren Aktuelle präklinische und klinische Ansätze. Ausgabe 12/2021
63. André T, Shiu K-K, Kim TW, Jensen BV, Jensen LH, Punt C, et al. Pembrolizumab in Microsatellite-Instability-High Advanced Colorectal Cancer. N Engl J Med; 2020;383:2207–18. DOI-Nr. 10.1056/NEJMoa2017699
64. Riella L V, Paterson AM, Sharpe AH, Chandraker A. Role of the PD-1 Pathway in the Immune Response. Am J Transplant. Wiley Periodicals Inc. C; 2012;12:2575–87. DOI-Nr.

10.1111/j.1600-6143.2012.04224.x
65. Han Y, Liu D, Li L. PD-1/PD-L1 pathway: current researches in cancer. Am J Cancer Res. 2020.
66. Freeman GJ, Long AJ, Iwai Y, Bourque K, Chernova T, Nishimura H, et al. Engagement of the PD-1 immunoinhibitory receptor by a novel B7 family member leads to negative regulation of lymphocyte activation. J Exp Med; 2000;192:1027–34. DOI-Nr. 10.1084/jem.192.7.1027
67. Latchman Y, Wood CR, Chernova T, Chaudhary D, Borde M, Chernova I, et al. PD-L2 is a second ligand for PD-1 and inhibits T cell activation. Nat Immunol. 2001 Mar;2(3):261-8. DOI-Nr. 10.1038/85330
68. Beenen AC, Sauerer T, Schaft N, Dörrie J. Beyond Cancer: Regulation and Function of PD-L1 in Health and Immune-Related Diseases. Int. J. Mol. Sci. **2022**, *23*, 8599. DOI-Nr. 10.3390/ijms23158599
69. Ning Y-M, Suzman D, Maher VE, Zhang L, Tang S, Ricks T, et al. FDA Approval Summary: Atezolizumab for the Treatment of Patients with Progressive Advanced Urothelial Carcinoma after Platinum-Containing Chemotherapy. Oncologist; 2017;22:743–9. DOI-Nr. 10.1634/the-oncologist.2017-0087
70. Pal SK, Hoffman-Censits J, Zheng H, Kaiser C, Tayama D, Bellmunt J. Atezolizumab in Platinum-treated Locally Advanced or Metastatic Urothelial Carcinoma: Clinical Experience from an Expanded Access Study in the United States. Eur Urol; 2018;73:800–6. DOI-Nr. 10.1016/j.eururo.2018.02.010
71. Workman CJ, Rice DS, Dugger KJ, Kurschner C, Vignali DA. Phenotypic analysis of the murine CD4-related glycoprotein, CD223 (LAG-3). Eur J Immunol. 2002 Aug;32(8):2255-63. DOI-Nr. 10.1002/1521-4141(200208)32:8<2255::AID-IMMU2255>3.0.CO;2-A
72. Triebel F. LAG-3: a regulator of T-cell and DC responses and its use in therapeutic vaccination. Trends Immunol; 2003;24:619–22. DOI-Nr. 10.1016/j.it.2003.10.001
73. Huo J-L, Wang Y-T, Fu W-J, Lu N, Liu Z-S. The promising immune checkpoint LAG-3 in cancer immunotherapy: from basic research to clinical application. Front Immunol; 2022;13:956090. DOI-Nr. 10.3389/fimmu.2022.956090
74. Triebel F, Jitsukawa S, Baixeras E, Roman-Roman S, Genevee C, Viegas-Pequignot E, et al. LAG-3, a novel lymphocyte activation gene closely related to CD4. J Exp Med; 1990;171:1393–405. DOI-Nr. 10.1084/jem.171.5.1393
75. Maruhashi T, Sugiura D, Okazaki IM, Okazaki T. LAG-3: from molecular functions to clinical applications. J Immunother Cancer; 2020;8:e001014. DOI-Nr. 10.1136/jitc-2020-001014
76. Huard B, Prigent P, Tournier M, Bruniquel D, Triebel F. CD4/major histocompatibility complex class II interaction analyzed with CD4- and lymphocyte activation gene-3 (LAG-3)-Ig fusion proteins. Eur J Immunol; 1995;25:2718–21. DOI-Nr. 10.1002/eji.1830250949

77. Long L, Zhang X, Chen F, Pan Q, Phiphatwatchara P, Zeng Y, et al. The promising immune checkpoint LAG-3: From tumor microenvironment to cancer immunotherapy. Genes and Cancer; 2018;9:176–89. DOI-Nr. 10.18632/genesandcancer.180

78. Sordo-bahamonde C, Lorenzo-herrero S, González-rodríguez AP, Payer ÁR, González-garcía E, López-soto A, et al. LAG-3 Blockade with Relatlimab (BMS-986016) Restores Anti-Leukemic Responses in Chronic Lymphocytic Leukemia. Cancers (Basel); 2021;13. DOI-Nr. 10.3390/cancers13092112

79. Chocarro L, Bocanegra A, Blanco E, Fernández-Rubio L, Arasanz H, Echaide M, et al. Cutting-Edge: Preclinical and Clinical Development of the First Approved Lag-3 Inhibitor. Cells 2022; DOI-Nr. 10.3390/cells11152351

80. Liebl MC, Hofmann TG. Identification of responders to immune checkpoint therapy: which biomarkers have the highest value? J Eur Acad Dermatology Venereol; 2019;33:52–6. DOI-Nr. 10.1111/jdv.15992

81. Paucek RD, Baltimore D, Li G. The Cellular Immunotherapy Revolution: Arming the Immune System for Precision Therapy. Trends Immunol; 2019;40:292–309. DOI-Nr. 10.1016/j.it.2019.02.002

82. Rad HS, Rad HS, Shiravand Y, Radfar P, Arpon D, Warkiani ME, et al. The Pandora's box of novel technologies that may revolutionize lung cancer. Lung Cancer. Elsevier; 2021;159:34–41. DOI-Nr. 10.1016/j.lungcan.2021.06.022

83. Kulasinghe A, Monkman J, Shah ET, Matigian N, Adams MN, O'Byrne K. Spatial Profiling Identifies Prognostic Features of Response to Adjuvant Therapy in Triple Negative Breast Cancer (TNBC). Front Oncol; 2021;11:1. DOI-Nr. 10.3389/fonc.2021.798296

84. Hazama S, Tamada K, Yamaguchi Y, Kawakami Y, Nagano H. Current status of immunotherapy against gastrointestinal cancers and its biomarkers: Perspective for precision immunotherapy. Ann Gastroenterol Surg; 2018;2:289. DOI-Nr. 10.1002/ags3.12180

85. Redmond WL, Linch SN. Combinatorial immunotherapeutic approaches to restore the function of anergic tumor-reactive cytotoxic CD8+ T cells. Hum Vaccin Immunother; 2016;12:2519. DOI-Nr. 10.1080/21645515.2016.1193277

86. Seledtsov VI, Goncharov AG, Seledtsova G V. Clinically feasible approaches to potentiating cancer cell-based immunotherapies Clinically feasible approaches to potentiating cancer cell-based immunotherapies. Human Vaccines & Immunotherapeutics 2015; DOI-Nr. 10.1080/21645515.2015.1009814

87. Kreiter S, María M, Barrio F, Cáncer A, Wirth TC, Kühnel F. Neoantigen Targeting-Dawn of a New Era in Cancer Immunotherapy? Front Immunol. 2017;8:1848. DOI-Nr. 10.3389/fimmu.2017.01848

88. Martin Lluesma S, Wolfer A, Harari A, Kandalaft LE. Cancer Vaccines in Ovarian Cancer:

How Can We Improve? Biomedicines. 2016 May 3;4(2):10. DOI-Nr. 10.3390/biomedicines4020010

89. Saeterdal I, Bjørheim J, Lislerud K, Gjertsen MK, Bukholm IK, Olsen OC, et al. Frameshift-mutation-derived peptides as tumor-specific antigens in inherited and spontaneous colorectal cancer. Proc Natl Acad Sci U S A. 2001 Nov 6;98(23):13255-60. DOI-Nr. 10.1073/pnas.231326898

90. Gebert J, Gelincik O, Oezcan-Wahlbrink M, Marshall JD, Hernandez-Sanchez A, Urban K, et al. Recurrent Frameshift Neoantigen Vaccine Elicits Protective Immunity With Reduced Tumor Burden and Improved Overall Survival in a Lynch Syndrome Mouse Model. Gastroenterology. 2021;161:1288-1302.e13. DOI-Nr. 10.1053/j.gastro.2021.06.073

91. Maletzki C, Gladbach YS, Hamed M, Fuellen G, Semmler ML, Stenzel J, et al. Cellular vaccination of MLH1−/− mice – an immunotherapeutic proof of concept study. Oncoimmunology; 2018;7. DOI-Nr. 10.1080/2162402X.2017.1408748

92. Giardiello FM, Allen JI, Axilbund JE, Boland CR, Burke CA, Burt RW, et al. Guidelines on genetic evaluation and management of lynch syndrome: A consensus statement by the US multi-society task force on colorectal cancer. Am J Gastroenterol; 2014;109:1159–79. DOI-Nr. 10.1038/ajg.2014.186

93. Peltomäki P, Vasen H. Mutations associated with HNPCC predisposition -- Update of ICG-HNPCC/INSiGHT mutation database. Dis Markers; 2004;20:269–76. DOI-Nr. 10.1155/2004/305058

94. Yao X, Buermeyer AB, Narayanan L, Tran D, Baker SM, Prolla TA, et al. Different mutator phenotypes in Mlh1- versus Pms2-deficient mice. Proc Natl Acad Sci U S A; 1999;96:6850–5. DOI-Nr. 10.1073/pnas.96.12.6850

95. Lee K, Tosti E, Edelmann W. Mouse models of DNA mismatch repair in cancer research. DNA Repair (Amst); 2016;38:140–6. DOI-Nr. 10.1016/j.dnarep.2015.11.015

96. Edelmann W, Cohen PE, Kane M, Lau K, Morrow B, Bennett S, et al. Meiotic pachytene arrest in MLH1-deficient mice. Cell; 1996;85:1125–34. DOI-Nr. 10.1016/s0092-8674(00)81312-4

97. Pussila M, Törönen P, Einarsdottir E, Katayama S, Krjutškov K, Holm L, et al. Mlh1 deficiency in normal mouse colon mucosa associates with chromosomally unstable colon cancer. Carcinogenesis; 2018;39:788. DOI-Nr. 10.1093/carcin/bgy056

98. Edelmann W, Yang K, Kuraguchi M, Heyer J, Lia M, Kneitz B, et al. Tumorigenesis in Mlh1 and Mlh1/Apc1638N mutant mice. Cancer Res. United States; 1999;59:1301–7.

99. Maletzki C, Beyrich F, Hühns M, Klar E, Linnebacher M. The mutational profile and infiltration pattern of murine MLH1-/- tumors: concurrences, disparities and cell line establishment for functional analysis. Oncotarget; 2016;7:53583. DOI-Nr. 10.18632/oncotarget.10677

100. Roskoski R. Cyclin-dependent protein serine/threonine kinase inhibitors as anticancer drugs. Pharmacol Res; 2019;139:471–88. DOI-Nr. 10.1016/j.phrs.2018.11.035
101. Bai J, Li Y, Zhang G. Cell cycle regulation and anticancer drug discovery. Cancer Biol Med; 2017;14:348. DOI-Nr. 10.20892/j.issn.2095-3941.2017.0033
102. Sánchez-Martínez C, Lallena MJ, Sanfeliciano SG, de Dios A. Cyclin dependent kinase (CDK) inhibitors as anticancer drugs: Recent advances (2015–2019). Bioorg Med Chem Lett. Pergamon; 2019;29:126637. DOI-Nr. 10.1016/j.bmcl.2019.126637
103. Giannone G, Tuninetti V, Ghisoni E, Genta S, Scotto G, Mittica G, et al. Role of Cyclin-Dependent Kinase Inhibitors in Endometrial Cancer. Int J Mol Sci; 2019;20. DOI-Nr. 10.3390/ijms20092353
104. Jardim DL, Millis SZ, Ross JS, Woo MS-A, Ali SM, Kurzrock R. Cyclin Pathway Genomic Alterations Across 190,247 Solid Tumors: Leveraging Large-Scale Data to Inform Therapeutic Directions. Oncologist. 2021;26:e78–89. DOI-Nr. 10.1634/theoncologist.2020-0509
105. Lim S, Kaldis P. Cdks, cyclins and CKIs: roles beyond cell cycle regulation. Development; 2013;140:3079–93. DOI-Nr. 10.1242/dev.091744
106. Parry D, Guzi T, Shanahan F, Davis N, Prabhavalkar D, Wiswell D, et al. Dinaciclib (SCH 727965), a novel and potent cyclin-dependent kinase inhibitor. Mol Cancer Ther; 2010;9:2344–53. DOI-Nr. 10.1158/1535-7163.MCT-10-0324
107. Huang J, Chen P, Liu K, Liu J, Zhou B, Wu R, et al. CDK1/2/5 inhibition overcomes IFNG-mediated adaptive immune resistance in pancreatic cancer. Gut. England; 2021;70:890–9. DOI-Nr. 10.1136/gutjnl-2019-320441
108. Kwiatkowski N, Zhang T, Rahl PB, Abraham BJ, Reddy J, Ficarro SB, et al. Targeting transcription regulation in cancer with a covalent CDK7 inhibitor. Nature. 2014;8. DOI-Nr. 10.1038/nature13393
109. Olson CM, Liang Y, Leggett A, Park WD, Li L, Mills CE, et al. Development of a Selective CDK7 Covalent Inhibitor Reveals Predominant Cell-Cycle Phenotype. Cell Chem Biol. Elsevier Ltd; 2019;26:792-803.e10. DOI-Nr. 10.1016/j.chembiol.2019.02.012
110. Li B, Wang B, Zhu C, Tang D, Pang J, Zhao J, et al. Cyclin-dependent kinase 7 inhibitor THZ1 in cancer therapy. Chronic Dis Transl Med; 2019;5:155–69. DOI-Nr. 10.1016/j.cdtm.2019.08.006
111. Riess C, Koczan D, Schneider B, Linke C, del Moral K, Classen CF, et al. Cyclin-dependent kinase inhibitors exert distinct effects on patient-derived 2D and 3D glioblastoma cell culture models. Cell death Discov; 2021;7. DOI-Nr. 10.1038/s41420-021-00423-1
112. Manohar SM, Joshi KS. Promising Anticancer Activity of Multitarget Cyclin Dependent Kinase Inhibitors against Human Colorectal Carcinoma Cells. Curr Mol Pharmacol. United Arab Emirates; 2022;15:1024–33. DOI-Nr. 10.2174/1874467215666220124125809
113. Rahaman MH, Lam F, Zhong L, Teo T, Adams J, Yu M, et al. Targeting CDK9 for

treatment of colorectal cancer. Mol Oncol; 2019;13:2178. DOI-Nr. 10.1002/1878-0261.12559
114. Patel H, Periyasamy M, Sava GP, Bondke A, Slafer BW, Kroll SHB, et al. ICEC0942, an Orally Bioavailable Selective Inhibitor of CDK7 for Cancer Treatment. Mol Cancer Ther; 2018;17:1156. DOI-Nr. 10.1158/1535-7163.MCT-16-0847
115. Goetz MP, Toi M, Campone M, Sohn J, Paluch-Shimon S, Huober J, et al. MONARCH 3: Abemaciclib As Initial Therapy for Advanced Breast Cancer. J Clin Oncol Off J Am Soc Clin Oncol. United States; 2017;35:3638–46. DOI-Nr. 10.1200/JCO.2017.75.6155
116. Hino H, Iriyama N, Kokuba H, Kazama H, Moriya S, Takano N, et al. Abemaciclib induces atypical cell death in cancer cells characterized by formation of cytoplasmic vacuoles derived from lysosomes. Cancer Sci; 2020;111:2132–45. DOI-Nr. 10.1111/cas.14419
117. Torres-Guzmán R, Calsina B, Hermoso A, Baquero C, Alvarez B, Amat J, et al. Preclinical characterization of abemaciclib in hormone receptor positive breast cancer. Oncotarget. 2017;8:69493–507. DOI-Nr. 10.18632/oncotarget.17778
118. Goel S, Decristo MJ, Watt AC, Brinjones H, Sceneay J, Li BB, et al. CDK4/6 inhibition triggers anti-tumour immunity. Nature; 2017;548:471–5. DOI-Nr. 10.1038/nature23465
119. Petroni G, Formenti SC, Chen-Kiang S, Galluzzi L. The ability of malignant cells to ignore inhibitory inputs from the microenvironment. DOI-Nr. 10.1038/nature01096
120. Schaer DA, Beckmann RP, Dempsey JA, Huber L, Forest A, Amaladas N, et al. The CDK4/6 Inhibitor Abemaciclib Induces a T Cell Inflamed Tumor Microenvironment and Enhances the Efficacy of PD-L1 Checkpoint Blockade. Cell Rep; 2018;22:2978–94. DOI-Nr. 10.1016/j.celrep.2018.02.053
121. Heckler M, Ali LR, Clancy-Thompson E, Qiang L, Ventre KS, Lenehan P, et al. Inhibition of CDK4/6 Promotes CD8 T-cell Memory Formation. Cancer Discov; 2021;11:2564–81. DOI-Nr. 10.1158/2159-8290.CD-20-1540
122. Sobhani N, Fassl A, Mondani G, Generali D, Otto T. Targeting Aberrant FGFR Signaling to Overcome CDK4/6 Inhibitor Resistance in Breast Cancer. Cells; 2021;10:1–14. DOI-Nr. 10.3390/cells10020293
123. Groenland SL, Martínez-Chávez A, van Dongen MGJ, Beijnen JH, Schinkel AH, Huitema ADR, et al. Clinical Pharmacokinetics and Pharmacodynamics of the Cyclin-Dependent Kinase 4 and 6 Inhibitors Palbociclib, Ribociclib, and Abemaciclib. Clin Pharmacokinet; 2020;59:1501–20. DOI-Nr. 10.1007/s40262-020-00930-x
124. George MA, Qureshi S, Omene C, Toppmeyer DL, Ganesan S. Clinical and Pharmacologic Differences of CDK4/6 Inhibitors in Breast Cancer. Front Oncol. Frontiers Media S.A.; 2021;11:2471. DOI-Nr. 10.3389/fonc.2021.693104
125. Riess C, Irmscher N, Salewski I, Strüder D, Classen CF, Große-Thie C, et al. Cyclin-dependent kinase inhibitors in head and neck cancer and glioblastoma-backbone or add-on in immune-oncology? Cancer Metastasis Rev; 2021;40:153–71. DOI-Nr. 10.1007/s10555-020-

09940-4
126. Parylo S, Vennepureddy A, Dhar V, Patibandla P, Sokoloff A. Role of cyclin-dependent kinase 4/6 inhibitors in the current and future eras of cancer treatment. J Oncol Pharm Pract; 2019;25:110–29. DOI-Nr. 10.1177/1078155218770904
127. Barroso-Sousa R, Shapiro GI, Tolaney SM. Clinical Development of the CDK4/6 Inhibitors Ribociclib and Abemaciclib in Breast Cancer. Breast Care (Basel) 2016; DOI-Nr. 10.1159/000447284
128. Klein ME, Kovatcheva M, Davis LE, Tap WD, Koff A. CDK4/6 Inhibitors: The Mechanism of Action May Not Be as Simple as Once Thought. Cancer Cell; 2018;34:9–20. DOI-Nr. 10.1016/j.ccell.2018.03.023
129. Knudsen ES, Hutcheson J, Vail P, Witkiewicz AK. Biological specificity of CDK4/6 inhibitors: dose response relationship, in vivo signaling, and composite response signature. Oncotarget. 2017. DOI-Nr. 10.18632/oncotarget.18435
130. Kloor M, Von Knebel Doeberitz M. The Immune Biology of Microsatellite-Unstable Cancer. Trends in Cancer; 2016;2:121–33. DOI-Nr. 10.1016/j.trecan.2016.02.004
131. Schwitalle Y, Kloor M, Eiermann S, Linnebacher M, Kienle P, Knaebel HP, et al. Immune Response Against Frameshift-Induced Neopeptides in HNPCC Patients and Healthy HNPCC Mutation Carriers. Gastroenterology. W.B. Saunders; 2008;134:988–97. DOI-Nr. 10.1053/j.gastro.2008.01.015
132. Roudko V, Bozkus CC, Greenbaum B, Lucas A, Samstein R, Bhardwaj N, et al. Lynch Syndrome and MSI-H Cancers: From Mechanisms to "Off-The-Shelf" Cancer Vaccines. Front Immunol. 2021 Sep 24;12:757804. DOI-Nr. 10.3389/fimmu.2021.757804
133. Md Sakib Hossain D, Javaid S, Cai M, Zhang C, Sawant A, Hinton M, et al. Dinaciclib induces immunogenic cell death and enhances anti-PD1-mediated tumor suppression. J Clin Invest; 2018;128:644–54. DOI-Nr. 10.1172/JCI94586
134. Zhang J, Bu X, Wang H, Zhu Y, Geng Y, Nihira NT, et al. Cyclin D-CDK4 kinase destabilizes PD-L1 via Cul3SPOP to control cancer immune surveillance. Nature; 2018;553:91. DOI-Nr. 10.1038/nature25015
135. Zhang QF, Li J, Jiang K, Wang R, Ge JL, Yang H, et al. CDK4/6 inhibition promotes immune infiltration in ovarian cancer and synergizes with PD-1 blockade in a B cell-dependent manner. Theranostics. Ivyspring International Publisher; 2020;10:10619–33. DOI-Nr. 10.7150/thno.44871
136. Jang HJ, Truong CY, Lo EM, Holmes HM, Ramos D, Ramineni M, et al. Inhibition of Cyclin Dependent Kinase 4/6 Overcomes Primary Resistance to Programmed Cell Death 1 Blockade in Malignant Mesothelioma. Ann Thorac Surg; 2021; DOI-Nr. 10.1016/j.athoracsur.2021.08.054
137. Schoenwaelder N, Krause M, Freitag T, Schneider B, Zonnur S, Zimpfer A, et al.

Preclinical Head and Neck Squamous Cell Carcinoma Models for Combined Targeted Therapy Approaches. Cancers (Basel); 2022;14:2484. DOI-Nr. 10.3390/cancers14102484

138. Gregory GP, Kumar S, Wang D, Mahadevan D, Walker P, Wagner-Johnston N, et al. Pembrolizumab plus dinaciclib in patients with hematologic malignancies: the phase 1b KEYNOTE-155 study. Blood Adv. 2022 Feb 22;6(4):1232-1242. DOI-Nr. 10.1182/bloodadvances.2021005872

139. Kortüm B, Campregher C, Lang M, Khare V, Pinter M, Evstatiev R, et al. Mesalazine and thymoquinone attenuate intestinal tumour development in Msh2loxP/loxP Villin-Cre mice. Gut. 2015;64:1905–12. DOI-Nr. 10.1136/gutjnl-2014-307663

140. Kucherlapati MH, Lee K, Nguyen AA, Clark AB, Hou HJ, Rosulek A, et al. An Msh2 conditional knockout mouse for studying intestinal cancer and testing anticancer agents. Gastroenterology. United States; 2010;138:993-1002.e1. DOI-Nr. 10.1053/j.gastro.2009.11.009

141. Gladbach YS, Wiegele L, Hamed M, Merkenschläger AM, Fuellen G, Junghanss C, et al. Unraveling the Heterogeneous Mutational Signature of Spontaneously Developing Tumors in MLH1 -/- Mice. Cancers (Basel); 2019;11. DOI-Nr. 10.3390/cancers11101485

142. Tomita M, Yasui H, Higashikawa K, Nakajima K, Takakura H, Shiga T, et al. Anti PD-1 treatment increases [18 F]FDG uptake by cancer cells in a mouse B16F10 melanoma model. EJNMMI Res 8, 82 (2018) DOI-Nr. 10.1186/s13550-018-0433-1

143. He H, Cen Y, Wang P, Zeng X, Zeng S, Li X, et al. The therapeutic effect of an autologous and allogenic mixed glioma cell lysate vaccine in a rat model. J Cancer Res Clin Oncol; 2022;1–14. DOI-Nr. 10.1007/s00432-022-04281-x

144. Dean JL, McClendon AK, Knudsen ES. Modification of the DNA damage response by therapeutic CDK4/6 inhibition. J Biol Chem; 2012;287:29075–87. DOI-Nr. 10.1074/jbc.M112.365494

145. Palmer AC, Izar B, Hwangbo H, Sorger PK. Predictable Clinical Benefits without Evidence of Synergy in Trials of Combination Therapies with Immune-Checkpoint Inhibitors. Clin Cancer Res; 2022;28:368–77. DOI-Nr. 10.1158/1078-0432.CCR-21-2275

146. FDA approves nivolumab plus ipilimumab and chemotherapy for first-line treatment of metastatic NSCLC | FDA. Available from: https://www.fda.gov/drugs/resources-information-approved-drugs/fda-approves-nivolumab-plus-ipilimumab-and-chemotherapy-first-line-treatment-metastatic-nsclc

147. Jiang L, Zhang C. Complete response with combined therapy in a patient with brain metastasis from nasopharyngeal carcinoma: case report and literature review. Journal of International Medical Research. 2023;51(1). DOI- Nr. 10.1177/03000605221147187

148. Heckler M, Ali LR, Clancy-Thompson E, Qiang L, Ventre KS, Lenehan P, et al. Inhibition of CDK4/6 Promotes CD8 T-cell Memory Formation. Cancer Discov; 2021;11:2564–81. DOI-

Nr. 10.1158/2159-8290.CD-20-1540
149. Lecoq I, Kopp KL, Chapellier M, Mantas P, Martinenaite E, Perez-Penco M, et al. CCL22-based peptide vaccines induce anti-cancer immunity by modulating tumor microenvironment. Oncoimmunology. 2022 Aug 29;11(1):2115655. DOI-Nr. 10.1080/2162402X.2022.2115655
150. Vavolizza RD, Petroni GR, Mauldin IS, Chianese-Bullock KA, Olson WC, Smith KT, et al. Phase I/II clinical trial of a helper peptide vaccine plus PD-1 blockade in PD-1 antibody-naïve and PD-1 antibody-experienced patients with melanoma (MEL64). J Immunother Cancer. 2022;10:5424. DOI-Nr. 10.1136/jitc-2022-005424corr1
151. Horn LA, Fousek K, Hamilton DH, Hodge JW, Zebala JA, Maeda DY, et al. Vaccine Increases the Diversity and Activation of Intratumoral T Cells in the Context of Combination Immunotherapy. Cancers 2021, Vol 13, Page 968; 2021;13:968. DOI-Nr. 10.3390/cancers13050968
152. Wilkinson Carlisle J, Jansen CS, Cardenas MA, Sobierajska E, Reyes AM, Greenwald R, et al. Clinical outcome following checkpoint therapy in renal cell carcinoma is associated with a burst of activated CD8 T cells in blood. J Immunother Cancer. 2022;10:4803. DOI-Nr. 10.1136/jitc-2022-004803
153. Salewski I, Henne J, Engster L, Krone P, Schneider B, Redwanz C, et al. CDK4/6 blockade provides an alternative approach for treatment of mismatch-repair deficient tumors. Oncoimmunology; 2022;11. DOI-Nr. 10.1080/2162402X.2022.2094583
154. Hegan DC, Narayanan L, Jirik FR, Edelmann W, Liskay RM, Glazer PM. Differing patterns of genetic instability in mice deficient in the mismatch repair genes Pms2, Mlh1, Msh2, Msh3 and Msh6. Carcinogenesis; 2006;27:2402–8. DOI-Nr. 10.1093/carcin/bgl079
155. Yajuk O, Baron M, Toker S, Zelter T, Fainsod-Levi T, Granot Z. The PD-L1/PD-1 Axis Blocks Neutrophil Cytotoxicity in Cancer. Cells. 2021 Jun 15;10(6):1510. DOI-Nr. 10.3390/cells10061510
156. Rodrigues EG, Travassos LR. Endogenous accumulation of IFN-gamma in IFN-gamma-R(-/-) mice increases resistance to B16F10-Nex2 murine melanoma: a model for direct IFN-gamma anti-tumor cytotoxicity in vitro and in vivo. Cytokines Cell Mol Ther; 2002;7:107–16. DOI-Nr. 10.1080/13684730310000121
157. Ait Ouakrim D, Dashti SG, Chau R, Buchanan DD, Clendenning M, Rosty C, et al. Aspirin, Ibuprofen, and the Risk of Colorectal Cancer in Lynch Syndrome. J Natl Cancer Inst. 2015;107:djv170. DOI-Nr. 10.1093/jnci/djv170
158. Cao Y, Nishihara R, Qian ZR, Song M, Mima K, Inamura K, et al. Regular Aspirin Use Associates With Lower Risk of Colorectal Cancers With Low Numbers of Tumor-Infiltrating Lymphocytes. Gastroenterology. 2016;151:879-892.e4. DOI-Nr. 10.1053/j.gastro.2016.07.030
159. Cramer DW, Titus-Ernstoff L, McKolanis JR, Welch WR, Vitonis AF, Berkowitz RS, et al. Conditions Associated with Antibodies Against the Tumor-Associated Antigen MUC1 and Their

Relationship to Risk for Ovarian Cancer. Cancer Epidemiol Biomarkers Prev; 2005;14:1125–31. DOI-Nr. 10.1158/1055-9965.EPI-05-0035

160. Santegoets SJAM, Stam AGM, Lougheed SM, Gall H, Jooss K, Sacks N, et al. Myeloid derived suppressor and dendritic cell subsets are related to clinical outcome in prostate cancer patients treated with prostate GVAX and ipilimumab. J Immunother cancer; 2014;2:1. DOI-Nr. 10.1186/s40425-014-0031-3

161. Mina M, Boldrini R, Citti A, Romania P, D'alicandro V, De Ioris M, et al. Tumor-infiltrating T lymphocytes improve clinical outcome of therapy-resistant neuroblastoma. Oncoimmunology. 2015 Apr 2;4(9):e1019981. DOI-Nr. 10.1080/2162402X.2015.1019981

162. Hdeib A, Sloan AE. Dendritic cell immunotherapy for solid tumors: evaluation of the DCVax® platform in the treatment of glioblastoma multiforme. CNS Oncol. 2015;4(2):63-9. DOI-Nr. 10.2217/cns.14.54

163. Banchereau J, Steinman RM. Dendritic cells and the control of immunity. Nature; 1998;392:245–52. DOI-Nr. 10.1038/32588

164. Meng X, Sun X, Liu Z, He Y. A novel era of cancer/testis antigen in cancer immunotherapy. Int Immunopharmacol. Elsevier; 2021;98:107889. DOI-Nr. 10.1016/j.intimp.2021.107889

165. Shou J, Mo F, Zhang S, Lu L, Han N, Liu L, et al. Combination treatment of radiofrequency ablation and peptide neoantigen vaccination: Promising modality for future cancer immunotherapy. Front Immunol. 2022 Sep 29;13:1000681. DOI-Nr. 10.3389/fimmu.2022.1000681

8. Original publications for cumulative dissertation

8.1 Publication 1

Salewski *et al. J Transl Med* (2020) 18:402
https://doi.org/10.1186/s12967-020-02570-y

Journal of Translational Medicine

RESEARCH Open Access

In vivo vaccination with cell line-derived whole tumor lysates: neoantigen quality, not quantity matters

Inken Salewski[1†], Yvonne Saara Gladbach[2,3,4†], Steffen Kuntoff[1], Nina Irmscher[1], Olga Hahn[5], Christian Junghanss[1] and Claudia Maletzki[1*]

Abstract

Background: Cancer vaccines provide a complex source of neoantigens. Still, increasing evidence reveals that the neoantigen quality rather than the quantity is predictive for treatment outcome.

Methods: Using the preclinical Mlh1$^{-/-}$ tumor model, we performed a side-by side comparison of two autologous cell-line derived tumor lysates (namely 328 and A7450 T1 M1) harboring different tumor mutational burden (TMB; i.e. ultra-high: 328; moderate-high: A7450 T1 M1). Mice received repetitive prophylactic or therapeutic applications of the vaccine. Tumor incidence, immune responses and tumor microenvironment was examined.

Results: Both tumor cell lysates delayed tumor formation in the prophylactic setting, with the A7450 T1 M1 lysate being more effective in decelerating tumor growth than the 328 lysate (median overall survival: 37 vs. 25 weeks). Comparable results were achieved in therapeutic setting and could be traced back to antigen-driven immune stimulation. Reactive T cells isolated from A7450 T1 M1-treated mice recognized autologous Mlh1$^{-/-}$ tumor cells in IFNγ ELISpot, but likewise YAC-1 cells, indicative for stimulation of both arms of the immune system. By deciphering local effects, vaccines shaped the tumor microenvironment differently. While A7450 T1 M1 prophylactically vaccinated tumors harbored low numbers of myeloid-derived suppressor cells (MDSC) and elevated CD8-T cell infiltrates, vaccination with the 328 lysate evoked MDSC infiltration. Similar effects were seen in the therapeutic setting with stable disease induction only upon A7450 T1 M1 vaccination. Untangling individual response profiles revealed strong infiltration with LAG3^{+} and PD-L1^{+} immune cells when treatments failed, but almost complete exclusion of checkpoint-expressing lymphocytes in long-term survivors.

Conclusions: By applying two tumor cell lysates we demonstrate that neoantigen quality outranks quantity. This should be considered prior to designing cancer vaccine-based combination approaches.

Keywords: Tumor lysate, Mutational load, MMR deficiency, In vivo imaging, Primary cell lines

Background

The idea of using whole tumor lysates as vaccines dates back to the late 1970ies and aims at the induction of a vigorous immune response against cancer [1]. Highly immunogenic tumor-derived neo-epitopes must be present to be recognized by cytotoxic T cells. Antigen (Ag)-loaded dendritic cells (DCs) are the most commonly used cell-based vaccines with proven safety and, notably, the

*Correspondence: claudia.maletzki@med.uni-rostock.de
†Inken Salewski and Yvonne Saara Gladbach contributed equally to this work
[1] Department of Medicine, Clinic III-Hematology, Oncology, Palliative Care, Rostock University Medical Center, Ernst-Heydemann-Str. 6, 18057 Rostock, Germany
Full list of author information is available at the end of the article

capability of providing long-lasting protective immunity [2–4]. As such, vaccines hold promise to delay or prevent cancer recurrence, particularly in early-stage disease patients, when immune-suppressive mechanisms are not firmly established. They conquer the limitations of classical peptide-based approaches by not creating favorable conditions for growth of tumor cell clones that lack the Ags present in the vaccine [5]. Still, therapeutic cancer vaccines have met limited clinical success [6, 7]. In most cases, the immune system is either polarized and/or has a limited tumor-specific T cell repertoire [8, 9].

Several strategies were employed to prepare Ags from whole tumor cells and thus produce a highly immunogenic vaccine. Common strategies include chemical treatment, radiation as well as repetitive freeze/thaw cycles. With these methods, standardized, applicable sources of tumor-specific Ags can be generated. Besides, tumor cell lysates are also useful in high-risk, tumor-free patients—especially for prophylactic approaches.

Lynch syndrome (LS), the most common hereditary cancer syndrome, represents the paragon for cancer vaccination approaches [10–12]. Affected patients suffer from a deleterious germline mutation in one of the mismatch repair genes (MMR) and develop a complex spectrum of solid cancers [13–15]. Having in mind that almost all tumors in LS patients are hypermutated and microsatellite instable (MSI), they are likely to express a huge amount of neo-Ags. These, in turn, may elicit an Ag-specific cytotoxic T-cell response [16].

To move forward in developing vaccination strategies, we employed the $MLH1^{-/-}$ mouse model that resembles features of the human LS counterpart [17, 18]. These mice develop spontaneous tumors at virtually 100% frequency [18] and are suitable for prophylactic as well as therapeutic approaches. Indeed, in our previous studies, we vaccinated mice with an allograft-derived whole tumor lysate [19, 20]. While this approach proved successful, direct transfer into the clinic might be compromised by the fact that tumor lysate preparation is only applicable for previously diseased patients with a high likelihood of relapse. Another critical and limiting factor is the amount of the original material and the timely delivery of the individually tailored vaccine. Hence, we addressed the question of whether cell-line derived tumor lysates might provide an alternative source of highly immunogenic tumor Ags. In a pilot study, we identified different outcomes upon vaccination with two individual cell line-derived lysates in the therapeutic setting [21]. We hypothesized that the mutational signature predicts response. Here, we refined our cell line-tailored vaccination approach aiming at a detailed understanding of the mechanisms underly-ing vaccination efficacy. Our results show that tumor cell lysates delay tumor formation and growth; still, the neo-Ag quality rather than the quantity is predictive for response.

Material and methods

Cell culture and tumor lysate preparation

$Mlh1^{-/-}$ cells (two gastrointestinal tumor (GIT) cell lines: 328, A7450 T1 M1 and one lymphoma cell lines: 1351) were established in our lab. YAC-1 cells were originally cultured in DMEM medium, supplemented with 10% FCS (fetal calf serum), 6 mM Glutamine, and penicillin/streptomycin antibiotics (all from Biochrom, Berlin, Germany). Tumor lysates were prepared from cell cultures in P15 as described [20]. Briefly, confluent cells were harvested and treated with four repetitive freeze/thaw cycles followed by 60 Gy irradiation and protein quantification. Lysate stocks were frozen at − 80 °C and used for in vivo application.

DC generation and co-culture

DCs were generated from murine femur and tibia as described [22]. Briefly, the resulting cell suspension was filtered (100 µm, Greiner-bio one, Kremsmünster, Austria) and centrifuged at 300×g (10 min, 4 °C). Cells were seeded in a 6-well plate (density: 3×10^5 cells/ml). GM-CSF was added (20 ng/ml, Immunotools, Friesoythe, Germany) cells were harvested every third day. Therefore, non-adherent cells were gently pipetted up and down, transferred in a centrifuge tube, pelleted (200×g, 8 min), the supernatant discarded and the pellet resuspended in freshly prepared medium. Cells were counted and re-cultured in DC medium containing GM-CSF with no other cytokines to generate highly pure DCs. On the 9th day, supernatant was collected and centrifuged. DCs were phenotyped using the following FITC-, PE-, APC-, and PE/Cy7-labeled antibodies (1 µg each): anti-CD11c (Biolegend, San Diego, CA), anti-CD83 (Biolegend), anti-CD11b (Immunotools), anti-CD40 (Biolegend), anti-CD80 (Immunotools), anti-CD86 (Immunotools), anti-MHC class I/II (Immunotools), and anti-CD19 (Immunotools). Afterwards, DCs were loaded with protein lysate (50 µg/tumor lysate). After 24 h of incubation, peripheral blood mononuclear cells were added in a ratio of 1:10 (DC:immune cell) [23, 24] and a co-culture was established. On the 5th day, Brefeldin A (5.0 µg/ml Biolegend) was used to enhance intracellular cytokine staining signals. The following fluorescent-labeled antibodies (1 µg each) were used: anti-CD3, anti-CD4, anti-CD8α, anti-CD25 (Immunotools), anti-IFN-γ, and anti-TNF-α (Biolegend). Immunophenotypic changes were determined using flow cytometry (BD FACSVerse™, BD Pharmingen, Heidelberg, Germany).

Visualization of whole exome sequencing data

! e cell lines 328 and A7450 T1 M1 were processed likewise [20, 21] for the visualization. With the complex Heatmap [25] R package, their patterns and correlations were revealed in oncoprint. ! e mutational profiles were filtered for the exclusive SNV separately with mutation filters such as mutation type (missense and nonsense) and those occurring in known annotated genes.

Furthermore, mapping the mutations and their statistics on a linear gene product (proteins of interest) was done with a 'lollipop' mutation diagram generator [30]. Based on the knowledge from the human MMR-D counterpart and general involvement in tumorigenesis, genes for further analysis were chosen with a high probability of mutating.

Mlh1$^{-/-}$ mouse model and in vivo vaccination protocol

Ethical statement

All animal experiments were approved by the German local authority: Landesamt für Landwirtschaft, Lebensmittelsicherheit und Fischerei Mecklenburg-Vorpommern (7221.3-1-026/17), under the German animal protection law and the EU Guideline 2010/63/EU. Mice were bred in the animal facility of the University Medical Center in Rostock under specific pathogen-free conditions. Mlh1 genotyping was done according to [26]. During their whole life-time, all animals received enrichment in the form of mouse-igloos (ANT Tierhaltungsbedarf, Buxtehude, Germany), nesting material (shredded tissue paper, Verbandmittel GmbH, Frankenberg, Deutschland) paper roles (75 × 38 mm, H 0528–151, ssniff-Spezialdiäten GmbH, Soest, Germany), and wooden sticks (40 × 16 × 10 mm, Abedd, Vienna, Austria). During the experiment, mice were kept in type III cages (Zoonlab GmbH, Castrop-Rauxel, Germany) at 12-h dark:light cycle, the temperature of 21 ± 2 °C, and relative humidity of 60 ± 20% with food (pellets, 10 mm, ssniff-Spezialdiäten GmbH, Soest, Germany) and tap water ad libitum.

Experimental protocol

A detailed treatment schedule is provided in Fig. 1. Briefly, prophylactic application was initiated when mice aged 8–10 weeks by four weekly boosts of tumor lysates (10 mg/kg bw, s.c., 328 vaccine: n = 10; A7450 T1 M1 vaccine: n = 9, respectively) followed by monthly applications (a total of 12 vaccinations). Control mice were left untreated (n = 15 mice). For the therapeutic vaccination approach, mice were given 4 weekly boosts. Vaccination was sustained (10 mg/kg bw, biweekly) until tumors progressed (max. 12 injections; n = 8 mice/group). Control mice were left untreated (n = 7 mice). Reduction of suffering during the trial was guaranteed by providing daily prepared soaked pellets, twice-daily monitoring of the health status using a score sheet and by applying humane endpoints (weight loss, any sign of pain or distress, or changes in social behavior). All mice were sacrificed before they became moribund to prevent pain and distress.

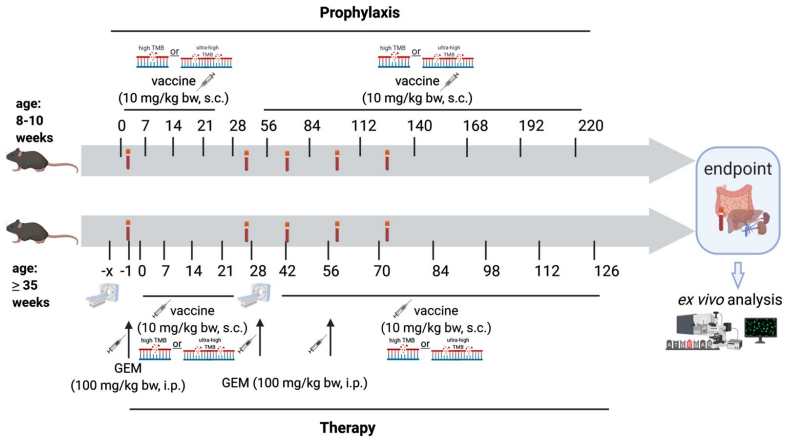

Fig. 1 Vaccination protocol. Mice were either given repetitive prophylactic or therapeutic injections of two different cell line-derived whole tumor lysates. In the case of therapeutic application, mice were additionally given 3 monthly injections of gemcitabine. The scheme was created with BioRender.com

Positron emission tomography/computed tomography (PET/CT) imaging

PET/CT imaging scans were performed on a small animal PET/CT scanner (Inveon PET/CT, Siemens Medical Solutions, Knoxville, TN, USA) according to a standard protocol as described before [19, 20].

Immune phenotyping and immuno"uorescence

Blood samples were taken routinely from the retrobulbar venous plexus. Blood samples were stained with a panel of conjugated monoclonal antibodies (mAb, 1 µg each) followed by lysis of erythrocytes (155 mM NH_4Cl, 10 mM $KHCO_3$ (both MERCK Millipore, Darmstadt, Germany), and 0.1 mM EDTA (Applichem, Darmstadt, Germany). Negative controls consisted of lymphocytes stained with appropriate isotypes (Biolegend, San Diego, USA). Cells were washed, resuspended in PBS and analyzed by flow cytometry on a Flow Cytometer (BD FACSVerse™, BD Pharmingen, CA, USA). Data analysis was performed using BD FACSuite software (BD Pharmingen).

Target proteins in 4 µM cryostat sections of tumor resection specimens were visualized as described [20] and documented on a confocal laser scanning microscope (LSM780, Zeiss, Jena, Germany) using 20× objectives.

Procartaplex Cytokine Assay

Cytokine levels in cell culture supernatants as well as plasma samples were determined according to the manufacturer's instructions of the Procartaplex™ multiplex immunoassay. Measurement as well as cytokine quantification was performed on a Bioplex 2000 (Bio-Rad Laboratories GmbH, Munich, Germany) in combination with the Bio-Plex Manager Software.

IFNγ ELISpot

2.5×10^3 targets/well ($Mlh1^{-/-}$ A7450, $Mlh1^{-/-}$ 328, $Mlh1^{-/-}$ 1351, and YAC-1 cells) were seeded in IFNγ–specific mAb (Mabtech, 3321-3)-coated, 96-well microtiter plates. Peripheral blood leukocytes (5×10^4 cells/well) or splenocytes (1×10^4 cells/well) were added in triplicates and co-cultured overnight. Finally, bound antibody (Mabtech, 3321-6) was visualized by BCIP/NBT (KPL, Gaithersburg, Maryland, USA); spots were counted using an ELISpot reader. Presented are the numbers of IFNγ-secreting cells corrected for background levels counted in the absence of target cells, which was always ≤ 5 spots/well. Target cells without effector cells showed no background level.

Statistics

All values are expressed as mean ± SD. In case of PET/CT data, raw tumor sizes are presented. After proving the assumption of normality (Kolmogorov–Smirnov test), differences between vaccinated and control mice were determined using the unpaired Student's t-test or one-way ANOVA (Bonferroni or Dunnett's multiple comparison). Kaplan–Meier survival analysis was done by applying the log rank (Mantel Cox) test. Statistical analyses were performed using GraphPad Prism 5 (San Diego, CA). % e criterion for significance was set to $p < 0.05$.

Results

In vitro characterization of antigen-sources

In this study, two $Mlh1^{-/-}$ cell lines established from spontaneous GIT were used. % e drug response of the cell lines 328 and A7450 T1 M1 was determined before and revealed no significant differences towards standard cytostatic drugs [19]. By assessing the basal secretion profile from supernatants, we indeed observed substantial variations. Focusing on cytokines associated with immune stimulation, A7450 cells generally secreted higher levels of GM-CSF, IL1b, and IL-18 (Fig. 2a, left panel). While all of these cytokines enhance NK cell activity and foster % 1 cell development, concentration of chemokines responsible for monocyte- and eosinophil-attraction, such as monocyte chemoattractant protein-1(MCP1), MCP3, and Eotaxin was higher in supernatants from 328 cells (Fig. 2a, right panel).

Based on these findings, a co-culture system of tumor-Ags-loaded DCs and lymphocytes was initiated. DCs were established from the bone marrow according to a standard protocol using GM-CSF [22]. We decided to use this method for DC generation because it delivers highly pure DCs (> 90% purity), constituting a mixture of immature and mature DCs (Fig. 2b). By flow cytometry, virtually all cells expressed DC-markers CD11c, CD83 as well as co-stimulatory molecules CD80/86. CD11b was reduced, mainly because of their activation status (Fig. 2b). In the co-culture setting, additional differences were seen in the T cell phenotype (Fig. 2c, d). DC-loaded with A7450 T1 M1 tumor lysate boosted the frequency of $CD3^+CD8^+$ T cells, which were activated and additionally positive for IFNγ. By contrast, the phenotypes of leukocytes from 328 lysate-loaded DCs changed faintly compared to the control (Fig. 2b).

Mutational pro$le of antigen-sources

% e selected genes of the oncoprint are known for the relevance for tumor initiation, progression, apoptosis, and suppressors functions (Fig. 3a). $Mlh1^{-/-}$ tumors harbor mutations in Pik3ca, Msh3, Braf, and/or Kras, and Erbb3 [21]. % e A7450 T1 M1 cell line harbors nonsense and missense single nucleotide variants (SNVs) in the Wnt signaling pathway regulator Apc gene. Further hotspots in pre-selected clinical relevant genes are occurring in tumor suppressors Arid1a as well as Fhit.

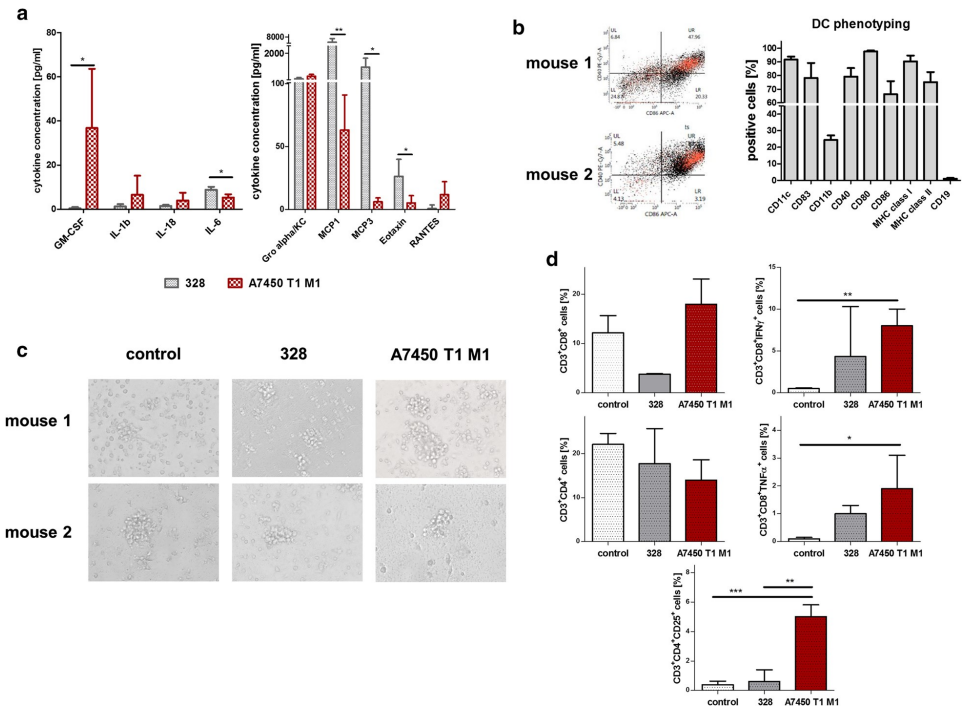

Fig. 2 Secretion profile and in vitro DC culture. **a** Cell culture supernatants were collected and analyzed using the Procartaplex™ multiplex immunoassay. Finally, cytokine and chemokine concentration were determined from three independent experiments. Given are the mean + SD. *p< 0.05; **p< 0.01; unpaired one-sided T-test. **b** Left panel: representative flow cytometry of DCs and right panel: quantitative phenotyping of DCs taken from three individual mice. Non-adherent cells were analyzed. Given are the % numbers of positive cells measured upon gating on viable cells (n = 3 mice). **c** Representative microscopic images of DCs loaded with tumor A7450 T1 M1 or 328 tumor lysate, respectively. Original magnification 10×. **d** Phenotyping of peripheral blood mononuclear cells after co-culture with loaded DCs (DC:immune cell ratio: 1:10). On the 5th day, Brefeldin A was used to enhance intracellular cytokine staining signals. Immunophenotypic changes were determined using flow cytometry, data analyses were performed using BD FACSuite software. Given are the % numbers of positive cells measured upon gating on viable cells. *p < 0.05; **p < 0.01; ***p < 0.001; one-way ANOVA (Bonferroni multiple comparison)

In a direct comparison, alterations are exclusively distributed. ! e cell line 328 acquired more missense SNVs in the pre-selected gene set, especially in EGFR signaling members as well as in Nf1. ! e 328 cell line had additional missense and nonsense Pole mutations. Taking the germline MMR-D into account, the increased number of gene mutations in affected tumor cells is conserved in the cell line 328 compared to A7450 T1 M1 (Fig. 3a).

In Arid1a, all of the 34 SNVs appear before or after the ARID/BRIGHT DNA binding domain (Fig. 3b), regulating cell proliferation, differentiation, and development [27], as well as the SWI/SNF-like complex subunit BAF250/Osa. Every single SNV is exclusive for the corresponding cell line, none are shared, and all of them are missense mutations.

! e prevalence and hotspot mutations in Tcerg1 and Wwox exclusively detected in the 328 cell line are shown in Fig. 3b. ! e mutational hotspot in Tcerg1 is Q1040H within the FF6 domain, the only amino acid change in this gene. FF domains play an essential role in binding the phosphorylated C-terminus of the RNA polymerase II. Furthermore, Tcerg1 is involved in regulating the transcriptional elongation and the pre-mRNA splicing [28]. In Wwox, we found three SNVs, which all affect the short-chain of the dehydrogenase/reductase domain.

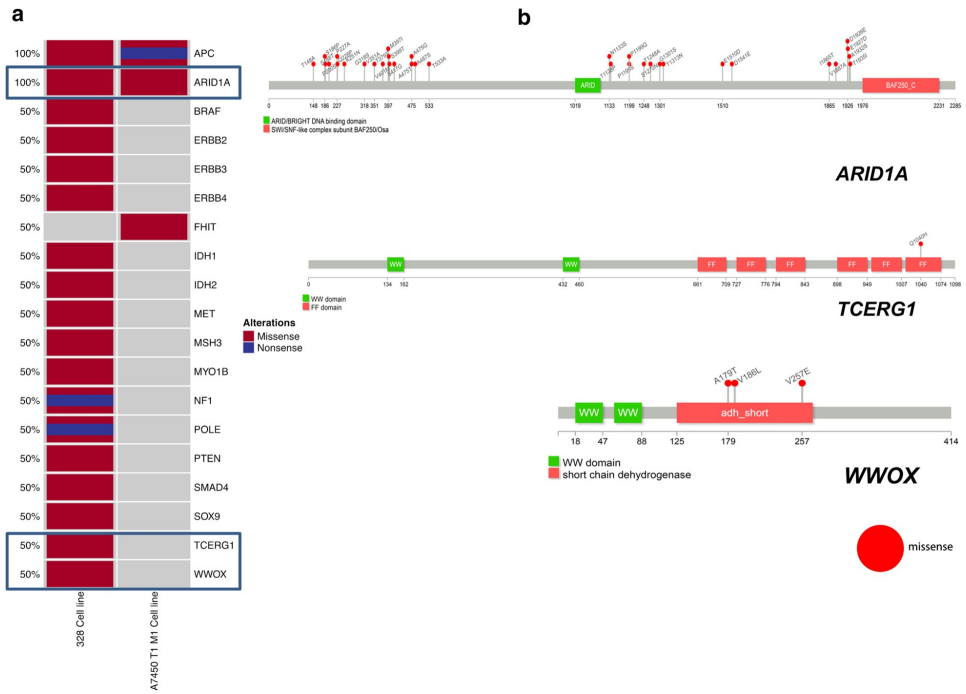

Fig. 3 Human counterpart hotspots in cell line development. **a** The presented oncoprint reveals patterns and correlations of the different cell lines 328 and A7450 T1 M1 with regard to tumor suppressive functions, tumor initiation, and progression. An overview of the non-synonymous alterations in genes of interest (rows) affecting the cell lines (columns) is provided with this way of visualization. **b** Prevalence and hotspot regions in Arid1a, Tcerg1, and Wwox. The colored regions show known gene/ protein domains, while the other regions are represented in dark grey. The missense mutations are depicted as a red lollipop in the cell lines, whereby each lollipop label shows an amino acid change with its corresponding location

For the mutational profile as a potential Ag-source, the MSI pathway [29, 30] and genes associated with MSI status [31] have an impact on survival (based on hazard ratio in the human counterpart) (Table 1). Except for Cope, the theme of exclusive and distinct SNVs within the 328 and A7450 T1 M1 cell lines continues. However, its influence on survival remains elusive and has no impact, since the alterations are yet unknown or silent. Overall, cell line 328 shows a more substantial amount of affected genes associated with overall survival and disease-free survival. #ese are Chmp5, Dhx32, Gadd45b, and Inadl.

#en, the coding microsatellite (cMS) mutational profile was analyzed comparatively on a panel of putative MSI target genes (Table 2 and [18]). Overall, A7450 T1 M1 cells harbored mutations in half of the markers. # e numbers of cMS mutations in 328 cells were lower (37%) and the genes affected differently, highlighting the individual profile even in these molecular closely matched Mlh1$^{-/-}$ cells that harbor the very same germline mutation. Shared mutations were found in seven candidate genes, such as Taf1b, Rfc3, Akt3, and Spen. While these genes are all classified as tumor suppressors, they may have a high likelihood of being causative for this type of tumor. By deciphering the differences between these two samples in more detail, we identified some exclusive mutations in Mlh1$^{-/-}$ A7450 T1 M1 cells whose resulting neo-Ags may have immunogenic potential. # e most promising candidates, in this case, are Senp6 and Rasal2. Consequently, we analyzed the frequency of spontaneous immune reactivity against the neoepitopes derived from a − 1 frameshift mutation in the cMS of these genes. However, in this test, no significant reactivity was detectable

Table 1 SNVs in MLH1$^{-/-}$ cell lines in tumor suppressor genes and potential association with survival

Gene	A7450 T1 M1	328	Survival		
BAX		NA		DFS	
CHMP5		MISSENSE	OS	DFS	DSS
COPE	NONE	SILENT	Unknown		
DHX32		SILENT	OS	DFS	
DYNLT3		NA		DFS	
GADD45B		NA	OS	DFS	DSS
INADL		NA	OS	DFS	DSS
MTRF1		NA		DFS	
NME7	NONE		OS	DFS	DSS
RAC3		SILENT	Unknown		
SNRNP40	NONE			DFS	
SRP9	NONE		Unknown		
TMEM14C	NONE		Unknown		

Based on COX p-value < 0.05

OS overall survival, *DFS* disease-free survival, *DSS* disease-speci"c survival

(data not shown), making these candidates unlikely to act as tumor rejection Ags.

Prolonged survival in the prophylactic setting

To test the immunogenicity of whole cancer vaccines on a more global level, Mlh1$^{-/-}$ mice received two independent tumor lysates, either harboring high (= 328, 167 mutations/Mb) or moderate (= A7450 T1 M1, 27 mutations/Mb) TMB [21] (Fig. 1).

Prophylactic vaccination yielded significantly prolonged cancer-free survival in Mlh1$^{-/-}$ A7450 T1 M1-treated mice. Median survival time was 37 weeks, whereas it was only 22 weeks in control mice ($p < 0.001$). " e Mlh1$^{-/-}$ 328 vaccine had a minor impact on survival, reaching a median survival of 25 weeks (Fig. 4a). " e tumor spectrum observed in this study largely covers the distribution seen in Mlh1$^{-/-}$ mice. Two thirds of Mlh1$^{-/-}$ A7450 T1 M1-treated mice developed GIT or generalized lymphomas in the spleen; remaining mice developed lymphomas in the thymus (1 case), skin malignancies (1 case) or died spontaneously (2 cases). Mice receiving the Mlh1$^{-/-}$ 328 tumor lysate showed a comparable tumor spectrum. Here, 70% suffered from GIT or generalized lymphomas in the spleen, one mouse developed a thymic lymphoma, and two mice died because of unknown malignancy (suspected lymphomagenesis).

" e survival benefit of mice vaccinated with the Mlh1$^{-/-}$ A7450 T1 M1 lysate was reflected by immunological changes in the peripheral blood. While T cell numbers only gradually increased, we observed elevated levels of circulating NK cells (Fig. 4b).

" en, the reactivity of peripheral blood leukocytes was assessed upon co-incubation with different target cells by IFNγ-ELISpot assay (Fig. 5a). Autologous Mlh1$^{-/-}$ tumor targets triggered IFNγ secretion of lymphocytes from vaccinated mice. " e highest reactivity was seen between days 56 and 84 and mainly against target cells that were used for vaccination. We even observed differences between the two vaccines; A7450 T1 M1 cells evoked IFNγ secretion more effectively from lymphocytes than 328 cells ($p < 0.01$). In line with the increased number of NK cells upon A7450 T1 M1 vaccination, leukocytes from vaccinated mice reacted against NK target cells YAC-1 ($p < 0.01$).

Tumor microenvironment

Next, the tumor microenvironment was studied in detail to explore the quantity and quality of leukocyte infiltrates. Prophylactic vaccination leveraged the microenvironment (Fig. 5b). " e Mlh1$^{-/-}$ A7450 T1 M1 vaccine largely prevented infiltration of CD11b^{+}/Gr1^{+} myeloid-derived suppressor cells and F4/80^{+} tumor-associated macrophages (TAMs). While these cell types were barely detectable, we observed high numbers of infiltrating CD11c^{+} DCs as well as CD8^{+} cytotoxic T cells (CTL). By contrast, the Mlh1$^{-/-}$ 328 lysate triggered MDSC infiltration in the tumor, CTL were occasionally found. PD1 expression was not altered by any vaccination and, thus, expression levels were highly comparable with control tumors.

Therapeutic vaccination

" en, we moved to the therapeutic approach (Fig. 1). " e survival benefit of mice treated with a lysate from the Mlh1$^{-/-}$ A7450 cells compared to the 328 lysate was shown before [21] and (Fig. 6a). Here, the median over-all survival was 11 weeks. By contrast, the 328 lysate failed to improve outcome, which was slightly longer than in untreated control mice (5 vs. 4 weeks). To see whether treatment can be improved by adding low-dose chemotherapy, the vaccination protocol was extended by gemcitabine given one day before treatment initiation, followed by 2 monthly injections (Figs. 1, 6a). With this combined chemo-vaccine, survival was prolonged in mice treated with cell-line derived tumor lysates 328 (9 weeks; $p < 0.05$ vs. control). With regard to the A7450 T1 M1+chemo group, there was a trend towards longer progression-free survival, yet this did not reach statistical significance (hazard ratio: 0.9).

Accompanying PET/CT imaging largely reflected the survival data (Fig. 6b). 328-vaccinated tumors progressed, with no gross changes compared to untreated controls. Gemcitabine in conjunction with the lysate yielded stable

Table 2 Mutational pro!le of MLH1$^{-/-}$ derived cell lines using an in-house panel of cMS marker

cMS Marker	APC	Tmem60	Senp6	Phactr4	Aste1	Taf1b	Sdccag1	Rasal2	Lig4	Bend5	Supt16	C8a	Kcnma1	Rfc3	ERCC5	DNAJC2	IL1F9	Clock	Akt3	Spen	Frequency	
Sample/ Repeat	A8	A8	A11	A10	A8	A8	A11	A8	A9	A8	A8	T8	A10	A10	A9	A8	A10	T9	T8	A8	(n)	(%)
328	wt	−1/−2	wt	wt	wt/−1	wt/−1	wt	wt	wt/−1	wt	wt/−1	wt	wt/−1	wt/−1	wt	−1	−1	wt/−1	wt/−1	wt/−1	12/32	37.50
7450 T1 M1	wt/−1	wt	wt/−1	−1	wt	wt/−1	−1	wt/−1	−1	wt/−1/−2	−1	MSI	wt/−1	wt/−1	wt/−1	wt	−1	wt	wt/−1	wt/−1	16/32	50.00

wt: wildtype; wt/−1: heterozygous mutation; −1: homozygous mutation

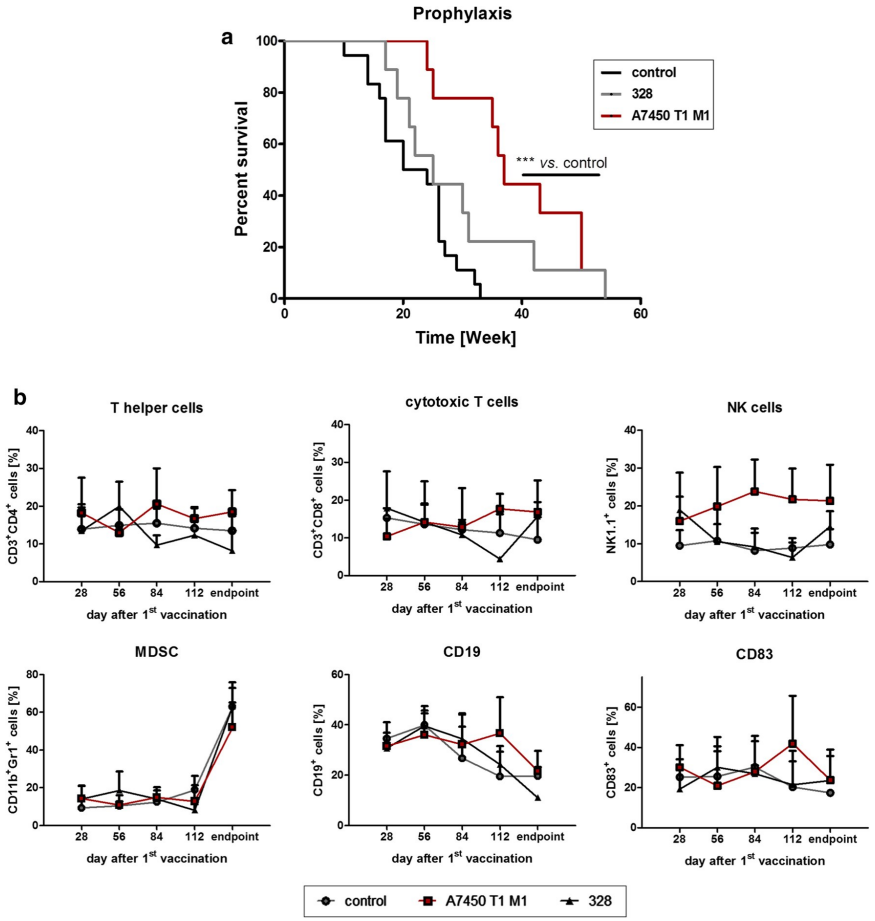

Fig. 4 Prophylactic approach. Mice received repetitive local applications of the Mlh1$^{-/-}$ A7450 T1 M1 and Mlh1$^{-/-}$ 328 vaccine, respectively (10 mg/kg bw, s.c., n = 9 mice/group). Control mice were left untreated (n = 15 mice). **a** Kaplan–Meier survival curve analysis. *p< 0.001 A7450 T1 M1 vs. control; Log-rank (Mantel–Cox) test. **b** Immune phenotyping of peripheral blood was done before and during the course of vaccination until the experimental endpoint. Samples were analyzed by flow cytometry on a FACSVerse™, data analyses were performed using BD FACSuite software. Given are the % numbers of positive cells measured upon gating on viable cells

disease. ! e same was true for tumors treated with the A7450 T1 M1 lysate, showing virtually no progression during the 1st weeks of treatment. Here again, combined chemo-immunotherapy improved tumor growth control. Individual tumors even tended to shrink (Fig. 6b). Still, the antitumoral stimulus provided by the combined chemo-vaccine was not strong enough to induce long-term regression, and tumors finally progressed.

Immunological changes upon vaccination

!erapeutic vaccination altered splenic immune cell composition. Spleens from 328-vaccinated mice tended to have reduced amounts of CTL (Fig. 6c). Levels of CD11b^{+}Gr1^{+} MDSC as well as CD69^{+} activated T cells remained similar to controls. Gemcitabine had no impact on immune cell distribution at all. Spleens from mice

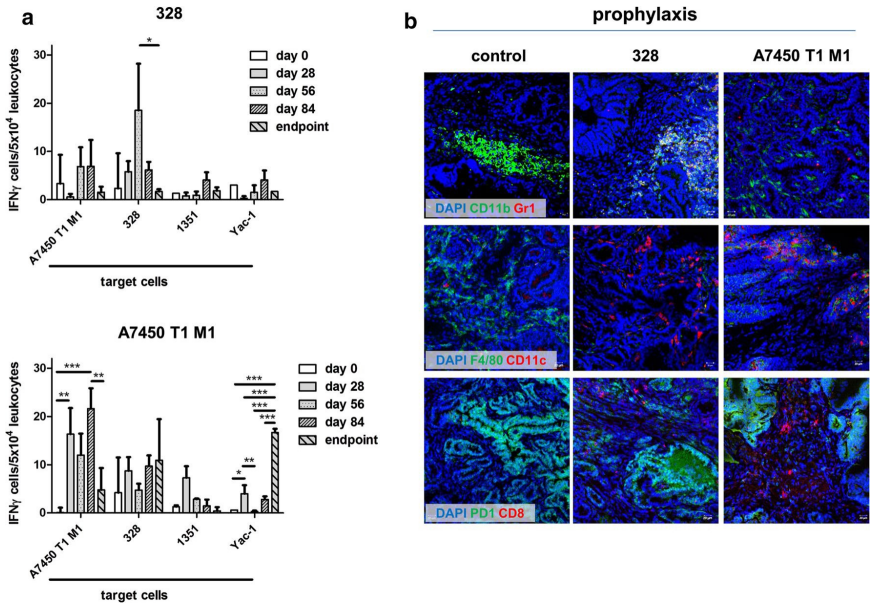

Fig. 5 IFNγ ELISpot and tumor microenvironment. **a** Reactivity of peripheral blood leukocytes against Mlh1$^{-/-}$ target cells as assessed during vaccination and at the experimental endpoint. The number of IFNγ secreting cells/5 × 10^4 effector cells was determined after overnight co-incubation and quantification on an ELISpot reader as described in material and methods. *p< 0.05; **p< 0.01; ***p< 0.001 one-way ANOVA (Bonferroni multiple comparison). **b** Immunofluorescence was done on 4 µM slides stained with mAbs as stated in "Material and methods" section. Cell nuclei were stained with DAPI. Control tumors were highly infiltrated with CD11b$^+$ granulocytes and F4/80$^+$ macrophages. The infiltration pattern changed dependent on the vaccine. Analyses were done on a laser scanning microscope (Zeiss) using 20× objectives

receiving the chemo-vaccine combinations had similar phenotypes as those treated with the 328 vaccine alone.

In contrast, the immune phenotype of spleens from A7450 T1 M1-vaccinated mice positively changed with significantly lower numbers of MDSCs but higher levels of activated CD69$^+$ T cells (Fig. 6c). "is effect was even independent of gemcitabine and thus related to the vaccine itself. Accompanying functional ELISpot analysis confirmed these findings with high reactivity against autologous target cells A7450 T1 M1 (Fig. 6d). Leukocytes from mice treated with the chemo-vaccine combination tended to have higher reactivity against NK cell targets YAC-1 compared to those getting the A7450 T1 M1 monotherapy. In line with the results from the prophylactic setting, there was no cross-reactivity against other Mlh1$^{-/-}$ tumor targets, i.e. 328 and 1351.

We finally examined whether alterations were evident on tumor resection specimens in situ. Generally, A7450 T1 M1 vaccinated tumors were more infiltrated than 328-treated tumors (Fig. 7). By delineating mice that had no response from those achieving stable disease in PET/CT, we indeed found clear differences in the tumor microenvironment. Tumors of short-term survivors (328) were highly infiltrated with TAMs and had higher numbers of LAG-3- and PD-L1-expressing lymphocytes (Fig. 7). Granulocytes were rarely detectable. Resection specimens from long-term survivors harbored few TAMs, virtually no MDSCs or LAG-3$^+$ lymphocytes. Hence, these data nicely reflect the in vivo response.

Discussion

Here, we used the Mlh1$^{-/-}$ mouse model and examined the protective value of two individual cancer vaccines made from autologous tumor cell cultures with different TMB [21]. "e two cell lines, 328 and A7450 T1 M1, show exclusively distributed non-synonymous alterations in the pre-selected clinical hotspot regions. Every single amino acid appears exclusively, with Arid1a and Apc, being the only genes shared from both cell lines. "is clearly shows that the tumors develop differently apart from the host, and with SNVs mainly affecting binding domains as well as occurring in tumor suppressors and

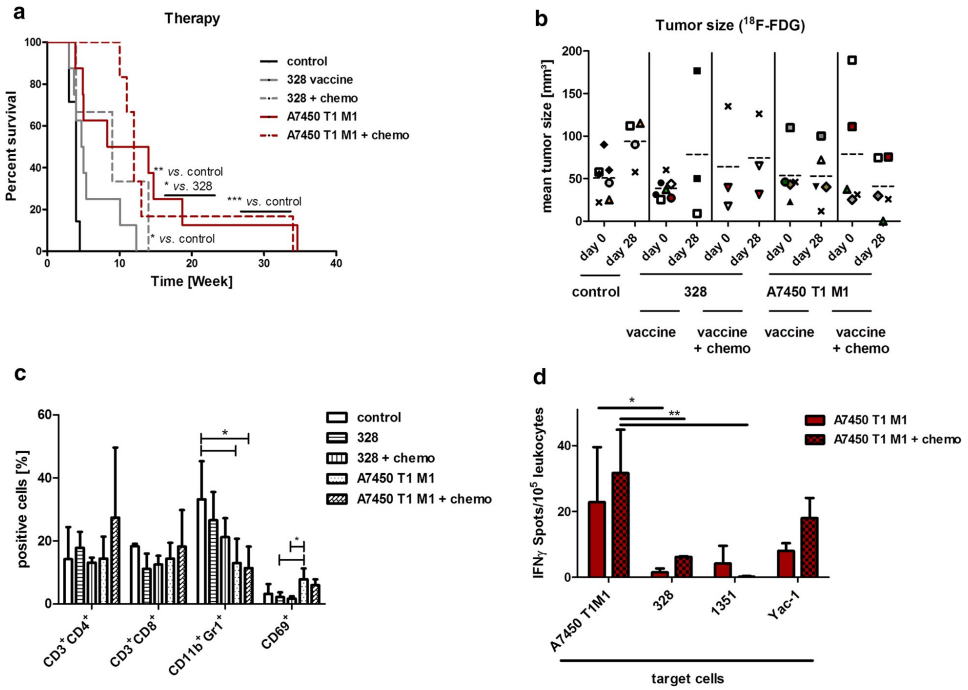

Fig. 6 Therapeutic approach. Mice received repetitive local applications of cell line derived vaccines A7450 T1 M1 and 328, respectively (10 mg/kg bw, s.c., n = 8 mice/group). Control mice were left untreated (n = 7 mice). Combined chemo-vaccination was done by adding gemcitabine (100 mg/kg bw; Mlh1$^{-/-}$ A7450 T1 M1: n = 6 and 328: n = 3 mice). **a** Kaplan–Meier survival curve analysis. *p < 0.05 328 + chemo vs. control; **p < 0.01 A7450 T1 M1 vs. control; *p < 0.05 A7450 T1 M1 vs. 328; Log-rank (Mantel–Cox) Test. **b** Mean tumor size determined by ^{18}F-FDG PET/CT. In vivo imaging was done before and during vaccination. Tumors sizes were quantified using the inveon software. The symbols were standardized between day 0 and day 28, and each symbol is representative of one mouse (average tumor size in given resulting from the detected number of tumors/mouse). **c** Flow cytometry of splenic leukocytes. Phenotyping was done on splenocytes from control (n = 5) and vaccinated mice receiving monotherapy (328 and A7450 T1 M1, 3–5 mice/group) or combinations with gemcitabine (n = 3–5 mice/group). * p < 0.05; one-way ANOVA (Dunnett's multiple comparison). **d** IFNγ ELISpot. Reactivity of splenocytes against MLH1$^{-/-}$ target cells as assessed at the experimental endpoint. The number of IFNγ secreting cells/5 × 10^4 effector cells was determined after overnight co-incubation and quantification on an ELISpot reader as described in material and methods. *p < 0.05; **p < 0.01; one-way ANOVA (Bonferroni multiple comparison)

interfering with the MSI status and/or the MSI signaling pathway.

By using cell lines for vaccination, this approach provides a virtually limitless source of neo-Ags, permits standardized, large-scale vaccine production, and is—from the economic point of view—very cost-effective [5]. To get an idea on the mutanome, whole-exome sequencing was performed on both cell lines in the very same passage later used for in vivo vaccination. Hypothetically, the number of neo-Ags correlates with immune activation and consequently, treatment outcome. However, we here provide evidence that the neo-Ag quality outranks quantity. By applying two vaccines that harbor the very same germline mutation, only one was able to activate T cells in vitro and mediated a survival benefit in the prophylactic situation. # e 328 cell line was established directly from an ultra-hypermutated GIT with aggressive in situ growth behavior. Indeed, the mutations found in this cell line were mostly associated with a worse prognosis. # e cell line A7450 T1 M1 was made from a moderately mutated GIT allografted in Mlh1$^{\pm}$ mice that gave rise to stable in vitro growth [21]. While these two cell lines show no significant differences in growth kinetics, phenotype (MHC-I$^+$, IDO^{low}, PD-L1$^+$)

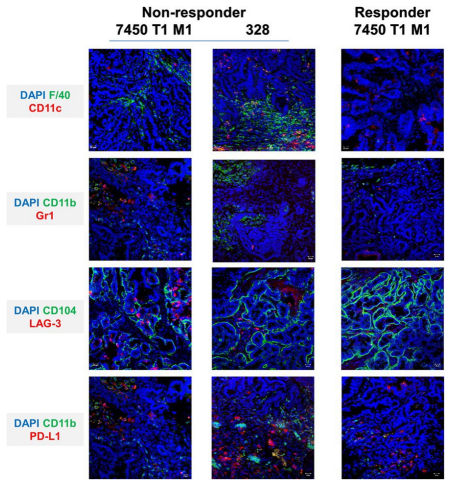

Fig. 7 Tumor microenvironment. Immunofluorescence was done on 4 µM slides stained with mAbs as stated in the material and methods section. Cell nuclei were stained with DAPI. Representative images are given showing either GIT in which treatment failed (left panel) or, as in the case of A7450 T1 M1, treatment succeeded. Differences in leukocytic infiltration are evident. Analyses were done on a laser scanning microscope (Zeiss) using 20× objectives

and drug response [19], their cytokine secretion profile greatly varies. A7450 T1 M1 cells secreted cytokines associated with favorable prognosis at least in colorectal cancer (such as GM-CSF, IL-1b) [32], with known ability to enhance NK cell activity and foster ! 1 cell development. By contrast, the secretion profile of 328 cells nicely matched with a prototypic immunosuppressive cell line. ! e high inter-individual heterogeneity was further validated by additional mutational analysis that focused on cMS mutations, which are exclusive for MMR-D tumors. In fact, these two cell lines harbored only a few shared cMS mutations. By examining the spontaneous immune reactivity against selected neoepitopes, we, however, failed to observe significant reactivity, leaving the neo-Ags that confer immune responses unidentified. Still, the survival benefit of Mlh1$^{-/-}$ A7450 T1 M1 vaccinated mice compared to those receiving the 328 lysate was reflected by systemic immunological changes. T cell numbers gradually increased, and mice had elevated levels of circulating NK cells, recognizing autologous target but also YAC-1 cells in ELISpot IFNγ assays. NK cells are a subset of innate lymphocytes with great potential to kill cancer cells directly, and thus, the elevated number of NK cells detected here may have also prevented early tumor formation [33–35]. Due to the sustained immunological pressure on (premalignant) tumor cells and the process of cancer editing, it is tempting to speculate that cancer cells either escaped NK cell control or directly induced loss of the NK cells' cytotoxic ability. ! e latter was just recently shown in a preclinical breast cancer model and uncovers novel clues on how cancer cells escape NK cell surveillance [36]. Still, the vaccine itself stimulated both arms of the immune system. ! o u g h this immune activating stimulus was not strong enough to prevent tumor formation it altered the microenvironment, especially upon Mlh1$^{-/-}$ A7450 T1 M1 vaccination. Here, numbers of tumor-infiltrating CD11c^{+} DCs were elevated; tumor-promoting MDSCs and TAMs low and provide a reasonable explanation for the delayed in vivo tumorigenesis compared to 328-vaccinated mice.

! e r a p e u t i c application prolonged progression-free survival, but again only when mice received the A7450 T1 M1 vaccine. ! e ultra-hypermutated-derived lysate 328 failed to provide a clear survival benefit. Adding chemotherapy to either vaccination improved the outcome by inducing long-term stable disease (≥ 4 weeks). Once more, tumor growth control was more effective in the A7450 T1 M1 combination group, assuming that the coupled application of the tumor lysate and low-dose chemotherapy induced immunogenic cell death. ! i s converted dying cancer cells into a vaccine vulnerable to be taken up by DC. ! e s e, in turn, activated T cells to kill tumor targets. In support of this, half of the mice received partial remission. Here, chemotherapy itself may play a supportive role in re-activating the immune system against Mlh1$^{-/-}$ tumors. Other preclinical studies likewise described boosted Ag cross-presentation, increased immune-supportive M1 macrophages, as well as circulating T cells upon gemcitabine [37, 38]. Indeed, spleens from treated mice in this study had higher numbers of activated T cells and significantly lower MDSC level. By unraveling the tumor microenvironment, differences became much more apparent, and tumors of long-term survivors had fewer immunosuppressive infiltrates (MDSCs, TAMs) than those that failed to respond. Whether responding tumors harbored less immunosuppressive infiltrates per se and were therefore better treatable by the given therapy or the applied regimen actively eliminated TAMs and MDSCs is a matter of speculation. Generally, the efficacy of cancer immunotherapy seems to be negatively correlated with MDSCs frequency and function [39, 40]. Still, a one-size-fits-all model does not exist. In pancreatic cancer patients, for instance, a high pre-vaccination MDSC value did not preclude an immune response [41], whereas higher MDSCs levels were associated with lower response rate in metastatic melanomas [42]. While most of these studies assessed pre-vaccination peripheral blood levels as biomarkers, the association between the attraction of immunosuppressive cells into

the tumor and the development of secondary resistance to immunotherapy is yet unknown. Several extrinsic as well as intrinsic factors foster resistance, especially after initial response. Treatment failure might be finally attributable to insufficient T-cell responses (transient, low avidity, low magnitude); poor T-cell homing to $MIh1^{-/-}$ tumors, dysfunction or death of T cells within the tumor, and immune escape mediated by upregulation of immune-checkpoint molecules LAG-3 and PD-L1. Hence, the balance between immune-mediated tumor prevention/elimination and escape is a narrow ridge [43, 44]. A previous study identified several potential therapy-resistance genes, confirmed in CRISPR-based screens [45]. IFNγ—initially associated with tumor immunity also enhances the activation of the PD-1 signaling axis. Indeed, we also diagnosed higher numbers of LAG-3- and PD-L1-expressing lymphocytes in tumors of short-term survivors (mainly 328), while resections specimens from long-term survivors harbored virtually no $LAG\text{-}3^{+}$ lymphocytes.

In humans, MMR-D tumors are often characterized by an increased density of intratumoral T cells and most patients are eligible to immunotherapy. Still, we here add evidence that the neo-Ag quality, rather than quantity defines response. #ese findings are supported by a recent study comparing pancreatic cancer and melanoma Ag load and T cell responses [46]. While the number of potential neo-Ags in pancreatic cancer samples was an order of magnitude lower than in melanoma, almost every tumor had a mutation that resulted in a predicted neo-Ag [47]. Comparable results were reported in hepatocellular carcinoma where the number of predicted neo-Ags did unexpectedly not correlate with effector and regulatory immune cell infiltration [48]. To discriminate immunogenic epitopes from a background set of mutated peptides, non-synonymous mutations should principally confer antitumoral vaccine activity. Hence, we tested the spontaneous immune response against a panel of putative immunogenic peptides. Still, in this setting no significant immune response was detectable, leaving the exact tumor rejection Ags unidentified.

To improve vaccine efficacy prospectively, some additional aspects must be considered: (I) the choice of the right target Ags, whose mutation frequency is high and ideally shared among cancers; (II) the time-interval and dosing of vaccines; (III) the route of application; (IV) the choice of adjuvant and/or combinatorial agent as well as (V) a change of the standard of care in humans from the tumor to the host by treating patients with immunotherapy in first-line and thus before a history of previous anti-cancer chemotherapy.

Finally, we would like to mention that there are some limitations to this study. Firstly, we only injected vaccines without additional adjuvants that might play a supporting role in immune stimulation. Secondly, mice were vaccinated with a lysate of only one cell line instead of different ones. Hence, there is a possibility that we have missed certain Ags that evoke immune responses when applied together and thus individual tumor clones may have been unrecognized.

Conclusions

Prophylactic as well as therapeutic vaccination with whole tumor lysates delay tumor growth. Still, not only tumor mutational burden but also neoantigen quality predict vaccination efficacy. In addition to the number of mutations provided by a vaccine, the ability to evoke T cell responses and induce an inflamed tumor microenvironment is crucial for treatment responses.

Abbreviations

Ag: Antigen; cMS: Coding microsatellite; DC: Dendritic cell; GIT: Gastrointestinal tumor; MDSC: Myeloid-derived suppressor cells; MMR-D: Mismatch repair deficiency; TAM: Tumor-associated macrophages; TMB: Tumor mutational burden; MSI: Microsatellite instability.

Acknowledgements

We gratefully thank Mrs. Ilona Klamfuss for breeding mice, Brigitte Vollmar and Bernd Krause for their continuous support in their efforts of chairing the Core Facility of Multimodal Small Animal Imaging. We also gratefully acknowledge the excellent technical assistance of Mrs. Joanna Förster. Furthermore, we thank Carina Bergner and Anja Gummesson, radiopharmacy team of the Department of Nuclear Medicine of the University Medical Centre Rostock, for providing ^{18}F-FDG for the small animal PET/CT experiments.

Authors' contributions

CM—conducted the study, performed the experiments, analyzed data and wrote the manuscript; YSG—analyzed whole exome sequencing data; IS, SK, and OH—performed in vivo and in vitro experiments; CJ—critically revised the manuscript. All authors read and approved the final manuscript.

Funding

Open Access funding enabled and organized by Projekt DEAL. This work was supported by grants from the German research foundation to CM [DFG Grant numbers MA5799/2-1 and MA5799/2-2].

Availability of data and materials

The datasets used and/or analyzed during the current study are available from the corresponding author on reasonable request.

Consent for publication

All authors have agreed to publish this article.

Competing interests

"No potential conflict of interest was reported by the authors."

Author details

[1] Department of Medicine, Clinic III-Hematology, Oncology, Palliative Care, Rostock University Medical Center, Ernst-Heydemann-Str. 6, 18057 Rostock, Germany. [2] Institute for Biostatistics and Informatics in Medicine and Ageing Research (IBIMA), Rostock University Medical Center, University of Rostock, 18057 Rostock, Germany. [3] Faculty of Biosciences, Heidelberg University, 69120 Heidelberg, Germany. [4] Division of Applied Bioinformatics, German Cancer Research Center (DKFZ) and National Center for Tumor Diseases (NCT), Heidelberg, Germany. [5] Department of Cell Biology, Rostock University Medical Center, 18057 Rostock, Germany.

Received: 3 August 2020 Accepted: 12 October 2020
Published online: 21 October 2020

References

1. NH Sarkar DH Moore 1978 Immunization of mice against murine mammary tumor virus infection and mammary tumor development Cancer Res 38 1468 72
2. FE González A Gleisner F Falcón-Beas F Osorio MN López F Salazar-Onfray 2014 Tumor cell lysates as immunogenic sources for cancer vaccine design Hum Vaccines Immunother 10 3261 9 https://doi.org/10.4161/21645515.2014.982996
3. S Hazama K Tamada Y Yamaguchi Y Kawakami H Nagano 2018 Current status of immunotherapy against gastrointestinal cancers and its biomarkers: perspective for precision immunotherapy Ann Gastroenterol Surg 2 289 303
4. WL Redmond SN Linch 2016 Combinatorial immunotherapeutic approaches to restore the function of anergic tumor-reactive cytotoxic CD8(+) T cells Hum Vaccines Immunother 12 2519 2522
5. VI Seledtsov AG Goncharov GV Seledtsova 2015 Clinically feasible approaches to potentiating cancer cell-based immunotherapies Hum Vaccines Immunother 11 851 869
6. S Martin Lluesma A Wolfer A Harari L Kandalaft 2016 Cancer vaccines in ovarian cancer: how can we improve? Biomedicines 4 10
7. TC Wirth F Kühnel 2017 Neoantigen targeting—Dawn of a new era in cancer immunotherapy? Front Immunol 8 1848
8. U Sahin Ö Türeci 2018 Personalized vaccines for cancer immunotherapy Science (80–) 359 1355 60 https://doi.org/10.1126/science.aar7112
9. MJ Elsas van T Hall van SH Burg van der 2020 Future challenges in cancer resistance to immunotherapy Cancers 12 935
10. A Spira ML Disis JT Schiller E Vilar TR Rebbeck R Bejar 2016 Leveraging premalignant biology for immune-based cancer prevention Proc Natl Acad Sci 113 10750 10758
11. K Chang MW Taggart L Reyes-Uribe E Borras E Riquelme RM Barnett 2018 Immune profiling of premalignant lesions in patients with lynch syndrome JAMA Oncol 4 1085 1092
12. M Kloor M Knebel Doeberitz Von 2016 The immune biology of microsatellite-unstable cancer Trends Cancer 2 121 33 https://doi.org/10.1016/j.trecan.2016.02.004
13. H Binder L Hopp MR Schweiger S Hoffmann F Juhling M Kerick 2017 Genomic and transcriptomic heterogeneity of colorectal tumours arising in Lynch syndrome J Pathol 243 242 254
14. P Moller T Seppala I Bernstein E Holinski-Feder P Sala DG Evans 2017 Cancer incidence and survival in Lynch syndrome patients receiving colonoscopic and gynaecological surveillance: first report from the prospective Lynch syndrome database Gut 66 464 472
15. HT Lynch PM Lynch SJ Lanspa CL Snyder JF Lynch CR Boland 2009 Review of the Lynch syndrome: history, molecular genetics, screening, differential diagnosis, and medicolegal ramifications Clin Genet 76 1 18
16. S Majumder R Shah J Elias M Manoharan P Shah A Kumari 2018 A cancer vaccine approach for personalized treatment of Lynch Syndrome Sci Rep 8 1 14
17. W Edelmann K Yang M Kuraguchi W Edelmann K Yang M Kuraguchi 1999 Tumorigenesis in Mlh1 and Mlh1/Apc1638N mutant mice Cancer Res 59 1301 7
18. C Maletzki F Beyrich M Hühns E Klar M Linnebacher 2016 The mutational profile and infiltration pattern of murine MLH1-/-tumors—concurrences, disparities and cell line establishment for functional analysis Oncotarget 7 53583
19. C Maletzki L Wiegele I Nassar J Stenzel C Junghanss 2019 Chemo-immunotherapy improves long- term survival in a preclinical model of MMR-D-related cancer J ImmunoTher Cancer 7 1 14
20. C Maletzki YS Gladbach M Hamed G Fuellen M-L Semmler J Stenzel 2018 Cellular vaccination of MLH1 − / − mice—an immunotherapeutic proof of concept study Oncoimmunology 7 e1408748
21. YS Gladbach L Wiegele M Hamed AM Merkenschläger G Fuellen C Junghanss 2019 Unraveling the heterogeneous mutational signature of spontaneously developing tumors in MLH1$^{-/-}$ mice Cancers 11 1485
22. MB Lutz N Kukutsch AL Ogilvie S Rößner F Koch N Romani 1999 An advanced culture method for generating large quantities of highly pure dendritic cells from mouse bone marrow J Immunol Methods 223 77 92
23. UE Höpken I Lehmann J Droese M Lipp T Schüler A Rehm 2005 The ratio between dendritic cells and T cells determines the outcome of their encounter: proliferation versus deletion Eur J Immunol 35 2851 2863
24. M Dauer B Obermaier J Herten C Haerle K Pohl S Rothenfusser 2003 Mature dendritic cells derived from human monocytes within 48 hours: a novel strategy for dendritic cell differentiation from blood precursors J Immunol 170 4069 4076
25. Z Gu R Eils M Schlesner 2016 Complex heatmaps reveal patterns and correlations in multidimensional genomic data Bioinformatics 32 2847 2849
26. W Edelmann K Yang M Kuraguchi J Heyer M Lia B Kneitz 1999 Tumorigenesis in Mlh1 and Mlh1 / Apc1638N mutant mice Cancer Res 59 1301 1307
27. J Iwahara M Iwahara GW Daughdrill J Ford 2002 The structure of the Dead ringer-DNA complex reveals how AT-rich interaction domains (ARIDs) recognize DNA EMBO J 21 1197 209
28. J Liu S Fan CJ Lee AL Greenleaf P Zhou 2013 Specific interaction of the transcription elongation regulator TCERG1 with RNA polymerase II Requires simultaneous phosphorylation at Ser2, Ser5, and Ser7 within the carboxyl-terminal domain repeat J Biol Chem 288 10890 901
29. DN Slenter M Kutmon K Hanspers A Riutta J Windsor N Nunes 2018 WikiPathways: a multifaceted pathway database bridging metabolomics to other omics research Nucleic Acids Res 46 D661 D667
30. M Kanehisa S Goto 2000 KEGG: kyoto encyclopedia of genes and genomes Nucleic Acids Res 28 27 30
31. C Yu H Hong S Zhang Y Zong J Ma A Lu 2019 Identification of key genes and pathways involved in microsatellite instability in colorectal cancer Mol Med Rep 19 2065 2076
32. CA Nebiker J Han S Eppenberger-Castori G Iezzi C Hirt F Amicarella 2014 GM-CSF production by tumor cells is associated with improved survival in colorectal cancer Clin Cancer Res 20 3094 106
33. B Isaacson O Mandelboim 2019 Natural killer cells control metastasis via structural editing of primary tumors in mice Cancer Immunol Immunother 68 1721 4
34. M Alvarez F Simonetta J Baker AR Morrison AS Wenokur A Pierini 2020 Indirect impact of PD-1/PD-L1 blockade on a murine model of NK cell exhaustion Front Immunol 11 7 https://doi.org/10.3389/fimmu.2020.00007/full
35. CIM Dahlberg D Sarhan M Chrobok AD Duru E Alici 2015 Natural killer cell-based therapies targeting cancer: possible strategies to gain and sustain anti-tumor activity Front Immunol 6 605
36. IS Chan H Knútsdóttir G Ramakrishnan V Padmanaban M Warrier JC Ramirez 2020 Cancer cells educate natural killer cells to a metastasis-promoting cell state J Cell Biol 219 e202001134
37. L Rettig S Seidenberg I Parvanova P Samaras A Knuth S Pascolo 2011 Gemcitabine depletes regulatory T-cells in human and mice and enhances triggering of vaccine-specific cytotoxic T-cells Int J Cancer 129 832 838
38. E Suzuki V Kapoor AS Jassar LR Kaiser SM Albelda 2005 Gemcitabine selectively eliminates splenic Gr-1+/CD11b + myeloid suppressor cells in tumor-bearing animals and enhances antitumor immune activity Clin Cancer Res 11 6713 6721
39. GL Hansen G Gaudernack PF Brunsvig M Cvancarova JA Kyte 2015 Immunological factors influencing clinical outcome in lung cancer patients after telomerase peptide vaccination Cancer Immunol Immunother 64 1609 21
40. A Martens K Wistuba-Hamprecht M Geukes Foppen J Yuan MA Postow P Wong 2016 Baseline peripheral blood biomarkers associated with clinical outcome of advanced melanoma patients treated with ipilimumab Clin Cancer Res 22 2908 18
41. NE Annels VE Shaw RF Gabitass L Billingham P Corrie M Eatock 2014 The effects of gemcitabine and capecitabine combination chemotherapy and of low-dose adjuvant GM-CSF on the levels of myeloid-derived suppressor cells in patients with advanced pancreatic cancer Cancer Immunol Immunother 63 175 83
42. J Weber G Gibney R Kudchadkar B Yu P Cheng AJ Martinez 2016 Phase I/II study of metastatic melanoma patients treated with nivolumab who had progressed after ipilimumab Cancer Immunol Res 4 345 53
43. JL Benci B Xu Y Qiu TJ Wu H Dada C Twyman-Saint Victor 2016 Tumor interferon signaling regulates a multigenic resistance program to immune checkpoint blockade Cell 167 1540 1554.e12
44. CL Slingluff 2020 Building on the promise of cancer vaccines for solid tumors Clin Cancer Res 26 529 31

45. RT Manguso HW Pope MD Zimmer FD Brown KB Yates BC Miller 2017 In vivo CRISPR screening identifies Ptpn2 as a cancer immunotherapy target Nature 547 413 418
46. P Bailey DK Chang MA Forget FAS Lucas HA Alvarez C Haymaker 2016 Exploiting the neoantigen landscape for immunotherapy of pancreatic ductal adenocarcinoma Sci Rep 6 35848
47. JS Bowers SR Bailey MP Rubinstein CM Paulos ER Camp 2019 Genomics meets immunity in pancreatic cancer: current research and future directions for pancreatic adenocarcinoma immunotherapy Oncol Rev 13 102 13
48. A Mauriello R Zeuli B Cavalluzzo A Petrizzo ML Tornesello FM Buonaguro 2019 High somatic mutation and neoantigen burden do not correlate with decreased progression-free survival in hcc patients not undergoing immunotherapy Cancers 11 1824

Publisher's Note

8.2 Publication 2

Cancer Immunology, Immunotherapy
https://doi.org/10.1007/s00262-021-02933-4

ORIGINAL ARTICLE

Combined vaccine-immune-checkpoint inhibition constitutes a promising strategy for treatment of dMMR tumors

Inken Salewski[1] · Ste"en Kunto"[1] · Andreas Kuemmel[2,3] · Rico Feldtmann[2,3] · Stephan B. Felix[2,3] · Larissa Henze[1] · Christian Junghanss[1] · Claudia Maletzki[1]

Received: 19 October 2020 / Accepted: 29 March 2021

Abstract

Background Mlh1-knock-out-driven mismatch-repair-deficient (dMMR) tumors can be targeted immunologically. By applying therapeutic tumor vaccination, tumor growth is delayed but escape mechanisms evolve, including upregulation of immune-checkpoint molecules (LAG-3, PD-L1). To counteract immune escape, we investigated the therapeutic activity of a combined tumor vaccine-immune-checkpoint inhibitor therapy using α-PD-L1.

Design In this trial, Mlh1-knock-out mice with established gastrointestinal tumors received single or thrice injections of α-PD-L1 monoclonal antibody clone 6E11 (2.5 mg/kg bw, q2w, i.v.) either alone or in combination with the vaccine. Longitudinal flow cytometry and PET/CT imaging studies were followed by ex vivo functional immunological and gene expression assays.

Results 6E11 monotherapy slightly increased median overall survival (mOS: 6.0 weeks vs. control 4.0 weeks). Increasing the number of injections ($n = 3$) improved therapy outcome (mOS: 9.2 weeks) and was significantly boosted by combining 6E11 with the vaccine (mOS: 19.4 weeks vs. 10.2 weeks vaccine monotherapy). Accompanying PET/CT imaging confirmed treatment-induced tumor growth control, with the strongest inhibition in the combination group. Three mice (30%) achieved a complete remission and showed long-term survival. Decreased levels of circulating splenic and intratumoral myeloid-derived suppressor cells (MDSC) and decreased numbers of immune-checkpoint-expressing splenic T cells (LAG-3, CTLA-4) accompanied therapeutic effects. Gene expression and protein analysis of residual tumors revealed downregulation of PI3K/Akt/Wnt-and TGF-signaling, leading to T cell infiltration, reduced numbers of macrophages, neutrophils and MDSC.

Conclusions By successful uncoupling of the PD-1/PD-L1 axis, we provide further evidence for the safe and successful application of immunotherapies to combat dMMR-driven malignancies that warrants further investigation.

Keywords α-PD-L1 · MMR deficiency · In vivo imaging · Tumor microenvironment · Long-term survival

Abbreviations

cMS	Coding microsatellite
CTL	Cytotoxic T-lymphocytes
DC	Dendritic cells
dMMR	Mismatch repair deficiency
GIT	Gastrointestinal tumor
ICI	Immune-checkpoint inhibitors
MDSC	Myeloid-derived suppressor cells
TMB	Tumor mutational burden

Inken Salewski and Steffen Kuntoff have contributed equally to this work.

✉ Claudia Maletzki
claudia.maletzki@med.uni-rostock.de

[1] Department of Medicine Clinic III - Hematology, Oncology, Palliative Medicine, Rostock University Medical Center, Ernst-Heydemann-Str. 6, 18057 Rostock, Germany

[2] Department of Internal Medicine B, Cardiology, University Medicine Greifswald, Greifswald, Germany

[3] DZHK (German Centre for Cardiovascular Research), Partner Site Greifswald, Greifswald, Germany

Background

Immunotherapy with immune-checkpoint inhibitors (ICI) has become a mainstay of treatment for a range of solid cancers, including melanoma, bladder cancer, non-small cell lung cancer and Hodgkin's lymphoma [1–5]. CTLA-4, PD-1, or PD-L1 are the so far most studied checkpoint molecules and ICI widely applied in the clinic to improve

Published online: 18 April 2021

patients' prognosis. This blockade reactivates exhausted T-cells, prevents T-cell inhibition, and promotes effector T-cell proliferation to stimulate T-cell-mediated tumor cell killing [6–8]. Atezolizumab, Avelumab and Durvalumab are FDA approved as PD-L1 blocking antibodies. Monotherapy results in antitumor immune responses yet have a limited long-term therapeutic efficacy in most cases.

Lessons learned from the last years identified mismatch-repair deficiency (dMMR) as a molecular subtype with high response rates toward ICI. DMMR-driven carcinogenesis emerges sporadically because of MMR gene promoter hypermethylation or as part of defined hereditary tumor syndromes such as Lynch Syndrome and constitutional mismatch-repair deficiency [9–14]. The spectrum of cancer types related to dMMR is complex and includes, among others, gastrointestinal, endometrial and urothelial cancers [15]. A hallmark of dMMR tumors – irrespective of organ manifestation – is an ultramutated tumor phenotype (= TMB high), leading to a high abundance of frameshifted neo-epitopes on the tumor cells' surface. This latter feature underlines the tremendous potential for immunological targeting of dMMR cancers [15–17]. Indeed, in 2017, the FDA approved α-PD-1 ICI Pembrolizumab and Nivolumab for treatment of dMMR cancers agnostic of cancer site [18], which was extended lately for the first-line treatment of patients with un-resectable or metastatic dMMR colorectal cancer (CRC). Pre-existing Th type1 immune responses and high numbers of tumor-infiltrating $CD8^+$ T-cell clones (= IFNγ signature) constitute positive predictive biomarkers [19]. However, roughly 25% of patients show intrinsic resistance and in most cases initially responding patients gradually develop resistance, highlighting the necessity of improving treatment options [20–23]. As for PD-L1, limited preclinical data exist. PD-L1 expression on tumor-infiltrating lymphocytes is thought to be a potential predictor for patients' response to α-PD-1 therapy, but it is not well established for dMMR cancers because of the generally low expression [24, 25]. A recent phase II study in patients with dMMR metastatic or unresectable CRC revealed antitumor activity of Avelumab monotherapy [26]. Additional clinical trials are ongoing with different combinations being employed. One of them is based on tumor lysates or specific neoantigen-derived peptides. The former act as "global" vaccines and induce objective responses in some patients. To refine combination approaches preclinically, we employed the Mlh1 knock-out mouse model for dMMR-related diseases. Preceding vaccination approaches yielded prolonged overall survival in the therapeutic and prophylactic setting [27, 28]. Residual tumor cells showed an upregulation of immune-checkpoint molecules as part of acquired resistance. To counteract vaccination-induced immune escape and improve overall survival, we here applied a murine α-PD-L1 antibody (clone: 6E11) in combination with repeated vaccination.

Methods

Cell culture & vaccine preparation

Cells were cultured in DMEM medium, supplemented with 10% FCS (fetal calf serum), 6 mM Glutamine, and antibiotics (all from Biochrom, Berlin, Germany). The tumor lysate was prepared from a A7450 tumor allograft as described [29].

$Mlh1^{-/-}$ mouse model and in vivo treatment protocol

Ethical statement

The German local authority approved all animal experiments: Landesamt für Landwirtschaft, Lebensmittelsicherheit und Fischerei Mecklenburg-Vorpommern (7221.3-1-026/17; -026/17-3), under the German animal protection law and the EU Guideline 2010/63/EU. Mice were bred in the animal facility of the University Medical Center in Rostock under specific pathogen-free conditions. Mlh1 genotyping was done according to [21]. During their whole lifetime, all animals got enrichment in the form of mouse-igloos (ANT Tierhaltungsbedarf, Buxtehude, Germany), nesting material (shredded tissue paper, Verbandmittel GmbH, Frankenberg, Germany), paper roles (75 × 38 mm, H 0528–151, ssniff-Spezialdiäten GmbH), and wooden sticks (40 × 16 × 10 mm, Abedd, Vienna, Austria). During the experiment, mice were kept in type III cages (Zoonlab GmbH, Castrop-Rauxel, Germany) at 12-h dark:light cycle, the temperature of 21 ± 2 °C, and relative humidity of 60 ± 20% with food (pellets, 10 mm, ssniff-Spezialdiäten GmbH, Soest, Germany) and tap water ad libitum.

Experimental protocol

Mice with PET/CT proven gastrointestinal tumors (GIT), located in the duodenum, were conducted to therapy using four weekly tumor lysate boosts. Vaccination was sustained (10 mg/kg bw, biweekly, $n = 10$ mice) until tumors progressed, but for a maximum of 12 times. Treatment with α-PD-L1 (clone 6E11, kindly provided by Genentech, a subsidiary of Roche, South San Francisco, USA, dissolved in PBS) given at 2.5 mg/kg bw intravenously was done once ($n = 4$ mice) or thrice ($n = 10$ mice) every second week (q2wx3). Mice receiving the combination of α-PD-L1 were given vaccine first, followed by α-PD-L1 injection. Here again, combinations included single or triple α-PD-L1

applications ($n = 10$ mice/group; q2wx1 and q2wx3). Control mice were left untreated ($n = 10$ mice). Reduction of suffering was guaranteed by providing daily prepared soaked pellets, twice-daily monitoring of the health status using a score sheet and by applying humane endpoints (weight loss > 15%, pain/distress, changes in social behavior). All mice were sacrificed before they became moribund to prevent pain and distress. At this time, blood samples, spleens, lymph nodes and GIT were removed for further analyses.

PET/CT imaging

PET/CT imaging scans were performed on a small animal PET/CT scanner (Inveon PET/CT, Siemens Medical Solutions, Knoxville, TN, USA) according to a standard protocol as described before [30]. Briefly, mice were anesthetized by isoflurane (1–3%, supplemented with oxygen) and received a mean dose of 16.03 ± 1.10 MBq $^{[18F]}$FDG intravenously via a microcatheter placed in a tail vein. Static PET scans were acquired using a small animal micro PET/CT scan-ner (Inveon PET/CT Siemens, Knoxville, TN, USA). The PET image reconstruction method consisted of a 2-dimen-sional ordered subset expectation maximization algorithm (2D-OSEM) with four iterations and six subsets. Attenuation correction was performed on the basis whole body CT scan and a decay correction for [^{18}F] was applied. PET images were corrected for random coincidences, dead time and scatter. By marking the entire tumors, starting at the edge and cutting through the whole $^{[18F]}$FDG-enriched tumor, volumes and SUVs were determined. This was done by using Inveon Research Workplace 4.2 software.

Immune phenotyping

Blood samples were taken routinely from the retrobulbar venous plexus. Single cell suspensions of spleens and GIT were obtained upon passing them through a cell strainer (100 µm). Samples (2×10^5/Well) were stained with a panel of conjugated monoclonal antibodies (mAb, 1 µg each) followed by lysis of erythrocytes (155 mM NH_4Cl (MERCK Millipore, Darmstadt, Germany), 10 mM $KHCO_3$ (MERCK Millipore) and 0.1 mM EDTA (Applichem, Darmstadt, Germany). Negative controls consisted of lymphocytes stained with the appropriate isotypes (Biolegend, San Diego, USA). Cells were washed, resuspended in PBS and analyzed by flow cytometry on a Flow Cytometer (BD FACSVerse™, BD Pharmingen). Data analysis was performed using BD FACSuite software (BD Pharmingen).

Procartaplex cytokine assay

Cytokine levels in plasma samples were determined according to the manufacturer's instructions of the Procartaplex™ multiplex immunoassay (Thermo Fisher Scientific, Schwerte, Germany). Measurement as well as cytokine quantification was performed on a Bioplex 2000 (Bio-Rad Laboratories GmbH, Munich, Germany) in combination with the BioPlex Manager Software. Absolute plasma cytokine and chemokine level are presented [ng/ml].

Fragment length analysis of cMS target genes

A panel of non-coding and coding MS marker was analyzed as described before [31]. MSI is defined by mono- and/or bialellic band shifts usually characterized by deletions (indicated with minus symbol + number).

Nanostring targeted gene expression profiling

The T cell–inflamed tumor microenvironment was analyzed by targeted gene expression profiling of tumor RNA from fresh frozen or Tissue-Tek® embedded treatment and control samples ($n = 3$ samples/group). Total RNA was isolated using the RNeasy Mini Kit according to the manufacturers' instruction (Qiagen, Hilden, Germany). Total RNA concentrations were measured using the NanoDrop ND1000 (Thermo Fisher Scientific). Gene expression analysis was conducted on the NanoString nCounter gene expression platform (NanoString Technologies, Seattle, WA) applying the PanCancer IO 360™ Panel. This panel enables digital profiling of 770 genes that shape the tumor-immune interface and allows for characterization of pathways relevant in immune response and escape. Quality control, normalization and data analysis was done by applying the nSolver™ Analysis Software 4.0 including nCounter Advanced Analysis (version 2.0.115). Data are presented as Heatmap and log10 (p value) as well as log2 fold change.

Immunofluorescence

Cryostat sections of 4 µm were air-dried and fixed in cold pure methanol for 8 min. Unspecific binding sites were blocked in 2% BSA (Roth) for 2 h followed by incubation with 1 µg of the following FITC- and PE-labeled mAbs: CD4, CD8α, CD11b, Gr1 (Immunotools, Friesoythe, Germany), CD11c, CD104, LAG-3, PD-1, F4/80 and PD-L1 (Biolegend). Sections were washed, embedded in Roti Mount Flour Care DAPI (Roth, Karlsruhe)and target proteins visualized on a confocal laser scanning microscope (LSM780, Zeiss, Jena, Germany) using 20× objectives.

IFN-γ ELISpot

2.5×10^3 targets/well (2 GIT cell lines: Mlh1$^{-/-}$ A7450, Mlh1$^{-/-}$ 328, 1 lymphoma cell line: Mlh1$^{-/-}$ 1351, and YAC-1 cells) were seeded in IFNγ–specific mAb (Mabtech,

3321–3)–coated, 96-well microtiter plates. Peripheral blood leukocytes (5×10^4/Well) or splenocytes (1×10^4/well) from vaccinated and control mice were added in triplicates and co-cultured overnight. Bound antibody (Mabtech, 3321–6) was visualized by BCIP/NBT (KPL, Gaithersburg, Maryland, USA); spots were counted using an ELISpot reader. Presented are the numbers of IFNγ–secreting cells per 10,000 effector cells corrected for background levels counted in the absence of target cells, which was always ≤ 5 spots/well. Target cells without effector cells showed no background level.

Statistics

All values are expressed as mean ± SD. After proving the assumption of normality (Kolmogorov–Smirnov test), differences between vaccinated and control mice were determined using the unpaired Student's t test or one-way ANOVA (Bonferroni or Dunnett's multiple comparison). Kaplan–Meier survival analysis was done by applying the log rank (Mantel Cox) test. Statistical analyses were performed using GraphPad Prism 5 (San Diego, CA). The criterion for significance was set to $p < 0.05$.

Results

Combination of α-PD-L1 and vaccines significantly improves outcome of Mlh1$^{-/-}$ mice

In a first cohort, the ICI α-PD-L1 was administered once because of its long half-value period. Effects on survival were only marginal (Fig. 1a) and may indicate that MLH1$^{-/-}$- associated tumors are refractory to ICI monotherapy. By combining single α-PD-L1 with the vaccine (combination 1), overall survival was not significantly improved. In the next step, α-PD-L1 was given three times, to see whether tumors are indeed ICI-refractory or single application was simply not sufficient to induce immune responses in this

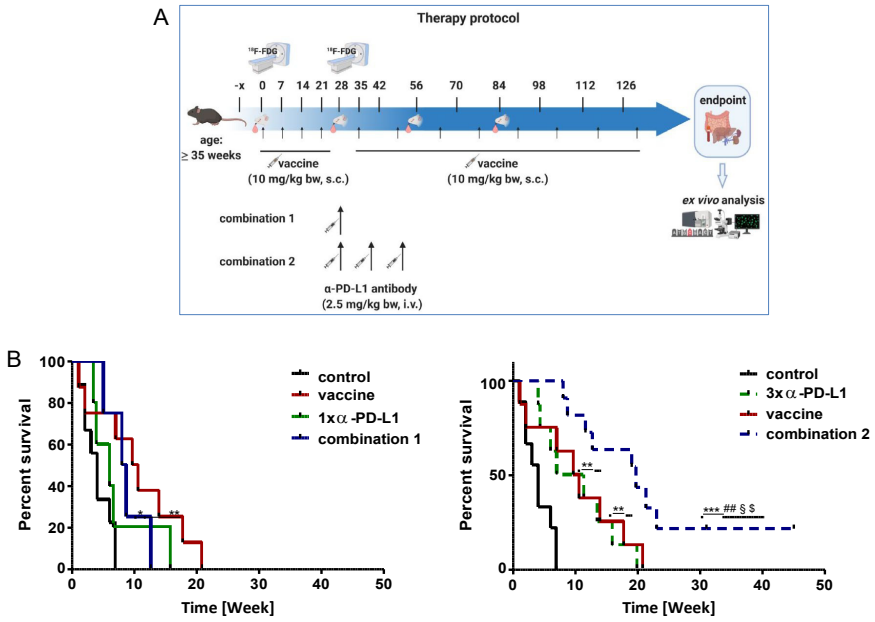

Fig. 1 Therapy protocol and Kaplan–Meier survival curve **a** Schematic overview on the treatment protocol, including time points for blood collection and PET/CT imaging **b** Log rank survival analy-sis of treated and control mice. Mice with confirmed GIT received four weekly injections of the tumor lysates (= vaccine; 10 mg/kg bw, biweekly, $n = 10$ mice) until tumors progressed (maximum 12 injections). Treatment with α-PD-L1 (clone 6E11, Genentech) given at 2.5 mg/kg bw intravenously was done **a** once ($n = 4$ mice) or **b** thrice ($n = 10$ mice) every second week (q2wx3). Mice receiving the combination were given vaccine first, followed by α-PD-L1 injection. Here again, combinations included **a** single or **b** triple α-PD-L1 applications ($n = 10$ mice/group). Control mice were left untreated ($n = 10$ mice). $^*p < 0.05$ versus control; $^{**}p < 0.01$ versus control; $^{***}p < 0.001$ versus control; $^{\#\#}p < 0.01$ versus 1x α-PD-L1; §$p < 0.05$ versus 3x α-PD-L1; $p < 0.05$ versus vaccine

model. Indeed, thrice α-PD-L1 injection extended the life span of mice to a degree comparable to the vaccine monotherapy (Fig. 1b). In combination with the vaccine (= combination 2), α-PD-L1 antibody treatment could even quintuple the life of mice from four weeks (control) to ~ 20 weeks ($p < 0.001$ vs. control; $p < 0.01$ vs. 1x α-PD-L1; $p < 0.05$ vs. 3x α-PD-L1; $p < 0.05$ vs. vaccine). Hence, this combination partially abrogated intrinsic ICI resistance and we consequently continued to move on with the triple α-PD-L1 treatment (combination 2, hereafter referred as combination) for subsequent functional analyses.

Combinational therapy leads to tumor reduction

Longitudinal PET/CT measurement revealed significant tumor size reduction by either therapy (vaccine, α-PD-L1 and combination) compared to controls (Fig. 2a). Still, analysis of the tumor size within the treatment groups identified significant reduction over time only in the combination (Exemplary pictures are given in Fig. 2b) finally resulting in partial or even complete remission. For the latter, this promising result was seen in three mice. Two of them remained alive until the experimental endpoint and one mouse had to be euthanized because of a progressive cutaneous benign lesion (week 23).

Peripheral immune activation by vaccine-based immunotherapy

To investigate the immunological changes during therapy, blood was taken from mice every four weeks and analyzed via flow cytometry (Fig. 3a). The vaccine treatment-induced a temporary increase in $CD3^+/CD4^+$ T-helper cells at day 84 which was not seen in the other groups. The level of $CD3^+/CD8^+$ cytotoxic T-lymphocytes (CTL) remained constant over time, while the amount of NK cells increased continually in all three treatment groups. The $CD11b^+/Gr1^+$ MDSC was doubled during the therapy with every treatment. The effects on $CD19^+$ B-lymphocytes were oppositional. B-lymphocytes increased in the combination and decreased during vaccine or α-PD-L1 treatment. $CD83^+$ dendritic cells (DC) were mainly found in mice treated with the vaccine only or the combination, likely because of stimulating the humoral arm of the immune system.

To investigate changes in the cytokine levels that act as growth factors, we analyzed plasma levels from different time points and at the end using a multiplex cytokine assay. TNF-α showed only marginal changes with the vaccine, a remarkable peak at day 56 in the α-PD-L1 treatment and a constant slight increase over time in the combination (Fig. 3b). This latter increase was also seen for the chemoattractant MIP1β. The IL10 level fluctuated in all three treatments. In contrast, the vaccine-induced IL13, while it remained unaffected upon α-PD-L1 treatment and decreased in the combination group, indicative for minor relevance of Th2-cytokines in treatment response. The levels of RANTES and Eotaxin decreased with vaccination, but for α-PD-L1 and the combination it initially increased.

Changes in important sites for immune reactions: spleens and residual tumors

Additionally to the blood immune-monitoring, spleens and residual tumors were resected at the experimental endpoint

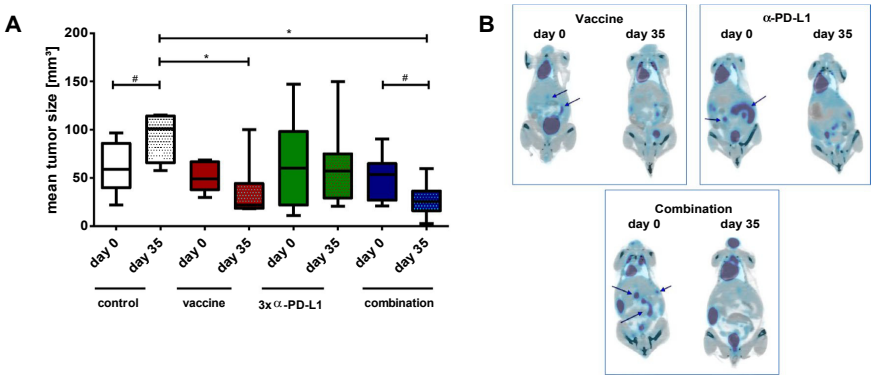

Fig. 2 PET/CT imaging **a** PET/CT analysis for quantification of mean tumor volume [mm^3]. Represented are the mean tumor sizes ± SD at start of treatment and after 28 days of treatment ($n = 4–10$ mice/group and time-point); *$p < 0.05$ versus control, one-way ANOVA (Bonferroni's multiple comparison test); #$p < 0.05$ versus day 0; t-test **b** Representative PET/CT scans from mice receiving the vaccine (upper left), the a-PD-L1 antibody (upper right) or a combination of both (lower). Arrows indicate measurable tumor nodules in the gut

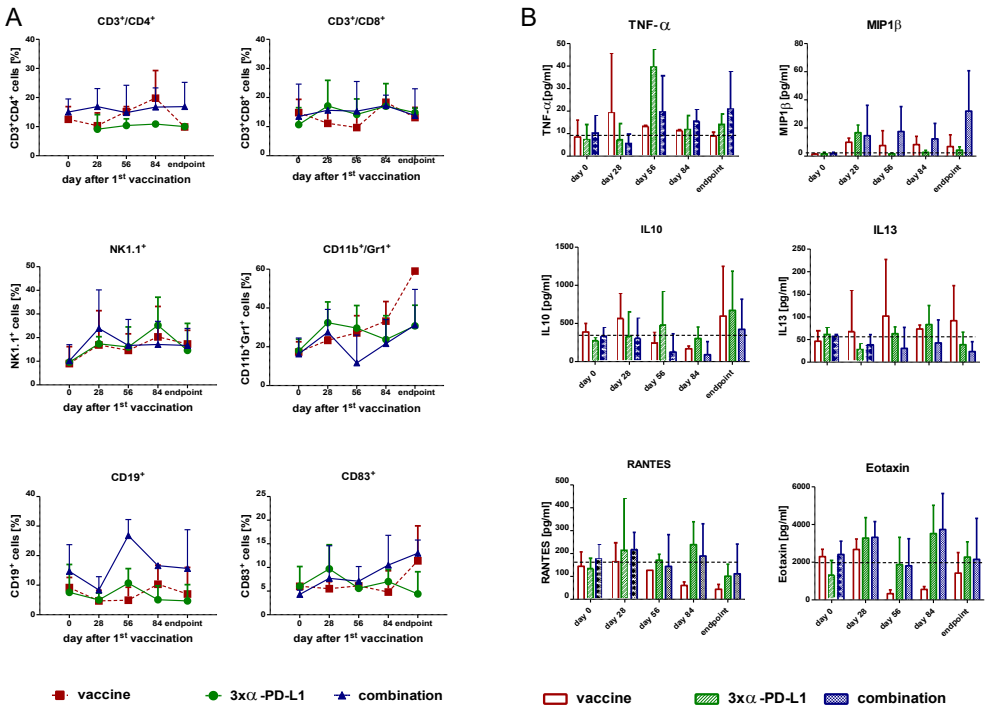

Fig. 3 Longitudinal flow cytometric phenotyping and plasma cytokine level **a** Phenotyping of peripheral blood leukocytes was done before, during therapy and at the endpoint. Therefore, blood was collected via the retrobulbar venous plexus and stained with antibodies. Given are the percentage numbers of positive cells ± SD resulting from 20,000 events measured on a flow cytometer. **b** Plasma cytokine levels from mice with immunotherapy and controls (upper graph). Differences between tumor-free and tumor-bearing mice (lower graphs). Plasma samples were collected at the experimental endpoint and cytokine levels determined as described in material and methods. Given are the mean cytokine level ± SD

and infiltrating cells analyzed by flow cytometry. In spleens, levels of $CD3^+/CD4^+$ T-helper cells and $CD3^+/CD8^+$ CTL did not change with the therapies. By contrast, levels of $CD11b^+/Gr1^+$ MDSC decreased and the $CD83^+$ DC significantly increased in all treatment groups with a trend toward stronger effects in the combination ($p < 0.05$; and $p < 0.01$ vs. control; Fig. 4). The amount of $PD\text{-}1^+$ cells increased slightly, $PD\text{-}L1^+$ cells reduced. $LAG\text{-}3^+$ cells decreased significantly, especially in the α-PD-L1 and the combination treatment ($p < 0.05$; and $p < 0.01$ vs. control). The same effect was seen for $CTLA4^+$ cells ($p < 0.05$; $p < 0.01$; $p < 0.001$ vs. control and vaccine) and $TIM\text{-}3^+$ cells.

Residual tumors harbored higher numbers of infiltrating $CD3^+/CD4^+$ T-helper cells and $CD3^+/CD8^+$ CTL, particularly for the combination group. $CD11b^+/Gr1^+$ MDSC increased with α-PD-L1 treatment and dropped in the combination ($p < 0.05$ vs. α-PD-L1). Levels of $CD83^+$ DC were constant and similar to the control, while $CD200R^+$ cells reduced in the combination ($p < 0.05$ vs. α-PD-L1). Looking at the frequency of immune-checkpoint molecules, there were additional differences. The abundance of $PD\text{-}1^+$ cells remained unchanged in all groups, $PD\text{-}L1^+$ cells increased with α-PD-L1 treatment and decreased in the combination ($p < 0.01$ vs. α-PD-L1). Infiltrating $LAG\text{-}3^+$ cell numbers were high in the monotherapies, whereas $CTLA4^+$ infiltration was mainly confined to groups of the vaccine (vaccine monotherapy and combination). Still, $TIM\text{-}3^+$ cells decreased significantly upon combination ($p < 0.01$ vs. control).

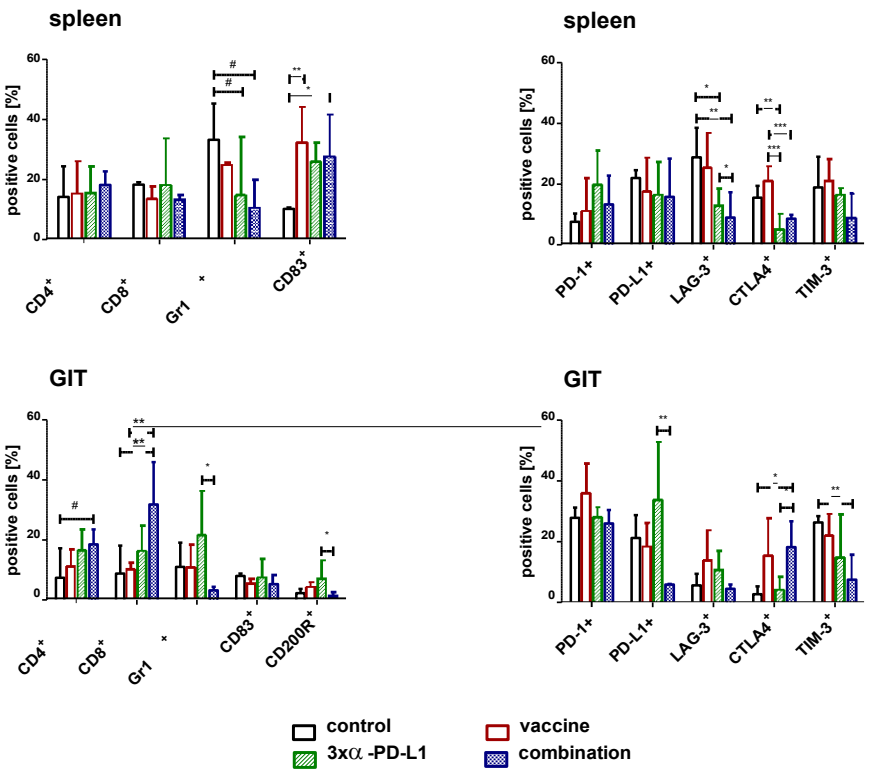

Fig. 4 Flow cytometric phenotyping of spleen and GIT cells. Phenotyping was done at the endpoint. Therefore, mice were euthanatized, organs removed and single cell suspensions stained with the appropriate antibodies. Given are the percentage numbers of positive cells ± SD resulting from 20,000 events measured on a flow cytometer. $*p < 0.05$; $**p < 0.01$; $***p < 0.001$ one-way ANOVA (Bonferroni's multiple comparison test); $^{\#}p < 0.05$ one-way ANOVA (Dunnett's multiple comparison test)

Gene expression analysis identifies downregulation of PI3K/Akt/Wnt-and TGF-signaling

To have a closer look on the complex interplay between the tumor microenvironment and immune response, the PanCancer IO 360 Gene Expression Panel was applied (Fig. 5).

The cluster, left to the heat map (Fig. 5a), schematically illustrates the relations of the three individuals of the four treatment groups dependent on their tumor-infiltrating lymphocyte (TIL) levels. The amounts of different immune cells differ the most in the combination group compared to the other groups. Here, overall immune cell expression levels increased in two of three individuals. Treatment with α-PD-L1 also changed immune cell expression patterns compared to the control and vaccine treatment.

Total TIL levels (Fig. 5b, upper left) were elevated in the α-PD-L1 and the combination therapy, because of increasing amounts of cytotoxic T and B cells (upper and middle). Conspicuously, levels of exhausted $CD8^+$ T cells and neutrophils exclusively decreased in the combination (middle and lower). Macrophages only decreased in the vaccine and combination group.

As can be taken from Fig. 5c, effects on common signaling pathways in the combination group correlate more with the vaccine therapy than with α-PD-L1 treatment. In detail, the myeloid compartment, *TGF*-beta and *Wnt* signaling pathways were downregulated in all treatment groups in comparison with the control. Additionally in the combination group, genes related to angiogenesis and PI3K/Akt pathway were downregulated. For the latter, *LAMA1* and *Comp* were downregulated, whereas the

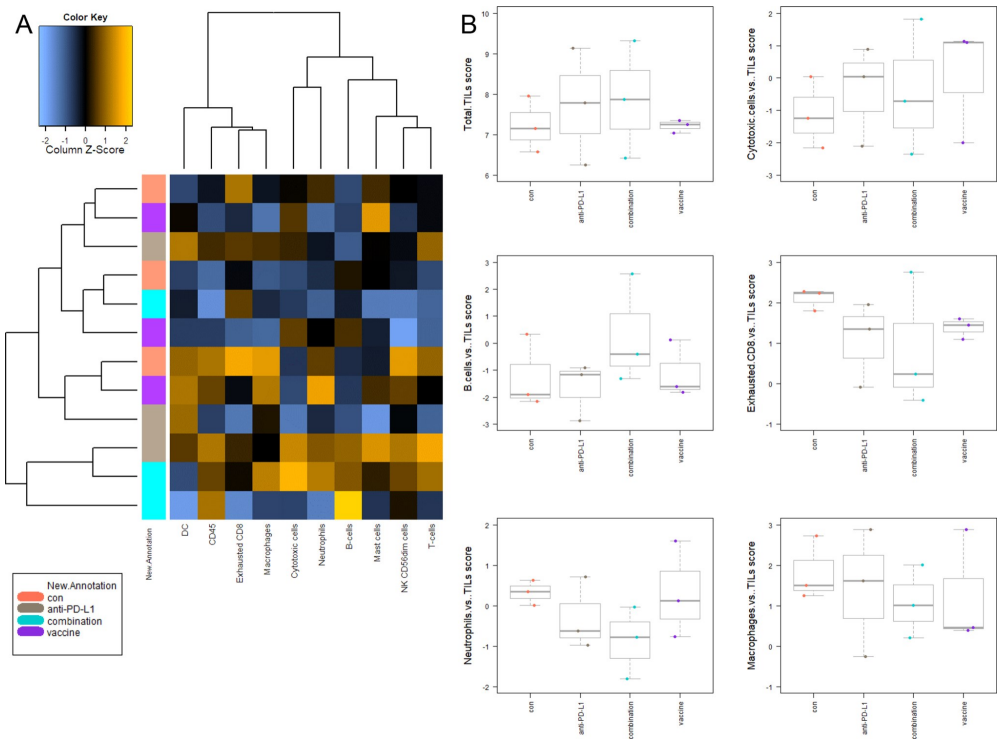

Fig. 5 PanCancer gene expression analysis of treated and control tumors **a** Heatmap showing raw abundance of cell types in each sample. Orange shows high abundance; blue indicates low abundance **b** Relative abundances measuring various contrasts between cell types reported for each group. Data result from $n = 3$ samples/group. (**c, d**) Affected pathways in treated and control tumors **c** Directed global significance statistics measure the extent to which a gene set's genes are up or downregulated with the variable. Red denotes gene sets whose genes exhibit extensive over-expression with the covariate, blue denotes gene sets with extensive under-expression **d** Scores of selected pathways shown for each group. Increasing scores correspond to an increasing expression. Data result from $n = 3$ samples/group

phosphatase *PTEN*, a well-established tumor suppressor was upregulated (Fig. 5d). Genes for costimulatory signaling and lymphoid compartment were higher in tumors of mice receiving α-PD-L1 and the combination, whereas no changes were seen in the vaccine group. Furthermore, the JAK/STAT signaling was activated by the combination (Fig. 5d).

We summarize the detailed analysis of differential expression at the gene set level (supplementary Fig. 1). In the combination, genes belonging to the interferon signaling (such as *H2-Q1/H2-Q2, Ifi203,* and *Vcam1*) and cytotoxicity (*Gzma* and *Tnfsf10*) were upregulated, whereas all genes of the myeloid compartment genes were downregulated (including *Ly6C1*, *Olr1,* and *Ccl20*).

Combination therapy alters the tumor microenvironment

While above findings already showed changes between individual treatment groups, we additionally studied the tumor microenvironment by immunofluorescence (Fig. 6).

MDSC and F4/80$^+$ tumor-associated macrophages (TAM) were detectable in control tumors, indicative a suppressive microenvironment. While MDSC were effectively eliminated upon therapy, irrespective of the applied treatment regimen, only the combination was able to impact on numbers of infiltrating TAM (Fig. 6a, b). Besides, CD11c$^+$ cells increased in the combination. Numbers of CD4$^+$ T-helper cells remained the same, while the CD8$^+$ CTL increased. This resulted in a

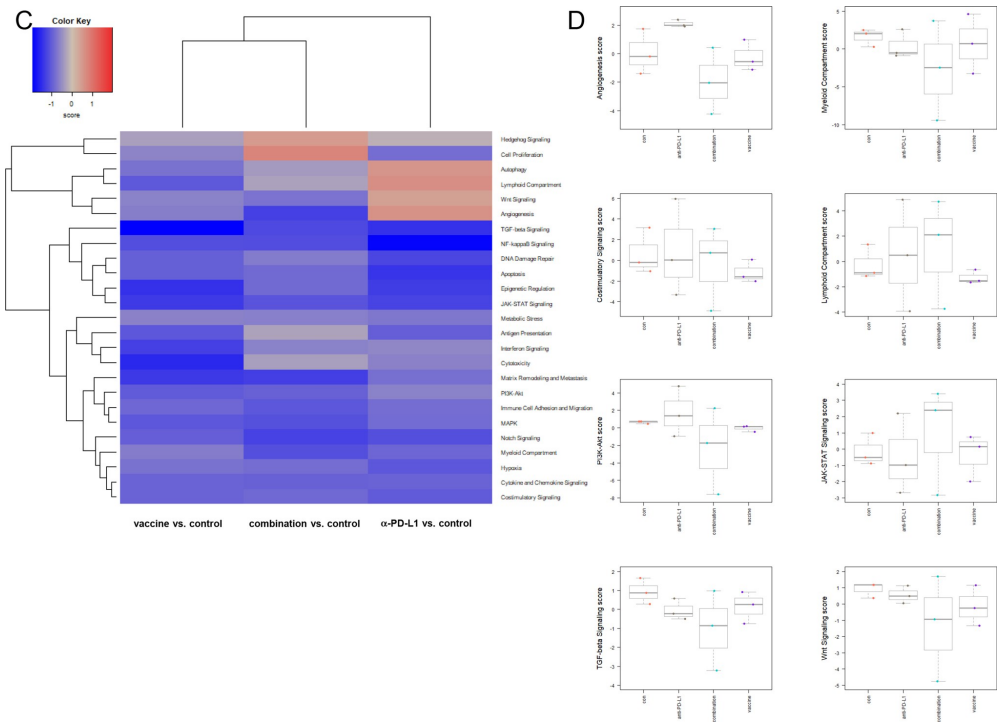

Fig. 5 (continued)

significant difference between the vaccine and the α-PD-L1 treatment (Fig. 6c, d). Vice versa, the amount of LAG-3$^+$ T-cells significantly increased upon vaccine treatment but significantly decreased upon α-PD-L1 and the combination. These results were similar to the levels of PD-L1$^+$ cells, which significantly decreased in these two groups (Fig. 6c, d). Though PD1 was highly abundant on tumor cells, we observed intratumoral differences, ranging from high to low PD1 expression within individual specimen (supplementary Fig. 2). This was, however, treatment-independent.

Treatment-induced molecular changes in cMS

Residual tumors of the different treatment groups were scanned for typical gene mutations at cMS (Fig. 7a, b). Depending on the treatment, tumors harbored different mutation frequencies in cMS. *NKtr1* and *Kcnma1* (left of the dotted line) had the lowest mutation rates for the control, whereas the treatments resulted in high mutation rates. Noticeably, GIT from all three treatment groups showed no mutation in *Spen*, *Apc* and *Casc3* (highlighted with the gray box in the middle), while a mutation rate of 20–30% was evidently in control tumors. Residual tumors from the combination harbored the lowest mutation frequencies in *Akt3*, *Clock*, *Il1F9* and *Rfc3* (highlighted with the right gray box), especially compared with α-PD-L1 treatment (= 100% mutation frequency).

ELISpot analysis reveals increased immune activation upon combination treatment

To asses immune activation, IFN-γ secretion by T-lymphocytes was detected by ELISpot-assays after coincubation of splenocytes from treated and control mice with different cancer cell lines (A7450 T1 M1, 328, 1351, and Yac-1) (Fig. 7c). Splenocytes of mice from the combination group responded with significantly higher IFN-γ secretion than those treated with α-PD-L1. NK cell reactivity was excluded by lacking IFN-γ secretion against Yac-1 cells. Notably, IFN-γ secretion levels against 1351 MLH1$^{-/-}$ lymphoma cells were the lowest irrespective of the treatment.

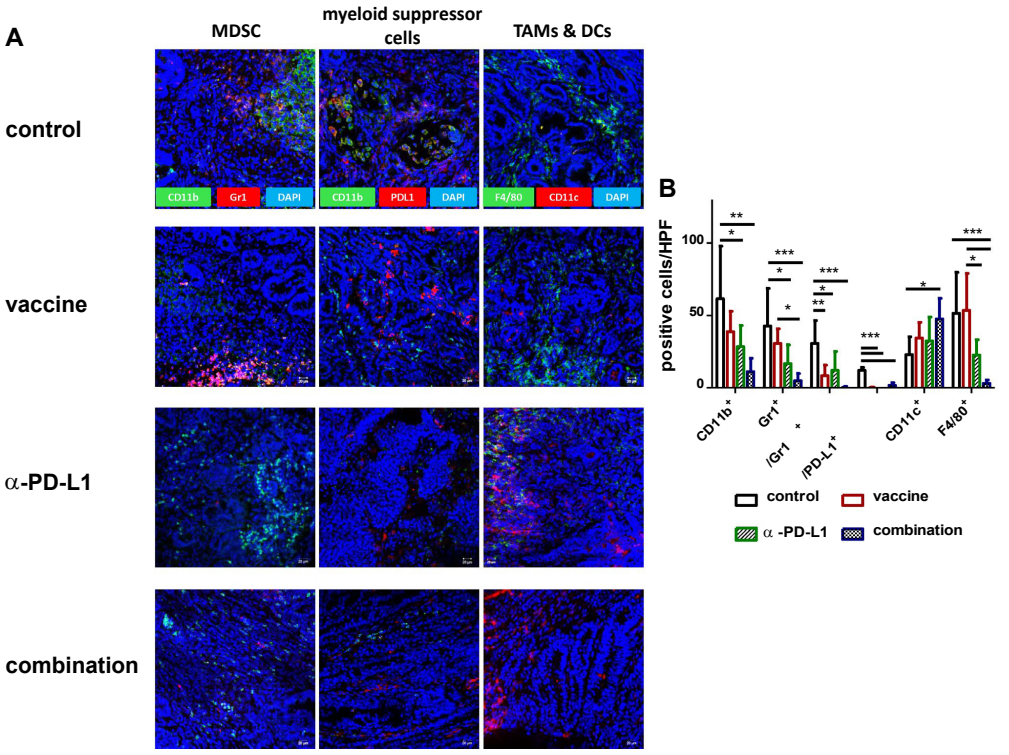

Fig. 6 Immunofluorescence **a, c** Residual Mlh1$^{-/-}$ GIT were resected after therapeutic vaccination and cryostat sections of 4 µm prepared. Tumor microenvironment was studied upon staining with specific mAbs, followed by nuclear staining with DAPI. Pictures were taken on a laser scanning microscope (Zeiss) using 20× objectives. **b, d** Quantification of infiltrating immune cells. At least three pictures were taken from each slide and numbers of infiltrating cells counted. Data are given as infiltrates/HPF. Mean + SD, $n \geq 3$ samples/group; *$p < 0.05$, **p<0.01; ***p<0.001 one-way ANOVA (Bonferroni's multiple comparison test)

Discussion

In this study, we describe a strategy to combine active tumor vaccination with an ICI in a clinically relevant dMMR mouse model [32]. DMMR is associated with high tumor mutational burden [33–35] and thus harbors a tentatively high likelihood of being susceptible to immunotherapy.

Using a murine α-PD-L1 antibody, monotherapy itself marginally improved outcome after single application. By increasing the number of injections, overall survival of Mlh1$^{-/-}$ mice extended to a degree comparable to the vaccine monotherapy. The latter was prepared from a whole tumor lysate with proven antitumor activity from previous studies [27, 36]. Hence, both treatments prolonged mice' survival suffering from highly aggressive Mlh1$^{-/-}$-driven GIT. Given the fact that Mlh1$^{-/-}$ tumors, despite their high TMB, do not have a high IFNγ signature and are not targetable by ICI per se, the improved outcome after α-PD-L1 monotherapy is intriguing. It is therefore unlikely that mice' outcome after targeting the PD-L1 axis is better if α-PD-L1 antibodies are applied more often or over a longer time. Rather targeting both MHC-I and II restricted tumor epitopes—with whole tumor lysates—in combination with PD-L1 blockade seems necessary to affect growth of poorly immunogenic and thus ICI refractory, immunologically cold/warm tumors, as recently shown for triple-negative breast cancer [37]. So far, we can only speculate on the survival benefit of mice treated with the α-PD-L1 antibody in monotherapy. In a very recent study on dMMR gastric cancer, CD68^{+}CD163^{-} M1-like macrophages were identified as prerequisites for efficient PD-L1/PD-1 blockade because of specific chemokine receptor expression likely

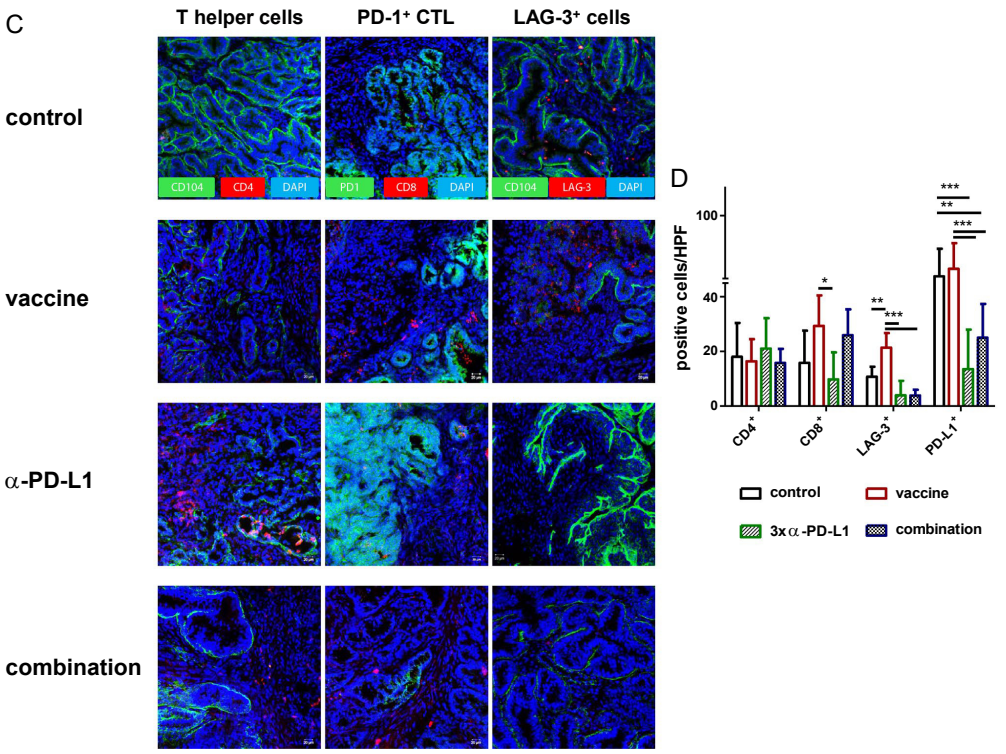

Fig. 6 (continued)

activating CTL [38]. The α-PD-L1 antibody itself may have also induced immune-independent apoptosis and autophagy in $Mlh1^{-/-}$ cells. In addition to our RNA expression data, showing signaling pathway alteration, increased release of reactive oxygen species and cytochrome-c was found in atezolizumab-treated osteosarcoma cells, ultimately leading to mitochondrial-related apoptosis [39].

Another interesting finding of our study was the upregulation of angiogenesis pathways under α-PD-L1 monotherapy, adding further credence for combined checkpoint-angiogenesis inhibition, currently tested in clinical trials [40, 41].

However, dosing schedules and accurate timing of each combination partner remain undefined for combined vaccine and ICI strategies. Here, we performed alternating treatment starting with vaccine first. The rationale is based on our previous observations in which repetitive vaccine monotherapy provoked upregulation of immune-checkpoint-molecules on residual tumors [27]. To counteract therapy-induced upregulation, we here applied α-PD-L1 therapy during vaccination. This combined treatment yielded complete remission in 30% of mice, finally resulting in significantly improved overall survival. Although complete remission was not achieved in all mice, we would like to stress the point that tumor burden massively reduced in the combination likely because of inducing a T cell–inflamed tumor microenvironment. Other studies reported superior effects when checkpoint-inhibition was given after cessation of the vaccine [42]. Still, the significantly prolonged overall survival of $MLH1^{-/-}$ mice achieved in this study argues in favor of concomitant application. By applying dual immune-checkpoint blockade (such as α- or α-LAG-3) one may expect even better and long-term tumor growth control.

Most previous trials focused on α-PD-1 antibodies to increase antitumoral effects of vaccine-induced immunity [43–45]. Rare preclinical data exist on vaccine-α-PD-L1 combinations. A recent study described prolonged survival and increased tumor cell apoptosis in a hepatocellular carcinoma model treated with a combined DC vaccine and α-PD-L1 inhibitor [46], supported by findings from Ji et al., reporting reactivation of neoantigen-specific CTL

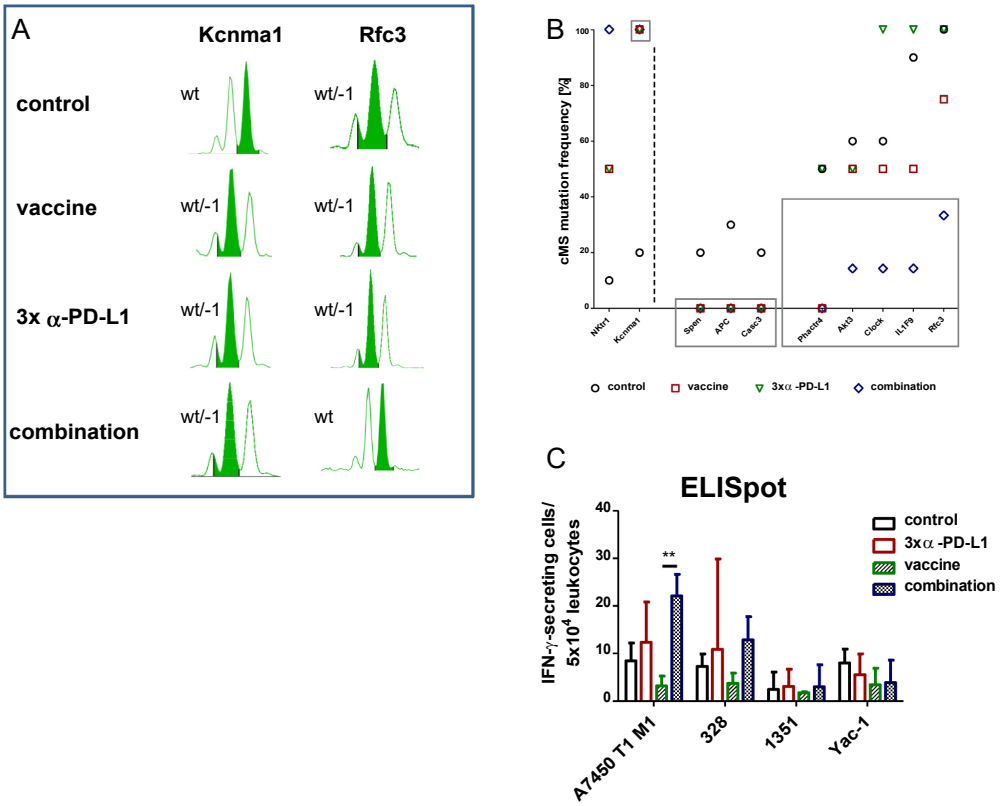

Fig. 7 Fragment length analysis of cMS mutations in Mlh1$^{-/-}$ target genes and IFN-γ ELISpot **a** Representative pattern of cMS markers. MSI is defined by mono- and/or bialellic band shifts characterized by deletions (indicated with minus symbol + number). The wild type peak is highlighted in green **b** Quantitative cMS analysis using a panel of predefined Mlh1$^{-/-}$ target genes. Represented is the mutation frequency of selected target genes in mice from the control (n = 10), vaccine (n = 4), α-PD-L1 (n = 4), and combination 2 (n = 7). Note the differences in mutational frequency between control and treated mice indicating loss of single cell clones (= no mutation detected, such as *Spen, Apc, Casc3*) mainly in the combination 2 group (gray frame) **c** Reactivity of splenocytes against target cells (Mlh1$^{-/-}$ 7450 T1 M1, Mlh1$^{-/-}$ 328, Mlh1$^{-/-}$ 1351, and YAC-1) was examined after overnight co-incubation. Lymphocytes were isolated from mice of the following groups: control (n = 3), vaccine (n = 5), α-PD-L1 (n = 4) and combination 2 (n = 4). Highest reactivity was seen in the combination treatment. Given is the mean ± SD, **p<0.01 one-way ANOVA (Bonferroni's multiple comparison test)

by combined α-PD-L1 peptide vaccination [47]. Likewise, Sun et al. found enhanced tumor-antigen-specific immunity upon combined vaccine-PD-L1-blockade [48]. By reversing the immunosuppressive status of the micromilieu, PD-L1 is indeed a promising target. Here, we also identified a shaped tumor microenvironment accompanied by peripheral immune activation. By performing a detailed and longitudinal analysis, we found decreased numbers of circulating MDSC and T cell exhaustion markers after combined treatment. Accompanying in-depth gene expression analysis of residual tumors identified increased numbers of total TIL, mainly being cytotoxic T and B cells. Vice versa, levels of exhausted CD8$^+$ T cells, tumor-associated macrophages and neutrophils reduced in the combination group. Neutrophils are a group of tumor-associated cells which, in conjunction with MDSC, play a major role during cancer development and progression. Their specific location within the tumor (i.e., intra-, peritumoral or stromal) has prognostic relevance [49]. Abundance of tumor-associated neutrophils may even correlate with local TGFβ expression; in fact, TGFβ blocking improves outcome in preclinical cancer models [49]. In support of this, TGF-signaling was downregulated here

upon combination and likely facilitated conquering primary resistance to checkpoint inhibition [50]. Though not analyzed in detail here, reduced TGFβ signaling may have also exerted a tumor-intrinsic effect finally blocking the EMT-like transition and preventing Mlh1$^{-/-}$-driven tumor progression [50]. Additional common pathways with prognostic relevance that were altered by the vaccine-α-PD-L1 combination include PI3K/Akt and Wnt-signaling as well as genes responsible for angiogenesis, matrix remodeling and metastasis. By contrast, genes belonging to the JAK/STAT signaling were upregulated, indicative for enhanced immune-related crosstalk to eradicate Mlh1$^{-/-}$ tumor cells via IFN-γ [51]. These cumulative data nicely explain the improved overall survival in mice treated with the combined vaccine-α-PD-L1 approach.

While most pronounced effects were in fact seen in the combination therapy and thus interpretable as synergistic, the monotherapy itself modulated the tumor microenvironment. Anti-PD-L1 treatment-induced genes relevant for autophagy and downregulated NF-κB-signaling, which is in line with data from a recent trial on triple-negative breast cancer cells, treated with Atezolizumab [52]. Upon vaccination, matrix remodeling/metastasis-related genes and genes of the Wnt-and TGF-signaling were downregulated and a direct indicator of successful reversal of intrinsic resistance. Indeed, tumor-intrinsic β-catenin activation prevents T cell priming and infiltration into the tumor microenvironment and results in resistance to anti-PD-L1/anti-CTLA-4 therapy [53]. Vice versa, Wnt-pathway suppression restores DC infiltration, a phenomenon seen here upon therapy characterized by elevated levels of tumor-infiltrating CD11c^{+} DC that confirm successful therapy-related downregulation of the Wnt-pathway.

Inter-individual differences throughout the treatment groups reflect the different overall survival times of mice. Here, short-term survivors had low TIL scores and vice versa. Teasing out what are the (patient-) individual baseline differences is the challenge for the next wave of pre- and clinical trials with immunotherapy to refine treatment on the long run.

Another interesting finding was the altered molecular pro-file in typical cMS marker upon treatment. One may specu-late that treatment successfully eliminated single mutated clones, whereas other emerged under the immune-selective pressure. We identified somatic cMS mutations in *NKtr1* and *Kcnma1* in all treatment groups that were infrequent in control tumors. By contrast, somatic mutations in *Spen*, *Apc,* and *Casc3* were no longer detectable. Notably, residual tumors from the combination therapy harbored the lowest mutation frequencies in *Akt3*, *Clock*, *Il1F9,* and *Rfc3*, especially compared with α-PD-L1 treatment (= 100% mutation frequency).

Among others, question remains why some tumors regressed, while others finally progressed. Sustained tumor IFN signaling induces PD-L1 expression on tumor and immune cells and is considered a acquired resistance mechanism [54]. However, this only partially explains the different in vivo response. Reports from human dMMR CRC describe contradictory PD-L1 abundance on tumor-infiltrating lymphocytes or tumor cells [55, 56]. Its role to mediate immune escape is undebatable and results from a phase II study already confirmed antitumor activity of Avelumab with manageable toxicity in most, but clearly not all patients with previously treated dMMR mCRC and recurrent/persistent endometrial cancer [26, 57]. Heterogeneity among tumors, such as the varying TMB, different genomic variations (in cMS), Indoleamine 2,3-Dioxygenase 1-based immune escape, and the activated Wnt/β-catenin signaling may provide an explanation for the difference seen here. Understanding how Mlh1$^{-/-}$ tumor and immune cells react to our treatments holds promise for novel immune-modulating strategies and will hopefully help to guide the way for clinical vaccine-based immune-checkpoint regimens.

Conclusion

Tumor-lysate vaccination in combination with α-PD-L1 prolongs the lifetime of Mlh1 knock-out mice significantly and shows strong tumor growth inhibition via downregulation of PI3K/Akt/Wnt-and TGF-signaling. This combination regimen results in decreased levels of myeloid-derived suppressor cells (MDSC), splenic and intratumoral checkpoint-expressing T cells (PD-L1, LAG-3 and CTLA-4) and therefore positively modulates the tumor microenvironment. Combined vaccine-immune-checkpoint inhibition provides a safe approach especially for patients having a likelihood of being non-responsive toward immune-checkpoint monotherapy.

Supplementary Information The online version contains supplementary material available at https://doi.org/10.1007/s00262-021-02933-4.

Acknowledgements We gratefully thank Genentech, a subsidiary of Roche, South San Francisco, USA for providing the clone 6E11 for in vivo experiments. We additionally thank Mrs. Ilona Klamfuss for breeding mice, Brigitte Vollmar and Bernd Krause for their continuous support in their efforts of chairing the Core Facility of Multimodal Small Animal Imaging. We also gratefully acknowledge the excellent technical assistance of Mrs. Joanna Förster. Furthermore, we thank Carina Bergner and Anja Gummesson, radiopharmacy team of the Department of Nuclear Medicine of the University Medical Center Rostock, for providing ^{18}F-FDG for the small animal PET/CT experiments.

Authors' contribution CM was involved in conducted the study, performed the in vivo experiments, analyzed data and wrote the manuscript; IS and SK performed ex vivo experiments, analyzed data and participated in writing; AK and RF were involved in performed nanostring analysis; LH and CJ critically revised the manuscript.

Funding Open Access funding enabled and organized by Projekt DEAL. This work was supported by a grant from the German research foundation to CM [DFG Grant Number MA5799/2-1 and MA5799/2-2].

Availability of data and material The datasets used and/or analyzed during the current study are available from the corresponding author on reasonable request.

Declarations

Competing interest The authors declare no competing interests.

Ethics approval and consent to participate The German local authority approved all animal experiments: Landesamt für Landwirtschaft, Lebensmittelsicherheit und Fischerei Mecklenburg-Vorpommern (7221.3-1-026/17; -026/17–3), under the German animal protection law and the EU Guideline 2010/63/EU.

Consent for publication Genentech, a subsidiary of Roche, South San Francisco, USA gave their consent for publication.

References

1. Cousin S, Seneschal J, Italiano A (2018) Toxicity profiles of immunotherapy. Pharmacol Ther 181:91–100
2. Pistillo MP, Carosio R, Grillo F et al (2020) Phenotypic characterization of tumor CTLA-4 expression in melanoma tissues and its possible role in clinical response to Ipilimumab. Clin Immunol. https://doi.org/10.1016/j.clim.2020.108428
3. Suzman DL, Agrawal S, Ning Y et al (2019) FDA approval summary: Atezolizumab or Pembrolizumab for the treatment of patients with advanced Urothelial carcinoma ineligible for cisplatin-containing chemotherapy. Oncologist 24:563–569. https://doi.org/10.1634/theoncologist.2018-0084
4. Crist M, Balar A (2017) Atezolizumab in invasive and metastatic urothelial carcinoma. Expert Rev Clin Pharmacol 10:1295–1301. https://doi.org/10.1080/17512433.2017.1389275
5. Plimack ER, Bellmunt J, Gupta S et al (2017) Safety and activity of pembrolizumab in patients with locally advanced or metastatic urothelial cancer (KEYNOTE-012): a non-randomised, open-label, phase 1b study. Lancet Oncol 18:212–220. https://doi.org/10.1016/S1470-2045(17)30007-4
6. Leng C, Li Y, Qin J et al (2016) Relationship between expression of PD-L1 and PD-L2 on esophageal squamous cell carcinoma and the antitumor effects of CD8+ T cells. Oncol Rep 35:699–708. https://doi.org/10.3892/or.2015.4435
7. Kalim M, Iqbal Khan MS, Zhan J (2020) Programmed cell death ligand-1: a dynamic immune checkpoint in cancer therapy. Chem Biol Drug Des 95:552–566
8. Liu J, Zhang S, Hu Y et al (2016) Targeting PD-1 and Tim-3 pathways to reverse CD8 T-cell exhaustion and enhance ex vivo T-cell responses to autologous dendritic/tumor vaccines. J Immunother 39:171–180. https://doi.org/10.1097/CJI.0000000000000122
9. Siegel RL, Torre LA, Soerjomataram I et al (2019) Global patterns and trends in colorectal cancer incidence in young adults. Gut. https://doi.org/10.1136/gutjnl-2019-319511
10. Evrard C, Tachon G, Randrian V et al (2019) Microsatellite Instability: diagnosis, heterogeneity, discordance, and clinical impact in colorectal cancer. Cancers (Basel) 11:1567. https://doi.org/10.3390/cancers11101567
11. Ait Ouakrim D, Dashti SG, Chau R et al (2015) Aspirin, Ibuprofen, and the Risk of Colorectal Cancer in Lynch Syndrome. J Natl Cancer Inst 107:djv170. https://doi.org/10.1093/jnci/djv170
12. Seth S, Ager A, Arends MJ, Frayling IM (2018) Lynch syndrome – cancer pathways, heterogeneity and immune escape. J Pathol 246:129–133. https://doi.org/10.1002/path.5139
13. Bodo S, Colas C, Buhard O et al (2015) Diagnosis of constitutional mismatch repair-deficiency syndrome based on microsatellite instability and lymphocyte tolerance to methylating agents. Gastroenterology 149:1017–1029. https://doi.org/10.1053/j.gastro.2015.06.013
14. Wimmer K, Kratz CP (2010) Constitutional mismatch repair-deficiency syndrome. Haematologica 95:699–701. https://doi.org/10.3324/haematol.2009.021626
15. Luchini C, Bibeau F, Ligtenberg MJL et al (2019) ESMO recommendations on microsatellite instability testing for immunotherapy in cancer, and its relationship with PD-1/PD-L1 expression and tumour mutational burden: a systematic review-based approach. Ann Oncol 30:1232–1243. https://doi.org/10.1093/annonc/mdz116
16. Le DT, Durham JN, Smith KN et al (2017) Mismatch repair deficiency predicts response of solid tumors to PD-1 blockade. Science 357:409–413. https://doi.org/10.1126/science.aan6733
17. Campbell BB, Light N, Fabrizio D et al (2017) Comprehensive analysis of hypermutation in human cancer. Cell 171:1042-1056.e10. https://doi.org/10.1016/j.cell.2017.09.048
18. Lemery S, Keegan P, Pazdur R (2017) First FDA approval agnostic of cancer site—when a biomarker defines the indication. N Engl J Med 377:1409–1412
19. Loupakis F, Depetris I, Biason P et al (2020) Prediction of benefit from checkpoint inhibitors in mismatch repair deficient metastatic colorectal cancer: role of tumor infiltrating lymphocytes. Oncologist. https://doi.org/10.1634/theoncologist.2019-0611
20. Ariyan CE, Brady MS, Siegelbaum RH et al (2018) Robust antitumor responses result from local chemotherapy and CTLA-4 blockade. Cancer Immunol Res 6:189–200. https://doi.org/10.1158/2326-6066.CIR-17-0356
21. Bozorgmehr F, Hommertgen A, Krisam J et al (2019) Fostering efficacy of anti-PD-1-treatment: nivolumab plus radiotherapy in advanced non-small cell lung cancer - study protocol of the FORCE trial. BMC Cancer. https://doi.org/10.1186/s12885-019-6205-0
22. Sullivan RJ, Hamid O, Gonzalez R et al (2019) Atezolizumab plus cobimetinib and vemurafenib in BRAF-mutated melanoma patients. Nat Med 25:929–935
23. Sahin IH, Akce M, Alese O et al (2019) Immune checkpoint inhibitors for the treatment of MSI-H/MMR-D colorectal cancer and a perspective on resistance mechanisms. Br J Cancer 121:809–818
24. Kong P, Wang J, Song Z et al (2019) Circulating lymphocytes, PD-L1 expression on tumor-infiltrating lymphocytes, and survival of colorectal cancer patients with different mismatch repair gene status. J Cancer 10:1745–1754. https://doi.org/10.7150/jca.25187
25. Le DT, Uram JN, Wang H et al (2015) PD-1 blockade in tumors with mismatch-repair deficiency. N Engl J Med 372:2509–2520. https://doi.org/10.1056/NEJMoa1500596

26. Kim JH, Kim SY, Baek JY et al (2020) A phase II study of avelumab monotherapy in patients with mismatch repair-deficient/microsatellite instability-high or *pole*-mutated metastatic or unresectable colorectal cancer. Cancer Res Treat. https://doi.org/10.4143/crt.2020.218
27. Maletzki C, Gladbach YS, Hamed M et al (2018) Cellular vaccination of MLH1$^{-/-}$ mice–an immunotherapeutic proof of concept study. Oncoimmunology 7:e1408748. https://doi.org/10.1080/2162402X.2017.1408748
28. Maletzki C, Wiegele L, Nassar I et al (2019) Chemo-immunotherapy improves long-term survival in a preclinical model of MMR-D-related cancer. J Immunother Cancer 7:1–14. https://doi.org/10.1186/s40425-018-0476-x
29. Maletzki C, Gladbach YS, Hamed M et al (2018) Cellular vaccination of MLH1$^{-/-}$mice–an immunotherapeutic proof of concept study. Oncoimmunology. https://doi.org/10.1080/2162402X.2017.1408748
30. Maletzki C, Beyrich F, Hühns M et al (2016) The mutational profile and infiltration pattern of murine MLH1$^{-/-}$ tumors: concurrences, disparities and cell line establishment for functional analysis. Oncotarget. https://doi.org/10.18632/oncotarget.10677
31. Maletzki C, Huehns M, Bauer I et al (2017) Frameshift mutational target gene analysis identifies similarities and differences in constitutional mismatch repair-deficiency and lynch syndrome. Mol Carcinog 56:1753–1764. https://doi.org/10.1002/mc.22632
32. Edelmann W, Yang K, Kuraguchi M et al (1999) Tumorigenesis in Mlh1 and Mlh1 / Apc1638N mutant mice. Cancer Res 59:1301–1307
33. Chae YK, Anker JF, Bais P, Namburi S (2018) Mutations in DNA repair genes are associated with increased neo-antigen load and activated T cell infiltration in lung adenocarcinoma. Oncotarget 9:7949–7960
34. Chang L, Chang M, Chang HM, Chang F (2018) Microsatellite instability: a predictive biomarker for cancer immunotherapy. Appl Immunohistochem Mol Morphol 26:e15–e21
35. Salem ME, Puccini A, Grothey A et al (2018) Landscape of tumor mutation load, mismatch repair deficiency, and PD-L1 expression in a large patient cohort of gastrointestinal cancers. Mol Cancer Res 16:805–812. https://doi.org/10.1158/1541-7786.MCR-17-0735
36. Maletzki C, Wiegele L, Nassar I et al (2019) Chemo-immunotherapy improves long- term survival in a preclinical model of MMR-D-related cancer. J Immunother Cancer 7:1–14
37. Feola S, Capasso C, Fusciello M et al (2018) Oncolytic vaccines increase the response to PD-L1 blockade in immunogenic and poorly immunogenic tumors. Oncoimmunology. https://doi.org/10.1080/2162402X.2018.1457596
38. Zhao R, Wan Q, Wang Y et al (2021) M1-like TAMs are required for the efficacy of PD-L1/PD-1 blockades in gastric cancer. Oncoimmunology. https://doi.org/10.1080/2162402X.2020.1862520
39. Liu Z, Wang H, Hu C et al (2021) Targeting autophagy enhances atezolizumab-induced mitochondria-related apoptosis in osteosarcoma. Cell Death Dis. https://doi.org/10.1038/s41419-021-03449-6
40. Lee MS, Ryoo BY, Hsu CH et al (2020) Atezolizumab with or without bevacizumab in unresectable hepatocellular carcinoma (GO30140): an open-label, multicentre, phase 1b study. Lancet Oncol 21:808–820. https://doi.org/10.1016/S1470-2045(20)30156-X
41. McDermott DF, Huseni MA, Atkins MB et al (2018) Clinical activity and molecular correlates of response to atezolizumab alone or in combination with bevacizumab versus sunitinib in renal cell carcinoma. Nat Med 24:749–757. https://doi.org/10.1038/s41591-018-0053-3
42. Kodumudi KN, Ramamoorthi G, Snyder C et al (2019) Sequential Anti-PD1 therapy following dendritic cell vaccination improves survival in a HER2 mammary carcinoma model and identifies a critical role for CD4 T cells in mediating the response. Front Immunol 10:1939. https://doi.org/10.3389/fimmu.2019.01939
43. Yoo SY, Badrinath N, Jeong S-N et al (2020) Overcoming tumor resistance to oncolyticvaccinia virus with Anti-PD-1-based combination therapy by inducing antitumor immunity in the tumor microenvironment. Vaccines 8:321. https://doi.org/10.3390/vaccines8020321
44. Kadam P, Sharma S (2020) Pd-1 immune checkpoint blockade promotes therapeutic cancer vaccine to eradicate lung cancer. Vaccines 8:1–13. https://doi.org/10.3390/vaccines8020317
45. Xu G, Feng D, Yao Y et al (2020) Listeria-based hepatocellular carcinoma vaccine facilitates anti-PD-1 therapy by regulating macrophage polarization. Oncogene 39:1429–1444. https://doi.org/10.1038/s41388-019-1072-3
46. Teng CF, Wang T, Wu TH et al (2020) Combination therapy with dendritic cell vaccine and programmed death ligand 1 immune checkpoint inhibitor for hepatocellular carcinoma in an orthotopic mouse model. Ther Adv Med Oncol. https://doi.org/10.1177/1758835920922034
47. Ji S, Lee J, Lee ES et al (2021) B16 melanoma control by anti-PD-L1 requires CD8+ T cells and NK cells: application of anti-PD-L1 Abs and Trp2 peptide vaccines. Hum Vaccines Immunother. https://doi.org/10.1080/21645515.2020.1866951
48. Sun NY, Chen YL, Wu WY et al (2019) Blockade of PD-L1 enhances cancer immunotherapy by regulating dendritic cell maturation and macrophage polarization. Cancers (Basel). https://doi.org/10.3390/cancers11091400
49. Shaul ME, Fridlender ZG (2019) Tumour-associated neutrophils in patients with cancer. Nat Rev Clin Oncol 16:601–620
50. Canè S, Van Snick J, Uyttenhove C et al (2021) TGFβ1 neutralization displays therapeutic efficacy through both an immunomodulatory and a non-immune tumor-intrinsic mechanism. J Immunother Cancer 9:e001798. https://doi.org/10.1136/jitc-2020-001798
51. Rieth J, Subramanian S (2018) Mechanisms of intrinsic tumor resistance to immunotherapy. Int J Mol Sci 19:1340. https://doi.org/10.3390/ijms19051340
52. Saleh R, Taha RZ, Nair VS et al (2019) PD-L1 blockade by atezolizumab downregulates signaling pathways associated with tumor growth, metastasis, and hypoxia in human triple negative breast cancer. Cancers (Basel). https://doi.org/10.3390/cancers11081050
53. Spranger S, Bao R, Gajewski TF (2015) Melanoma-intrinsic *β*-catenin signalling prevents anti-tumour immunity. Nature 523:231–235. https://doi.org/10.1038/nature14404
54. Benci JL, Xu B, Qiu Y et al (2016) Tumor interferon signaling regulates a multigenic resistance program to immune checkpoint blockade. Cell 167:1540-1554.e12. https://doi.org/10.1016/j.cell.2016.11.022
55. Ho HL, Chou TY, Yang SH et al (2019) PD-L1 is a double-edged sword in colorectal cancer: the prognostic value of PD-L1 depends on the cell type expressing PD-L1. J Cancer Res Clin Oncol 145:1785–1794. https://doi.org/10.1007/s00432-019-02942-y
56. Korehisa S, Oki E, Iimori M et al (2018) Clinical significance of programmed cell death-ligand 1 expression and the immune microenvironment at the invasive front of colorectal cancers with high microsatellite instability. Int J Cancer 142:822–832. https://doi.org/10.1002/ijc.31107
57. Konstantinopoulos PA, Luo W, Liu JF et al (2019) Phase II study of avelumab in patients with mismatch repair deficient and mismatch repair proficient recurrent/persistent endometrial cancer. J Clin Oncol 37:2786–2794. https://doi.org/10.1200/JCO.19.01021

8.3 Publication 3

International Journal of *Molecular Sciences*

MDPI

Article

Combined Gemcitabine and Immune-Checkpoint Inhibition Conquers Anti-PD-L1 Resistance in Low-Immunogenic Mismatch Repair-Deficient Tumors

Inken Salewski [1,†], Julia Henne [1,†], Leonie Engster [1], Bjoern Schneider [2], Heiko Lemcke [3,4], Anna Skorska [3,4], Peggy Berlin [5], Larissa Henze [1], Christian Junghanss [1] and Claudia Maletzki [1,*]

[1] Department of Medicine, Clinic III–Hematology, Oncology, Palliative Medicine, Rostock University Medical Center, University of Rostock, 18057 Rostock, Germany; Inken.salewski@med.uni-rostock.de (I.S.); julia.henne@uni-rostock.de (J.H.); leonie.engster@uni-rostock.de (L.E.); Larissa.henze@med.uni-rostock.de (L.H.); Christian.junghanss@med.uni-rostock.de (C.J.)
[2] Institute of Pathology, Rostock University Medical Center, University of Rostock, 18057 Rostock, Germany; bjoern.schneider@med.uni-rostock.de
[3] Department of Cardiac Surgery, Reference and Translation Center for Cardiac Stem Cell Therapy (RTC), Rostock University Medical Center, University of Rostock, 18057 Rostock, Germany; Heiko.Lemcke@med.uni-rostock.de (H.L.); anna.skorska@med.uni-rostock.de (A.S.)
[4] Faculty of Interdisciplinary Research, Department Life, Light & Matter, University Rostock, 18057 Rostock, Germany
[5] Division of Gastroenterology and Endocrinology, Department of Medicine II, Rostock University Medical Center, University of Rostock, 18057 Rostock, Germany; peggy.berlin@med.uni-rostock.de
* Correspondence: claudia.maletzki@med.uni-rostock.de
† Authors contributed equally.

Abstract: Tumors arising in the context of Lynch Syndrome or constitutional mismatch repair deficiency are hypermutated and have a good response towards immune-checkpoint inhibitors (ICIs), including α-PD-L1 antibodies. However, in most cases, resistance mechanisms evolve. To improve outcomes and prevent resistance development, combination approaches are warranted. Herein, we applied a combined regimen with an α-PD-L1 antibody and gemcitabine in a preclinical tumor model to activate endogenous antitumor immune responses. $Mlh1^{-/-}$ mice with established gastrointestinal tumors received the α-PD-L1 antibody (clone 6E11; 2.5 mg/kg bw, i.v., q2wx3) and gemcitabine (100 mg/kg bw, i.p., q4wx3) in mono- or combination therapy. Survival and tumor growth were recorded. Immunological changes in the blood were routinely examined via multi-color flow cytometry and complemented by ex vivo frameshift mutation analysis to identify alterations in $Mlh1^{-/-}$-tumor-associated target genes. The combined therapy of α-PD-L1 and gemcitabine prolonged median overall survival of $Mlh1^{-/-}$ mice from four weeks in the untreated control group to 12 weeks, accompanied by therapy-induced tumor growth inhibition, as measured by $^{[18F]}$-FDG PET/CT. Plasma cytokine levels of IL13, TNFα, and MIP1β were increased and also higher than in mice receiving either monotherapy. Circulating splenic and intratumoral myeloid-derived suppressor cells (MDSCs), as well as M2 macrophages, were markedly reduced. Besides, residual tumor specimens from combi-treated mice had increased numbers of infiltrating cytotoxic T-cells. Frameshift mutations in APC, Tmem60, and Casc3 were no longer detectable upon treatment, likely because of the successful eradication of single mutated cell clones. By contrast, novel mutations appeared. Collectively, we herein confirm the safe application of combined chemo-immunotherapy by long-term tumor growth control to prevent the development of resistance mechanisms.

Keywords: immune checkpoint inhibitor; MMR deficiency; in vivo imaging; tumor microenvironment; genetic model; coding microsatellite mutations

!"#!$%&'(
!"#$%&'

Citation: Salewski, I.; Henne, J.; Engster, L.; Schneider, B.; Lemcke, H.; Skorska, A.; Berlin, P.; Henze, L.; Junghanss, C.; Maletzki, C. Combined Gemcitabine and Immune-Checkpoint Inhibition Conquers Anti-PD-L1 Resistance in Low-Immunogenic Mismatch Repair-Deficient Tumors. Int. J. Mol. Sci. **2021**, 22, 5990. https://doi.org/10.3390/ijms22115990

Academic Editors: Yoland C. Antill and Paul James

Received: 19 May 2021
Accepted: 31 May 2021
Published: 1 June 2021

Publisher's Note: MDPI stays neutral with regard to jurisdictional claims in published maps and institutional affiliations.

1. Introduction

Conventional oncological treatment regimens include surgery, radiation, and chemotherapy. While the latter is a widely applied treatment option for primary and metastatic diseases, the side effects are complex, including myelosuppression. Cancer immunotherapy is a safe and effective treatment option, and immune-checkpoint inhibitors (ICIs) are widely used nowadays, both in research and clinically to force tumor cell killing via reactivation of exhausted T-cells. Additional to the already established α-PD1 and α-CTLA-4 antibodies, the FDA recently approved atezolizumab, avelumab, and durvalumab as antibodies against PD-L1, because of proven long-lasting immune-responses in certain patient cohorts [1–3].

Lynch Syndrome and constitutional mismatch repair deficiency (dMMR) are two hereditary cancer syndromes with a high likelihood of having a good response towards ICIs. In both syndromes, germline mutations in one of the mismatch-repair genes constitute the oncogenic driver, resulting in early-onset tumorigenesis [4–11]. Lynch Syndrome carriers frequently harbor MLH1 or MSH2 germline mutations, whereas, in constitutional mismatch repair deficiency, germline PMS2 and MSH6 mutations dominate. A hallmark of all dMMR-driven tumors is the high tumor mutational burden, often characterized by frameshift mutations in coding microsatellites (cMS) of tumor suppressor genes. This hyper- or ultra-hypermutated phenotype directly correlates with the level of immunity and contributes to the approval of the α-PD-1 antibody pembrolizumab for 1st-line treatment of patients with unresectable or metastatic dMMR colorectal cancer (CRC) [12,13]. The SAMCO-PRODIGE 54 randomized phase II trial is currently evaluating avelumab vs. standard 2nd-line treatment chemotherapy in metastatic dMMR CRC patients [14]. Additional studies are ongoing, including 1st and 2nd-line treatment schedules (clinical trials.gov).

While the enthusiasm of ICIs is often thwarted by resistance mechanisms and relapse upon successful ICI-tailored therapy, combination therapies are actively tested. A very promising approach is the combination of chemotherapeutics, based on the observation that some drugs activate endogenous antitumor immune responses [15]. These include direct effects such as the induction of immunogenic cell death, but also indirect effects via cytotoxic T cell activation and tumor infiltration. These encouraging results have contributed to the initiation of clinical trials for α-PD-L1-based chemo-immunotherapy to treat solid tumors (NCT03572400, NCT03324282, NCT03093922). Furthermore, even tumors with low mutational load (Lynch syndrome subtype G2) acquire a higher mutational burden by chemotherapy [16,17]. Gemcitabine is among the most promising drugs. Acting like a classical cytotoxic drug by inhibiting DNA synthesis, this substance has the capacity to activate the immune system and shift the tumor microenvironment towards an inflammatory milieu [18,19]. Indeed, in our previous study on $Mlh1^{-/-}$ mice, this drug, in conjunction with a whole tumor vaccine, prolonged survival via immune modulation [20]. To move on, we combined gemcitabine chemotherapy with an α-PD-L1 ICI and analyzed the outcome.

2. Results

2.1. In Vitro Analysis

Two cell lines, A7450 T1 M1 and 328, established from mouse duodenal tumors were used for preliminary in vitro experiments. The former cell line, A7450 T1 M1, was generated upon in vivo expansion, whereas 328 cells could be established from the primary tumor. Both cell lines are highly heterogenic in terms of morphology, growth kinetics, mutational profile, and drug response [21,22]. To test the efficacy of ultra-low-dose chemotherapy (CTX) treatment, a colony formation assay was performed. Figure 1A shows representative crystal violet stainings. Experiments revealed individual responses, with more evident growth inhibition in A7450 T1 M1 cells than in 328 cells (Figure 1A). For the former, cell density was approximately 20% lower after low-dose CTX treatment and remained decreased even after 6 days of rest. For the 328 cells, a decelerated response profile was observed with a lack of initial growth inhibition, but reduced cell numbers after an

additional 6 days of rest, finally reaching an inhibition of 15%. The numbers of viable cell colonies were thus below controls. Then, a semi-autologous short-term co-culture system was used to analyze the impact of the immune system. Tumor and immune cells were co-cultured in the presence of CTX, α-PD-L1, or a combination of both, and residual cells were counted after 72 h via flow cytometry (Figure 1B). Treatment with α-PD-L1 stimulated immune-mediated killing of A7450 T1 M1, but not 328 cells. CTX itself had no influence on tumor cell numbers. The combination of both agents boosted the immune-mediated killing of A7450 T1 M1 cells. Here again, 328 cells were resistant towards killing, and cell numbers even increased (Figure 1B). Then, the immune cells were stained for typical surface antigens to check for activation and exhaustion markers. Numbers of $Lag3^+$ T-lymphocytes increased in the combination (Figure 1C). $PD\text{-}L1^+$ and $PD\text{-}1^+$ cells were lower in T-lymphocytes exposed to A7450 T1 M1 cells and the combination therapy, while both markers were elevated under α-PD-L1 treatment. No change was seen for the 328-edited lymphocytes, irrespective of the treatment. Likewise, numbers of $CD4^+CD25^+Foxp3^+$ regulatory T cells were lower in lymphocytes co-cultured with A7450 T1 M1 cells and the combination therapy.

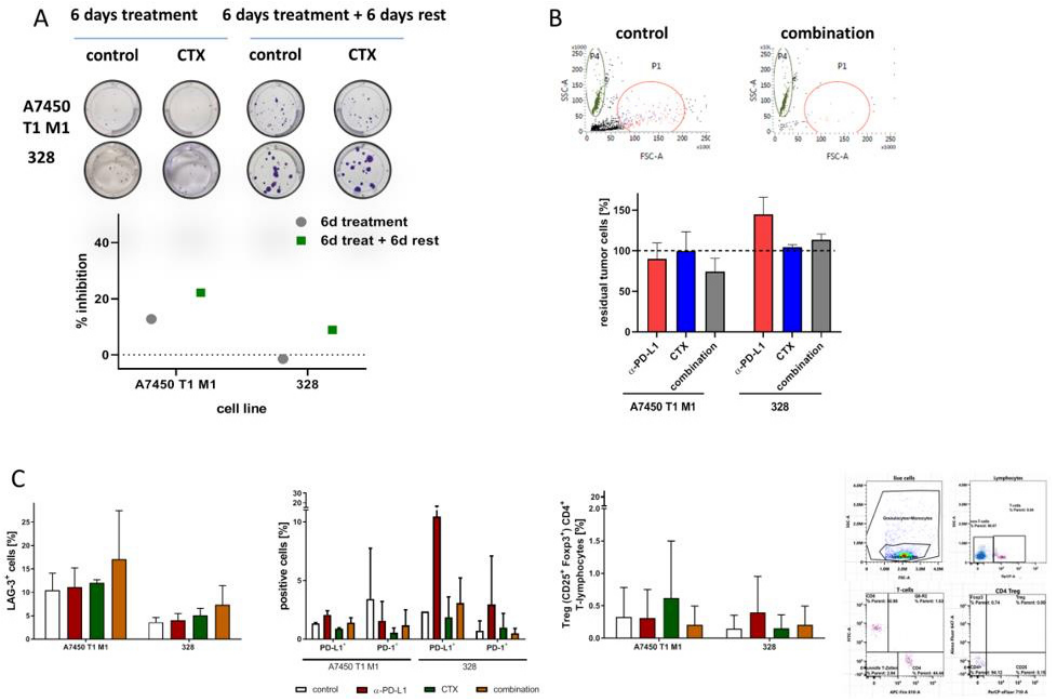

Figure 1. In vitro colony formation assay and co-culture. (**A**) Colony formation assay. $Mlh1^{-/-}$ cell lines A7450 T1 M1 and 328 were treated for 6 days with gemcitabine. Colonies were counted either directly after treatment or after an additional 6 days of rest. (**B**) Co-culture of tumor cells with murine immune cells. After 72 h, cells were counted and (**C**) immune cells were phenotyped. The gating strategy is shown on the right side, next to the bar charts. Events shown within the dot plots represent mean of the numbers of positive cells ± SD resulting from 20,000 events.

Hence, though differences did not reach statistical significance, the above data hinted towards the successful elimination of tumor cells because of immune-editing.

2.2. Combination of α-PD-L1 and CTX Prolongs the Survival of Mlh1$^{-/-}$ Mice

Then, we tested our treatment strategy in an in vivo Mlh1$^{-/-}$ model (see the workflow, Figure 2). Mice with an already diagnosed gastrointestinal tumor (GIT) received the α-PD-L1 antibody, CTX, a combination of both, or were left untreated (tumor size at the starting point: ≈50 mm^3). Survival time of the mice was significantly influenced by the different treatments. Monotherapies with either α-PD-L1 or CTX doubled the survival rate from 4 weeks (median survival) to around 6 to 7 weeks ($p < 0.05$ vs. control). The combination of both therapies has even prolonged overall survival, reaching 12 weeks ($p < 0.0001$ vs. control, Figure 2B). Accompanying longitudinal tumor volume analysis using $^{[18F]}$-FDG PET/CT revealed effective tumor growth control in all three treatment groups and significantly decreased tumor size in the combination group ($p < 0.05$ vs. control, Figure 2C). Although differences were insignificant between treatment groups, we want to emphasize that all mice in the combination group received follow-up screening, whereas only 75% and 50% of mice in the α-PD-L1 and CTX group, respectively, were available for PET/CT screening. The remaining mice had to be euthanized because of progressive disease. The combination therapy induced stable disease (SD) or partial response (PR) in 43% and 43% of mice, respectively. In the monotherapies, less than 50% of mice experienced SD or PR, and all control mice suffered from progressive disease (Figure 2C).

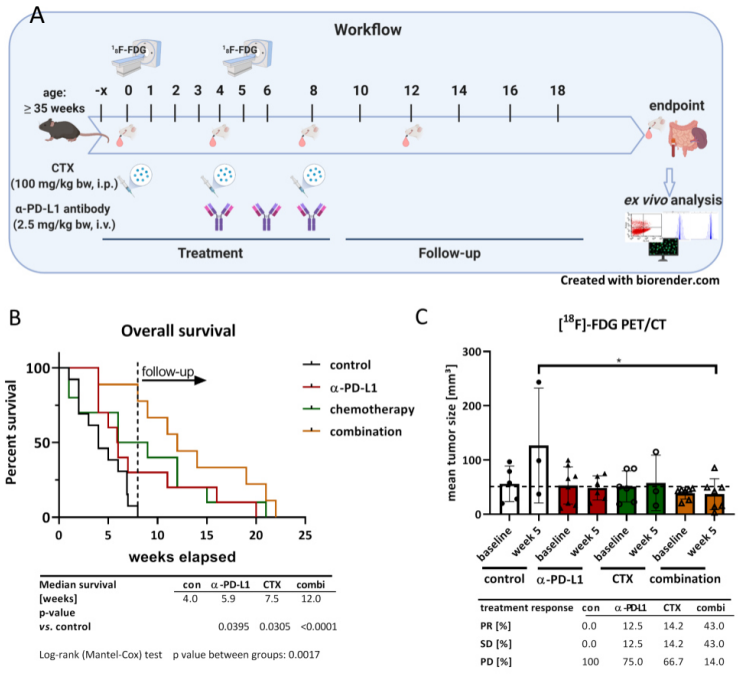

Figure 2. Therapy protocol and Kaplan-Meier survival curve. (**A**) Schematic therapeutic protocol including PET/CT imaging, blood collection and endpoint procedure. (**B**) Kaplan-Meier survival curve. Mice were treated with α-PD-L1 (clone 6E11, Genentech, 2.5 mg/kg bw, i.v., q2w), gemcitabine (100 mg/kg bw, i.p., q4wx3, CTX = chemotherapy), or a combination of chemotherapy, followed by α-PD-L1 antibody therapy four weeks later. (**C**) Tumor progression under therapy, measured with $^{[18F]}$FDG PET/CT. The mean tumor volume ± SD in mm^3 are shown. Measurements were taken at start of the respective therapy and 5 weeks later (n = 3–8 mice/group and time-point). * $p < 0.05$; one-way ANOVA (Dunnett's multiple comparison test).

2.3. Peripheral Immune Activation by Combinational Therapy

Furthermore, immunological changes in the blood were recorded routinely via flow cytometry (Figure 3). The plasma was analyzed using a multiplex cytokine assay (Figure 3A). IL10 and RANTES concentrations did not change over time in any of the four groups, whereas, in the combination, IL13, TNFα, MIP1β, and EOTAXIN levels increased, which might be due to an increase in cytokine-secreting T cells. Besides, α-PD-L1 monotherapy also increased MIP1β concentration to the same level as the combination treatment. Additional flow cytometric phenotyping of blood samples showed quite similar levels of positive cells in both monotherapy groups, while the combination therapy induced $CD3^+CD4^+$ T-helper cells significantly after 12 weeks of treatment ($p < 0.01$ combination vs. α-PD-L1; $p < 0.01$ combination vs. CTX, Figure 3B). Moreover, the $CD3^+CD8^+$ cytotoxic T cells increased by trend in the combination group as well as $CD83^+$ cells, indicative of activated B-cells and dendritic cells. The numbers of $CD11b^+GR1^+$ myeloid-derived suppressor cells (MDSCs) did not differ between individual treatment groups.

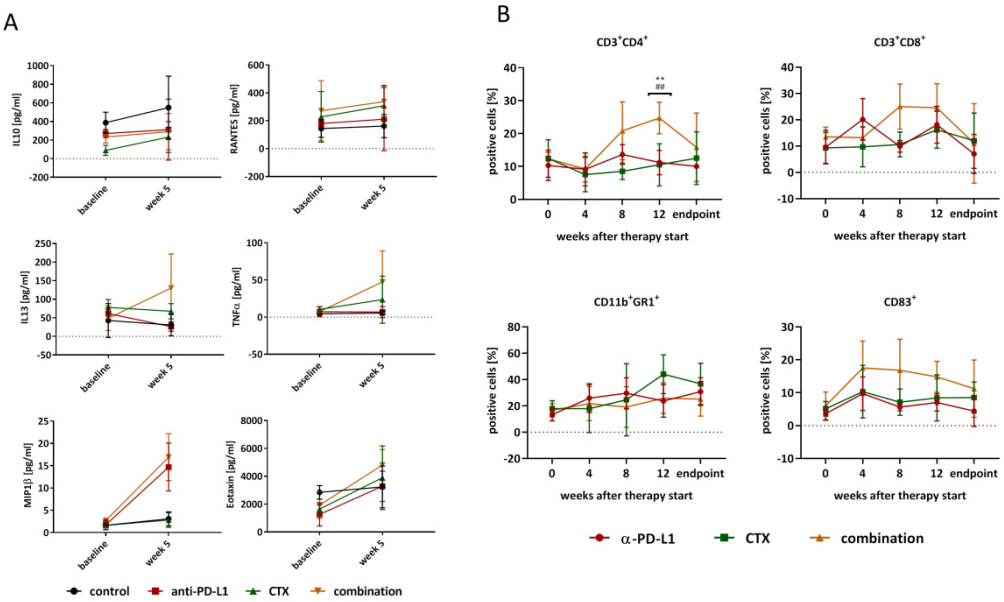

Figure 3. Quantification of plasma cytokine levels and assessment of immunologically relevant markers in the blood. (**A**) Cytokine levels in the plasma were analyzed at beginning of therapy and after 5 weeks. The y-axis shows the mean cytokine levels ± SD. (**B**) Every four weeks, blood was taken from mice under therapy to investigate immunological changes via flow cytometry. Represented are the numbers of positive cells ± SD resulting from 20,000 events, n = 3–5 mice/group. ** $p <$ 0.01 vs. CTX; one-way ANOVA (Bonferroni's multiple comparison test); ## $p < 0.01$ vs. α-PD-L1 monotherapy one-way ANOVA (Dunnett's multiple comparison test).

2.4. Spleens and Residual Tumors Change Their Immunological Profile

At the endpoint, either determined by humane endpoints or after several weeks of follow-up observation, spleens and residual tumors were analyzed using flow cytometry (Figure 4). Similar to the blood, numbers of $CD3^+CD4^+$ T-helper cells significantly increased in the spleen after combinational treatment ($p < 0.05$ vs. control). $CD3^+CD8^+$ cytotoxic T cells and $CD83^+$ cells were slightly increased after all three therapies. In contrast, $CD11b^+GR1^+$ MDSCs and $CD200R^+$ cells decreased upon treatment. The therapy effect on tumor infiltrating T cells goes hand in hand with the effect in the spleen. All three groups

were characterized by increased T cell levels, reaching significance in the combination ($CD3^+CD8^+$ T cells, $p < 0.05$ vs. control). The percentage of $CD11b^+GR1^+$ MDSCs was as high as in the control in the monotherapies but decreased significantly after combination therapy. The numbers of $CD83^+$ cells did not change considerably but declined in the α-PD-L1 monotherapy. No effect was seen for $CD200R^+$ cells, implicating a minor role in the immune regulatory functions of CD200-CD200R interaction.

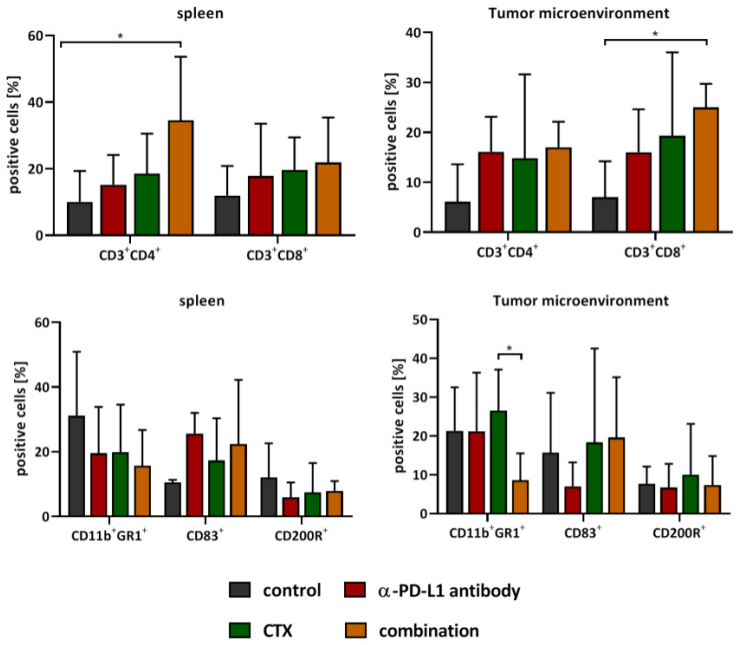

Figure 4. Flow cytometric phenotyping of spleens and tumor microenvironment. At the endpoint, spleen and tumor were resected. The single cell suspension was stained with respective antibodies and screened for immunological markers via flow cytometry. Represented are the numbers of positive cells ± SD resulting from 20,000 events, n = 3–5 mice/group. * $p < 0.05$ one-way ANOVA (Bonferroni's multiple comparison test).

In addition to flow cytometry, the tumor microenvironment was studied in detail by fluorescence microscopy (Figures 5 and 6). The amount of cytotoxic T-lymphocytes was higher upon CTX and the combination treatment. T-helper cells additionally increased by CTX. MDSCs were only visible in the control and CTX groups, and thus effectively eliminated by the α-PD-L1 antibody. M2 macrophages and DCs were present in all groups, but their density and location differed between groups (Figure 5). PD-1 expressing M2 macrophages vanished in the combination, in a similar manner to regulatory granulocytes, which were more abundant in the control and CTX groups. Hence, the α-PD-L1 antibody itself shaped the tumor microenvironment by eradicating immunosuppressive cell populations (i.e., $CD11b^+PD\text{-}L1^+$, $CD206^+PD1^+$) and promoting infiltration of antigen-presenting cells ($CD11c^+$). In support of this, we also found significantly higher levels of $IRF5^+$ cells within tumor sections treated with the α-PD-L1 antibody alone or in combination with CTX (Figure 6A,B). In most cases, $IRF5^+$ cells co-localized with $PD1^+$ cells in the lymphoid compartment within the tumors (Figure 6C). Hence, IRF5 may constitute a direct indicator for successful immune activation in α-PD-L1-based regimens.

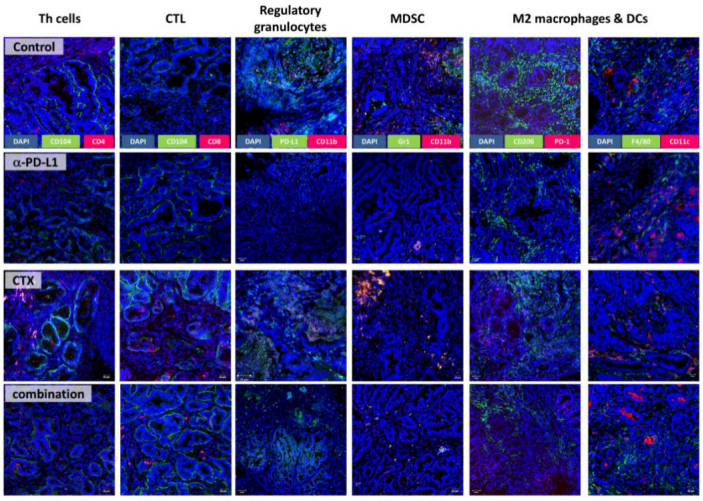

Figure 5. Immunofluorescence. Mlh1$^{-/-}$ GIT cryostat sections of 4 µm were prepared and the tumor microenvironment was studied upon staining with specific monoclonal antibodies, followed by nuclear staining with DAPI. Images were taken using a laser scanning microscope, Elyra PS.1 (Zeiss), and 20× objective.

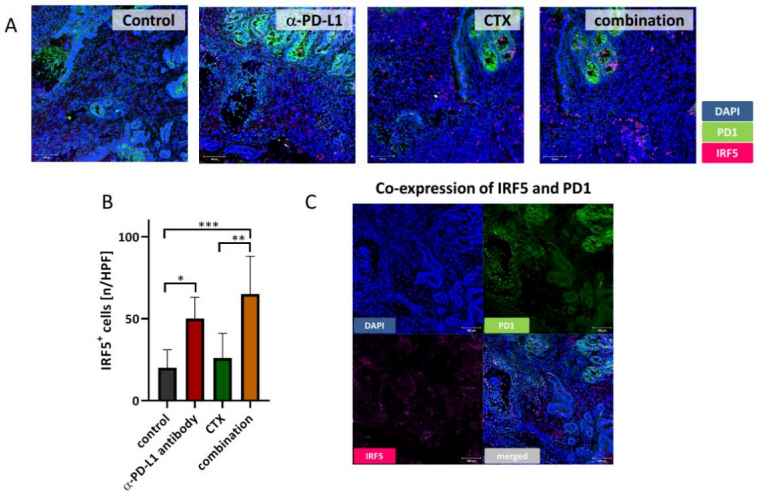

Figure 6. IRF5 immunofluorescence. (**A**) Mlh1$^{-/-}$ GIT cryostat sections of 4 µm were prepared and stained with Alexa488-conjugated anti-PD1 antibody and primary rabbit anti-IRF5 antibody, followed by staining with a secondary Alexa647-labeled antibody. Nuclei were counterstained with DAPI. Pictures were taken on a laser scanning microscope (Zeiss) using 20× objectives. (**B**) Quantification of IRF5^{+} infiltrating immune cells. At least three images were taken from each slide and numbers of infiltrating cells counted. Data are given as infiltrates/high power field (HPF). Mean + SD, n ≥ 3 samples/group; * $p < 0.05$; ** $p < 0.01$; *** $p < 0.001$; one-way ANOVA (Bonferroni's multiple comparison test). (**C**) Representative immunofluorescence images show co-localization of IRF5^{+} cells and PD1^{+} cells (single planes and merged channels).

2.5. Treatment with α-PD-L1 Induced Molecular Changes in cMS of dMMR-Target Genes

The therapies not only induced immunological changes but also influenced the mutational frequency in Mlh1$^{-/-}$ tumors (Figure 7). Both α-PD-L1 mono- and combinational therapy increased the overall mutation frequency of the tumor (Figure 7A). Figure 7B shows the mutation frequencies in dMMR-target genes. Frameshift mutations in APC, Tmem60, and Casc3 were no longer detectable upon treatment, likely because of eradicating single mutated cell clones. By contrast, novel mutations appeared (Figure 7B,C). Mutation frequencies in cMS repeats of MDC1 slightly increased after α-PD-L1 monotherapy and CTX. Additionally, cMS mutation frequencies in Senp6, Mbd6, and Lig4 increased after α-PD-L1 monotherapy. Since this trend was not seen in the combination, specific elimination is likely. Lig4 is the only exception. Here, cMS mutations were only detectable upon treatment but remained comparably low in the combination. CTX monotherapy alone triggered mutations in cMS of MDC1, Mbd6, and Lig4.

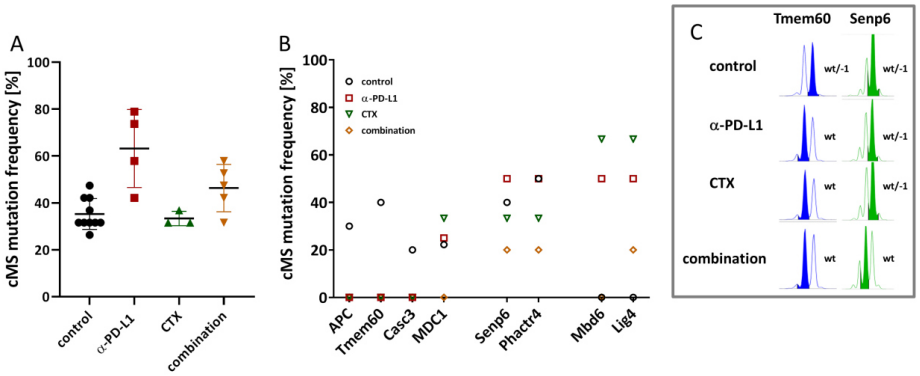

Figure 7. cMS mutation frequency. (**A**) Fragment length analysis was used to detect frameshift mutations in selected cMS. Overall mutational frequency in residual tumors revealed higher mutational load after α-PD-L1 monotherapy and the combination. (**B**) The cMS mutation frequency in selected Mlh1$^{-/-}$ target genes differed among the four therapy groups. In some genes, the results even indicated loss of single cell clones (APC, Tmem60, and Casc3). (**C**) Representative band shifts of two cMS loci in Tmem60 and Senp6 target genes. Wt—wildtype; wt/−1—wildtype/−1 s.

3. Discussion

In the present study, we targeted the PD-1/PD-L1 axis additional to conventional CTX to enhance the survival of Mlh1$^{-/-}$ mice. This strategy is based on the idea of utilizing CTX as an immunogenic cell death (ICD) inductor. Indeed, several reports from the literature provided sufficient data confirming ICD induction by cytostatic or cytotoxic drugs. These include, among others, anthracyclines such as doxorubicin, mitoxantrone, and oxaliplatin [23–26]. Besides, we recently described successful ICD induction by the deoxycytidine nucleoside analogue gemcitabine, characterized by reduced amounts of intracellular IDO-1, increased levels of surface-bound CalR, and elevated HMGB1 secretion [20]. To boost CTX-initiated immune responses, we here added an α-PD-L1 antibody and performed in vitro as well as in vivo analyses. Using a semi-autologous in vitro co-culture system, we provide evidence for the successful targeting of dMMR epithelial Mlh1$^{-/-}$ murine tumor cells. However, the therapeutic outcome was highly individual among the two cell lines, A7450 T1 M1 and 328, nicely reflecting the heterogeneity among dMMR tumors patients, even in cases harboring the same MMR mutation [27,28]. The cell line Mlh1$^{-/-}$ 328 is highly resistant and representative of a low-immunogenic subtype [21,22], which was confirmed further in this study. For the A7450 T1 M1 cells, the combination proved superior compared to either monotherapy with CTX or α-PD-L1 blockade. By studying the immune cells' phenotype in-depth, we identified differences in

specific activation and immune-regulatory markers. Numbers of PD-L1$^+$ and PD-1$^+$ as well as CD4$^+$CD25$^+$Foxp3$^+$ regulatory T cells were exclusively lower in lymphocytes co-cultured with A7450 T1 M1 cells and the combination therapies. In 328 cells, no such differences were seen. Successful elimination of tumor cells is thus a likely result of creating an ICD-mediated inflamed, immunogenic tumor environment that enabled T cell-mediated killing. However, this regimen may only succeed in cases of at least moderate tumor immunity.

Using the Mlh1$^{-/-}$ mouse model, we transferred the therapeutic CTX-α-PD-L1 therapy approach in the preclinical situation. Monotherapy of CTX or α-PD-L1 prolonged the overall survival of tumor-bearing mice, which was additionally improved by applying the combination of both agents. Hence, this setting proved safe and effective in our hands. By applying PET/CT staging, induction of SD or PR was seen in >80% of mice, respectively, and thus confirmed successful long-term effects of the applied regimen. Monotherapy of either agent yielded objective response in roughly 25% of mice, matching with clinical data, in which comparable or even superior response towards ICB compared to CTX monotherapy was already proven [29,30]. By combining immunogenic CTX, outcomes for patients with solid tumors were considerably improved. An example of successful chemo-immunotherapy is the combination of platinum CTX with PD-1/PD-L1 inhibitors [31–33], which has now become the standard 1st-line option for advanced PD-L1$^+$ non-small cell lung cancer [34].

With the aim of inducing long-term immunological memory, longitudinal immune profiling revealed elevated plasma levels of IL13, TNFα, EOTAXIN, and MIP1β in the combination, accompanied by higher numbers of cytokine-secreting T-helper cells. The latter is likely attributable to the α-PD-L1 antibody since MIP1β levels additionally increased under this monotherapy. CTX monotherapy did not influence cytokines, with levels being comparable to controls. Another study on pancreatic carcinomas described the consistently high synthesis of CCL/CXCL chemokines and TGF-β-associated signals by gemcitabine after long-term treatment [35]. Alteration of disease course after combined gemcitabine and α-PD-1 treatment was only reached if mice also underwent genetic or pharmacologic ablation of TGF-β signaling. Though we have not analyzed TGF-β-signaling in depth, one may speculate that if induced at all, the α-PD-L1 antibody itself may have neutralized such effects. In support of this, we detected higher numbers of circulating CD83$^+$ cells as well as CD3$^+$CD8$^+$ cytotoxic T cells in the combination group. Both cell types are involved in immune-mediated inflammation, either as antigen-presenting or effector cells. Hence, the dosing interval seems pivotal. CTX was given here three times with long treatment-free intervals, rendering the establishment of additional immunosuppressive cytokine barriers quite unlikely. Another point worth mentioning is the missing impact on circulating MDSCs. This highly immunosuppressive myeloid subtype is well-known for its capacity to facilitate tumor progression—both directly and indirectly [36–40]. The notion that we did not see any differences in numbers of circulating and splenic MDSCs in any treatment group matches with recent studies [41] and may explain the final relapse of Mlh1$^{-/-}$ tumors. Generally, a high frequency of memory cells and low numbers of immunosuppres-sive cells are indicative of a good response, though individual differences exist [42]. The Mlh1$^{-/-}$ mouse model is representative for immunosuppressive subtypes, thus, convert-ing immune regulatory cells into pro-inflammatory cell types seem challenging. Still, the combination was able to shape the local tumor microenvironment. This included effective elimination of MDSCs and massive reduction of M2 macrophages even after several weeks of after-care, and vice versa; cytotoxic T lymphocytes increased, attributable to successful re-activation of antigen-driven immune responses. This finding is in line with increasing evidence on a broader remodeling of the tumor microenvironment by ICI than previously anticipated [43]. Although the lymphoid compartment is the main target for ICI, other immune cell populations, including myeloid cells, are affected as well [44]. In support of this, we also found higher levels of IRF5$^+$ cells within tumor sections treated with the α-PD-L1 antibody alone or in the combination, often co-localized with PD1$^+$ cells. IRF5 regulates type I IFN signaling and cytokines/chemokines with lymphocyte-chemotactic

activities, such as RANTES. MIP1α/β and is considered a specific marker of inflammatory macrophages [45]. Such positive immune-modulating effects were mainly attributable to the α-PD-L1 antibody, while the CTX itself shaped the tumor microenvironment less efficiently. Here, numbers of MDSCs remained similar between controls and treated mice. Another recent study even reported boosted intratumoral MDSC accumulation by 5-FU that counteracted T and NK cell infiltration, thus abrogating the anti-tumor efficacy of PD-L1 blockade [46]. Such immunosuppressive effects were not seen in our study. In contrast, a positive effect on the immune system was seen here, by slightly elevated numbers of circulating as well as tumor-infiltrating cytotoxic and T helper cells. Other studies likewise reported very low toxicity on T cells and increased $CD8^+$ cytotoxic T cell infiltration upon combined application of low, non-cytotoxic doses of gemcitabine, a Chk1 Inhibitor, and α-PD-L1 antibody [19,47]. Hence, gemcitabine is indeed a very interesting and promising backbone for combination therapies with ICIs.

While dMMR constitutes a predictive biomarker for ICI-based regimens, recent evidence demonstrates that AT-rich interaction domain 1A (ARID1A) deficiency is associated with high antitumor immunity and good response towards ICI-monotherapy [48]. Indeed, tumors arising in $Mlh1^{-/-}$ mice harbor multiple ARID1A missense mutations, resulting in loss-of-function of this tumor suppressor [22]. Hence, the observed clinical response seen here upon mono- and combination therapy with α-PD-L1 adds another piece of evidence for the causative relevance of ARID1A mutations in dMMR-driven cancers. In support of this, a complete pathologic response after two months of combined mFOLFOX6 with pembrolizumab therapy was recently reported in a Lynch syndrome patient suffering from an ARID1A mutated and tumor mutational burden (TMB) high dMMR CRC [49]. It is therefore tempting to speculate that the combination therapy is indeed beneficial for ARID1A-mutated dMMR tumors. Besides, the finding that PD-L1 expression is generally low in dMMR CRCs and not predictive in response to ICIs [50,51] warrants further investigations on ARID1A mutation status as a predictive biomarker.

Another interesting finding of our current study was the observed striking difference in the mutational profile of the selected cMS marker. The monotherapies as well as their combination altered cMS frequency. Single mutated clones vanished, especially in the combination. By contrast, novel mutations appeared under CTX or ICI monotherapy and provide another explanation for final relapse. Though not analyzed in detail here, we speculate higher TMB after mono- than combination therapy. Notably, the most significant changes were seen after α-PD-L1 monotherapy.

Finally, the patients' responses towards ICB are so individual, and determinants of such distinct reactions are just at the beginning of being understood. There is an increasing body of evidence pointing towards TMB, immune cell densities, and types in the tumor microenvironment, as well as expression levels of PD-1/PD-L1 and cytokines as legitimate factors. Elucidating the determinants of response and resistance are key to improving treatment strategies prospectively.

4. Materials and Methods

4.1. Cell Culture

$Mlh1^{-/-}$ tumor cells were established in our lab and basically characterized [22,52]. Cells were cultured in DMEM medium, supplemented with 10% FCS (fetal calf serum), 6mM Glutamine, and antibiotics (all from Biochrom, Berlin, Germany). Prior to analysis, cells were harvested, washed with PBS, and counted.

4.2. Colony Formation Assay

Cells were cultured as described above. For colony formation assay, a standard protocol was used as described before [53]. Briefly, 500 cells per well were seeded in a 6 well plate and incubated overnight. Thereafter, cells were treated with 0.24 nM gemcitabine or left untreated. After 6 days medium was removed and remaining cells were stained with 500 µL 0.2% crystal violet for 10 min on a rocking plate. Then, the wells were washed 5

times with PBS. For the second group, drug-containing medium was removed after 6 days, and cells were rested with medium for additional 6 days. Afterwards, the amount of colonies was analyzed using ImageJ-win64.

4.3. Co-Culture Experiments

Harvested cells were stained with 5 µM CMFDA for 15 min at 37 °C. Cells were washed with PBS and seeded in a 24 well plate at a density of 20,000 cells per well. On the next day, 0.24 nM gemcitabine was added. Immune cells were harvested from peripheral blood samples routinely taken from $Mlh1^{-/-}$ mice. Around 100 µL of pooled blood was incubated with erythrocyte lysis buffer (155 mM NH_4Cl (MERCK Millipore, Darmstadt, Germany), 10 mM $KHCO_3$ (MERCK Millipore), and 0.1 mM EDTA (Applichem, Darmstadt, Germany)) for 15 min, then stopped with PBS. Approximately 200,000 blood cells (E:T ratio: 1:10) were seeded per well. After 24 h, α-PD-L1 (10 µg/mL) was added. Tumor cells were counted with fluorescent microsphere beads (1.4 ⇥ 105 beads/mL, size: 10 µm, Polysciences, Hirschberg an der Bergstrasse, Germany) on a Flow Cytometer (BD FACSVerse™, BD Pharmingen, Heidelberg, Germany). Data analysis was performed using BD FACSuite software (BD Pharmingen). Additionally, immune cells were stained with a panel of conjugated monoclonal antibodies (mAb, 0.125 µg to 1.5 µg each) and measured on a spectral flow cytometer (Cytek™ Aurora, Amsterdam, The Netherlands). Data were analyzed using SpectroFlow™ Version 2.2.0.3.

4.4. $Mlh1^{-/-}$ Mouse Model and In Vivo Treatment Protocol

4.4.1. Institutional Review Board Statement

The German local authority approved all animal experiments on 27 June 2017: "Landesamt für Landwirtschaft, Lebensmittelsicherheit und Fischerei Mecklenburg-Vorpommern" (approval number: 7221.3-1-026/17; -026/17-3), under the German animal protection law and the EU Guideline 2010/63/EU. Mice were bred in the animal facility of the University Medical Center in Rostock under specific pathogen-free conditions. Mlh1 genotyping was done according to [21]. During their whole life-time, all animals got enrichment in the form of mouse-igloos (ANT Tierhaltungsbedarf, Buxtehude, Germany), nesting material (shredded tissue paper, Verbandmittel GmbH, Frankenberg, Germany), paper roles (75 ⇥ 38 mm, H 0528–151, ssniff-Spezialdiäten GmbH, Cologne, Germany), and wooden sticks (40 ⇥ 16 ⇥ 10 mm, Abedd, Vienna, Austria). During the experiment, mice were kept in type III cages (Zoonlab GmbH, Castrop-Rauxel, Germany) at 12-h dark:light cycle, the temperature of 21 ± 2 °C, and relative humidity of 60 ± 20% with food (pellets, 10 mm, ssniff-Spezialdiäten GmbH, Soest, Germany) and tap water ad libitum.

4.4.2. Experimental Protocol

Mice with PET/CT proven GIT (located in the duodenum) were taken into therapy. α-PD-L1 antibody (clone 6E11, kindly provided by Genentech, a subsidiary of Roche, South San Francisco, CA, USA) was dissolved in PBS and given intravenously (dose: 2.5 mg/kg bw, n = 10 mice) every 2 weeks, and gemcitabine (CTX, 100 mg/kg bw) intraperitoneal every 4 weeks (n = 10 mice), for a total of 3 times. In combination (n = 9 mice), CTX was given first, and after four weeks, α-PD-L1 antibody treatment started. Control mice were untreated (n = 9 mice). A treatment schedule is depicted in Figure 1. To prevent suffering of the mice, soaked pellets were offered and, additionally, humane endpoints (weight loss >15%, pain/distress, changes in social behavior) were applied. Before mice became moribund, they were sacrificed and blood, spleen, lymph nodes and GIT were removed for further analyses.

4.5. PET/CT Imaging

PET/CT imaging scans were performed on a small animal PET/CT scanner (Inveon PET/CT, Siemens Medical Solutions, Knoxville, TN, USA) according to a standard protocol as described before [54,55]. The PET image reconstruction method consisted of a

2-dimensional ordered subset expectation maximization algorithm (2D-OSEM) with four iterations and six subsets. Attenuation correction was performed on the basis that whole-body CT scan and a decay correction for [18F] was applied. PET images were corrected for random coincidences, dead time, and scatter. By marking the entire tumors, starting at the edge and cutting through the whole $^{[18F]}$FDG-enriched tumor, volumes and SUVs were determined using Inveon Research Workplace 4.2 software (Siemens Medical Solutions USA, Knoxville, Tennessee).

4.6. Immune Phenotyping

Blood samples were taken from anaesthetized mice every 6 weeks (retrobulbar venous plexus). Single cell suspensions of spleens and GIT were obtained upon passing them through a cell strainer (100 µm). Samples (2 × 10^5/well) were stained with a panel of conjugated monoclonal antibodies (mAb, 1 µg each) followed by lysis of erythrocytes. Negative controls consisted of lymphocytes stained with the appropriate isotypes (Biolegend, San Diego, CA, USA) or unstained cells. Cells were washed, solved in PBS, and analyzed on a flow cytometer (BD FACSVerse™, BD Pharmingen). Data analysis was performed using BD FACSuite software (BD Pharmingen).

4.7. Procartaplex Cytokine Assay

Cytokine levels in plasma samples were determined according to the manufacturer's instructions of the Procartaplex™ multiplex immunoassay (Thermo Fisher Scientific, Schwerte, Germany). Measurement and cytokine quantification was performed on a Bioplex 2000 (Bio-Rad Laboratories GmbH, Munich, Germany) in combination with the Bio-Plex Manager Software. Absolute plasma cytokine and chemokine level are presented [pg/mL].

4.8. Fragment Length Analysis of cMS Target Genes

Fragment length analysis was done from multiplexed PCRs of gDNA (25 ng/sample) from tumor and normal tissue as described [22]. To identify potential Mlh1 target genes, a panel (n = 20 marker) was screened. Primers were designed using Primer3 software (Elixir Estonia, Tartu, Estonia) to yield short amplicons (≅200 bp). Frameshift mutations were detected by mono- and/or biallelic band shifts, usually characterized by deletions.

4.9. Immunofluorescence

Air-dried cryostat sections (4 µm thickness) were fixed (methanol, 8 min). Unspecific binding sites were blocked in 2% BSA (Roth, Karlsruhe, Germany) for 1 h followed by incubation with 1 µg of the following AlexaFluor488, AlexaFluor594, and AlexaFluor 647-labeled mAbs: CD4, CD8α, CD11b, Gr1, CD11c, F4/80, CD104, CD206, PD-1, and PD-L1 (all from Biolegend). For intracellular stainings, slides were fixed in 4% paraformaldehyde w/o methanol (Thermo Scientific, Darmstadt, Germany, 30min) and cells permeabilized in 0.5% Triton X−100 (Sigma-Aldrich, Darmstadt, Germany, 15 min). After blocking with 2% BSA (Serva, Heidelberg, Germany), slides were incubated with the monoclonal rabbit anti-IRF5 antibody (1:50; ThermoFisher Scientific, Darmstadt, Germany) overnight at 4 °C, followed by a secondary goat anti-rabbit Alexa647 antibody (1:500; Cell Signaling, Frankfurt am Main, Germany). Sections were washed, embedded in Roti Mount Flour Care DAPI (Roth), and target proteins visualized on a confocal laser scanning microscope (Elyra 7, Zeiss, Jena, Germany) using 20× objectives. $IRF5^+$ cells were quantified by counting individual positive cells in three high power fields per sample (n = 3/group).

4.10. Statistics

All values are expressed as mean ± SD. After proving the assumption of normality (Kolmogorov-Smirnov test), differences between vaccinated and control mice were determined using the unpaired Student's t-test or one-way ANOVA (Bonferroni or Dunnett's multiple comparison). Kaplan-Meier survival analysis was done by applying the log rank

(Mantel Cox) test. Statistical analyses were performed using GraphPad Prism 8.0.2 (San Diego, CA, USA). The criterion for significance was set to $p < 0.05$.

5. Conclusions

The combination of gemcitabine and α-PD-L1 prolongs the lifetime of $Mlh1^{-/-}$ mice significantly via long-term tumor growth control. The treatment modulates the tumor microenvironment by eliminating MDSCs and massive reductions of M2 macrophages counterbalanced by an increase in cytotoxic T cells. Patients would profit from a combinational chemo- and ICI therapy, to prevent development of resistance mechanisms.

Author Contributions: Conceptualization, C.M.; methodology, C.M., I.S., J.H., and L.E.; software, I.S. and J.H. validation, C.M.; formal analysis, C.M. and I.S.; investigation, C.M..; data curation, C.M., I.S., J.H., L.E., and B.S.; writing—original draft preparation, I.S.; writing—review and editing, C.M., H.L., A.S., P.B., C.J., and L.H.; visualization, I.S., J.H., and P.B.; supervision, C.M.; project administration, C.M.; funding acquisition, C.M. All authors have read and agreed to the published version of the manuscript.

Funding: This research was funded by the German research foundation, grant number MA5799/2-2.

Institutional Review Board Statement: The study was conducted according to the guidelines of the Declaration of Helsinki, and approved by the Institutional Review Board (or Ethics Committee) of the German local authority on 27 June 2017: "Landesamt für Landwirtschaft, Lebensmittelsicherheit und Fischerei Mecklenburg-Vorpommern" (approval number: 7221.3-1-026/17; -026/17-3), under the German animal protection law and the EU Guideline 2010/63/EU.

Informed Consent Statement: Not applicable.

Data Availability Statement: Data are available from the corresponding author upon reasonable request.

Acknowledgments: We gratefully thank Genentech, a subsidiary of Roche, South San Francisco, USA for providing the clone 6E11 for in vivo experiments. We additionally thank Ilona Klamfuss and Chantal von Hörsten for breeding mice, Brigitte Vollmar and Bernd Krause for their continuous support in their efforts of chairing the Core Facility of Multimodal Small Animal Imaging. We also gratefully acknowledge the excellent technical assistance of Joanna Förster, as well as support from the Core Facility for Cell Sorting & Cell Analysis, Laboratory for Clinical Immunology, University Medical Center Rostock. Furthermore, we thank Carina Bergner and Anja Gummesson, radiopharmacy team of the Department of Nuclear Medicine of the University Medical Centre Rostock, for providing 18F-FDG for the small animal PET/CT experiments.

Conflicts of Interest: The authors declare no conflict of interest. The funders had no role in the design of the study; in the collection, analyses, or interpretation of data; in the writing of the manuscript; or in the decision to publish the results.

References

1. Ning, Y.; Suzman, D.; Maher, V.E.; Zhang, L.; Tang, S.; Ricks, T.; Palmby, T.; Fu, W.; Liu, Q.; Goldberg, K.B.; et al. FDA Approval Summary: Atezolizumab for the Treatment of Patients with Progressive Advanced Urothelial Carcinoma after Platinum-Containing Chemotherapy. Oncologist **2017**, 22, 743–749. [CrossRef] [PubMed]
2. Pal, S.K.; Hoffman-Censits, J.; Zheng, H.; Kaiser, C.; Tayama, D.; Bellmunt, J. Atezolizumab in Platinum-treated Locally Advanced or Metastatic Urothelial Carcinoma: Clinical Experience from an Expanded Access Study in the United States. Eur. Urol. **2018**, 73, 800–806. [CrossRef] [PubMed]
3. Solomon, B.; Young, R.J.; Rischin, D. Head and neck squamous cell carcinoma: Genomics and emerging biomarkers for immunomodulatory cancer treatments. Semin. Cancer Biol. **2018**, 52, 228–240. [CrossRef] [PubMed]
4. Pearlman, R.; Frankel, W.L.; Swanson, B.; Zhao, W.; Yilmaz, A.; Miller, K.; Bacher, J.; Bigley, C.; Nelsen, L.; Goodfellow, P.J.; et al. Prevalence and Spectrum of Germline Cancer Susceptibility Gene Mutations Among Patients With Early-Onset Colorectal Cancer. JAMA Oncol. **2017**, 3, 464–471. [CrossRef] [PubMed]
5. Imai, K.; Yamamoto, H. Carcinogenesis and microsatellite instability: The interrelationship between genetics and epigenetics. Carcinogenesis **2008**, 29, 673–680. [CrossRef]
6. Álvaro, E.; Cano, J.M.; García, J.L.; Brandáriz, L.; Olmedillas-López, S.; Arriba, M.; Rueda, D.; Rodríguez, Y.; Cañete, Á.; Arribas, J.; et al. Clinical and molecular comparative study of colorectal cancer based on age-of-onset and tumor location: Two main criteria for subclassifying colorectal cancer. Int. J. Mol. Sci. **2019**, 20, 968. [CrossRef]

7. Evrard, C.; Tachon, G.; Randrian, V.; Karayan-Tapon, L.; Tougeron, D. Microsatellite Instability: Diagnosis, Heterogeneity, Discordance, and Clinical Impact in Colorectal Cancer. Cancers **2019**, 11, 1567. [CrossRef]
8. Wimmer, K.; Rosenbaum, T.; Messiaen, L. Connections between constitutional mismatch repair deficiency syndrome and neurofibromatosis type 1. Clin. Genet. **2017**, 91, 507–519. [CrossRef]
9. Tabori, U.; Hansford, J.R.; Achatz, M.I.; Kratz, C.P.; Plon, S.E.; Frebourg, T.; Brugieres, L. Clinical management and tumor surveillance recommendations of inherited mismatch repair deficiency in childhood. Clin. Cancer Res. **2017**, 23, e32–e37. [CrossRef] [PubMed]
10. Bakry, D.; Aronson, M.; Durno, C.; Rimawi, H.; Farah, R.; Alharbi, Q.K.; Alharbi, M.; Shamvil, A.; Ben-Shachar, S.; Mistry, M.; et al. Genetic and clinical determinants of constitutional mismatch repair deficiency syndrome: Report from the constitutional mismatch repair deficiency consortium. Eur. J. Cancer **2014**, 50, 987–996. [CrossRef]
11. Aronson, M.; Colas, C.; Shuen, A.; Hampel, H.; Foulkes, W.D.; Baris Feldman, H.; Goldberg, Y.; Muleris, M.; Wolfe Schneider, K.; McGee, R.B.; et al. Diagnostic criteria for constitutional mismatch repair deficiency (CMMRD): Recommendations from the international consensus working group. J. Med. Genet. **2021**. [CrossRef] [PubMed]
12. Tan, E.; Sahin, I.H. Defining the current role of immune checkpoint inhibitors in the treatment of mismatch repair-deficient/microsatellite stability-high colorectal cancer and shedding light on future approaches. Expert Rev. Gastroenterol. Hepatol. **2021**, 1–8. [CrossRef] [PubMed]
13. Trullas, A.; Delgado, J.; Genazzani, A.; Mueller-Berghaus, J.; Migali, C.; Müller-Egert, S.; Zander, H.; Enzmann, H.; Pignatti, F. The EMA assessment of pembrolizumab as monotherapy for the first-line treatment of adult patients with metastatic microsatellite instability-high or mismatch repair deficient colorectal cancer. ESMO Open **2021**, 6, 100145. [CrossRef] [PubMed]
14. Taïeb, J.; André, T.; El Hajbi, F.; Barbier, E.; Toullec, C.; Kim, S.; Bouche, O.; Di Fiore, F.; Chauvenet, M.; Perrier, H.; et al. Avelumab versus standard second line treatment chemotherapy in metastatic colorectal cancer patients with microsatellite instability: The SAMCO-PRODIGE 54 randomised phase II trial. Dig. Liver Dis. **2020**, 53, 318–323. [CrossRef] [PubMed]
15. Li, J.-Y.; Chen, Y.-P.; Li, Y.-Q.; Liu, N.; Ma, J. Chemotherapeutic and targeted agents can modulate the tumor microenvironment and increase the efficacy of immune checkpoint blockades. Mol. Cancer **2021**, 20, 27. [CrossRef] [PubMed]
16. Seth, S.; Ager, A.; Arends, M.J.; Frayling, I.M. Lynch syndrome—Cancer pathways, heterogeneity and immune escape. J. Pathol. **2018**, 246, 129–133. [CrossRef]
17. Binder, H.; Hopp, L.; Schweiger, M.R.; Hoffmann, S.; Juhling, F.; Kerick, M.; Timmermann, B.; Siebert, S.; Grimm, C.; Nersisyan, L.; et al. Genomic and transcriptomic heterogeneity of colorectal tumours arising in Lynch syndrome. J. Pathol. **2017**, 243, 242–254. [CrossRef] [PubMed]
18. Parente, P.; Parcesepe, P.; Covelli, C.; Olivieri, N.; Remo, A.; Pancione, M.; Latiano, T.P.; Graziano, P.; Maiello, E.; Giordano, G. Crosstalk between the tumor microenvironment and immune system in pancreatic ductal adenocarcinoma: Potential targets for new therapeutic approaches. Gastroenterol. Res. Pract. **2018**, 2018. [CrossRef]
19. Sen, T.; Della Corte, C.M.; Milutinovic, S.; Cardnell, R.J.; Diao, L.; Ramkumar, K.; Gay, C.M.; Stewart, C.A.; Fan, Y.; Shen, L.; et al. Combination Treatment of the Oral CHK1 Inhibitor, SRA737, and Low-Dose Gemcitabine Enhances the Effect of Programmed Death Ligand 1 Blockade by Modulating the Immune Microenvironment in SCLC. J. Thorac. Oncol. **2019**, 14, 2152–2163. [CrossRef]
20. Maletzki, C.; Wiegele, L.; Nassar, I.; Stenzel, J.; Junghanss, C. Chemo-immunotherapy improves long-term survival in a preclinical model of MMR-D-related cancer. J. Immunother. Cancer **2019**, 7, 1–4. [CrossRef]
21. Salewski, I.; Gladbach, Y.S.; Kuntoff, S.; Irmscher, N.; Hahn, O.; Junghanss, C.; Maletzki, C. In vivo vaccination with cell line-derived whole tumor lysates: Neoantigen quality, not quantity matters. J. Transl. Med. **2020**, 18, 1–5. [CrossRef]
22. Gladbach, Y.S.; Wiegele, L.; Hamed, M.; Merkenschläger, A.M.; Fuellen, G.; Junghanss, C.; Maletzki, C. Unraveling the Heterogeneous Mutational Signature of Spontaneously Developing Tumors in MLH1−/− Mice. Cancers **2019**, 11, 1485. [CrossRef] [PubMed]
23. Machiels, J.P.H.; Todd Reilly, R.T.; Emens, L.A.; Ercolini, A.M.; Lei, R.Y.; Weintraub, D.; Okoye, F.I.; Jaffee, E.M. Cyclophosphamide, doxorubicin, and paclitaxel enhance the antitumor immune response of granulocyte/macrophage-colony stimulating factor-secreting whole-cell vaccines in HER-2/neu tolerized mice. Cancer Res. **2001**, 61, 3689–3697.
24. Sukkurwala, A.Q.; Adjemian, S.; Senovilla, L.; Michaud, M.; Spaggiari, S.; Vacchelli, E.; Baracco, E.E.; Galluzzi, L.; Zitvogel, L.; Kepp, O.; et al. Screening of novel immunogenic cell death inducers within the NCI mechanistic diversity set. Oncoimmunology **2014**, 3, e28473. [CrossRef] [PubMed]
25. Hato, S.V.; Khong, A.; De Vries, I.J.M.; Lesterhuis, W.J. Molecular pathways: The immunogenic effects of platinum-based chemotherapeutics. Clin. Cancer Res. **2014**, 20, 2831–2837. [CrossRef] [PubMed]
26. Gebremeskel, S.; Johnston, B. Concepts and mechanisms underlying chemotherapy induced immunogenic cell death: Impact on clinical studies and considerations for combined therapies. Oncotarget **2015**, 6, 41600–41619. [CrossRef] [PubMed]
27. Cui, G. The Mechanisms Leading to Distinct Responses to PD-1/PD-L1 Blockades in Colorectal Cancers With Different MSI Statuses. Front. Oncol. **2021**, 11. [CrossRef]
28. Wang, T.; Lee, L.H.; Vyas, M.; Zhang, L.; Ganesh, K.; Firat, C.; Segal, N.H.; Desai, A.; Hechtman, J.F.; Ntiamoah, P.; et al. Colorectal carcinoma with double somatic mismatch repair gene inactivation: Clinical and pathological characteristics and response to immune checkpoint blockade. Mod. Pathol. **2019**, 32, 1551–1562. [CrossRef]

29. Marabelle, A.; Le, D.T.; Ascierto, P.A.; Di Giacomo, A.M.; de Jesus-Acosta, A.; Delord, J.P.; Geva, R.; Gottfried, M.; Penel, N.; Hansen, A.R.; et al. Efficacy of pembrolizumab in patients with noncolorectal high microsatellite instability/ mismatch repair–deficient cancer: Results from the phase II KEYNOTE-158 study. J. Clin. Oncol. **2020**, 38, 1–10. [CrossRef]
30. André, T.; Shiu, K.-K.; Kim, T.W.; Jensen, B.V.; Jensen, L.H.; Punt, C.; Smith, D.; Garcia-Carbonero, R.; Benavides, M.; Gibbs, P.; et al. Pembrolizumab in Microsatellite-Instability–High Advanced Colorectal Cancer. N. Engl. J. Med. **2020**, 383, 2207–2218. [CrossRef]
31. Rizvi, N.A.; Hellmann, M.D.; Brahmer, J.R.; Juergens, R.A.; Borghaei, H.; Gettinger, S.; Chow, L.Q.; Gerber, D.E.; Laurie, S.A.; Goldman, J.W.; et al. Nivolumab in combination with platinum-based doublet chemotherapy for first-line treatment of advanced non-small-cell lung cancer. J. Clin. Oncol. **2016**, 34, 2969–2979. [CrossRef] [PubMed]
32. Kanda, S.; Goto, K.; Shiraishi, H.; Kubo, E.; Tanaka, A.; Utsumi, H.; Sunami, K.; Kitazono, S.; Mizugaki, H.; Horinouchi, H.; et al. Safety and efficacy of nivolumab and standard chemotherapy drug combination in patients with advanced non-small-cell lung cancer: A four arms phase Ib study. Ann. Oncol. **2016**, 27, 2242–2250. [CrossRef] [PubMed]
33. Fujimoto, N.; Aoe, K.; Kozuki, T.; Oze, I.; Kato, K.; Kishimoto, T.; Hotta, K. A Phase II Trial of First-Line Combination Chemotherapy With Cisplatin, Pemetrexed, and Nivolumab for Unresectable Malignant Pleural Mesothelioma: A Study Protocol. Clin. Lung Cancer **2018**, 19, e705–e707. [CrossRef]
34. Dudnik, E.; Moskovitz, M.; Rottenberg, Y.; Lobachov, A.; Mandelboim, R.; Shochat, T.; Urban, D.; Wollner, M.; Nechushtan, H.; Rotem, O.; et al. Pembrolizumab as a monotherapy or in combination with platinum-based chemotherapy in advanced non-small cell lung cancer with PD-L1 tumor proportion score (TPS) ≥50%: Real-world data. Oncoimmunology **2021**, 10. [CrossRef]
35. Principe, D.R.; Narbutis, M.; Kumar, S.; Park, A.; Viswakarma, N.; Dorman, M.J.; Kamath, S.D.; Grippo, P.J.; Fishel, M.L.; Hwang, R.F.; et al. Long-term gemcitabine treatment reshapes the pancreatic tumor microenvironment and sensitizes murine carcinoma to combination immunotherapy. Cancer Res. **2020**, 80, 3101–3115. [CrossRef]
36. Baba, Y.; Nomoto, D.; Okadome, K.; Ishimoto, T.; Iwatsuki, M.; Miyamoto, Y.; Yoshida, N.; Baba, H. Tumor immune microenvironment and immune checkpoint inhibitors in esophageal squamous cell carcinoma. Cancer Sci. **2020**, 111, 3132–3141. [CrossRef] [PubMed]
37. Seledtsov, V.I.; Goncharov, A.G.; Seledtsova, G.V. Clinically feasible approaches to potentiating cancer cell-based immunotherapies. Hum. Vaccines Immunother. **2015**, 11, 851–869. [CrossRef]
38. Martens, A.; Wistuba-Hamprecht, K.; Geukes Foppen, M.; Yuan, J.; Postow, M.A.; Wong, P.; Romano, E.; Khammari, A.; Dreno, B.; Capone, M.; et al. Baseline Peripheral Blood Biomarkers Associated with Clinical Outcome of Advanced Melanoma Patients Treated with Ipilimumab. Clin. Cancer Res. **2016**, 22, 2908–2918. [CrossRef]
39. Weber, R.; Fleming, V.; Hu, X.; Nagibin, V.; Groth, C.; Altevogt, P.; Utikal, J.; Umansky, V. Myeloid-Derived Suppressor Cells Hinder the Anti-Cancer Activity of Immune Checkpoint Inhibitors. Front. Immunol. **2018**, 9, 1310. [CrossRef]
40. Liu, Y.; Wei, G.; Cheng, W.A.; Dong, Z.; Sun, H.; Lee, V.Y.; Cha, S.-C.; Smith, D.L.; Kwak, L.W.; Qin, H. Targeting myeloid-derived suppressor cells for cancer immunotherapy. Cancer Immunol. Immunother. **2018**, 67, 1181–1195. [CrossRef]
41. Ahn, J.-H.; Lee, B.-H.; Kim, S.-E.; Kwon, B.-E.; Jeong, H.; Choi, J.R.; Kim, M.J.; Park, Y.; Kim, B.S.; Kim, D.H.; et al. A Novel Anti-PD-L1 Antibody Exhibits Antitumor Effects on Multiple Myeloma in Murine Models via Antibody-Dependent Cellular Cytotoxicity. Biomol. Ther. **2020**, 29, 166–174. [CrossRef] [PubMed]
42. Hernandez, C.; Arasanz, H.; Chocarro, L.; Bocanegra, A.; Zuazo, M.; Fernandez-Hinojal, G.; Blanco, E.; Vera, R.; Escors, D.; Kochan, G. Systemic blood immune cell populations as biomarkers for the outcome of immune checkpoint inhibitor therapies. Int. J. Mol. Sci. **2020**, 21, 2411. [CrossRef] [PubMed]
43. Wang, X.; Yang, X.; Zhang, C.; Wang, Y.; Cheng, T.; Duan, L.; Tong, Z.; Tan, S.; Zhang, H.; Saw, P.E.; et al. Tumor cell-intrinsic PD-1 receptor is a tumor suppressor and mediates resistance to PD-1 blockade therapy. Proc. Natl. Acad. Sci. USA **2020**, 117, 6640–6650. [CrossRef] [PubMed]
44. Gubin, M.M.; Esaulova, E.; Ward, J.P.; Malkova, O.N.; Runci, D.; Wong, P.; Noguchi, T.; Arthur, C.D.; Meng, W.; Alspach, E.; et al. High-Dimensional Analysis Delineates Myeloid and Lymphoid Compartment Remodeling during Successful Immune-Checkpoint Cancer Therapy. Cell **2018**, 175, 1014–1030. [CrossRef]
45. Weiss, M.; Blazek, K.; Byrne, A.J.; Perocheau, D.P.; Udalova, I.A. IRF5 Is a Specific Marker of Inflammatory Macrophages In Vivo. Mediat. Inflamm. **2013**, 2013, 1–9. [CrossRef]
46. Kwong, T.T.; Wong, C.H.; Zhou, J.Y.; Cheng, A.S.L.; Sung, J.J.Y.; Chan, A.W.H.; Chan, S.L. Chemotherapy-induced recruitment of myeloid-derived suppressor cells abrogates efficacy of immune checkpoint blockade. JHEP Rep. **2021**, 3, 100224. [CrossRef] [PubMed]
47. Suzuki, E.; Sun, J.; Kapoor, V.; Jassar, A.S.; Albelda, S.M. Gemcitabine has significant immunomodulatory activity in murine tumor models independent of its cytotoxic effects. Cancer Biol. Ther. **2007**, 6, 880–885. [CrossRef]
48. Okamura, R.; Kato, S.; Lee, S.; Jimenez, R.E.; Sicklick, J.K.; Kurzrock, R. ARID1A alterations function as a biomarker for longer progression-free survival after anti-PD-1/PD-L1 immunotherapy. J. Immunother. Cancer **2020**, 8, e000438. [CrossRef]
49. Armstrong, S.; Al-Ghawi, H.; Helft, P.; House, M.G.; Spittler, A.J.; Wu, H.H.; Shahda, S. Two Months of Therapy: A Case of Pathologic Complete Response to Chemoimmunotherapy in a Patient With Metastatic Colorectal Cancer. Clin. Colorectal Cancer **2018**, 17, e229–e232. [CrossRef]
50. Lizardo, D.Y.; Kuang, C.; Hao, S.; Yu, J.; Huang, Y.; Zhang, L. Immunotherapy efficacy on mismatch repair-deficient colorectal cancer: From bench to bedside. Biochim. Biophys. Acta Rev. Cancer **2020**, 1874, 188447. [CrossRef]

51. Konstantinopoulos, P.A.; Luo, W.; Liu, J.F.; Gulhan, D.C.; Krasner, C.; Ishizuka, J.J.; Gockley, A.A.; Buss, M.; Growdon, W.B.; Crowe, H.; et al. Phase II study of avelumab in patients with mismatch repair deficient and mismatch repair proficient recurrent/persistent endometrial cancer. J. Clin. Oncol. **2019**, 37, 2786–2794. [CrossRef] [PubMed]
52. Maletzki, C.; Beyrich, F.; Hühns, M.; Klar, E.; Linnebacher, M. The mutational profile and infiltration pattern of murine MLH1$^{-/-}$ tumors: Concurrences, disparities and cell line establishment for functional analysis. Oncotarget **2016**, 7, 53583–53598. [CrossRef] [PubMed]
53. Franken, N.A.P.; Rodermond, H.M.; Stap, J.; Haveman, J.; van Bree, C. Clonogenic assay of cells in vitro. Nat. Protoc. **2006**, 1, 2315–2319. [CrossRef] [PubMed]
54. Maletzki, C.; Gladbach, Y.S.; Hamed, M.; Fuellen, G.; Semmler, M.-L.; Stenzel, J.; Linnebacher, M. Cellular vaccination of MLH1$^{-/-}$ mice–an immunotherapeutic proof of concept study. Oncoimmunology **2018**, 7, e1408748. [CrossRef] [PubMed]
55. Rohde, S.; Lindner, T.; Polei, S.; Stenzel, J.; Borufka, L.; Achilles, S.; Hartmann, E.; Lange, F.; Maletzki, C.; Linnebacher, M.; et al. Application of in vivo imaging techniques to monitor therapeutic efficiency of PLX4720 in an experimental model of microsatellite instable colorectal cancer. Oncotarget **2017**, 8, 69756–69767. [CrossRef]

8.4 Publication 4

OncoImmunology

ISSN: (Print) (Online) Journal homepage: https://www.tandfonline.com/loi/koni20

CDK4/6 blockade provides an alternative approach for treatment of mismatch-repair deficient tumors

Inken Salewski, Julia Henne, Leonie Engster, Paula Krone, Bjoern Schneider, Caterina Redwanz, Heiko Lemcke, Larissa Henze, Christian Junghanss & Claudia Maletzki

To cite this article: Inken Salewski, Julia Henne, Leonie Engster, Paula Krone, Bjoern Schneider, Caterina Redwanz, Heiko Lemcke, Larissa Henze, Christian Junghanss & Claudia Maletzki (2022) CDK4/6 blockade provides an alternative approach for treatment of mismatch-repair deficient tumors, OncoImmunology, 11:1, 2094583, DOI: 10.1080/2162402X.2022.2094583

To link to this article: https://doi.org/10.1080/2162402X.2022.2094583

ONCOIMMUNOLOGY
2022, VOL. 11, NO. 1, e2094583 (20 pages)
https://doi.org/10.1080/2162402X.2022.2094583

Taylor & Francis
Taylor & Francis Group

ORIGINAL RESEARCH

OPEN ACCESS Check for updates

CDK4/6 blockade provides an alternative approach for treatment of mismatch-repair de!cient tumors

Inken Salewski[a], Julia Henne[a], Leonie Engster[a], Paula Krone[a], Bjoern Schneider[b], Caterina Redwanz[c,d], Heiko Lemcke[e,f], Larissa Henze[a], Christian Junghanss[a], and Claudia Maletzki[a]

[a]–Hematology, Oncology, Palliative Medicine, Rostock University Medical Center, University of RostockDepartment of Medicine, Clinic III , Rostock, Germany; [b]Institute of Pathology, Rostock University Medical Center, University of Rostock, Rostock, Germany; [c]Department of Internal Medicine B, Cardiology, University Medicine Greifswald, Germany; [d]Department of Internal Medicine B, Cardiology, University Medicine Greifswald, Greifswald, Germany; DZHK (German Center for Cardiovascular Research), Partner Site Greifswald, Germany; [e]Department of Cardiac Surgery, Reference and Translation Center for Cardiac Stem Cell Therapy (RTC), Rostock University Medical Center, University of Rostock, Rostock, Germany; [f]Faculty of Interdisciplinary Research, Department Life, Light & Matter, Department of Cardiology, Rostock University Medical Center, University of Rostock, Rostock, Germany

ABSTRACT

Mismatch repair-de!cient (dMMR) tumors show a good response toward immune checkpoint inhibitors (ICI), but developing resistance impairs patients' outcomes. Here, we compared the therapeutic potential of an α-PD-L1 antibody with the CDK4/6 inhibitor abemaciclib in two preclinical mouse models of dMMR cancer, focusing on immune-modulatory e#ects of either treatment. Abemaciclib monotherapy signi!cantly prolonged overall survival of $Mlh1^{-/-}$ and $Msh2^{loxP/loxP;TgTg(Vil1\text{-}cre)}$ mice ($Mlh1^{-/-}$: 14.5 wks vs. 9.0 wks (α-PD-L1), and 3.5 wks (control); $Msh2^{loxP/loxP;TgTg(Vil1\text{-}cre)}$: 11.7 wks vs. 9.6 wks (α-PD-L1), and 2.0 wks (control)). The combination was not superior to either monotherapy. PET/CT imaging revealed individual response pro!les, with best clinical responses seen with abemaciclib mono- and combination therapy. Therapeutic e#ects were accompanied by increasing numbers of tumor-in!ltrating $CD4^+/CD8^+$ T-cells and lower numbers of M2-macrophages. Levels of T cell exhaustion markers and regulatory T cell counts declined. Expression analysis identi!ed higher numbers of dendritic cells and neutrophils within tumors together with high expression of DNA damage repair genes as part of the global stress response. In $Mlh1^{-/-}$ tumors, abemaciclib suppressed the PI3K/Akt pathway and led to induction of Mxd4/Myc. The immune-modulatory potential of abemaciclib renders this compound ideal for dMMR patients not eligible for ICI treatment.

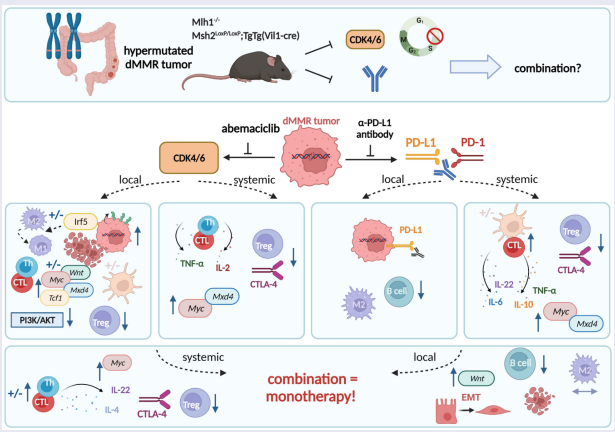

ARTICLE HISTORY
Received 4 April 2022
Revised 22 June 2022
Accepted 22 June 2022

Two genetic mouse models of spontaneous dMMR-driven tumorigenesis were used in this preclinical therapy trial. Tumor-bearing $Mlh1^{-/-}$ or $Msh2^{loxP/loxP;TgTg(Vil1-cre)}$ mice received the CDK4/6 inhibitor abemaciclib, the α-PD-L1 monoclonal antibody or a combination of both agents, in which abemaciclib was given as lead-in therapy. Abemaciclib led to an increase of tumor-infiltrating T helper (Th) cells and cytotoxic T cells (CTL), dendritic cells, as well as IRF5-driven polarization of M2 macrophages,

CONTACT Claudia Maletzki claudia.maletzki@med.uni-rostock.de Department of Medicine, Clinic III-Hematology, Oncology, Palliative Care Rostock University Medical Center, Schillingallee 70, Rostock D-18057, Germany

Supplemental data for this article can be accessed online at https://doi.org/10.1080/2162402X.2022.2094583

upregulation of Mxd4, and activation of the Wnt-signaling. Blood phenotyping revealed reduced levels of T cell exhaustion markers as well as regulatory T cell counts, attributable to Tc-mediated IL-2 secretion. While monotherapy with the α-PD-L1 monoclonal antibody had slightly different local and systemic effects, the combination approach was not superior to either monotherapy. Notably, most beneficial abemaciclib-mediated immune-modulatory effects were even repealed. Instead, the combination triggered epithelial-mesenchymal transition (EMT), raising caution for CDK-immune-checkpoint-inhibitor combination approaches. ±: indicates strain-specific differences.

Introduction

Mismatch-repair-deficiency (dMMR) arises as a consequence of MLH1 gene promoter hypermethylation (= sporadic form) or secondary to a germline MMR mutation (= hereditary form). In either case, dMMR is associated with high immunogenicity. Patients harboring dMMR tumors are thus predestined to be treated with immune-checkpoint inhibitors (ICIs). ICIs reactivate exhausted T cells, prevent T cell inhibition, and force T cell-mediated tumor killing.[1] Consequently, Programmed death 1 (PD-1) blockade has emerged as a highly effective treatment strategy and the positive results seen in many patients have contributed to the FDA and EMA approval for first-line therapy of unresectable or metastatic dMMR cancer.[2,3]

Recent data describe superior effects of α-PD-L1 antibodies compared to α-PD-1 antibodies in blocking PD-1/PD-L1 signaling.[4] PD-L1 is upregulated in the tumor microenvironment and is found in a large variety of tumors. In recent clinical trials on dMMR patients, the α-PD-L1 antibody Avelumab has first proven safe[5] and was then compared with standard chemotherapy for treatment of dMMR colorectal cancer patients.[6] Clinical responses up to complete remissions were seen in many cases. Our preclinical data additionally support the use of α-PD-L1 antibodies either alone or in conjunction with cytostatic drugs and immunotherapy.[7,8] Still, in most cases, resistance mechanisms evolve finally contributing to relapse.[9]

To improve outcomes, ICIs should be combined with other (targeted) agents. A very attractive option is the selective cyclin-dependent kinase 4/6 inhibitor (CDKI) abemaciclib.[10] Abemaciclib stops the cell cycle at G1, induces swollen and dysfunctional lysosomes, and triggers apoptosis/necrosis in tumor cells.[11–13] This CDK4/6 inhibitor is currently approved for treatment of both early and advanced/metastatic breast cancer, however, more immunogenic tumor types, such as dMMR-related cancers, should be considered as well. The rationale for this is based on the increasing body of evidence that abemaciclib stimulates antitumor immune responses by inducing an "inflamed" microenvironment finally contributing to T cell activation and improved T cell function.[14–17] Actually, a recent study reported transformation of $CD8^+$ T cells into memory cells upon CDK4/6 inhibition to expand the long-term immunity and efficacy of the cancer treatment – an effect frequently seen after ICI treatment.[18] CDK blockade may thus become an interesting option for dMMR patients not eligible for ICI treatment. The notion that many patients harbor preformed antitumoral immune responses that can be re-activated (or boosted) by immunotherapy additionally argues in favor of using immune-modulating CDKIs for treatment of dMMR-related malignancies.[19–21]

Using the two preclinical $Mlh1^{-/-}$ and $Msh2^{loxP/loxP;TgTg(Vil1-cre)}$ mouse models of spontaneous tumorigenesis,[22–25] we initiated a proof-of-concept study and compared the efficacy of a murine α-PD-L1 antibody (clone 6E11) with the CDK4/6 inhibitor abemaciclib either alone or in combination.

We could show that low-dose abemaciclib treatment is as effective as α-PD-L1 therapy, but its combination is not superior to the respective monotherapy. Hence, we propose abemaciclib monotherapy as a good alternative for treatment of dMMR patients that cannot be treated with ICI.

Methods

In vitro experiments

Cell culture

Two $MLH1^{-/-}$ tumor cell lines 328 and A7450 T1 M1 were established and characterized in our lab.[25,26] Cell culture was performed in DMEM/Ham's F12 medium, supplemented with 10% FCS (fetal calf serum), 6 mM Glutamine, and antibiotics (all from Biochrom, Berlin, Germany). Treatment was done with selected CDKIs at doses corresponding to IC_{30} values: (I) abemaciclib (= abema): 1 µM; (II) dinaciclib (= dina): 100 nM; (III) THZ-1: 0.83 µM. Doses were validated before via dose response curve analyses.

Apoptosis/necrosis, cell cycle analysis, and immunogenic cell death

Cells were treated with abema, dina, or THZ-1 for 72 hours, harvested and stained with 0.2 µM Yo-Pro 1 iodide (Thermo Scientific, Ex/Em 491/509 nm; blue laser 488 nm, 20 min, RT). Cells were washed and mixed with 7-AAD viability staining solution (250 ng, Biolegend, San Diego, United States) before measurements. For cell cycle analysis, cells were harvested and incubated with ice-cold 70% ethanol over night at −20°C. 1 mg/ml RNase (Carl Roth, Karlsruhe, Germany) was preheated at 37°C for 90 min. Ethanol fixed cells were washed twice with 2 ml PBS and centrifuged at 300 g for 10 min. Each sample was mixed with 500 µl of preheated RNase and incubated for 45 min in the water bath at 37°C. Cells were washed twice with 2 ml PBS and centrifuged at 300 g for 10 min. Cells were resuspended with 400 µl propidium iodide (50 µg/ml) and incubated for at least 30 min in the fridge covered from light.

For immunogenic cell death assessment, cells were treated with abemaciclib for 48 h and 72 hours. Supernatants were collected and amounts of high-mobility group protein 1 (HMGB1) were measurement by ELISA according to the manufacturers' instructions (Abbexa, Cambridge, UK). Cells were harvested and incubated with a polyclonal rabbit CalR primary antibody (1:50; Abgent, San Diego, CA, USA, 30 min, 4°C), followed by a secondary FITC-labeled antibody (donkey anti

rabbit, 1:50; Biolegend, 30 min, 4°C). Control cells were stained with the secondary FITC-labeled antibody. Measurements were performed on a FACSVerse Cytometer (BD Pharmingen, San Diego, USA). Data analysis was performed using BD FACSuite software (BD Pharmingen).

Colony formation assay

Five hundred cells/well were seeded in 6-well plates and were allowed to rest overnight. Cells were treated with abema, dina or were left untreated. After 6 days, medium was removed and cells were stained with 500 µl 0.2% crystal violet for 10 min on a rocking plate, followed by washing steps. Some cells were allowed to rest with medium for additional 6 days. Then, they were stained the same way with crystal violet. The number of colonies was evaluated using ImageJ-win64.

Co-culture assay

Tumor cells were harvested and stained with 5 µM CMFDA (15 min, 37°C, 5% CO_2). Twenty-thousand cells/well were seeded in a 24-well plate. After 24 hours, 200,000 blood cells/well, which were lysed with erythrocyte lysis buffer (155 mM NH4Cl (MERCK Millipore, Darmstadt, Germany), 10 mM KHCO3 (MERCK Millipore), and 0.1 mM EDTA (Applichem, Darmstadt, Germany)) were added. Abemaciclib was used at 1 µM. After 24 hours, 10 µg/ml α-PD-L1 was added. After additional 48 hours, tumor cells were harvested. To quantify residual tumor cells, fluorescent microsphere beads (1.4×10^5 beads/ml, size: 10 µm, Polyscience, Hirschberg an der Bergstrasse, Germany) were used. Measurements were performed on a FACSVerse Cytometer (BD Pharmingen). Data analysis was performed using BD FACSuite software (BD Pharmingen).

Immunofluorescence of cytoskeleton and ROS

The cytoskeleton and formation of reactive oxygen species (ROS) was visualized. Cells were treated twice with 1 µM abemaciclib for 72 hours and stained with 7.5 µM ROS Brite 670 (AAT Bioquest, CA, USA, 30 min, 37°C) followed by 125 nM Mitolite Green (AAT Bioquest) staining (45 min, 37°C). Cells were fixed with 4% PFA (30 min, RT), washed thrice with PBS and permeabilized with 0.2% TritonX-100 (15 min, RT). Afterward, Phalloidin-iFluor 594 conjugate (AAT Bioquest) dissolved 1:1000 in 1% BSA was added (30 min, RT), followed by three washing steps and 2 min staining with 1.5 µg/ml DAPI.

In vivo experiments

Ethical Statement

The German local authority approved all animal experiments: Landesamt für Landwirtschaft, Lebensmittelsicherheit und Fischerei Mecklenburg-Vorpommern (7221.3-1-062/19; –025/20), under the German animal protection law and the EU Guideline 2010/63/EU. Mice were bred in the animal facility of the University Medical Center in Rostock under specific pathogen-free conditions. Mlh1 genotyping was done according to [21] and Msh2 genotyping was done according to.[22,23] During their whole life-time, all animals received enrichment in the form of mouse-igloos (ANT Tierhaltungsbedarf, Buxtehude, Germany), nesting material (shredded tissue paper, Verbandmittel GmbH, Frankenberg, Deutschland), paper roles (75 × 38 mm, H 0528–151, ssniff-Spezialdiäten GmbH, Soest, Germany), and wooden sticks (40 × 16 × 10 mm, Abedd, Vienna, Austria). During the experiment, mice were kept in type III cages (Zoonlab GmbH, Castrop-Rauxel, Germany) at 12-h dark:light cycle, the temperature of 21 ± 2°C, and relative humidity of 60 ± 20% with food (pellets, 10 mm, ssniff-Spezialdiäten GmbH, Soest, Germany) and tap water ad libitum. When mice were subjected to treatment (= time of tumor development), they were given daily-prepared soaked pellets to ensure proper food intake.

Experimental protocol

Mice with validated gastrointestinal tumor via PET/CT were taken into therapy. Mice received abemaciclib (oral gavage, 75 mg/kg body weight (bw), 1x/week, 8 times in total (q1wx8), $Mlh1^{-/-}$ n = 7 mice, $Msh2^{loxP/loxP;TgTg(Vil1-cre)}$ n = 9 mice) and α-PD-L1 antibody (i.p., 2.5 mg/kg bw, biweekly), three times in total (q2wx3), $Mlh1^{-/-}$ n = 7 mice, $Msh2^{loxP/loxP;TgTg(Vil1-cre)}$ n = 10 mice). The α-PD-L1 antibody, clone 6E11, was kindly provided by Genentech, a subsidiary of Roche, South San Francisco, USA. Mice receiving the combination were given abemaciclib first as lead-in, followed by α-PD-L1 injection ($Mlh1^{-/-}$ n = 7 mice, $Msh2^{loxP/loxP;TgTg(Vil1-cre)}$ n = 10 mice). Control mice were left untreated ($Mlh1^{-/-}$ n = 6 mice, $Msh2^{loxP/loxP;TgTg(Vil1-cre)}$ n = 10 mice) or received the isotype control antibody (i.p. 2.5 mg/kg bw, $Mlh1^{-/-}$ n = 7 mice, $Msh2:^{loxP/loxP;TgTg(Vil1-cre)}$ n = 7 mice). The health status was monitored daily using a score sheet. Reduction of suffering was ensured by applying humane endpoints (weight loss >15%, pain, changes in social behavior). All mice were sacrificed before they became moribund to prevent pain and distress. Mice were sacrificed due to human endpoints (as outlined above + progressive disease, defined by tumor volume >300 mm^3), followed by removal of blood, spleen, and tumor.

PET/CT imaging

The tumor size was measured via PET/CT measurements on a small animal PET/CT scanner (Inveon PET/CT, Siemens Medical Solutions, Knoxville, TN, USA) in accordance to a standard protocol as described before.[25] Mice were anesthetized using isoflurane and received FDG intravenously. Evaluation of the images was performed as described before.[8] Treatment outcome determined according to clinical staging as follows: (I) progressive disease (PD) = tumor volume >25% vs. baseline (= day 0); (II) stable disease (SD): tumor volume similar to initial staging (≤25% vs. day 0); (III) partial response (PR): tumor volume 50% lower or more vs. baseline (=day 0). Follow-up was done at day 30 (= short-term) and, in some cases, at ~day 50 (= long-term follow-up).

Immune phenotyping

Blood was taken routinely from anesthetized mice (retrobulbar venous plexus). Spleen and tumor tissues were dissociated. Single cells were stained with a panel of conjugated monoclonal antibodies (mAb, 0.125 µg to 1.5 µg each). Zombie NIR™ Fixable Viability Kit by Biolegend (San Diego, United States) staining

was performed following the protocol Zombie NIR™ Fixable Viability Kit by Biolegend, extracellular staining was performed following the protocol BD Horizon Briliant Stain Buffer (BD Bioscience), followed by lysis and intracellular staining using the protocol of True-Nuclear™ Transcription Factor Buffer Set by Biolegend. Measurements were performed on a spectral flow cytometer (Cytek™ Aurora). For extracellular stainings Gr1 Alexa Fluor700, CD8 FITC, CD4 APC Fire, CD11b BV570, PD-L1 BV421, NK1.1 BV605, CD19 Spark Blue (Biolegend), CD25 PerCP-eFluor710 (Thermofisher), CD83 BV750, PD-1 BV650 (BD Bioscience) and for intracellular stainings CTLA-4 PE/Cy7, CD3 PerCP, and Foxp3 Alexa Fluor 647 (Biolegend) were used. Data were analyzed using SpectroFlow™ Version 2.2.0.3. and FlowJo™ Version 10.6.1.

Multiplex cytokine assay

Cytokine levels of the plasma were measured using a multi-analyte flow assay kit following the instructions of the manufacturer (LEGENDplex™, Biolegend). Measurements were performed on a spectral flow cytometer (Cytek™ Aurora). Data were analyzed using the manufacturer's online Software. Absolute plasma cytokine levels are presented [ng/ml].

Fragment length analysis

Tumor gDNA was isolated using the Wizard Genomic DNA Purification Kit (Promega). An established panel of coding- and non-coding MS marker was evaluated using the fragment length analysis as described before.[27]

Nanostring targeted gene expression profiling

Tumor RNA was isolated from cryostat sections using the RNeasy Mini Kit (Qiagen). Then, the RNA was analyzed using Nanostring analysis as described before.[8]

Quantitative real-time PCR

RNA was isolated using the RNeasy Mini Kit (Qiagen). 1 µg mRNA and 50 ng random Hexamer Primer were incubated for 10 min at 70°C. Sample-mixes were completed with 5x RT buffer complete, dNTPs and 200 units reverase. cDNA was synthesized using the PCR cycler 120 min at 45°C and for 10 min at 70°C. 25 ng cDNA was used for quantitative real-time PCR with the SensiFAST Probe Lo-ROX Kit (Bioline, Memphis, Tennessee, USA). Predesigned Taqman gene expression assays were used: 6-FAM-3′BHQ-1 Mxd4 (Mm00487523_m1), 6-FAM-3′BHQ-1 cMyc (Mm00487804_m1), 5-VIC-3′BHQ-1 Agr2 (Mm01291804_m1), 6-FAM-3′BHQ-1 Tgfb1 (Mm01178820_m1), 6-FAM-3′BHQ-1 Vimentin (Mm01333430_m1), 5-VIC-3′BHQ-1 N-Cadherin (Mm01162497_m1), 6-FAM-3′BHQ-1 Fpr2 (Mm00484464_s1), 5-VIC-3′BHQ-1 Csf1 (Mm00432686_m1), 6-FAM-3′BHQ-1 Csf2 (Mm01290062_m1), 5-VIC-3′BHQ-1 Tcf1/Pcbd2 (Mm01342270_m1), and 6-FAM-3′BHQ-1 Alox5 (Mm01182747_m1). Self-designed 5-VIC-3′BHQ-1 GAPDH was applied as housekeeping gene. Reaction was performed in the light cycler Viia7 (Applied Biosystems, Foster City, USA) with the following PCR conditions: 95°C for 10 min, 40 cycles of 15 s at 95°C, and 1 min at 60°C. All reactions were run in triplicates. The mRNA levels of target genes were normalized to GAPDH. Reactions were performed in triplicate wells. The expression level of each sample was considered by calculating $2^{-\Delta CT}$ ($\Delta Ct = Ct_{target} - Ct_{Housekeeping\ gene}$), followed by $2^{-\Delta\Delta CT}$ quantification, taking values of untreated controls as calibrator.

Immunofluorescence

Cryostat sections of 4 µm were fixed in cold pure methanol for 8 min, air-dried and unspecific binding site blocked (2% BSA, 2 h) followed by staining with Alexa Fluor 488, Alexa Fluor 594 and Alexa Fluor 647 labeled antibodies CD3, CD4, CD8, CD206, F4/80, CD11b, Gr1, PD-L1, PD-1, and Irf5 (Biolegend). Sections were washed and embedded in Roti Mount Fluor Care DAPI (Roth, Karlsruhe). Visualization was performed on a confocal laser scanning microscope (ZEISS Elyra 7 Confocal Laser Microscope, Zeiss, Jena, Germany). The infiltration pattern was quantified. For infiltrating $CD3^+CD4^+$ T helper cells and $CD3^+CD8^+$ cytotoxic T cells, numbers were counted in 2–3 high power fields (HPFs)/slide. For regulatory granulocytes and tumor-associated macrophages (TAM), the infiltration pattern was semi-quantitatively analyzed using a scoring system. 0 = no; 1 = mild (1–20 cells/HPF); 2 = moderate (21–40 cells/HPF); 3 = strong (>40 cells/HPF).

Statistics

GraphPad PRISM software, version 8.0.2 (GraphPad Software, San Diego, CA, USA) was used to perform statistical evaluation. All data are presented as mean + SEM. Data are depicted as scatter plots and bar charts, with individual values representing a single value of an individual mouse. Data showing baseline and follow-up are given as dots connected with a line. The value of significance was set to $p < .05$. The data were first tested for normality conducting Shapiro-Wilk test. Then, in case of normality, one-way ANOVA (Tukey´s multiple comparison) or unpaired T-Test was accomplished or in case of non-parametric data Kruskal-Wallis or U-Test was performed. Kaplan Meyer survival curves were analyzed using the log rank (Mantel Cox) test. In case of blood phenotyping, outliers were eliminated, when they were above or below the average plus/minus two times the standard deviation.

Dimensionality Reduction Analysis (t-SNE)

Individual fcs files were imported into FlowJo software (version 10.6.1) (FlowJo, Ashland, Oregon). Ten thousand cells per file (six files per treatment group concerning tumor data, and eight files per treatment group concerning blood and spleen data) were randomly selected and merged into one concatenated file. T-SNE algorithm provided by FlowJo software was performed only on gated live cells. The output was a t-SNE map which we show as a dot-plot. The t-SNE dimensions were used on the original gates to create the overlay t-SNE maps.

Results

In vitro effects of CDK blockade and α-PD-L1 treatment

Before performing animal experiments, the two murine $Mlh1^{-/-}$ tumor cell lines A7450 T1 M1 and 328 were used to evaluate the effects of different CDK inhibitors on cell cycle,

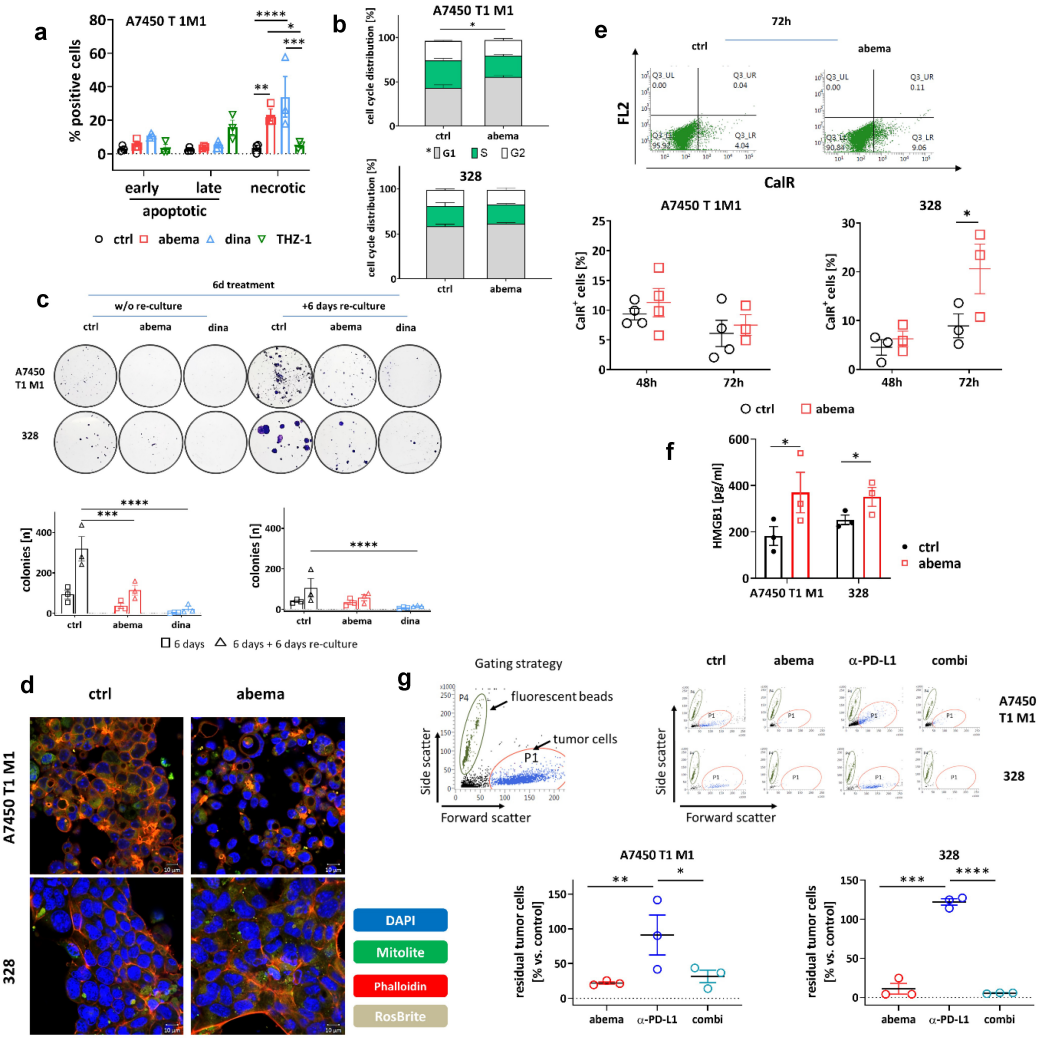

Figure 1. In vitro analysis on Mlh1$^{-/-}$ tumor cells. (a) Apoptosis/necrosis quantification. Mlh1$^{-/-}$ A7450 T1 M1 tumor cells were treated with CDKIs for 72 h and apoptosis/necrosis was quantified from Yo-Pro1/PI-stained cells. n = 3 independent experiments, *p < .05; ** p > .01; ***p < .001; two-way ANOVA (Tukey's multiple comparisons test). (b) Cell cycle analysis after 48 h of treatment with abemaciclib. n = 4 independent experiments, *p < .05; t-test. (c) Colony formation assay after treatment with abemaciclib or dinaciclib. Two experimental conditions were studied: (i) 6 days treatment and direct analysis and (II) 6 days treatment + 6 days re-culture without (w/o) treatment (= reconvalescence). Thereafter, colonies were counted using ImageJ software. n = 3 independent experiments, *p < .05; ***p < .001; ****p < .0001; two-way ANOVA (Tukey's multiple comparisons test). (d) Detection of ROS (RosBrite), cytoskeleton (Phalloidin) and mitochondria (mitolite) after 48 h of treatment with abemaciclib. Representative images are shown out of n = 3 independent experiments. Read out was done with the ZEISS Elyra 7 Confocal Laser Microscope (Zeiss). Original magnification 400 x. (e) Flow cytometric measurement of CalR-positive cells after 48 h and 72 h of treatment. n = 3–4 independent experiments. (f) HMGB1 secretion after 72 h of treatment. HMGB1 levels were determined from supernatants of MLH1$^{-/-}$ tumor cells. Control cells were left untreated. Experiments were repeated three times each of them performed in duplicates. *p < .05. (g) Co-culture of tumor and immune cells. Tumor and immune cells were simultaneously treated for 1 × 72 h with abemaciclib, α-PD-L1 antibody or a combination. The effector to target ratio was 1:10. Residual tumor cells were counted by adding fluorescent beads. Read out was done via flow cytometry. Representative dot plots of tumor cells treated with immune cells and drugs are shown. n = 3 independent experiments, *p < .05; **p < .01, ***p < .001; ****p < .0001, One-way ANOVA (Tukey's multiple comparisons test). (a-g) All data are given as mean + SEM. Doses used in each experiment are as follows: abemaciclib: 1 μM, dinaciclib: 0.1 μM, THZ-1: 0.83 μM; α-PD-L1 antibody: 10 μg/ml.

proliferation, morphology, and immunogenic cell death (Figure 1a–e). In some experiments, the α-PD-L1 antibody was added and combinations were tested (Figure 1e, f).

The selective CDK4/6 inhibitor abemaciclib and the global CDK1/2/5/9 inhibitor dinaciclib significantly increased the number of necrotic cells. By contrast, selective CDK7 inhibition by THZ-1 did not induce significant cell death (Figure 1a). Abemaciclib led to a G1-arrest in A7450 T1 M1 cells, whereas in 328, the number of cells in the G1-phase was slightly reduced (Figure 1b). Upon dinaciclib, the number of cells in S-phase increased in both cell lines. Using a classical colony formation assay, the number of A7450 T1 M1 colonies was reduced after abemaciclib and even more pronounced after dinaciclib treatment (Figure 1c), both after 6 days of treatment and significantly after additional 6 days of rest.

Then, we focused on abemaciclib for further studies. This agent affected the cytoskeleton and reduced mitochondria of A7450 T1 M1 cells. By contrast, reactive oxygen species remained unchanged (Figure 1d). In 328, we did not observe such strong changes in colony formation, cytoskeleton, and mitochondria, but reactive oxygen species were slightly decreased. The amount of CaIR^{+} A7450 T1 M1 cells was comparable to controls, while in 328 cells, surface-bound CaIR was more abundant after 72 hours of abemaciclib treatment (Figure 1e). Likewise, HMGB1 levels significantly increased, indicative for induction of immunogenic cell death (figure 1f).

In a subsequent co-culture assay, the impact of immune cells on the tumor cell viability was investigated (Figure 1g). Abemaciclib alone and its combination with α-PD-L1 reduced tumor cell numbers significantly.

Taken together, CDKIs have individual effects on MMR-D tumor cells. The immune-stimulating potential of abemaciclib may interact with immune-checkpoint blockade. To address this further, we initiated a proof-of-concept in vivo therapy trial.

Prolonged survival and e!ective tumor growth control under mono- and combination therapy

We included two preclinical mouse models of spontaneous, dMMR-driven tumorigenesis. Mlh1$^{-/-}$ mice harbor a constitutional knock out, whereas in Msh2$^{loxP/loxP;TgTg(Vil1-cre)}$ mice, a conditional knock out in the gut is the driver for tumor formation.[23,25,28] These mice share some features commonly related to dMMR, such as a high tumor mutational burden, and an inflamed tumor microenvironment. However, the infiltration pattern of specific immunological subtypes differs, nicely reflecting the clinical presentation of dMMR-related cancer (Table 1). Hence, these models are ideal tools for preclinical response analysis.

Treatment with abemaciclib was given weekly at a dose of 75 mg/kg bw because of its therapeutic activity in vitro even after drug removal and its capacity to stimulate the immune system.[14,16,18,29] The treatment schedule of the α-PD-L1 antibody was adopted to our previous study[8] with a biweekly application route at a dose of 2.5 mg/kg bw. Tumor growth was monitored in both mouse models before and after treatment using ^{18}F-FDG PET/CT (please see Figure 2a for experimental protocol).

Monotherapy with α-PD-L1 and abemaciclib reduced tumor sizes in Mlh1$^{-/-}$ mice (Figure 2b, $p < .05$ abemaciclib vs. control). The combination approach, in which abemaciclib was given as lead-in, had comparable effects. Control and isotype-treated mice showed the expected increased tumor sizes. By dissecting the response rates in more detail, we identified partial response or stable disease in all mice receiving abemaciclib or the combination. By contrast, partial response was only seen in one case after α-PD-L1 monotherapy and in neither mouse of the control groups (Figure 2b, d).

The response pattern of Msh2$^{loxP/loxP;TgTg(Vil1-cre)}$ mice was comparable to those of Mlh1$^{-/-}$ mice (Figure 2c, e). Short-term follow-up was available for all mice receiving treatment, whereas, in the controls, only half of them underwent follow-up because of disease progression. 66.0% of mice had partial response or stable disease under abemaciclib and 44.4% mice under combination therapy (vs. 37.5% in the α -PD-L1 and neither in the control groups).

Long-term follow-up (> day 50) principally confirmed the good response toward abemaciclib in both mouse strains (figure 2f, g). Fifty percent of mice showed partial response. The α-PD-L1 primarily induced stable disease. The response pattern toward monotherapy was not confirmed in the combination. Here, 50% of Mlh1$^{-/-}$ mice had partial response, while all Msh2$^{loxP/loxP;TgTg(Vil1-cre)}$ mice suffered from progressive disease (figure 2f, g).

All three therapies significantly improved the outcome in both mouse strains (Mlh1$^{-/-}$: $p < .001$, Msh2:$^{loxP/loxP;TgTg(Vil1-cre)}$ $p < .001$, Figure 2h,i). Median overall survival of Mlh1$^{-/-}$ mice receiving abemaciclib alone was 14.5 weeks and thus even better than under α-PD-L1 monotherapy (9.0 weeks). In Msh2$^{loxP/loxP;TgTg(Vil1-cre)}$ mice, both monotherapies yielded comparable outcomes (abemaciclib vs. α-PD-L1: 11.7 vs. 9.6 wks). Still, the combination was not superior to either monotherapy.

To check whether potential hepatotoxic effects of the applied regimens may account for treatment failure in the combination group, routine histology was done. This analysis revealed massive focal lymphocytic and granulocytic infiltration in livers from mice treated with abemaciclib or α-PD-L1 monotherapy (supplementary Figure S1, 63x magnification of single lymphocytes and granulocytes in the left corner, infiltrates are marked with a black arrow). While this was a likely result of the systemic immune stimulation, such strong lymphocytic infiltration was only partially preserved in the combination treatment, with single necrotic areas arising (black arrow). We conclude antagonistic instead of synergistic effects of combined CDK4/6 – immune-checkpoint blockade in these two preclinical dMMR tumor models.

Treatment-related immunological changes in the periphery and spleen

To get an idea on the mechanisms underlying this individual response pattern in vivo, plasma samples were taken from control and treatment groups at baseline (=before treatment) and after therapy (= experimental endpoint). A panel of cytokine markers was studied to cover the most relevant Th1 and Th2-specific cytokines and to track the changes under therapy (Figure 3).

Table 1. Overview on similarities and disparities between $Mlh1^{-/-}$ and $Msh2^{loxP/loxP\ Villin\ Cre}$ mice

Characteristic			$Mlh1^{-/-}$	$Msh2^{loxP/loxP\ Villin\ Cre}$
Strain specificity and model establishment	Mouse	Mouse strain	C57Bl/6	C57Bl/6
		Type of knock out	Constitutional	Conditional, gut
		Spontaneous tumor formation	Yes	Yes
Clinicopathological characteristics	Human	Frequency of the underlying MMR defect in human	~35 %	~ 40%
		Human disease counterpart	Lynch syndrome and constitutional mismatch repair deficiency	Lynch syndrome
		Human lifetime risk of tumorigenesis	♂: 27 – 74 % ♀: 22 – 53 %	♂: 27 – 74 % ♀: 22 – 53 %
	Mouse	Murine mean age of onset	26 weeks (lymphoma), 35 weeks (GIT)	35 weeks (GIT)
		Tumor penetrance	High, >90 %	High, >95 %
		Tumor spectrum	LS-associated tumors ≥ hematological malignancies (lymphoma) > others (skin)	LS-associated tumors
		Manifestation	Jejunum	Jejunum
		Metastastic spread	Not in GIT, lymphomas: yes	No
		MHC class I expression	100% positive	100% positive
		MSI in mononucleotide repeats	High	High
		MSI in coding mononucleotide repeats	Low	High
Tumor microenvironment	Mouse	Cytotoxic T-cells	Low	Moderate
		T helper cells	Low	Low
		MDSC	Moderate	Moderate
		TAM	Moderate	High
		PD-L1	Low	Moderate
Treatment response towards		Immune checkpoint inhibition (α-PD-L1)	Poor > moderate	Moderate
		CDK4/6 inhibition	Good	Good
		Combined ICI/CDKI	Missing	Missing
Immunological effects upon CDKI treatment		Circulation	IL-2 and TNF-α secretion; Treg, B cells ; MDSC	IL-2, TNF-α, IL-6 secretion, IL-10 secretion; B cells,Treg, $CTLA\text{-}4^+$ cells ; MDSC
		Spleen	Mxd4	Treg, $CTLA\text{-}4^+$ cells
		Tumor	Mxd4, cMyc, TGF-b; $CTLA\text{-}4^+$ cells; DC myeloid cells ; TAM ;	Agr2 ; B cells; Treg ; TAM
Pathway alteration upon CDKI treatment		DNA Damage repair	Induced	Unaffected
		PI3K-Akt	Downregulated	Unaffected
		Wnt signaling	Activated	Unaffected
		Epigenetic regulation	Downregulated	Induced
		JAK-STAT signaling	Downregulated	Induced
		EMT	Activated (boosted in the combination)	Not induced

TIL - tumor-infiltrating lymphocytes; GIT - gastrointestinal tumor; MDSC - myeloid-derived suppressor cells; TAM - tumor-associated macrophages; CDK - cyclin-dependent kinase; CDKI - cyclin-dependent kinase inhibitor; ICI - immune checkpoint inhibition; DC - dendritic cells; EMT - epithelial-mesenchymal transition.

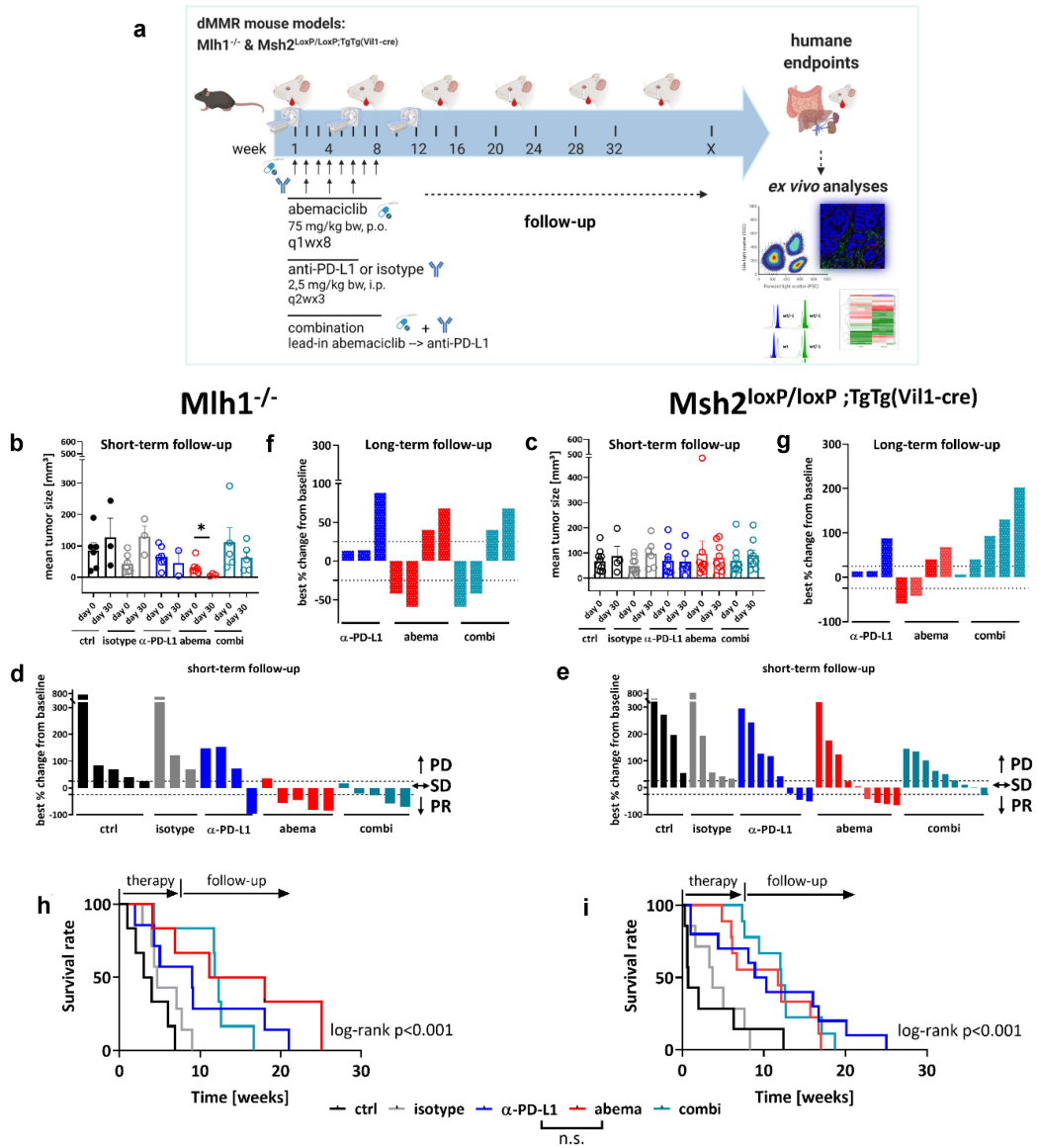

Figure 2. Treatment schedule, longitudinal ^{18}F-FDG PET/CT imaging in vivo and overall survival of Mlh1$^{-/-}$ and Msh2$^{loxP/loxP;TgTg(Vil1-cre)}$ mice. (a) Experimental protocol. Mice with gastrointestinal tumors were conducted to mono- or combination therapy. Abemaciclib: 1x/week, 8 times in total (q1wx8); α-PD-L1: biweekly, 3 times in total (q2wx3); combination: abemaciclib first (=lead-in), followed by α-PD-L1 injection. (b – g) Baseline and follow-up PET/CT imaging of individual mice. (b, c) Data are presented in column (each dot stands for an individual mouse). (D, E, F, G) data are presented as best % change from baseline according to clinical definitions and depicted for each individual mouse either after short-term (day 30) (d, e) or long-term follow-up (~day 50) (f, g); PD – progressive disease (tumor volume > 25% vs. baseline), SD – stable disease (tumor volume similar to initial staging (≤ 25% vs. day 0); PR – partial response (tumor volume 50% lower or more vs. baseline). (h, i) Kaplan-Meier survival curve. Mlh1$^{-/-}$: isotype vs. α-PD-L1: p < .05; control vs. abemaciclib: p < .01; control vs. combination: p < .01; ctrl: n = 6, isotype: n = 7, α-PD-L1 n = 7, abemaciclib: n = 6, combination n = 6. Msh2$^{loxP/loxP\ VillinCre:}$ isotype vs. α-PD-L1: p < .05; control vs. abemaciclib: p < .01; control vs. combination: p < .001. ctrl: n = 10, isotype: n = 7, α-PD-L1 n = 10, abemaciclib: n = 9, combination n = 9. Log-rank analysis (Mantel Cox).

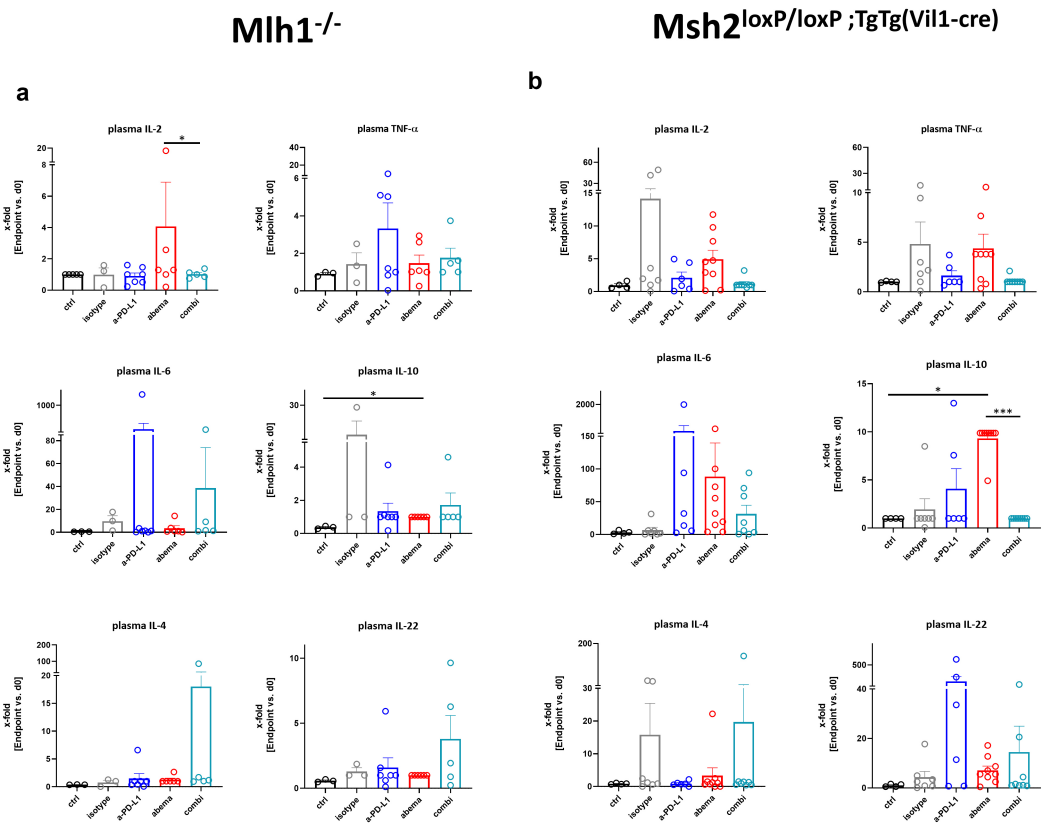

Figure 3. Cytokine levels of plasma from Mlh1$^{-/-}$ and Msh2$^{loxP/loxP;TgTg(Vil1-cre)}$ mice. (a) Mlh1$^{-/-}$ and (b) Msh2.$^{loxP/loxP;TgTg(Vil1-cre)}$ Plasma samples were collected before treatment (= baseline) and at the experimental endpoint. Cytokine levels were determined as described in material and methods. Given is the x-fold change of the indicated marker in comparison to day 0 (= baseline). Mlh1$^{-/-}$: ctrl: n = 3, isotype: n = 3, α-PD-L1 n = 7, abemaciclib: n = 6, combination n = 5. Msh2$^{loxP/loxP\ VillinCre}$: ctrl: n = 4, isotype: n = 7, α-PD-L1 n = 6, abemaciclib: n = 9, combination n = 8. *p < .05; ***p < .001, Kruskal-Wallis test (Dunn's multiple comparisons test). (a-b) All data are given as mean + SEM.

Monotherapy with abemaciclib induced IL-2 secretion in Mlh1$^{-/-}$ mice, while the α-PD-L1 antibody evoked TNF-α and IL-6 release (Figure 3a). However, this did not reach statistical significance. In mice receiving the combination, we detected increased levels of IL-4 and IL-22. IL-10 was not altered under therapy. In Msh2$^{loxP/loxP;TgTg(Vil1-cre)}$ mice, IL-2, TNF-α, IL-6, and IL-10 level were higher under abemaciclib treatment (Figure 3b). The α-PD-L1 monotherapy led to a strong increase of IL-6 and IL-22 (Figure 3b and supplementary Figure S2A). The combination triggered the release of IL-6 and IL-22 secretion, but not to a degree comparable to either monotherapy.

While these data already hinted toward individual effects on the immune system, we then focused on blood phenotyping to dissect the immunological changes in detail. Therefore, a panel of specific antibodies was used to quantify numbers of circulating T cell subpopulations (including exhausted and activated T cells), NK cells, B cells, and myeloid-derived suppressor cells (MDSC) via flow cytometry (Figure 4, supplementary Figure S2B, C).

This analysis identified decreased levels of regulatory T cells (Tregs) in Mlh1$^{-/-}$ and Msh2$^{loxP/loxP;TgTg(Vil1-cre)}$ mice and in all treatment groups (Figure 4a, b). In Mlh1$^{-/-}$ mice, CTLA-4^{+} cells showed only reduced levels under α-PD-L1 mono- and combination therapy (Figure 4c). This was additionally seen for CD19^{+} cells (supplementary Figure S2B). In contrast, the percentage of MDSCs was highly increased in the combination. NK cells remained unchanged (supplementary Figure S2B).

Comparable effects on Tregs and exhaustion markers were evident in Msh2$^{loxP/loxP;TgTg(Vil1-cre)}$ mice (Figure 4b, d). Exemplarily shown for CTLA-4^{+} T cells, the percentage of circulating cells was reduced under all three treatments (Figure 4d). Notably, both monotherapies reduced the amounts of exhausted PD-1^{+} T cells (not shown). The MDSCs, B cells, and NK cells showed diverging results, with the former showing treatment-related increases (supplementary Figure S2C).

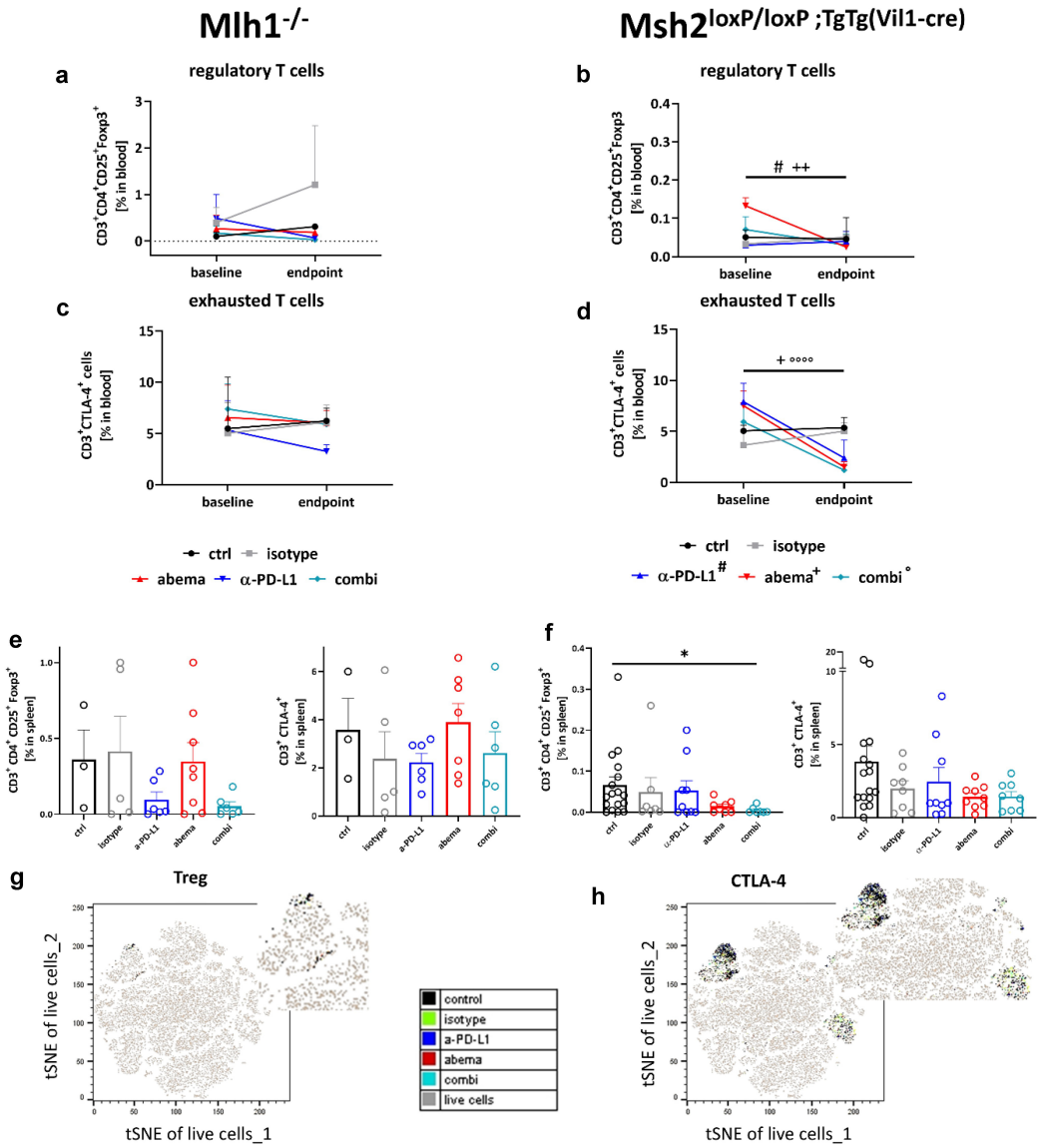

Figure 4. Spectral flow cytometry of peripheral blood and spleens from Mlh1$^{-/-}$ and Msh2$^{loxP/loxP;TgTg(Vil1-cre)}$ mice. (a – d) Blood phenotyping. Given is the number of % immune cells before treatment (= baseline) and at the experimental endpoint resulting from 100,000 events measured on a flow cytometer. Mlh1$^{-/-}$ n = 3–8 mice/group, Msh2$^{loxP/loxP;TgTg(Vil1-cre)}$ n = 7–9 mice/group. $^{\#}p < .05$ endpoint vs. day 0 α-PD-L1; $^{+}p < .05$ endpoint vs. day 0 abemaciclib; $^{++}p < .01$ endpoint vs. day 0 abemaciclib, $^{\circ\circ\circ\circ}p < .0001$ endpoint vs. day 0 combination. Kruskal-Wallis test (Dunn's multiple comparisons test). (e – h) Spleen phenotyping. Given is the number of % immune cells at the experimental endpoint resulting from 100,000 events measured on a flow cytometer. $^{*}p < .05$; Kruskal-Wallis test (Dunn's multiple comparisons test). (g, h) tSNE plots showing single T cell subpopulations of spleens from Msh2$^{loxP/loxP;TgTg(Vil1-cre)}$ mice. The expression profile of the exhaustion marker CTLA-4 as well as Tregs were illustrated for the treatment and control groups, respectively.

Next, we focused on splenic T cells (Figure 4e, f). In Mlh1$^{-/-}$ mice, Tregs were only reduced under a-PD-L1 mono – and combination treatment (Figure 4e). Abemaciclib alone did not change the amount of Tregs. Also, exhausted T cells remained unchanged under therapy. In Msh2$^{loxP/loxP;TgTg(Vil1-cre)}$ mice, abemaciclib alone and in combination with α-PD-L1 reduced

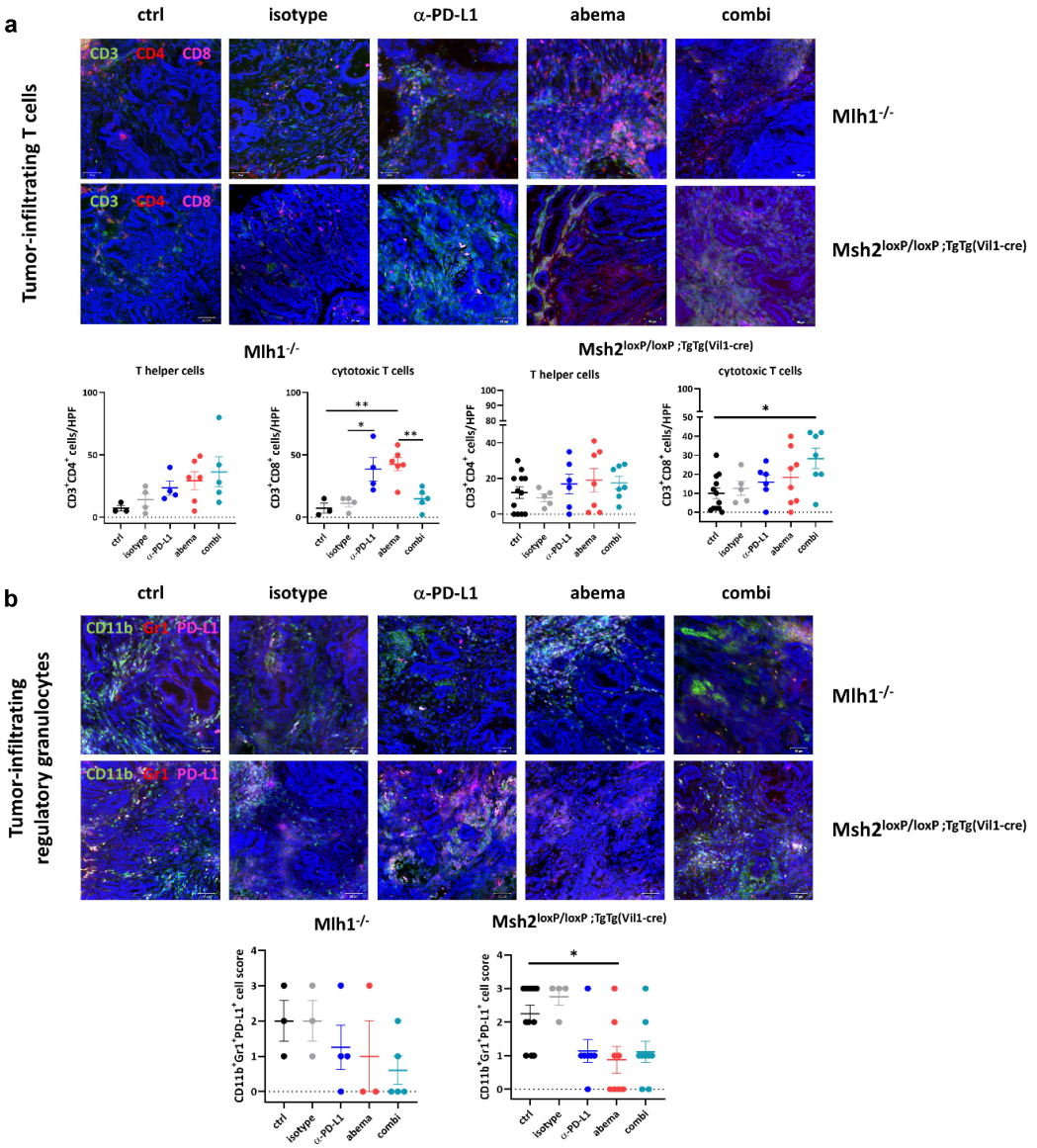

Figure 5. Immunofluorescence of tumor specimens from Mlh1$^{-/-}$ and Msh2$^{loxP/loxP;TgTg(Vil1-cre)}$ mice. Residual tumor slides were fixed, stained and embedded. Confocal laser scanning microscopy was done on a Zeiss Elyra 7 microscope. The infiltration pattern of T cells, regulatory and tumor-associated macrophages differed between individual treatment groups. In most cases, the differences reached statistical significance. Upper panel: representative images of tumor slides; lower panel: quantitative analysis of tumor-infiltrating immune cells. (a, d) Given is the number of infiltrating CD3$^+$CD4$^+$ T helper cells, CD3$^+$CD8$^+$ cytotoxic T cells and IRF5$^+$ macrophages counted in 2–3 HPFs/slide with n = 3–10 mice/group. (b, c) The infiltration pattern was semi-quantitatively analyzed using a scoring system. 0 = no; 1 = mild; 2 = moderate; 3 = strong. Each symbol represents one case. *p < .05; **p < .01, Two-way ANOVA (Tukey's multiple comparisons test).

the numbers of Tregs and CTLA-4$^+$ T cells (figure 4f), which is additionally illustrated as tSNE plot in Figure 4g,h Every dot represents one cell. Cells with similar surface markers are located next to each other. In the left upper part of the plot the Tregs are highlighted. As expected, they are all located very close in one cluster. Larger distances might be due to other expressed surface markers, which were not relevant for our gating of Tregs.

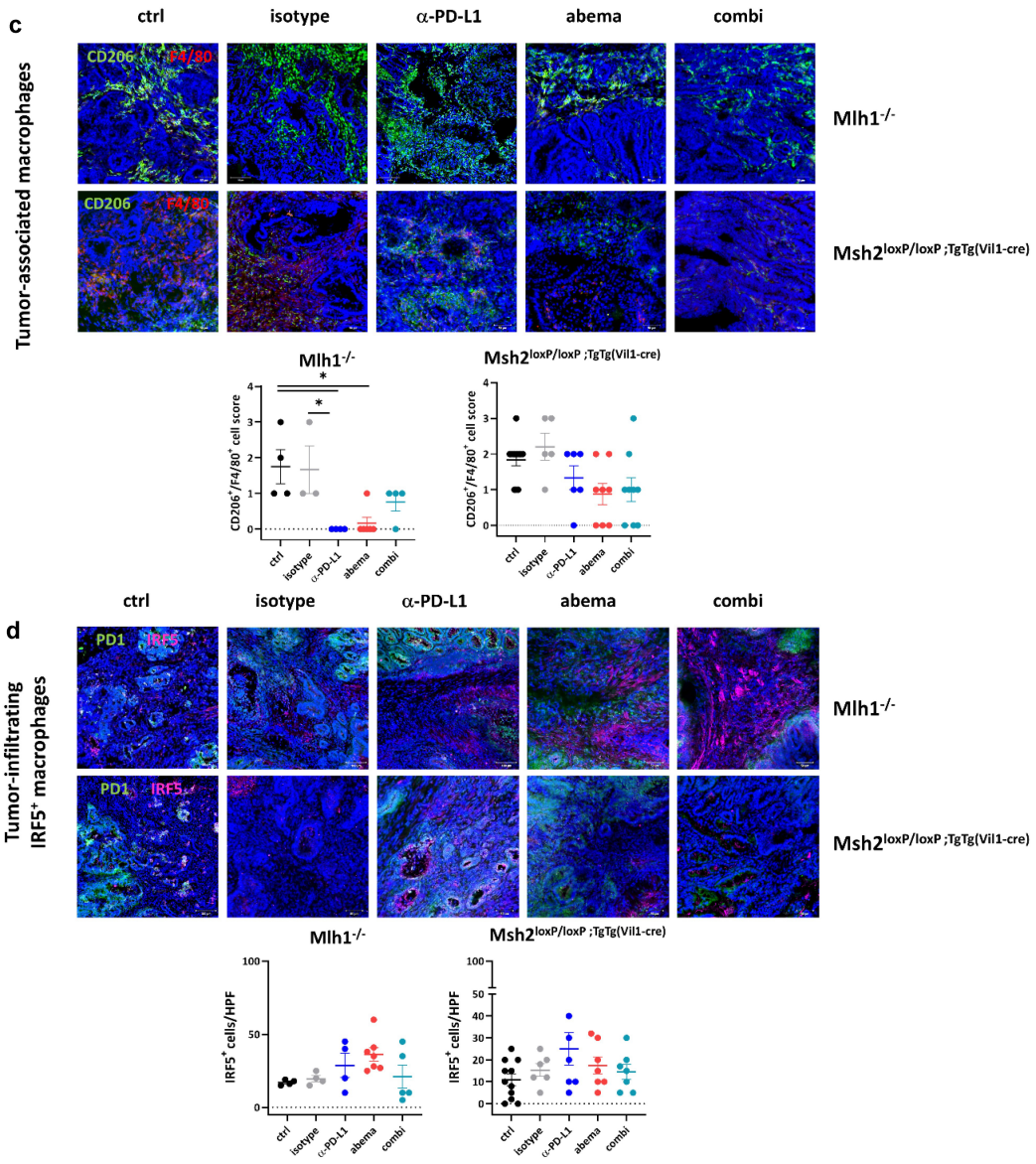

Figure 5. (Continued)

Treatment-related changes in the tumor microenvironment

The individual effects of either treatment on circulating immune cells were then studied in the local tumor microenvironment. Here, we quantified infiltrating T cells, regulatory $CD11b^+Gr1^+PD\text{-}L1^+$ granulocytes, tumor-associated macrophages (TAMs), and $IRF5^+$ M1 macrophages (Figure 5).

Abemaciclib and α-PD-L1 monotherapy triggered focal $CD3^+CD4^+$ and $CD3^+CD8^+$ T-cell infiltration, especially in $Mlh1^{-/-}$ mice (Figure 5a). Cytotoxic T cell numbers were even significantly elevated under abemaciclib and α-PD-L1 monotherapy in $MLH1^{-/-}$ mice, whereas in the combination treatment, this massive immune stimulation was partially abrogated (Figure 5a). In $Msh2^{loxP/loxP;TgTg(Vil1-cre)}$ mice, infiltrating T cell numbers increased upon treatment (Figure 5a). The

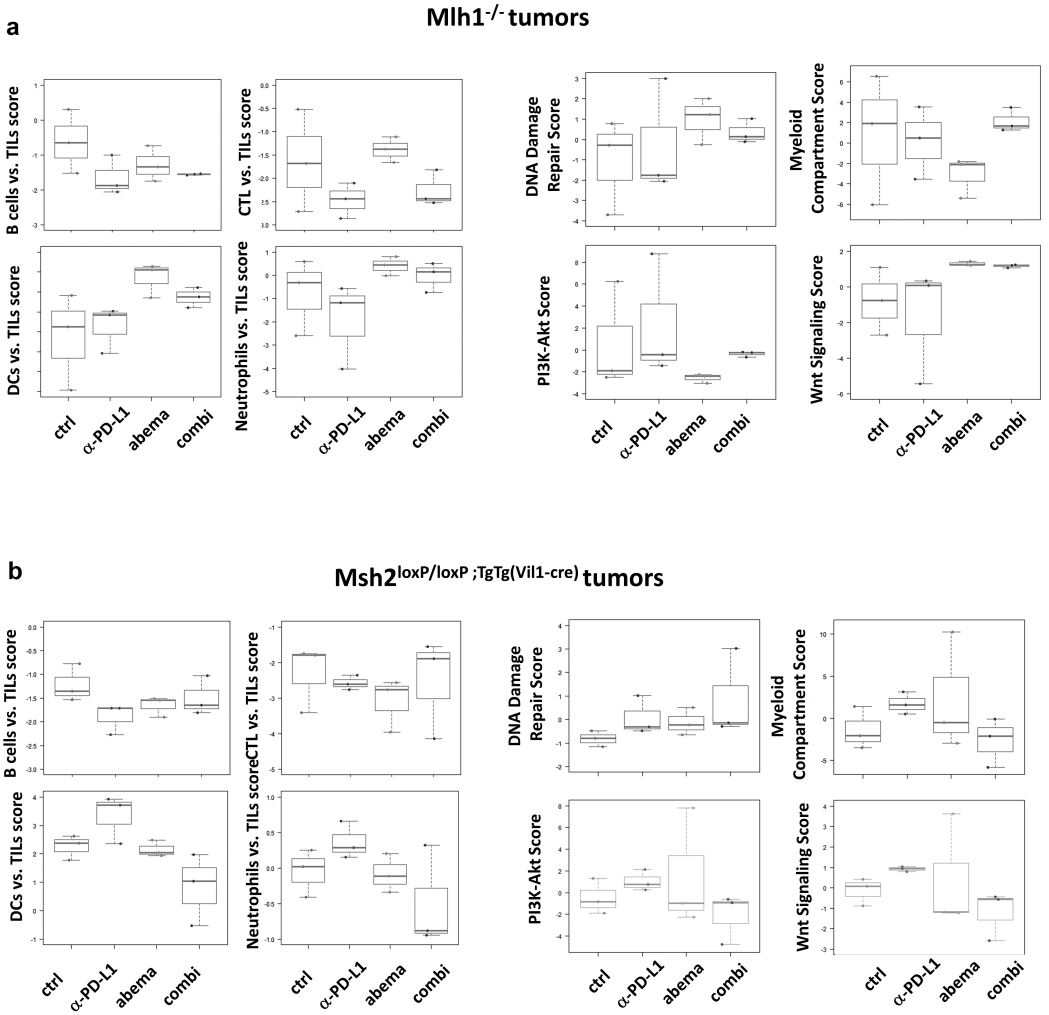

Figure 6. Nanostring gene expression analysis of tumors from Mlh1$^{-/-}$ and Msh2$^{loxP/loxP;TgTg(Vil1-cre)}$ mice. The PanCancer IO 360 Gene Expression Panel was applied. Relative abundances measuring various contrasts between cell types reported for each group. Data result from n = 3 samples/group.

overall higher infiltration with T cells was accompanied by decreased numbers of regulatory granulocytes and TAMs in both mouse strains (Figure 5b, c). Quite in line, IRF5, which leads to M1 polarization, was more abundant in abemaciclib-treated tumors and additionally slightly higher upon α-PD-L1 blockade (Figure 5d). This positive immunomodulatory effect was negated almost completely in both mouse strains receiving the combination.

Supplemental flow cytometric assessment of MLH1$^{-/-}$ and Msh2$^{loxP/loxP;TgTg(Vil1-cre)}$ tumors identified decreased numbers of Tregs in the combination groups (supplementary Figure S3).

The amount of CTLA-4^{+} T cells increased in tumors of Mlh1$^{-/-}$ mice upon abemaciclib mono- and combination therapy, but remained unchanged in Msh2$^{loxP/loxP;TgTg(Vil1-cre)}$ tumors.

To get a detailed overview of the tumor-infiltrating leukocyte (TIL) compartments and identify treatment-related pathway alterations in-depth, the PanCancer IO 360 Gene Expression Panel was applied (Figure 6 and supplementary Figure S4). B cell levels decreased under all therapies in both mouse strains. In Mlh1$^{-/-}$ mice, abemaciclib increased the level of cytotoxic T cells within the TIL compartment. Dendritic cell (DC) and neutrophil levels were contrary between the two

mouse strains. Abemaciclib mono- and combination therapy increased the level of both cell types in Mlh1$^{-/-}$ mice, while in Msh2$^{loxP/loxP;TgTg(Vil1-cre)}$ mice, it was the other way round.

DNA damage repair genes, such as Rad51, MGMT, and Exo1 were higher expressed under abemaciclib mono- and combination therapy in both mouse lines (Figure 6). A comparable effect was seen on Wnt signaling, which was highly activated in these two treatment groups, espe-cially in Mlh1$^{-/-}$ mice. Vice versa, the myeloid compart-ment score as well as genes related to PI3K/Akt or Jak/ STAT signaling were reduced (Figure 6, and supplemen-tary Figure S4). Additionally altered genes included those involved in epigenetic regulation and hypoxia. Here again, Mlh1$^{-/-}$ and Msh2$^{loxP/loxP;TgTg(Vil1-cre)}$ mice responded contrarily (supplementary Figure S4A,C). In the combina-tion, these strong immune-modulatory effects were almost completely neutralized as illustrated in a heatmap (supple-mentary Figure S4B, D). Here, the contradictory effects of both monotherapies (abemaciclib, α-PD-L1) on cellular pathways are shown. In Mlh1$^{-/-}$ mice, abemaciclib led to a significant downregulation of most pathways (depicted in blue), but the α-PD-L1 antibody activated them (depicted in red). In the combination, these opposite effects were blunted. In Msh2loxP/loxP;TgTg(Vil1−cre) mice, the differences were weaker, still, a comparable trend was seen for most pathway alterations, providing a likely explanation for the missing benefit in vivo.

Treatment-associated gene expression changes in the tumor microenvironment and spleen

The above findings indicated Wnt activation by abemaci-clib as well as epigenetic modulation by either treatment. Since these mechanisms are drivers of epithelial-mesenchymal transition (EMT), we determined whether this may also play a role here and provide another expla-nation for the different treatment responses seen under mono- and combination therapy. Therefore, the expres-sion levels of the EMT markers Tgfb1, Vimentin, N-Cadherin, and Fpr2 were studied by qPCR (Figure 7).

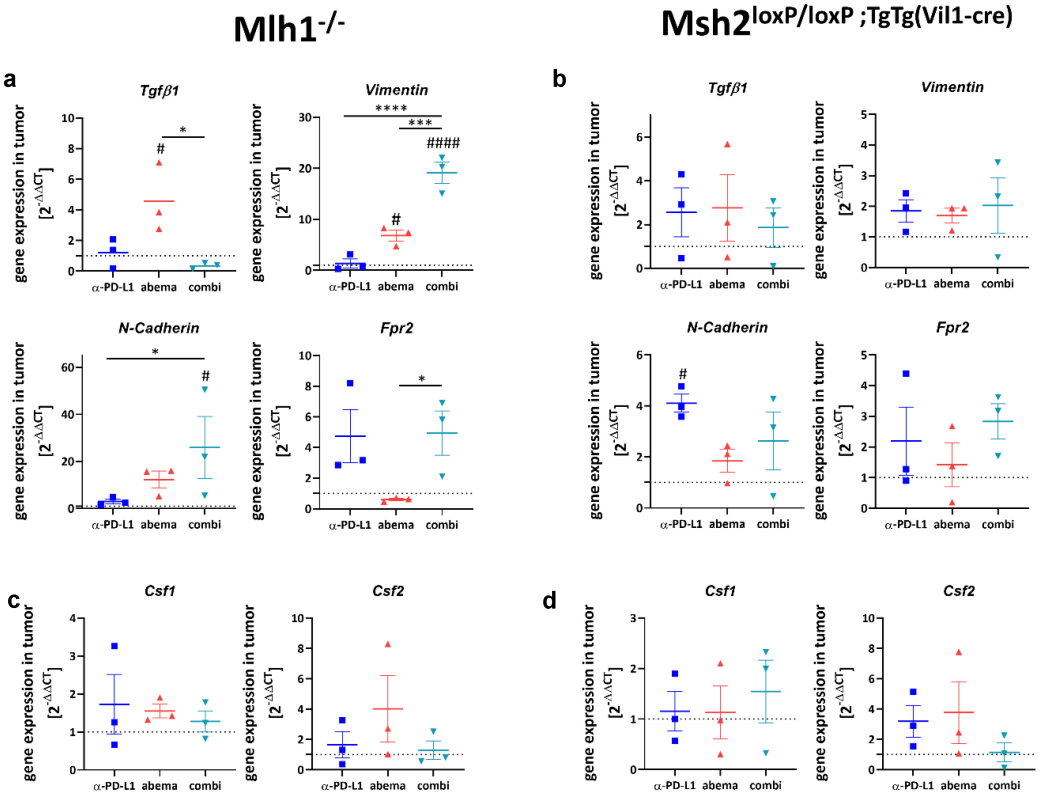

Figure 7. Expression levels of selected genes and functional immunological analysis. (a-f) Total RNA from tumors (A-F) and spleens (g, h) was reverse transcribed into cDNA and qPCR was done as described in material and methods. All data are given as $2^{-\Delta\Delta CT}$ values + SEM. Analysis was done in triplicates with n = 3 mice/group, respectively, * p < .05; *** p < .001; **** p < .0001; # p < .05; ## p < .01; #### p < .0001 vs. control. One-way ANOVA (Tukey's multiple comparisons test) or Kruskal-Wallis test (Dunn's multiple comparisons test).

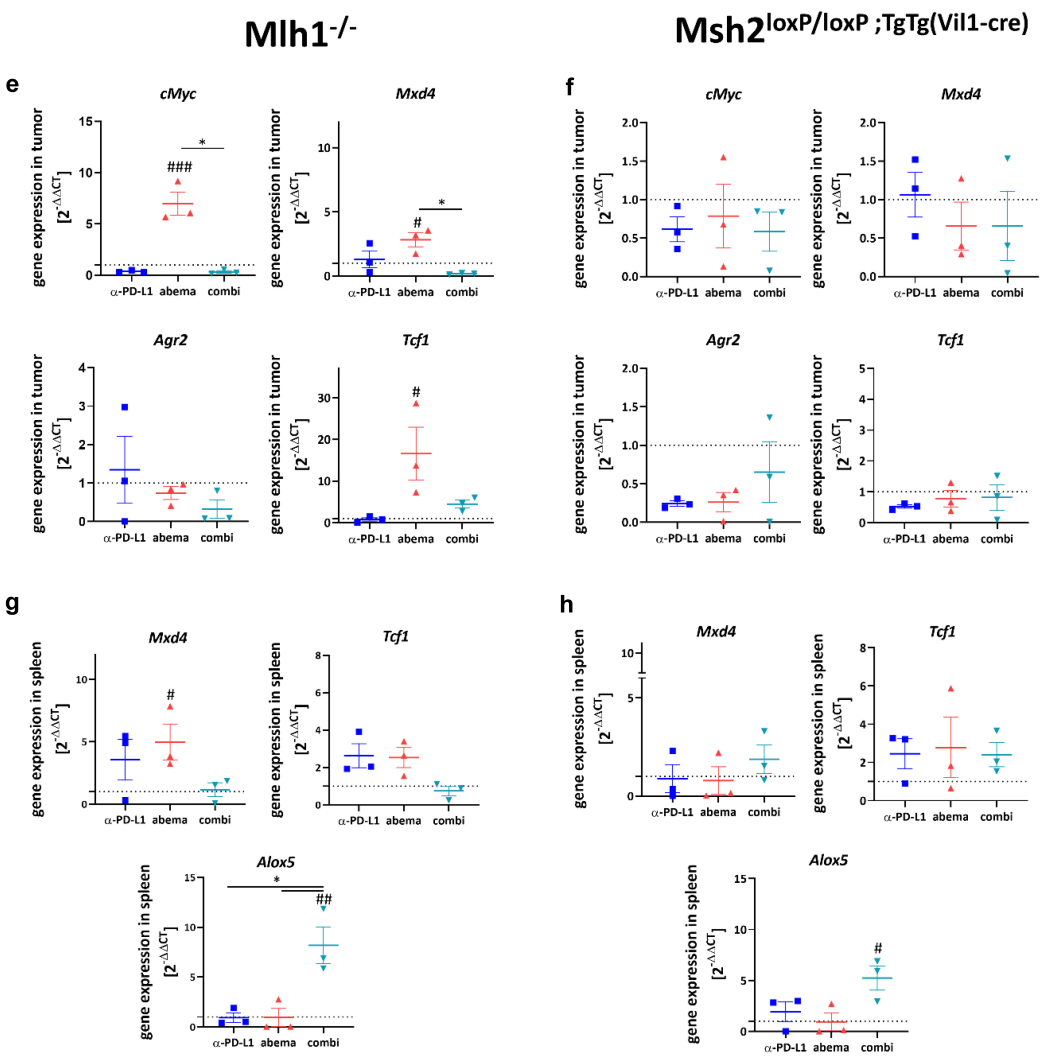

Figure 7. (Continued)

Monotherapy with abemaciclib upregulated Tgfb1, Vimentin, and N-Cadherin, but effectively suppressed Fpr2 in Mlh1$^{-/-}$ mice (Figure 7a). The α-PD-L1 antibody had no or opposite effects on gene expression. In mice receiving the combination, Vimentin, N-Cadherin, and Fpr2 were highly upregulated in residual tumors. The latter is a chemoattractant receptor of G-protein-coupled receptors, which, in conjunction with the EMT effectors Vimentin and N-Cadherin, triggers cancer invasion.[30]

In Msh2$^{loxP/loxP;TgTg(Vil1-cre)}$ mice, no such clear correlations were seen. Abemaciclib alone had no impact on EMT markers (Figure 7b). By contrast, α-PD-L1 treatment upregulated N-Cadherin and Fpr2. Heterogenous effects were seen in the combination group, showing slightly elevated expression levels of Vimentin, N-Cadherin, and Fpr2.

Then, the impact on macrophages was studied (Figure 7c, d). Csf1 and Csf2 were used as markers for macrophage polarization. Although statistical significance was not reached, we

observed a trend toward a higher expression of Csf2 vs. Csf1 in both mouse strains treated with abemaciclib or α-PD-L1. Csf2 is associated with an M1-like phenotype, which supports our above findings on M1-polarization upon monotherapy. Notably, in both mouse models receiving the combination, Csf1 and Csf2 were comparable to controls.

Next, we checked genes related to cancer immunity and T cell activation (cMyc, Mxd4, Agr2, Tcf-1).[18,31] Abemaciclib induced a significant upregulation of Myc and Mxd4 in $Mlh1^{-/-}$, but not $Msh2^{loxP/loxP;TgTg(Vil1-cre)}$ tumors. Also, Tcf1, a transcription factor of the Wnt signaling pathway and Treg suppressor,[32] was highly upregulated. Tcf-1 was recently identified in intratumoral memory $CD8^+$ T cells with stem cell-like properties.[31] Notably, no such changes were seen upon α-PD-L1 mono- or combination therapy (Figure 7e). The tumor-promoting anterior gradient-2 (Agr2) was found reduced in all mice ($Mlh1^{-/-}$ and $Msh2^{loxP/loxP;TgTg(Vil1-cre)}$) receiving abemaciclib alone or in combination with α-PD-L1 (figure 7f).

These results prompted us to check for the expression of immunologically and functionally relevant genes in the spleen (Figure 7g, h). Abemaciclib, but not the other treatment regimens, induced Mxd4 and Tcf1 in spleens of $Mlh1^{-/-}$ mice. As anticipated, no significant alterations were detectable in $Msh2^{loxP/loxP;TgTg(Vil1-cre)}$ mice in either treatment. By contrast, Alox5, a neutrophil and macrophage marker with pro-inflammatory and tumor-promoting activity,[33] was highly elevated in both mouse lines receiving the combination.

Finally, mutations in dMMR-specific target genes were examined (supplementary Figure S5). The overall mutation frequency in the tumor compared to normal tissue was slightly elevated under abemaciclib therapy in $Mlh1^{-/-}$ mice (supplementary Figure S5). In addition, abemaciclib was the only treatment that led to mutations in Mdm2 and Ncapd2 and also in combination therapy to mutations in Spen and FAS. For Taf1b, Kcnma1, and Rfc3 nearly all treatments triggered mutations. In $Msh2^{loxP/loxP;TgTg(Vil1-cre)}$ mice, α-PD-L1 mono- and combination therapy led to slightly decreased mutation frequency, whereas for the displayed genes, all treatments induced mutations.

Discussion

Using two clinically relevant mouse models of spontaneous dMMR-driven tumorigeneses, we report that low-dose abemaciclib treatment is as effective as immune-checkpoint blockade, while the combination is not superior to either monotherapy.

Abemaciclib is approved for high-risk early and advanced/metastatic breast cancer.[34] The underlying mode of action includes decreased cell proliferation and induction of senescence.[13,35,36] Here, we also found increased numbers of apoptotic and necrotic cells, a G1-arrest, and impaired colony formation abilities of murine dMMR tumor cells. The latter effect was evident after several days of treatment rest, which is in line with abemaciclibs' ability to suppress DNA synthesis even after drug removal.[13] In a co-culture system of $Mlh1^{-/-}$ tumor and semi-autologous immune cells, abemaciclib boosted cytotoxic effects to an amount much higher than the therapeutic α-PD-L1 antibody. Hence, we confirm the strong immune-stimulating potential of this CDKI.[14,15,37] This finding may expand the spectrum of tumors eligible for CDK inhibition.[38]

In a proof-of-concept in vivo trial, abemaciclib was given therapeutically to tumor-bearing $Mlh1^{-/-}$ and Msh2loxP/loxP; TgTg(Vil1−cre) mice. While both mouse strains responded to CDK4/6 inhibition, disease control was better in the former. Notably, 80% of mice underwent partial remission, finally resulting in significantly prolonged overall survival. In $Msh2^{loxP/loxP;TgTg(Vil1-cre)}$ mice, the overall survival was similarly extended, but longitudinal PET/CT imaging yielded heterogeneous effects on tumor sizes. The survival benefit was comparable to PD-L1 blockade, which improved the outcome by several weeks. Noteworthy, in this context, is the fact that treatment was given once a week as opposed to most preclinical studies in which a daily treatment regimen is applied.[12,36,37,39] The rationale for this dose reduction is based on the fact that dMMR tumors are highly immunogenic per se and pre-formed immune responses may exist.[19,20,40] Accordingly, the primary aim was to re-activate the immune system rather than inducing de novo T cell immune responses.[14,16,18,29] With this reduced dosing schedule, abemaciclib still triggered immune modulation, characterized by enhanced secretion of Th1 and Th2-specific cytokines. This was accompanied by reduced numbers of circulating, and to some degree also splenic, $CD4^+CD25^+FOXP3^+$ regulatory T cells – likely due to the CDKI-mediated repression of DNA methyltransferase 1[15]. Tregs express CDK6 at higher levels than effector T cells, making them more vulnerable to CDK inhibition.[15,41] This fact explains why abemaciclib does not impair effector T cell functions. Although these immunological changes emerged in both models, we identified striking differences in the response profile between $Mlh1^{-/-}$ and $Msh2^{loxP/loxP;TgTg(Vil1-cre)}$ mice. Given the fact that both strains develop dMMR-related tumors in the gastrointestinal tract (jejunum) spontaneously, this finding is intriguing. However, the mutational driver (Mlh1 vs. Msh2) and the resulting tumor microenvironment (T cells vs. TAMs vs. MDSCs vs. PD-L1 positivity) varies. This is consistent with the human counterpart, e.g. in the tumor mutational burden.[42]

Recent studies describe the restoration of the T cell function by CDK4/6 blockade.[15,18,37,38,43] By dissecting the local immune response in detail, we found significantly increased numbers of cytotoxic T cells and DCs within the TIL compartment, especially in $Mlh1^{-/-}$ mice. Vice versa, numbers of TAMs decreased, accompanied by rising numbers of $IRF5^+$ cells, reduced levels of the myeloid compartment as well as genes related to PI3K/Akt signaling. Higher expression of IRF5 leads to M1 polarization and the formation of a pro-inflammatory, antitumoral phenotype.[44] Comparable positive immune-modulating side-effects were recently reported for dinaciclib, turning the microenvironment of immunologically 'cold' pancreatic cancers into a 'hot' one.[45] Yet, the plasticity of macrophages may result in dual activation or a mixed M1/M2-like phenotype[46] as seen here upon abemaciclib treatment via upregulation of CSF1 and CSF2. The latter supports the differentiation of hematopoietic myeloid cells[47] and plays an important role in macrophage polarization by enhancing antigen

presentation and DC formation.[48] Here, abemaciclib-treated Mlh1$^{-/-}$ tumors had elevated numbers of DCs, likely because of CSF2-driven M1 polarization. In the combination, the beneficial effects of the monotherapies were blunted by suppressing activated pathways. Such striking differences in specific subpopulations were primarily detectable in tumors from Mlh1$^{-/-}$ mice, while Msh2$^{loxP/loxP;TgTg(Vil1-cre)}$ mice responded differently and effects were often weaker. The exact underlying reason for this model-individual response is not known. A recent study classified inherited and sporadic human dMMR endometrial tumors into distinct immunological entities.[49] Apart from this, dMMR-related malignancies are often grouped together and responses compared to proficient MMR-tumors, without MMR-subclassification, i.e. MLH1, MSH2, MSH6, or PMS2.[50] Hence, we can only speculate on the cause for the different responses seen here, such as: (I) these two dMMR models were created by different methods (Cre-lox System vs. constitutional knock out), the impact of either method on antitumoral immune function is inestimable; (II) Msh2$^{loxP/loxP;TgTg(Vil1-cre)}$ mice are bred homozygous, while Mlh1$^{-/-}$ mice are offsprings of heterozygous littermates; (III) the mutational load within coding microsatellites and the loci affected by a specific mutation within tumors differs; and (IV) the tumor microenvironment is heterogeneous.

When looking at regulatory granulocytes, another immunesuppressive subpopulation, only marginal changes were seen. Likewise, circulating and splenic MDSCs increased during after-care and may eventually have contributed to relapse. In support of this, gene expression analysis identified higher amounts of neutrophils within MLH1$^{-/-}$ and Msh2$^{loxP/loxP;TgTg(Vil1-cre)}$ tumors, together with high levels of DNA damage repair genes as part of the global stress-response. Another interesting finding of our preclinical in vivo trial is the activation of the Wnt pathway, which was again higher in MLH1$^{-/-}$ mice. This effect has been described before as a result of GSK3β inhibition by abemaciclib.[51] GSK3β is an integral kinase within the β-catenin destruction complex. Its specific inhibition by abemaciclib does not apply to other CDK4/6 inhibitors and prospective studies will have to show whether WNT/β-catenin activation constitutes a potentially harmful side effect. One of the conceivable effector mechanisms is the induction of epithelial-mesenchymal transformation (EMT), characterized by invasion and enhanced motility.[52] Indeed, abemaciclib triggered vimentin and N-cadherin expression, especially in Mlh1$^{-/-}$ mice, but effectively suppressed Fpr2, which is also involved in invasion and metastasis.[53,54] We, therefore, conclude a compensatory mechanism to counteract abemaciclib-driven EMT. In the combination, no such "protective" effects were seen, with expression levels of EMT-markers being equal to or higher than in either monotherapy. Therefore, we propose EMT-driven tumor progression as one of the mechanisms that contribute to treatment failure. This hypothesis is supported by comparable findings in Msh2$^{loxP/loxP;TgTg(Vil1-cre)}$ mice. Although the effects were weaker, we observed a trend toward a higher expression of EMT markers in the combination group.

Another positive effect of CDK4/6 inhibition was recently described on the transcription factor Mxd4, a negative regulator of MYC.[18] Interestingly, we also found the upregulation of Mxd4 after abemaciclib therapy in tumors and spleens of Mlh1$^{-/-}$ mice, but in contrast to Heckler et al.,[18] we additionally detected higher expression levels of cMyc. Furthermore, the previously described formation of CD8^{+} effector memory cells[18] was not confirmed by us (not shown). Despite effective anti-tumor treatment, we conclude a missing long-term immunity, quite possibly attributable to the low-dose and short-term therapy. The fact that neither tumors nor spleens from Msh2$^{loxP/loxP;TgTg(Vil1-cre)}$ mice showed any changes in these two genes confirm the better outcome of Mlh1$^{-/-}$ mice functionally.

Considering the effectiveness of PD-L1 blockade, overall survival was comparable between both mouse strains. Msh2$^{loxP/loxP;TgTg(Vil1-cre)}$ mice tended to benefit more from ICI, likely because of the higher PD-L1 abundance within the tumor stroma. The immunological effects of PD-L1 blockade can be summarized as follows: ICI-monotherapy triggered IL-6 release in both mouse strains, accompanied by reduced levels of exhausted T cells in the blood and slightly elevated levels of tumor-infiltrating T helper and cytotoxic cells. In the TIL compartment, regulatory granulocytes and TAMs faintly decreased. Tregs were only lower in the circulation of both mouse strains. Vice versa, splenic or tumor-infiltrating Treg numbers marginally changed. Although we detected higher expression levels of genes involved in antigen presentation, apoptosis, and interferon signaling in tumors of Msh2$^{loxP/loxP;TgTg(Vil1-cre)}$ mice, the overall immune stimulation was lower as seen for abemaciclib and the beneficial effects were consistently attenuated in the combination. With regard to EMT, ICIs are thought to have a minor direct impact.[55] This is in line with our findings, in which N-cadherin was the only elevated gene after α-PD-L1 blockade in Msh2$^{loxP/loxP;TgTg(Vil1-cre)}$ mice. Apart from this, no impact was seen on either marker, suggesting no interference with EMT at least in these models.

Finally, the question remains why the combination failed to surpass the respective monotherapy. Preexisting effector T cell levels and dynamic changes in circulating myeloid cells were previously identified as decisive factors for response to combined CDK4/6-immune-checkpoint inhibition (palbociclib + pembrolizumab) in metastatic breast cancer.[43] Here, we did not see such beneficial effects under combination therapy. Tumor growth control and overall survival were not better than in the respective monotherapy. Immunologically, both mouse strains responded with elevated levels of IL-4 in the plasma. IL-4 activates T helper cells, indicating at least partial maintenance of immune stimulation. In support of this, circulating, splenic, and tumor-infiltrating numbers of exhausted T cells were reduced to a degree comparable to abemaciclib monotherapy. In contrast, Mlh1$^{-/-}$ tumors had reduced cytotoxic T cell levels, which were replaced by TAMs. The latter may have stimulated EMT, characterized by high vimentin, N-cadherin, and Fpr2 expression. In Msh2$^{loxP/loxP;TgTg(Vil1-cre)}$ mice, overall effects were weaker, still, a comparable trend toward neutralizing beneficial effects of either monotherapy, such as apoptosis, co-stimulation, immune cell adhesion, and migration, was seen. Although this finding is somehow underwhelming, it supports recent findings, in which no significant difference in the anti-tumor response was seen compared with the activity of abemaciclib monotherapy.[29,37] By applying a simultaneous setting, the strong immune-modulatory effects

of abemaciclib are not boosted and in some cases, they are even dismantled. This finding complies with results from the phase Ia/Ib PACT study in which patients with advanced, refractory solid tumors received an α-PD-L1 inhibitor as monotherapy or in combination with abemaciclib.[56] Lead-in CDK inhibition was not feasible due to hepatotoxicity.[56] Detailed immunological analyses were not done in this clinical trial leaving the impact on the immune system unanswered.

To the best of our knowledge, this is the first comprehensive preclinical study reporting the immune-modulatory and therapeutic activity of abemaciclib on dMMR tumors. We not only provide another piece of evidence for the broad entity-overlapping potential of this selective CDKI but additionally propose an interesting option for dMMR patients not eligible for ICI treatment. However, caution is given when abemaciclib is used as lead-in therapy in combination with α-PD-L1, and follow-up studies are warranted to identify ideal combination partners for CDKI as an immunotherapy backbone.

List of abbreviations

abema – abemaciclib
cMS – coding microsatellite
combi – combination
ctrl – control
dina – dinaciclib
dMMR – Mismatch repair-deficient
ICI – immune checkpoint inhibitors
MDSC – myeloid-derived suppressor cell
ROS – reactive oxygen species
TAM – tumor-associated macrophages
Treg – regulatory T cells

Acknowledgments

We gratefully thank Genentech, a subsidiary of Roche, South San Francisco, USA, for providing the clone 6E11 for in vivo experiments. We additionally thank Mrs. Ilona Klamfuss and Ms. Chantal von Hoersten for breeding mice, Brigitte Vollmar and Bernd Krause for their continuous support in their efforts of chairing the Core Facility of Multimodal Small Animal Imaging. We also gratefully acknowledge the excellent technical assistance of Mrs. Joanna Förster. Furthermore, we thank Carina Bergner and Anja Gummesson, radiopharmacy team of the Department of Nuclear Medicine of the University Medical Centre Rostock, for providing ^{18}F-FDG for the small animal PET/CT experiments. We likewise thank the Core Facility for Cell Sorting & Cell Analysis, Laboratory for Clinical Immunology, University Medical Center Rostock (Mrs. Wendy Bergmann, Prof. Brigitte Müller-Hilke) for their continuous support and providing access to the technical devices. Moreover, we thank Prof. Winfried Edelmann and Prof. Christoph Gasche for providing $Msh2^{loxP/loxP;TgTg(Vil1\text{-}cre)}$ breeding pairs and giving the permission to breed mice in our facility.

Authors' contributions

IS – performed in vivo experiments, flow cytometry, analyzed data and participated in writing, LE, JH and PK – performed ex vivo analyses (staining of blood, spleen, and tumor samples, immunofluorescence, fragment length), BS – analyzed fragment length analyses; CR – performed Nanostring analysis, HL – provided assistance in confocal laser scanning microscopy, LH and CJ – critically revised the manuscript, CM – conducted the study and applied for grants, participated in the experiments, analyzed data, and wrote the manuscript.

Disclosure statement

No potential conflict of interest was reported by the authors.

Ethics approval and consent to participate

The German local authority approved all animal experiments: Landesamt für Landwirtschaft, Lebensmittelsicherheit und Fischerei Mecklenburg-Vorpommern (7221.3-1-062/19; −025/20), under the German animal protection law and the EU Guideline 2010/63/EU. All applicable international, national, and/or institutional guidelines for the care and use of animals were followed.

Data availability statement

All data generated or analyzed during this study are included in this published article [and its supplementary information files].

Funding

This work was supported by grants from the German research foundation [DFG grant number MA5799/2-1 and MA5799/2-2] and the Brigitte und Dr. Konstanze Wegener-Stiftung N/A to C; Deutsche Forschungsgemeinschaft.

References

1. Liu J, Zhang S, Hu Y, Yang Z, Li J, Liu X, Deng L, Wang Y, Zhang X, Jiang T, et al. Targeting PD-1 and Tim-3 pathways to reverse CD8 T-cell exhaustion and enhance ex vivo T-cell responses to autologous dendritic/tumor vaccines. J ImmunoTher. 2016;39(4):171–180. doi:10.1097/CJI.0000000000000122.
2. Tan E, Sahin IH. Defining the current role of immune checkpoint inhibitors in the treatment of mismatch repair-deficient/microsatellite stability-high colorectal cancer and shedding light on future approaches. Expert Rev Gastroenterol Hepatol. 2021 Feb 4;15(7):735–742. doi:10.1080/17474124.2021.1886077.
3. Lemery S, Keegan P, Pazdur R. First FDA approval agnostic of cancer site — when a biomarker defines the indication. N Engl J Med. 2017;377(15):1409–1412. doi:10.1056/NEJMp1709968.
4. Sousa Linhares A D, Battin C, Jutz S, Leitner J, Hafner C, Tobias J, Wiedermann U, Kundi M, Zlabinger GJ, Grabmeier-Pfistershammer K, et al. Therapeutic PD-L1 antibodies are more effective than PD-1 antibodies in blocking PD-1/PD-L1 signaling. Sci Reports. 2019;9(1):1–9. doi:10.1038/s41598-019-47910-1.
5. Kim JH, Kim SY, Baek JY, Cha YJ, Ahn JB, Kim HS, Lee K-W, Kim J-W, Kim T-Y, Chang WJ, et al. A phase II study of avelumab monotherapy in patients with mismatch repair-deficient/microsatellite instability-high or POLE-Mutated metastatic or unresectable colorectal cancer. Cancer Res Treat. 2020 Apr 24. doi:10.4143/crt.2020.218.
6. Taïeb J, André T, El Hajbi F, Barbier E, Toullec C, Kim S, Bouche O, Di Fiore F, Chauvenet M, Perrier H, et al. Avelumab versus standard second line treatment chemotherapy in metastatic colorectal cancer patients with microsatellite instability: the SAMCO-PRODIGE 54 randomised phase II trial. Dig Liver Dis. 2020;53(3):318–323. doi:10.1016/j.dld.2020.11.031.
7. Salewski I, Henne J, Engster L, Schneider B, Lemcke H, Skorska A, Berlin P, Henze L, Junghanss C, Maletzki C. Combined gemcitabine and immune-checkpoint inhibition conquers anti-PD-L1 resistance in low-immunogenic mismatch repair-deficient tumors. Int J Mol Sci. 2021;22(11):5990. doi:10.3390/IJMS22115990.
8. Salewski I, Kuntoff S, Kuemmel A, Feldtmann R, Felix SB, Henze L, Junghanss C, Maletzki C. Combined vaccine-immune-checkpoint inhibition constitutes

a promising strategy for treatment of dMMR tumors. Cancer Immunol Immunother. 2021;70(12):3405–3419. doi:10.1007/s00262-021-02933-4.
9. Sahin IH, Akce M, Alese O, Shaib W, Lesinski GB, El-Rayes B, Wu C. Immune checkpoint inhibitors for the treatment of MSI-H/MMR-D colorectal cancer and a perspective on resistance mechanisms. Br J Cancer. 2019;121(10):809–818. doi:10.1038/s41416-019-0599-y.
10. Goetz MP, Toi M, Campone M, Sohn J, Paluch-Shimon S, Huober J, Park IH, Trédan O, Chen SC, Manso L. MONARCH 3: Abemaciclib As Initial Therapy for Advanced Breast Cancer. J Clin Oncol. 2017 Nov 10;35(32): 3638–3646. doi:10.1200/JCO.2017.75.6155.
11. Hino H, Iriyama N, Kokuba H, Kazama H, Moriya S, Takano N, Hiramoto M, Aizawa S, Miyazawa K. Abemaciclib induces atypical cell death in cancer cells characterized by formation of cytoplasmic vacuoles derived from lysosomes. Cancer Sci. 2020;111(6):2132–2145. doi:10.1111/cas.14419.
12. Naz S, Sowers A, Choudhuri R, Wissler M, Gamson J, Mathias A, Cook JA, Mitchell JB. Abemaciclib, a selective CDK4/6 inhibitor, enhances the radiosensitivity of non–small cell lung cancer in vitro and in vivo. Clin.Cancer Res. 2018;24(16):3994–4005. doi:10.1158/1078-0432.CCR-17-3575/73825/AM/ABEMACICLIB-A-SELECTIVE-CDK4-6-INHIBITOR-ENHANCES.
13. Torres-Guzmán R, Calsina B, Hermoso A, Baquero C, Alvarez B, Amat J, McNulty AM, Gong X, Boehnke K, Du J, et al. Preclinical characterization of abemaciclib in hormone receptor positive breast cancer. Oncotarget. 2017;8(41):69493–69507. doi:10.18632/ONCOTARGET.17778.
14. Zhang QF, Li J, Jiang K, Wang R, Ge JL, Yang H, Liu SJ, Jia LT, Wang L, Chen BL. CDK4/6 inhibition promotes immune infiltration in ovarian cancer and synergizes with PD-1 blockade in a B cell-dependent manner. Theranostics. 2020;10(23):10619–10633. doi:10.7150/THNO.44871.
15. Petroni G, Formenti SC, Chen-Kiang S, Galluzzi L. Immunomodulation by anticancer cell cycle inhibitors. Nat. Rev. Immunol. 2020;20(11):669–679. doi:10.1038/S41577-020-0300-Y.
16. Goel S, Bergholz JS, Zhao JJ. Targeting CDK4 and CDK6 in cancer. Nat. Rev. 2022;22(6):356–372. doi:10.1038/S41568-022-00456-3.
17. Hurvitz SA, Martin M, Press MF, Chan D, Fernandez-Abad M, Petru E, Rostorfer R, Guarneri V, Huang CS, Barriga S, et al. Potent cell-cycle inhibition and upregulation of immune response with abemaciclib and anastrozole in Neomonarch, phase II neoadjuvant study in HR+/HER2- Breast cancer. Clin Cancer Res. 2020;26(3):566–580. doi:10.1158/1078-0432.CCR-19-1425.
18. Heckler M, Ali LR, Clancy-Thompson E, Qiang L, Ventre KS, Lenehan P, Roehle K, Luoma A, Boelaars K, Peters V, et al. Inhibition of CDK4/6 Promotes CD8 T-cell Memory Formation. Cancer Discov. 2021;11(10):2564–2581. doi:10.1158/2159-8290.CD-20-1540.
19. Roudko V, Cimen Bozkus C, Greenbaum B, Lucas A, Samstein R, Bhardwaj N. Lynch syndrome and MSI-H cancers: from mechanisms to "Off-The-Shelf" cancer vaccines. Front Immunol. 2021:12. doi:10.3389/FIMMU.2021.757804.
20. Schwitalle Y, Kloor M, Eiermann S, Linnebacher M, Kienle P, Knaebel HP, Tariverdian M, Benner A, Doeberitz MVONK. BASIC – ALIMENTARY TRACT immune response against frame-shift-induced neopeptides in HNPCC patients and healthy HNPCC mutation carriers. Gastroenterology. 2008;134(4):988–997. doi:10.1053/j.gastro.2008.01.015.
21. Kloor M, Von Knebel Doeberitz M. The immune biology of microsatellite-unstable cancer. Trends in Cancer. 2016;2(3):121–133. doi:10.1016/j.trecan.2016.02.004.
22. Kortüm B, Campregher C, Lang M, Khare V, Pinter M, Evstatiev R, Schmid G, Mittlböck M, Scharl T, Kucherlapati MH, et al. Mesalazine and thymoquinone attenuate intestinal tumour development in Msh2loxP/loxP Villin-Cre mice. Gut. 2015;64(12):1905–1912. doi:10.1136/gutjnl-2014-307663.
23. Kucherlapati MH, Lee K, Nguyen AA, Clark AB, Hou HJ, Rosulek A, Li H, Yang K, Fan K, Lipkin M, et al. An Msh2 conditional knockout mouse for studying intestinal cancer and testing anticancer agents. Gastroenterology. 2010;138(3):993–1002.e1. doi:10.1053/j.gastro.2009.11.009.
24. Edelmann W, Yang K, Kuraguchi M, Heyer J, Lia M, Kneitz B, Fan K, Brown AMC, Lipkin M, Kucherlapati R. Tumorigenesis in Mlh1 and Mlh1/Apc1638N Mutant Mice. Cancer Res. 1999;59:1301–1307.
25. Maletzki C, Beyrich F, Hühns M, Klar E, Linnebacher M. The mutational profile and infiltration pattern of murine MLH1-/- tumors: concurrences, disparities and cell line establishment for functional analysis. Oncotarget. 2016;7(33):53583–53598. doi:10.18632/oncotarget.10677.
26. Gladbach YS, Wiegele L, Hamed M, Merkenschläger AM, Fuellen G, Junghanss C, Maletzki C. Unraveling the heterogeneous mutational signature of spontaneously developing tumors in MLH1 -/- Mice. Cancers (Basel). 2019;11(10):1485. doi:10.3390/CANCERS11101485.
27. Maletzki C, Huehns M, Bauer I, Ripperger T, Mork MMMM, Vilar E, Klöcking S, Zettl H, Prall F, Linnebacher M. Frameshift mutational target gene analysis identifies similarities and differences in constitutional mismatch repair-deficiency and Lynch syndrome. Mol Carcinog. 2017;56(7):1753–1764. doi:10.1002/mc.22632.
28. Lee K, Tosti E, Edelmann W. Mouse models of DNA mismatch repair in cancer research. DNA Repair (Amst). 2015:1–7. doi:10.1016/j.dnarep.2015.11.015.
29. Goel S, DeCristo MJ, Watt AC, BrinJones H, Sceneay J, Li BB, Khan N, Ubellacker JM, Xie S, Metzger-Filho O, et al. CDK4/6 inhibition triggers anti-tumour immunity. Nature. 2017;548(7668):471–475. doi:10.1038/nature23465.
30. Usman S, Waseem NH, Nguyen TKN, Mohsin S, Jamal A, Teh MT, Waseem A. Vimentin is at the heart of epithelial mesenchymal transition (EMT) mediated metastasis. Cancers. 2021;13(19):4985. doi:10.3390/CANCERS13194985.
31. Wen S, Lu H, Wang D, Guo J, Dai W, Wang Z. TCF-1 maintains CD8 + T cell stemness in tumor microenvironment. J Leukoc Biol. 2021;110(3):585–590. doi:10.1002/JLB.5MR1120-778R.
32. Zhang J, Lyu T, Cao Y, Feng H. Role of TCF-1 in differentiation, exhaustion, and memory of CD8+ T cells: a review. FASEB J. 2021;35(5):e21549. doi:10.1096/FJ.202002566R.
33. Weigert A, Strack E, Snodgrass RG, Brüne B. mPGES-1 and ALOX5/-15 in tumor-associated macrophages. Cancer Metastasis Rev. 2018;37(2):317–334. doi:10.1007/S10555-018-9731-3.
34. Groenland SL, Martínez-Chávez A, van DongenMGJ, Beijnen JH, Schinkel AH, Huitema ADR, Steeghs N, van Dongen MGJ. Clinical pharmacokinetics and pharmacodynamics of the cyclin-dependent Kinase 4 and 6 inhibitors palbociclib, ribociclib, and abemaciclib. Clin Pharmacokinet. 2020;59(12):1501–1520. doi:10.1007/s40262-020-00930-x.
35. Klein ME, Kovatcheva M, Davis LE, Tap WD, Koff A. CDK4/6 inhibitors: the mechanism of action may not be as simple as once thought. Cancer Cell. 2018;34(1):9. doi:10.1016/J.CCELL.2018.03.023.
36. Knudsen ES, Hutcheson J, Vail P, Witkiewicz AK, Knudsen ES, Hutcheson J, Vail P, Witkiewicz AK. Biological specificity of CDK4/6 inhibitors: dose response relationship, in vivo signaling, and composite response signature. Oncotarget. 2017;8(27):43678–43691. doi:10.18632/ONCOTARGET.18435.
37. Schaer DA, Beckmann RP, Dempsey JA, Huber L, Forest A, Amaladas N, Li Y, Wang YC, Rasmussen ER, Chin D, et al. The CDK4/6 inhibitor abemaciclib induces a T cell inflamed tumor microenvironment and enhances the efficacy of PD-L1 checkpoint blockade. Cell Rep. 2018;22(11):2809–2817. doi:10.1016/j.celrep.2018.02.053.
38. Lelliott EJ, Sheppard KE, McArthur GA. Harnessing the immunotherapeutic potential of CDK4/6 inhibitors in melanoma: is timing everything? NPJ Precis Oncol. 2022;6(1):26. doi:10.1038/S41698-022-00273-9.

39. Dowless M, Lowery CD, Shackleford T, Renschler M, Stephens J, Flack R, Blosser W, Gupta S, Stewart J, Webster Y, et al. Abemaciclib is active in preclinical models of ewing sarcoma via multipronged regulation of cell cycle, DNA methylation, and interferon pathway signaling. Clin Cancer Res. 2018;24(23):6028–6039. doi:10.1158/1078-0432.CCR-18-1256.
40. Schwitalle Y, Linnebacher M, Ripberger E, Gebert J, von Knebel Doeberitz M. Immunogenic peptides generated by frameshift mutations in DNA mismatch repair-deficient cancer cells. Cancer Immun. 2004;4:14.
41. Rowell EA, Wang L, Chunder N, Hancock WW, Wells AD. Regulation of T cell differentiation and alloimmunity by the cyclin-dependent kinase inhibitor p18ink4c. PLoS One. 2014;9(3). doi:10.1371/JOURNAL.PONE.0091587.
42. Salem ME, Bodor JN, Puccini A, Xiu J, Goldberg RM, Grothey A, Korn WM, Shields AF, Worrilow WM, Kim ES, et al. Relationship between MLH1, PMS2, MSH2 and MSH6 gene-specific alterations and tumor mutational burden in 1057 microsatellite instability-high solid tumors. Int J Cancer. 2020;147 (10):2948–2956. doi:10.1002/ijc.33115.
43. Egelston C, Guo W, Yost S, Lee JS, Rose D, Avalos C, Ye J, Frankel P, Schmolze D, Waisman J, et al. Pre-existing effector T-cell levels and augmented myeloid cell composition denote response to CDK4/6 inhibitor palbociclib and pembrolizumab in hormone receptor-positive metastatic breast cancer. J Immunother Cancer. 2021;9(3):e002084. doi:10.1136/JITC-2020-002084.
44. Krausgruber T, Blazek K, Smallie T, Alzabin S, Lockstone H, Sahgal N, Hussell T, Feldmann M, Udalova IA. IRF5 promotes inflammatory macrophage polarization and TH1-TH17 responses. Nat Immunol. 2011;12(3):231–238. doi:10.1038/ni.1990.
45. Huang J, Chen P, Liu K, Liu J, Zhou B, Wu R, Peng Q, Liu Z-X, Li C, Kroemer G, et al. CDK1/2/5 inhibition overcomes IFNG-mediated adaptive immune resistance in pancreatic cancer. Gut. 2021;70(5):890–899. doi:10.1136/gutjnl-2019-320441.
46. Veremeyko T, Yung AWY, Anthony DC, Strekalova T, Ponomarev ED. Early growth response gene-2 is essential for M1 and M2 macrophage activation and plasticity by modulation of the transcription factor CEBPβ. Front Immunol. 2018;9(NOV):2515. doi:10.3389/FIMMU.2018.02515/BIBTEX.
47. Hercus TR, Thomas D, Guthridge MA, Ekert PG, King-Scott J, Parker MW, Lopez AF. The granulocyte-macrophage colony-stimulating factor receptor: linking its structure to cell signaling and its role in disease. Blood. 2009;114(7):1289–1298. doi:10.1182/BLOOD-2008-12-164004.
48. Cai H, Zhang Y, Wang J, Gu J. Defects in macrophage reprogramming in cancer therapy: the negative impact of PD-L1/PD-1. Front Immunol. 2021:12. doi:10.3389/FIMMU.2021.690869.
49. Ramchander NC, Ryan NAJ, Walker TDJ, Harries L, Bolton J, Bosse T, Evans DG, Crosbie EJ. Distinct immunological landscapes characterize inherited and sporadic mismatch repair deficient endometrial cancer. Front Immunol. 2020;11:10. doi:10.3389/FIMMU.2019.03023.
50. Willvonseder B, Stögbauer F, Steiger K, Jesinghaus M, Kuhn PH, Brambs C, Engel J, Bronger H, Schmidt GP, Haller B, et al. The immunologic tumor microenvironment in endometrioid endometrial cancer in the morphomolecular context: mutual correlations and prognostic impact depending on molecular alterations. Cancer Immunol Immunother. 2021;70(6):1679–1689. doi:10.1007/S00262-020-02813-3.
51. Cousins EM, Goldfarb D, Yan F, Roques J, Darr D, Johnson GL, Major MB. Competitive kinase enrichment proteomics reveals that abemaciclib inhibits GSK3β and activates WNT signaling. Mol Cancer Res. 2018;16(2):333–344. doi:10.1158/1541-7786.MCR-17-0468.
52. Huang Z, Zhang Z, Zhou C, Liu L, Huang C. Epithelial-mesenchymal transition: the history, regulatory mechanism, and cancer therapeutic opportunities. MedComm. 2022;3(2). doi:10.1002/MCO2.144.
53. Lu J, Zhao J, Jia C, Zhou L, Cai Y, Ni J, Ma J, Zheng M, Lu A. FPR2 enhances colorectal cancer progression by promoting EMT process. Neoplasma. 2019;66(5):785–791. doi:10.4149/NEO_2018_181123N890.
54. Xie X, Yang M, Ding Y, Yu L, Chen J. Formyl peptide receptor 2 expression predicts poor prognosis and promotes invasion and metastasis in epithelial ovarian cancer. Oncol Rep. 2017;38 (6):3297–3308. doi:10.3892/OR.2017.6034/HTML.
55. Taki M, Abiko K, Ukita M, Murakami R, Yamanoi K, Yamaguchi K, Hamanishi J, Baba T, Matsumura N, Mandai M. Tumor immune microenvironment during epithelial- mesenchymal transition. Clin Cancer Res. 2021;27(17):4669–4679. doi:10.1158/1078-0432.CCR-20-4459/672159/AM/TUMOR-IMMUNE-MICROENVIRONMENT-DURING-EPITHELIAL.
56. Patnaik A, Yap TA, Chung HC, de Miguel MJ, Bang Y-J, Lin -C-C, W-C S, Italiano A, Chow KH, Szpurka AM, et al. Safety and clinical activity of a new anti-PD-L1 antibody as monotherapy or combined with targeted therapy in advanced solid tumors: the PACT phase Ia/Ib Trial. Clin Cancer Res. 2021;27(5):1267–1277. doi:10.1158/1078-0432.CCR-20-2821.

9. Supplements

9.1 Own contribution to the publications

Publication 1: Conducting experiments and data analysis

Publication 2: Conducting experiments and data analysis, writing

Publication 3: Conducting experiments and data analysis, writing and creating the first draft of the manuscript

Publication 4: Conducting experiments, methodology and data analysis, writing and creating the first draft of the manuscript

9.2 Curriculum vitae

Personal information

Name:	M. Sc. Salewski
First name:	Inken
Date of birth:	06.12.1994
Nationality:	German

Education

01/2020 – 01/2023	PhD student in natural sciences / Scientific Assistant, Hematology, Oncology, Palliative Medicine, Rostock University Medical Center, University of Rostock Department of Medicine, Clinic III
07/2019 – 08/2019	Internship in Start-up *alpha-protein* in Bruchsal
10/2016 – 05/2019	Master of Science – University of Konstanz: *Cellular and Molecular Biology* Master thesis: *Functional analyses of cell cycle regulation by the interplay of kinases and phosphatases*
10/2013 – 08/2016	Bachelor of Science – University of Konstanz: *Biological Sciences* Bachelor thesis: *Influences of major morphogenetic pathways during Beloniform fish skeletal jaw development*
09/2005 – 06/2013	Margarete-Steiff-Gymnasium Giengen an der Brenz

9.3 Complete list of publications

9.3.1 Original work

Salewski I*, Gladbach YS*, Kuntoff S, Irmscher N, Hahn O, Junghanss C, Maletzki C. In vivo vaccination with cell line-derived whole tumor lysates: neoantigen quality, not quantity matters. J Transl Med. 2020 Oct 21;18(1):402. doi: 10.1186/s12967-020-02570-y. PMID: 33087163; PMCID: PMC7579816.
(IF 4.965)

Salewski I*, Kuntoff S*, Kuemmel A, Feldtmann R, Felix SB, Henze L, Junghanss C, Maletzki C. Combined vaccine-immune checkpoint inhibition constitutes a promising strategy for treatment of dMMR tumors. Cancer Immunol Immunother. 2021 Dec;70(12):3405-3419. doi: 10.1007/s00262-021-02933-4. Epub 2021 Apr 18. PMID: 33870463; PMCID: PMC8571220.
(IF 6.968)

Schoenwaelder N, **Salewski I**, Engel N, Krause M, Schneider B, Müller M, Riess C, Lemcke H, Skorska A, Grosse-Thie C, Junghanss C, Maletzki C. The Individual Effects of Cyclin-Dependent Kinase Inhibitors on Head and Neck Cancer Cells-A Systematic Analysis. Cancers (Basel). 2021 May 15;13(10):2396. doi: 10.3390/cancers13102396. PMID: 34063457; PMCID: PMC8157193.
(IF 2021 6.639)

Salewski I*, Henne J*, Engster L, Schneider B, Lemcke H, Skorska A, Berlin P, Henze L, Junghanss C, Maletzki C. Combined Gemcitabine and Immune checkpoint Inhibition Conquers Anti-PD-L1 Resistance in Low-Immunogenic Mismatch Repair-Deficient Tumors. Int J Mol Sci. 2021 Jun 1;22(11):5990. doi: 10.3390/ijms22115990. PMID: 34206051; PMCID: PMC8199186.
(IF 5.542)

Schoenwaelder N, Krause M, Freitag T, Schneider B, Zonnur S, Zimpfer A, Becker AS, **Salewski I**, Strüder DF, Lemcke H, Grosse-Thie C, Junghanss C, Maletzki C. Preclinical Head and Neck Squamous Cell Carcinoma Models for Combined Targeted Therapy Approaches. Cancers (Basel). 2022 May 18;14(10):2484. doi: 10.3390/cancers14102484. PMID: 35626088; PMCID: PMC9139292.
(IF 6.639)

Salewski I, Henne J, Engster L, Krone P, Schneider B, Redwanz C, Lemcke H, Henze L, Junghanss C, Maletzki C. CDK4/6 blockade provides an alternative approach for treatment of mismatch-repair deficient tumors. Oncoimmunology. 2022 Jul 11;11(1):2094583. doi: 10.1080/2162402X.2022.2094583. PMID: 35845723; PMCID: PMC9278458.
(IF 8.11)

* both authors contributed equally

9.3.2 Review articles

Riess C*, Irmscher N*, **Salewski I**, Strüder D, Classen CF, Große-Thie C, Junghanss C, Maletzki C. Cyclin-dependent kinase inhibitors in head and neck cancer and glioblastoma-backbone or add-on in immune-oncology? Cancer Metastasis Rev. 2021 Mar;40(1):153-171. doi: 10.1007/s10555-020-09940-4. Epub 2020 Nov 8. PMID: 33161487; PMCID: PMC7897202.
(IF 2020 9,26)

* both authors contributed equally

9.4 Conference contributions

Underlined you find the presenting author.

9.4.1 Talks

Inken Salewski, Steffen Kuntoff, Christian Junghanss, Claudia Maletzki, Effective tumor growth control by combined vaccine-immune checkpoint inhibition in MLH1$^{-/-}$ mice *ESMO virtuell*, 19.-21. September 2020

Inken Salewski, Steffen Kuntoff, Christian Junghanss, Claudia Maletzki, Combined vaccine-immune checkpoint inhibition significantly improves survival of Mlh1$^{-/-}$ mice *via* immune modulation *DGHO* virtuell*,* 09.-11. October 2020

Inken Salewski, Leonie Engster, Julia Henne, Larissa Henze, Christian Junghanss, Claudia Maletzki, CDK4/6 blockade is as effective as immune checkpoint-inhibition in tumor growth control of Mlh1$^{-/-}$ and *Msh2*$^{loxP/loxP}$ *Villin-Cre* mice *ESMO* hybrid, 16.-21. September 2021

Inken Salewski, Julia Henne, Leonie Engster, Bjoern Schneider, Heiko Lemcke, Anna Skorska, Peggy Berlin, Larissa Henze, Christian Junghanss, Claudia Maletzki, Combined gemcitabine and immune checkpoint inhibition conquers anti-PD-L1 resistance in low-immunogenic mismatch repair-deficient tumors *DGHO* hybrid*,* 01.-04. October 2021

Paula Krone, **Inken Salewski**, Julia Henne, Leonie Engster, Bjoern Schneider, Caterina Redwanz, Christian Junghanss, Claudia Maletzki, CDK4/6 blockade provides an alternative approach for treatment of mismatch-repair deficient tumors *DGHO* hybrid*,* 07.-10. October 2022

9.5 Danksagung

Zunächst bedanke ich mich bei Prof. Dr. Christian Junghanß für die Leitung der Abteilung.
Dann möchte ich mich natürlich bei PD Dr. Claudia Maletzki bedanken, die mir das Promotionsthema zur Verfügung gestellt hat, mir das Erlernen zahlreicher Methoden ermöglicht hat und immer mit erfahrenem Rat zur Seite stand.
Ebenfalls geht mein Dank an unsere Kooperationspartner Dr. Björn Schneider und Dr. Maja Hühns aus dem Institut der Pathologie, die nicht nur methodisch, sondern auch mit ihrem Wissen meine Arbeit unterstützten, genauso wie allen Tierpflegern und Mitarbeitern aus dem Rudolf-Zenker-Institut für Experimentelle Chirurgie/ Core Facility Zentrale Versuchstierhaltung, ohne die unsere *in vivo* Versuche nicht möglich gewesen wären. Zu den Kooperationspartnern zählen auch Wendy Bergmann und Michael Müller aus der Core Facility für Zellsortierung und Zellanalyse, die sowohl bei der Arbeit an den Geräten, als auch bei der Auswertung der Daten unterstützt haben. Selbstverständlich geht mein Dank auch meine medizinischen Doktoranden, die mich über die Jahre tatkräftig im Labor unterstützt haben.
Des Weiteren bedanke ich mich bei der gesamten Arbeitsgruppe der Hämatologie und Onkologie, die nicht nur für einen angenehmen Laboralltag sorgten, sondern auch für Spaß auf Grillfesten und Weihnachtsfeiern. Besonderer Dank geht hierbei an Nina Schönwälder, die mit mir die Hürden des Laboralltags gemeistert hat und bei Fragen und Problemen aller Art zu Seite stand.

Abschließend möchte ich mich bei meinen Freunden und meiner Familie bedanken, die mich trotz 1000 km Entfernung durchgehend unterstützt haben und an mich geglaubt haben. Ich danke euch.

9.6 Eidesstattliche Versicherung

Ich versichere eidesstattlich durch eigenhändige Unterschrift, dass ich die Arbeit selbstständig und ohne Benutzung anderer als der angegebenen Hilfsmittel angefertigt habe. Alle Stellen, die wörtlich oder sinngemäß aus Veröffentlichungen entnommen sind, habe ich als solche kenntlich gemacht.

Die Arbeit ist noch nicht veröffentlicht und ist in gleicher oder ähnlicher Weise noch nicht als Studienleistung zur Anerkennung oder Bewertung vorgelegt worden. Ich weiß, dass bei Abgabe einer falschen Versicherung die Prüfung als nicht bestanden zu gelten hat.

Rostock _____ _____

(Abgabedatum) (Vollständige Unterschrift)